

**BEHAVIOR OF TWO-SPAN CONTINUOUS PIER CAPS
WITH VARYING LEVELS OF PRESTRESS**

by

SARAH LONGSTRETH BILLINGTON, B.S.E.

THESIS

Presented to the Faculty of the Graduate School
of The University of Texas at Austin
in Partial Fulfillment
of the Requirements
for the Degree of

MASTER OF SCIENCE IN ENGINEERING

THE UNIVERSITY OF TEXAS AT AUSTIN

DECEMBER 1994

**BEHAVIOR OF TWO-SPAN CONTINUOUS PIER CAPS
WITH VARYING LEVELS OF PRESTRESS**

APPROVED BY:

John E. Breen

Michael E. Kreger

Copyright

by

Sarah Longstreth Billington

1994

*To my wonderful parents -
for their inspiring dedication to their professions
and their immeasurable love
for their children.*

ACKNOWLEDGEMENTS

The research program presented in this thesis was carried out at the Phil M. Ferguson Structural Engineering Laboratory at the University of Texas at Austin. Funding for this project was provided by the Texas Department of Transportation. The author was also supported by a National Science Foundation Graduate Research Fellowship. Any opinions, findings, conclusions or recommendations expressed in this publication are those of the author and do not necessarily reflect the views of the Foundation.

The most rewarding experience from this project was working with many wonderful people. I would especially like to thank my supervisor, Dr. John E. Breen. His remarkable ability to teach and inspire has been invaluable. His support, advice and patience are very much appreciated as well. I would also like to thank Dr. Michael E. Kreger for his guidance throughout many stages of this project.

I gratefully acknowledge my fellow student researchers on this project, Scott Armstrong, Rubén Salas and Bradley Wood. I have valued their continual advice, assistance and friendship throughout this project. It has been a pleasure to work with them.

A huge thank-you goes to Mohamed Najah, the primary undergraduate assistant for this project. His excellent productivity and inventiveness was an enormous help and always kept things interesting. (And I am particularly grateful that he quickly recovered from grinding his thumb, drinking Aqua-lube and attempting to rescue a falling 370-lb. dead-load block!) Many other assistants are deserving of thanks including Jim Doran, Craig Christie, Steve Smith, Todd Zatopek and David Vliet. They were all excellent workers and enjoyable to work with.

The help of the technicians and staff at Ferguson Lab is very much appreciated as well. I thank Pat Ball, Sharon Cunningham, Wayne Fontenot, Laurie Golding, Ryan Green, April Jenkins, Wayne Little, Ray Madonna, Beth Miller and Blake Stasney for all of their advice and help.

I would also like to express my gratitude for the assistance and friendship of all of my colleagues at the lab. I thank René Vignos, Erik Soderberg and Trey Hamilton as their collective help and great sense humor made the late hours and weekends in the lab enjoyable. A special thank-you goes to Valerie Andres and Jeffrey Schmitz for their help and friendship as well as their adventurous plots to ward off "thesis-writing-blues".

Most importantly I thank everyone in my family. They're absolutely wonderful and always make me smile.

Sarah Billington
Austin, TX
December, 1994

ABSTRACT

BEHAVIOR OF TWO-SPAN CONTINUOUS PIER CAPS WITH VARYING LEVELS OF PRESTRESS

by

Sarah Longstreth Billington, M.S.E..

The University of Texas at Austin, 1994

Supervisor: John E. Breen

There are currently two differing design philosophies present in American codes and standards. For conventionally reinforced members, design is based on the ultimate limit state with service limit state checks while members with prestressing steel are designed based on the service limit state with ultimate limit state checks. As well, there is presently no provision for using anything but full prestressing based on the service limit state if any prestressing is used. These differing philosophies often lead to confusion in design and in many cases uneconomical designs.

The goal of this study is to develop a clearer design method that may be applied to structures using varying amounts of non-prestressed and prestressed reinforcement. In particular, two-span continuous stocky beams are examined in conjunction with a unified design philosophy. The philosophy is one that bases flexural and shear designs on the ultimate limit state, carrying out adequate serviceability checks.

Four two-span continuous model beams were constructed and loaded to failure. The model designs included one conventionally reinforced and one fully prestressed design in accordance with the 1992 AASHTO Standard Specifications for Highway Bridges. Also designed were a model with 100% prestressed reinforcement to carry ultimate loads and a model with 71% prestressed reinforcement and 29% non-prestressed reinforcement to carry ultimate loads.

Behavior of these models during loading was recorded in terms of cracking behavior, load-deflection and moment-deflection response, moment redistribution, and ultimate load carrying capacity. Predicted fatigue capacity as well as constructability and economic considerations were examined. Many conclusions and design recommendations are made.

TABLE OF CONTENTS

LIST OF TABLES	xii
LIST OF FIGURES	xiv
CHAPTER 1 - INTRODUCTION	1
1.1 Problem Statement	1
1.2 Objectives	2
1.3 Scope	3
CHAPTER 2 - BACKGROUND	4
2.1 Introduction	4
2.2 Definitions and Concepts	5
2.2.1 The Ambiguity of "Partial Prestressing"	5
2.2.2 The Treatment of Prestress in Design and Analysis	11
2.3 History of Structural Concrete	16
2.3.1 Conventionally Reinforced Concrete	16
2.3.2 Prestressed Concrete	17
2.3.2.1 History	17
2.3.2.2 Formation of Committees, Organizations and Standards for Prestressed Concrete	19
2.3.2.3 Development of Design Philosophies and Practices of the U.S. Prestressing Industry	20
2.3.2.4 Present Situation for Prestressed Concrete Design in the U.S. ...	26
2.3.3 Mixed Design	27
2.3.3.1 The Debate between Full Prestressing and Mixed Reinforcement Design	28
2.3.4 Unified Design for Structural Concrete	33
2.3.5 Comparison with European Codes	35
2.4 Structural Concrete in the 1992 AASHTO Bridge Design Specifications	36
2.4.1 Reinforced Concrete Design	36
2.4.2 Prestressed Concrete Design	38
2.4.3 Problems with Current ACI and AASHTO Specifications	39

2.5 Proposed Integrated Design Methodology	40
2.6 Related Research - Literature Review	42
CHAPTER 3 - EXPERIMENTAL PROGRAM	46
3.1 Introduction	46
3.2 Modelling	46
3.2.1 Prototype and Model Dimensions	46
3.2.1.1 Modelling of Concrete	47
3.2.1.2 Modelling of Reinforcement	47
3.2.2 Prototype and Model Loads	51
3.2.2.1 Dead Load	51
3.2.2.2 Applied Loads	52
3.2.2.3 Construction Loads	53
3.2.2.4 Service and Factored Loads	53
3.2.3 Dead Load Blocks	54
3.3 Test Models	54
3.3.1 Designs According to 1992 AASHTO Bridge Design Specifications	55
3.3.1.1 Conventionally Reinforced - CB-RU	56
3.3.1.2 Fully Prestressed - CB-PS-100S	62
3.3.2 Designs According to Presented Integrated Design Method	68
3.3.2.1 100% Prestress for Factored Loads - CB-PU-100S	68
3.3.2.2 71% Prestress for Factored Loads - CB-PU-71S	78
3.4 Materials	85
3.4.1 Concrete	85
3.4.2 Non-prestressed Reinforcement	85
3.4.3 Prestressing Strand	86
3.4.4 Post-tensioning Duct	86
3.4.5 Grout	93
3.4.6 Anchorage Hardware	93
3.5 Fabrication	94
3.5.1 Reinforcing Cage and Strain Gages	94
3.5.2 Post-tensioning Duct	95
3.5.3 Concrete Placing and Curing	96

3.5.4	Placement of Model in Testing Frame	97
3.5.5	Application of Dead Load Blocks	97
3.5.6	Post-tensioning Procedure	97
3.5.7	Grouting Procedure	99
3.6	Test Set-up	101
3.6.1	Support System	101
3.6.2	Loading System	104
3.6.3	Instrumentation	104
3.6.3.1	Pressure Transducers and Load Cells	104
3.6.3.2	Strain Gages	105
3.6.3.3	Deflection Readings	105
3.7	Testing Procedure	111
3.7.1	Static Loading	111
3.7.2	Data Collection	111
3.7.2.1	Data Acquisition System	111
3.7.2.2	Deflection Measurements	111
3.7.2.3	Crack Width Measurements	112
3.7.3	Post-mortem Investigation	113
CHAPTER 4 - TEST RESULTS		114
4.1	Introduction	114
4.2	Designs According to AASHTO Bridge Specifications - 1992 edition	115
4.2.1	CB-RU-initial - Conventionally Reinforced	115
4.2.1.1	Cracking Behavior - CB-RU-initial	119
4.2.1.2	Moment-Strain Behavior - CB-RU-initial	120
4.2.1.3	Load-Deflection and Moment-Deflection Behavior - CB-RU-initial	128
4.2.2	CB-RU-final - Conventionally Reinforced	129
4.2.2.1	Cracking Behavior - CB-RU-final	129
4.2.2.2	Moment-Strain Behavior - CB-RU-final	134
4.2.2.3	Applied Load vs. Moment Behavior - CB-RU-final	141
4.2.2.4	Load-Deflection Behavior - CB-RU-final	141
4.2.2.5	Moment-Deflection Behavior - CB-RU-final	144

4.2.2.6	Post-mortem Investigation - CB-RU-final	145
4.2.2.7	Further Discussion - CB-RU-final	146
4.2.3	CB-PS-100S - Prestressed based on AASHTO (Service Load Design)	147
4.2.3.1	Cracking Behavior - CB-PS-100S	147
4.2.3.2	Moment-Strain Behavior - CB-PS-100S	153
4.2.3.3	Moment vs. Applied Load - CB-PS-100S	160
4.2.3.4	Load-Deflection Behavior - CB-PS-100S	162
4.2.3.5	Moment-Deflection Behavior - CB-PS-100S	162
4.2.3.6	Post-mortem Investigation - CB-PS-100S	165
4.2.3.7	Further Discussion - CB-PS-100S	165
4.3	Designs According to Proposed Integrated Design Method	167
4.3.1	CB-PU-100S - 100% Prestress Reinforcing (100% of nominal resistance provided by the prestressing strand)	167
4.3.1.1	Cracking Behavior - CB-PU-100S	167
4.3.1.2	Moment-Strain Behavior - CB-PU-100S	172
4.3.1.3	Moment vs. Applied Load Behavior - CB-PU-100S	178
4.3.1.4	Load-Deflection Behavior - CB-PU-100S	179
4.3.1.5	Moment-Deflection Behavior - CB-PU-100S	179
4.3.1.6	Post-mortem Investigation - CB-PU-100S	183
4.3.1.7	Further Discussion - CB-PU-100S	185
4.3.2	CB-PU-71S - 71% Prestress Reinforcing (71% of nominal resistance provided by the prestressing strand, 29% provided by non-prestressed steel)	185
4.3.2.1	Cracking Behavior - CB-PU-71S	185
4.3.2.2	Moment-Strain Behavior - CB-PU-71S	191
4.3.2.3	Moment vs. Applied Load Behavior - CB-PU-71S	197
4.3.2.4	Load-Deflection Behavior - CB-PU-71S	199
4.3.2.5	Moment-Deflection Behavior - CB-PU-71S	199
4.3.2.6	Post-mortem Investigation - CB-PU-71S	202
CHAPTER 5	COMPARISON OF TEST RESULTS	204
5.1	Introduction	204
5.2	First Cracking Behavior	204

5.3	Maximum Crack Width Envelopes	207
5.4	Measured vs. Predicted Crack Widths	210
5.5	Crack Distribution Characteristics	215
5.6	Moment Redistribution Behavior	222
5.7	Ultimate Behavior	222
5.8	Load-Deflection Behavior	224
5.9	Moment-Deflection Behavior	228
5.10	Fatigue Considerations	230
5.11	Constructability of Models	230
5.12	Economic Considerations	232
5.13	Design Recommendations	234
CHAPTER 6 - SUMMARY & CONCLUSIONS		236
6.1	Summary	236
6.2	Conclusions	238
APPENDIX A - Design Equations for Models CB-RU and CB-PU-100S		240
APPENDIX B - Fatigue Study for Model CB-PU-100S		249
REFERENCES		256
VITA		261

LIST OF TABLES

Table 3.1	Typical Span Length-to-Height and Shear Span-to-Effective Depth Ratios for San Antonio Y-project Straddle Bents	51
Table 3.2	Modelling of Reinforcement	51
Table 3.3	Comparison of Model and Prototype Designs for CB-RU	61
Table 3.4	Comparison of Model and Prototype Designs for CB-PS-100S	71
Table 3.5	Model and Corresponding Prototype Designs for CB-PU-100S	77
Table 3.6	Model and Corresponding Prototype Designs for CB-PU-71S	84
Table 3.7	Concrete Properties	86
Table 3.8	Grout Compressive Strengths	93
Table 4.1E	Maximum Crack Widths for CB-RU-initial, English Units	121
Table 4.1S	Maximum Crack Widths for CB-RU-initial, S.I. Units	122
Table 4.2E	Maximum Crack Widths for CB-RU-final, English Units	131
Table 4.2S	Maximum Crack Widths for CB-RU-final, S.I. Units	132
Table 4.3E	Maximum Crack Widths for CB-PS-100S, English Units	150
Table 4.3S	Maximum Crack Widths for CB-PS-100S, S.I. Units	151
Table 4.4E	Maximum Crack Widths for CB-PU-100S, English Units	170
Table 4.4S	Maximum Crack Widths for CB-PU-100S, S.I. Units	171
Table 4.5E	Maximum Crack Widths for CB-PU-71S, English Units	187
Table 4.5S	Maximum Crack Widths for CB-PU-71S, S.I. Units	188
Table 5.1	Comparison of First Cracking Predictions and Observed Behavior for all Models	206
Table 5.2	Comparison of Measured Crack Widths and Predicted Crack Widths under Service Loads	213
Table 5.3	Comparison of Measured Crack Widths and Predicted Crack Widths using Measured Steel Stresses under Service Loads	214
Table 5.4	Minimum Reinforcement Requirements in American Specifications and Codes	218
Table 5.5	Comparison of European Practice of Minimum Reinforcing for Crack Control of Members with Prestressed Reinforcement	220

Table 5.6	Comparison of Ultimate Applied Load Predictions and Observed Behavior for All Models	223
Table 5.7	Reinforcement Lengths and Weights for Each Model	233

LIST OF FIGURES

Figure 2.1a	Simply Supported Prestressed Beam	6
Figure 2.1b	Possible Names for Prestressing for Various Stress Distributions at Service Loads	6
Figure 2.2	Example Beams with Descriptions using Proposed New Terminology	8
Figure 2.3	Problems with Possible Definitions for Percentages of Prestress Reinforcing ...	10
Figure 2.4	Possible Treatments of Prestress	12
Figure 2.5	Treatment of Prestress for a Simply Supported Beam	13
Figure 2.6	Treatment of Prestress for a Two-span Continuous Beam	15
Figure 2.7	Development of Design Approaches for Prestressed Concrete in the United States	21
Figure 2.8	Development of Concrete Tensile Stress Limits for Prestressed Concrete Design in the United States	23
Figure 2.9a	Percent of Bridge Types versus Year Built as of May 1989	25
Figure 2.9b	Percent of Structurally Deficient Bridge Types versus Year Built as of May 1989	25
Figure 3.1a	Prototypical Designs from San Antonio "Y" Project, English units	48
Figure 3.1b	Prototypical Designs from San Antonio "Y" Project, S.I. units	49
Figure 3.2	Modelling of Prototype	50
Figure 3.3	Critical Moment and Shear Diagrams for Designs	57
Figure 3.4	Design of CB-RU - Conventionally Reinforced based on AASHTO	60
Figure 3.5	Moment Diagrams for Service and Unfactored Construction Loads	63
Figure 3.6	Factored Shear for Design of Post-tensioned Specimens	65
Figure 3.7	Anchor Zone Design Method for CB-PS-100S	67
Figure 3.8	Design of CB-PS-100S - "Fully" Prestressed based on AASHTO	69
Figure 3.9	Designed vs. Built Tendon Profile for CB-PS-100S	70
Figure 3.10	Compressive Stress Orientation in CB-PU-100S under Factored Loads for Shear Design	73
Figure 3.11a	Tensile Stress Orientation in CB-PU-100S under Service Loads	74
Figure 3.11b	Concrete Tensile Stresses in each element in terms of $\sqrt{f'_c}$	74
Figure 3.12	Design for CB-PU-100S - 100% Prestress for Ultimate Tensile Force	76

Figure 3.13	Compressive Stress Orientation in CB-PU-71S under Factored Loads for Shear	
	Design	80
Figure 3.14a	Tensile Stress Orientation in CB-PU-71S under Service Loads	81
Figure 3.14b	Concrete Tensile Stresses in Each Element in Terms of $\sqrt{f_c'}$	81
Figure 3.15	Design for CB-PU-71S - 71% Prestress for Ultimate Tensile Force	83
Figure 3.16	Stress-Strain Curve for No. 3 Deformed Reinforcement	87
Figure 3.17	Stress-Strain Curve for No. 2 Deformed Reinforcement from Sweden	88
Figure 3.18	Stress-Strain Curve for the $\Phi 5/32"$ (4.0 mm) Smooth Wire Reinforcement	89
Figure 3.19	Stress-Strain Curve for 12-gauge Smooth Cold-drawn Wire	90
Figure 3.20	Stress-Strain Curve for 1/2 in. (12.7 mm) Diameter Prestressing Strand	91
Figure 3.21	Stress-Strain Curve for 3/8 in. (9.5 mm) Diameter Prestressing Strand	92
Figure 3.22	Fabrication of Reinforcing Cage	94
Figure 3.23	Post-tensioning Duct Secured in Formwork before Placement of Concrete	95
Figure 3.24	Placement of Concrete	96
Figure 3.25	Dead Load Blocks Hanging from Model	98
Figure 3.26	Cross Section of Dead Load Blocks Hanging from Model	98
Figure 3.27	Set-up for Post-tensioning Operations	100
Figure 3.28	Preparing for Post-tensioning Procedures	100
Figure 3.29	Original Test Set-up	102
Figure 3.30	Final Test Set-up	103
Figure 3.31a	Strain Gauge Locations for CB-RU	106
Figure 3.31b	Strain Gauge Locations for CB-PS-100S	107
Figure 3.31c	Strain Gauge Locations for CB-PU-100S	108
Figure 3.31d	Strain Gauge Locations for CB-PU-71S	109
Figure 3.32	Deflection Measuring Systems for Final Set-up	110
Figure 3.33	Measuring of Crack Widths with an Optical Crack Monitor	112
Figure 3.34	Failed Test Specimen Opened for Post-Mortem Investigations	113
Figure 4.1	Analysis of Support Settlements using the Compatibility Method	117
Figure 4.2	Cracking of CB-RU-initial at Service Load Levels	119
Figure 4.3	Moment-Strain Behavior in the Negative Moment Region CB-RU-initial	123
Figure 4.4	Moment-Strain Behavior of Mid-Span Tensile Steel - CB-RU-initial	124
Figure 4.5	Moment-Strain Behavior of Side Face Crack Control Steel for CB-RU-initial .	126

Figure 4.6	Mid-Span Moment-Deflection Behavior for CB-RU-initial	128
Figure 4.7	Cracking of CB-RU-final at Ultimate Load Levels	130
Figure 4.8	Maximum Crack Width Envelope - CB-RU	133
Figure 4.9	Behavior of Side Face Crack Control Steel at Service Loads for Model	
	 CB-RU-final	134
Figure 4.10	Moment-Strain Behavior in the Negative Moment Region CB-RU-final	135
Figure 4.11	Moment-Strain Behavior of Mid-Span Tensile Steel - CB-RU-final	136
Figure 4.12	Center Support - Strain Behavior for Shear Stirrups - CB-RU-final	138
Figure 4.13	Moment-Strain Behavior of Side Face Crack Control Steel for CB-RU-final ..	139
Figure 4.14	Moment vs. Applied Load - CB-RU-final	142
Figure 4.15	Load-Deflection Behavior - CB-RU-final	143
Figure 4.16	Mid-Span Moment-Deflection Behavior for CB-RU-final	144
Figure 4.17	Failure Condition for CB-RU-final	145
Figure 4.18	Failure Condition for CB-RU-final - South Support, West Side	146
Figure 4.19	Cracking of CB-PS-100S at Ultimate Load Levels	149
Figure 4.20	Maximum Crack Width Envelope - CB-PS-100S	152
Figure 4.21	Moment-Strain Behavior for Non-Prestressed Steel in the Negative Moment	
	 Region - CB-PS-100S	154
Figure 4.22	Moment-Strain Behavior of Mid-Span Non-prestressed Tensile Steel -	
	 CB-PS-100S	155
Figure 4.23	Center Support - Strain Behavior for Shear Stirrups - CB-PS-100S	156
Figure 4.24	Shear-Stirrup Strain Behavior near North Mid-Span - CB-PS-100S	157
Figure 4.25	Moment-Strain Behavior of Side Face Crack Control Steel for CB-PS-100S ..	158
Figure 4.26	Moment vs. Applied Load - CB-PS-100S	161
Figure 4.27	Load-Deflection Behavior - CB-PS-100S	163
Figure 4.28	Mid-Span Moment-Deflection Behavior for CB-PS-100S	164
Figure 4.29	Post-mortem Investigation of Failed Cross-Section for CB-PS-100S	166
Figure 4.30	Crushing Failure of Mid-Span, North - CB-PS-100S	167
Figure 4.31	Cracking of CB-PU-100S at Ultimate Load Levels	168
Figure 4.32	Maximum Crack Width Envelope - CB-PU-100S	172
Figure 4.33	Moment-Strain Behavior for Non-Prestressed Steel in the Negative Moment	
	 Region - CB-PU-100S	174

Figure 4.34	Moment-Strain Behavior of Mid-Span Non-prestressed Tensile Steel - CB-PU-100S	175
Figure 4.35	Center Support - Strain Behavior for Steel Stirrups - CB-PU-100S	176
Figure 4.36	Moment-Strain Behavior of Side Face Crack Control Steel for CB-PU-100S ..	177
Figure 4.37	Moment vs. Applied Load - CB-PU-100S	180
Figure 4.38	Load-Deflection Behavior - CB-PU-100S	181
Figure 4.39	Mid-Span Moment-Deflection Behavior for CB-PU-100S	182
Figure 4.40	Crushing Failure of Mid-Span, North - CB-PU-100S	183
Figure 4.41	Post-mortem Investigation of Failed Cross-Section for CB-PU-100S	184
Figure 4.42	Cracking of CB-PU-71S at Ultimate Load Levels	186
Figure 4.43	Maximum Crack Width Envelope - CB-PU-71S	189
Figure 4.44	Behavior of Side Face Crack Control Steel at Service Loads for Model CB-PU-71S	190
Figure 4.45	Moment-Strain Behavior for Non-Prestressed Steel in the Negative Moment Region - CB-PU-71S	192
Figure 4.46	Moment-Strain Behavior of Mid-Span Non-prestressed Tensile Steel - CB-PU-71S	193
Figure 4.47	Center Support - Strain Behavior for Shear Stirrups - CB-PU-71S	194
Figure 4.48	Moment-Strain Behavior of Side Face Crack Control Steel for CB-PU-71S ...	195
Figure 4.49	Moment vs. Applied Load - CB-PU-71S	198
Figure 4.50	Load-Deflection Behavior - CB-PU-71S	200
Figure 4.51	Mid-Span Moment-Deflection Behavior for CB-PU-71S	201
Figure 4.52	Post-mortem Investigation of Failed Cross-Section for CB-PU-71S	202
Figure 4.53	Failure over the Center Support - CB-PU-71S	203
Figure 5.1	Maximum Crack Width Envelopes - All Models	208
Figure 5.2	Maximum Crack Width Envelopes for All Models	209
Figure 5.3	Comparison of Crack Distribution of all Models at the Service Limit State ...	216
Figure 5.4	Shear Deformation in Elastomeric Bearing Pads	225
Figure 5.5	Load-Deflection Behavior of All Models	226
Figure 5.6	Mid-Span Deflection for all Models under Service Loads	227
Figure 5.7	Moment-Deflection Curves for all Models	229
Figure 5.8	Cost of Reinforcing Steel for Prototypes of Each Model	234

Figure B.1	Concrete and Steel Strains in Initial Stage for Fatigue Study	251
Figure B.2	Cracked Section Analysis for Fatigue Study	253
Figure B.3	Stress Range for Prestressed Steel over Center Support - CB-PU-100S	254

CHAPTER 1

INTRODUCTION

1.1 Problem Statement

The traditional separation of conventionally reinforced concrete design from prestressed concrete design by treatment in separate chapters is a problem of concern in U.S. building codes and bridge design specifications. This is compounded by the present tendency of these standards to concentrate more on prescriptive and empirical equations for each type of design rather than clear overall behavioral models. This separation of design types and emphasis on prescriptive equations is often confusing to designers as it unnecessarily complicates the design of many types of elements.

One clear example of this is in the design of large-scale substructures as experienced by the Texas Department of Transportation in their elevated highway designs for the San Antonio Y-Project. With the design of the cantilever bents, it was often unclear as to whether the member should be designed as a deep beam or a corbel, each of which requires a different design theory (deep beam theory and shear friction theory respectively). As a result of the confusion and the lack of understandable behavioral models to follow, designers felt required to design the members fully for both methods. The final designs resulted in inefficient over-designed members that were not only uneconomical in material cost, but also difficult to construct due to the highly congested reinforcing cages.

Inefficient, over-designed members result from many large-scale deep straddle bent designs as well. Under current standards, if no prestressing is used, these members are designed primarily for the ultimate limit state with minimal checks for deflections and flexural reinforcement distribution to limit crack widths. If any prestressing is used the member must be designed to be fully prestressed to limit concrete tensile stresses at service loads to somewhat arbitrary levels. This excludes adding a limited amount of prestress to improve behavior of a primarily "non-prestressed" member. The design of large-scale deep members is therefore a good example in which designs could be greatly improved with the allowance of various levels of prestressing (anything less than "full") based on both strength and serviceability.

The recent LRFD (Load and Resistance Factored Design) proposal for an AASHTO Bridge Design Specification includes a section on "partially prestressed" design, essentially meaning the use of a mix of prestressed and non-prestressed reinforcement.[48] This is a positive step towards allowing for more

efficient designs. However, it artificially sets up yet another "class" of design with a new set of prescriptive rules. The IABSE (International Association of Bridge and Structural Engineers) Colloquium on Structural Concrete in 1991 specifically concluded that the introduction of such terms as "partially prestressed" is confusing and undesirable. The colloquium called for the development of a general unified design theory which would be applicable for the full spectrum from plain concrete through conventionally reinforced concrete to mixed design of prestressed and non-prestressed concrete to fully prestressed concrete.[61]

This idea leads to the concept of a unified design code covering all types of concrete design. An emphasis on performance standards and a better understanding of overall structural action with the help of clear behavioral models could alleviate many of the problems designers face using current standards. In particular such a unified design method would help with the design of unusual members that may not fall under clear-cut descriptions such as the large-scale cantilever and straddle bent caps of the San Antonio Y-Project.

1.2 Objectives

The objective of the overall research project of which this thesis is a part, is to investigate the behavior of large-scale stocky concrete substructures and to develop an integrated, unified design methodology for such members that would employ the use of clear behavioral models and allow for efficient combinations of prestressed and non-prestressed reinforcement.

The project has three areas of focus:

1. Cantilever bents - cantilever overhang only.
2. Cantilever bents - entire bent.
3. **Two-span continuous pier caps.**

The first area of focus involves investigations of the cantilever overhang portion of cantilever bents looking particularly at the effects of using varying amounts of prestressed and non-prestressed steel for the main flexural reinforcement, using hooked or T-headed reinforcing bars to anchor the main reinforcement, and using supplementary skin reinforcement for side face crack control. Alternate strut & tie models (i.e. inclined vs. vertical struts) were applied for shear design as well. Tests in this phase have been completed.[17,54] The second area of focus involves investigations of the behavior of entire cantilever bents (column, joint and overhang) designed with varying amounts and locations of prestressed and non-prestressed steel of the main flexural reinforcement. The use of T-headed reinforcement to anchor flexural

reinforcement and alternate strut & tie models for flexure and shear are investigated as well. Tests in this phase are in progress. The third area of focus and the subject of this thesis is a study of two-span continuous pier caps and involves investigations into the use of different combinations of prestressed and non-prestressed steel for the main flexural reinforcement and the resulting behavior of such designs.

1.3 Scope

The scope of this thesis is the reporting of an experimental investigation in which a series of two-span continuous beams similar to the beam portions of large-scale straddle bents were designed, constructed and loaded to failure to determine the behavior and efficiency of mixed combinations of prestressed and non-prestressed reinforcement. This thesis discusses the background of the problem of designing two-span continuous large-scale stocky beams, including the history and development of various design provisions in today's standards. An integrated, unified design method is then proposed and investigated. The testing program presented includes the selection of the prototype and model, variables to be investigated, a description of the test models, modelling techniques, materials, fabrication, test set-up, testing procedures and data collection. The test results are then presented and evaluated. Comparisons are drawn between the models, and constructability and economic considerations are discussed. Resulting design indications and recommendations for changes in the AASHTO Bridge Design Specifications are given. A final summary and conclusions are drawn.

CHAPTER 2

BACKGROUND

2.1 Introduction

...We are now [in] a period of optimization,... selecting the technically and economically best systems and methods,...We now envisage a period of critical reflection, questioning familiar and accepted practices, to ensure the best solutions for the service we expect from our structures. We have to check whether our philosophy of prestressed concrete is sound or whether it carries unwanted prejudices or ideologies...

- Fritz Leonhardt

The aim of this chapter is to review the historical development of the various types of structural concrete design currently referred to as reinforced concrete, prestressed concrete and partially prestressed concrete and to discuss their implementation in today's building codes and bridge design specifications. Different philosophies of design have existed since the introduction of these structural materials in the construction industry. Looking briefly into these philosophies and their effect on the different design procedures outlined in current standards in the United States and elsewhere, there are a number of inconsistencies, a lack of clear design models particularly for the design of large-scale, stocky continuous members, and a tendency to embrace old ideas despite new research and information that introduces more efficient approaches to design. There is now a definite need for and a tendency towards unifying these currently separate forms of design into one integrated method of design under the heading "Structural Concrete". This call for structural concrete has been ongoing for many years and is discussed here. An integrated unified design method to be investigated with experiments as well as a literature review of other related design method proposals and experiments are presented.

2.2 Definitions and Concepts

There are two major concepts relevant to this thesis that should be emphasized and well understood in order to examine the advantages or disadvantages of a unified design method. The first involves the problems with the term "partial" prestressing - which is defined differently by different individuals and groups. The second concept involves the treatment of prestressing as a resistance only or as a load and a resistance. Advantages and disadvantages of these treatments of prestressing are discussed.

2.2.1 The Ambiguity of "Partial Prestressing"

The term "partial prestressing" is awkward in that it can have a number of different meanings. The term is often used loosely and because of the different definitions, this leads to confusion. This can best be seen with an example. Consider two designs for a simply supported beam (Fig. 2.1). In the first design (Beam 1), two prestressed strands have been used for flexure design. In the second design (Beam 2), one prestressed strand and one mild steel deformed bar have been used for flexure design. Figure 2.1b shows different possible stress distributions in the section at service loads. Also shown are the various names or definitions ("full" or "partial") often assigned to the beams depending on the stress distribution at service loads. For Beam 1, Case I results in a stress distribution only of compression. In American usage, this beam would be called "fully prestressed". In Case II there is a small amount of tension at the bottom. Assuming this tensile stress is below an allowable limit (T_{allow}), this design may also be considered "fully prestressed". With Case III, the tensile stress at the bottom is larger than is "allowed", and this section is often referred to as "partially prestressed". However, due to the presence of prestressing strand only, some may still call it "fully prestressed". Looking at Beam 2, with the exact same three possible sectional stress distributions at service loads, each case would be referred to as "partially prestressed" in American usage simply due to the use of both prestressed and non-prestressed reinforcement to satisfy requirements for flexure.

These beams with three stress variations represent only some of the instances where the terms "partial" or "full" are often interchanged. There is also the possibility of using prestressing strand and not stressing it or stressing it to relatively low prestress levels. Some may call this "full prestressing", others "partial prestressing". In the case of most "fully prestressed" designs in the U.S., there is non-prestressed cage steel or steel for shrinkage and temperature that may act to increase the member's flexural capacity. These designs could then be referred to by some as "partially prestressed". However in American usage they are

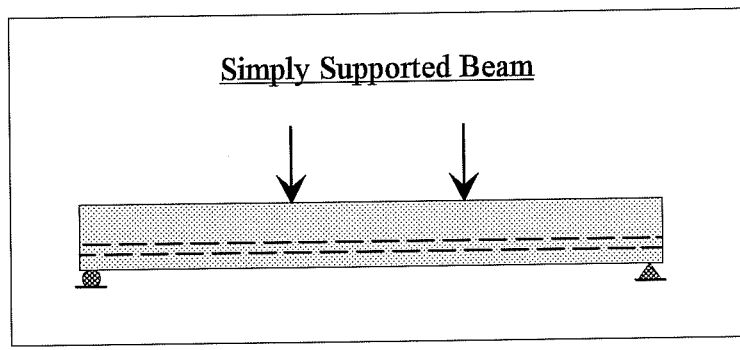


Figure 2.1a Simply Supported Prestressed Beam

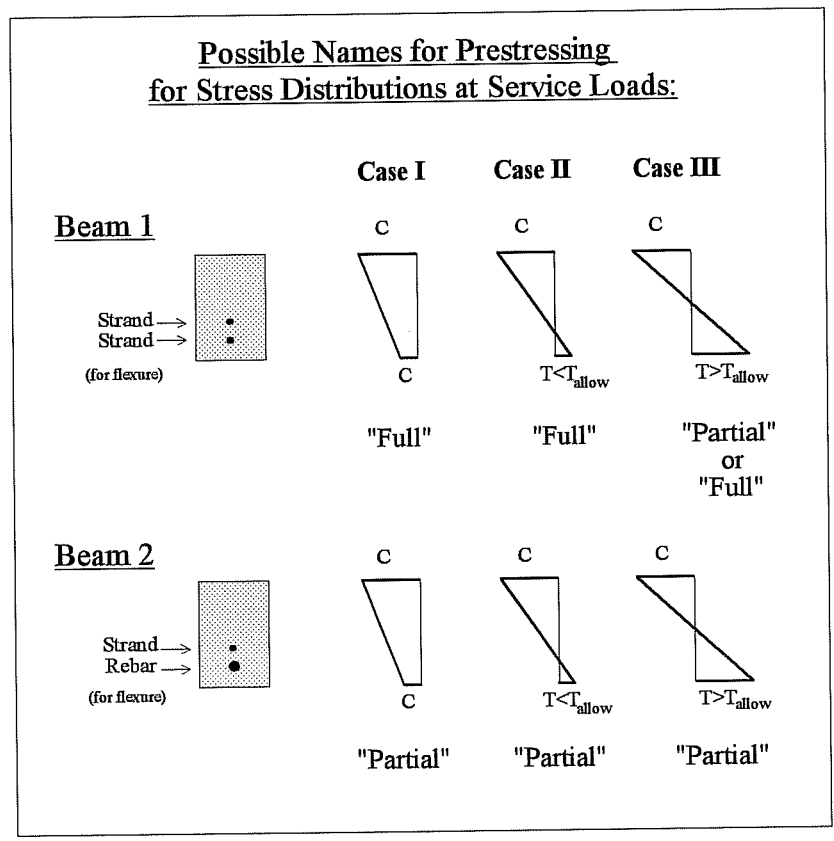


Figure 2.1b Possible Names for Prestressing for Various Stress Distributions at Service Loads

more typically referred to as "fully prestressed". These few examples show how almost any type of design with any amount of prestressed reinforcement may be referred to as either "fully" or "partially" prestressed despite the very different design and behavior implications of these designs. These different implications are not at all expressed by these names.

The term "partial prestressing" with its ambiguous meaning should therefore be avoided. One possible improvement to avoid confusion is to introduce clearer terminology and definitions. Such terms should recognize the important differences in behavior at ultimate and service limit states.

What is important at the ultimate limit state is that correct procedures have been used to determine the contribution of each type of reinforcement to the ultimate resistance. At this stage, the types of reinforcement may be referred to in terms of what percent of the nominal tensile force they provide. This would give a quick and clear understanding of what type of reinforcement is used to provide nominal resistance. This description can also serve as a starting point for design. With enough experience in mixed reinforcement design, designers may know to begin a certain type of design with a minimum or perhaps maximum of 70% of the ultimate tensile force being provided by the prestressing reinforcement (may be referred to as "70% Prestress Reinforcement based on the ultimate limit state"). The design would then be continued to check serviceability. In the examples of Figure 2.2, Beam 1 would be 52% Prestress Reinforcement" and Beam 2 would be "90% Prestress Reinforcement" based on the ultimate limit state. The strength of the non-prestressed steel at ultimate is assumed to be the yield strength of the steel and the strength of the prestressed steel is assumed to be the average stress in prestressing steel at ultimate load. Percentages would be calculated as follows:

$$\% PS Reinforcing = \frac{A_{ps} f_{su}^*}{A_{ps} f_{su}^* + A_s f_y} \times 100 \quad (2-1)$$

Where: A_{ps} : area of prestressing steel
 f_{su}^* : average stress in prestressing steel at ultimate load [9, Chapter 9]
 A_s : area of non-prestressing steel
 f_y : yield strength of non-prestressing steel

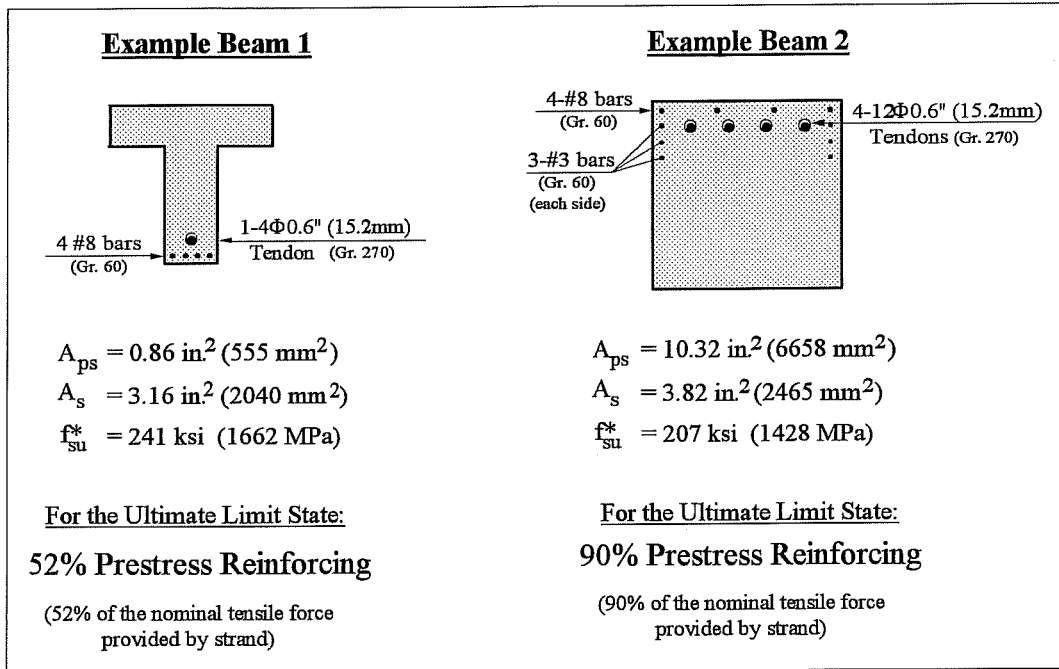


Figure 2.2 Example Beams with Descriptions using Proposed New Terminology

This type of definition is similar to the proposal of B. Thürlimann of Switzerland [63] where the degree of prestress in a member is defined by the ratio:

$$\lambda_p = \frac{A_p \sigma_{py}}{A_p \sigma_{py} + A_s \sigma_{sy}} \quad (2-2)$$

Where: λ_p : degree of prestress
 A_p : area of prestressing steel
 σ_{py} : yield strength of prestressing steel
 A_s : area of non-prestressing steel
 σ_{sy} : yield strength of non-prestressing steel

Thürlimann's definition uses the yield strength of the prestressing steel while the proposed new terminology uses the average stress in the prestressing steel at ultimate load. In this way, the proposed terminology is more directly related to the ultimate behavior of the element being discussed.

Comparisons between different designs or elements using such indices would be informative in terms of implying how ultimate loads are carried. These comparisons would best be made when similar procedures are used to determine the strengths of the materials at ultimate load.

At the service limit state, of primary interest is serviceability must be satisfied. The exact type and quantity of reinforcement used to do this is not of direct importance provided that serviceability is indeed satisfied. Different terminology for this limit state is not desired nor is it necessary.

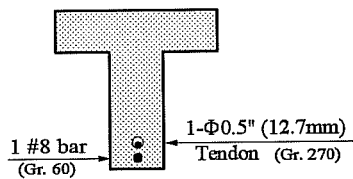
In terms of construction, a simple description explaining general amounts of prestressed versus non-prestressed reinforcement may be of interest to constructors. Constructors would be interested in knowing generally the degree of constructor-controlled prestressing operations which will be necessary, and any potential congestion problems. However, introducing new terms for this purpose leads to a "classification" of concrete. Boundaries would need to be set for terms such as "minimally prestressed", "moderately prestressed", or "largely prestressed" in order that they might correctly imply to the constructor the degree of required constructor-controlled prestressing operations. What these boundaries would be based on is questionable. They could be based on new percentages such as the percentage of area of steel that needs to be prestressed or the percentage of flexural reinforcing elements (bars or strands) that need to be prestressed. However, each of these new percentages in certain cases may not honestly or accurately give an understanding of the degree of required constructor-controlled prestressing operations or potential congestion problems of the reinforcing cages (see Figure 2.3). More importantly, introducing a new type of percentage could lead to confusion.

It would appear that boundaries could be set based on the previously proposed terminology where a design is described in terms of the percentage of nominal tensile strength provided by the prestress reinforcement. However, in the case of service load design, prestressing may provide 90% of the nominal tensile strength of a design while also providing 100% more strength than is required for ultimate load design. This is common in design in that often more prestressing reinforcement is required to control stresses at service loads than is required to carry ultimate loads. Such designs would be far more congested than a design based on ultimate loads where similarly 90% of the nominal tensile strength is provided by the prestressing reinforcement, yet the nominal resistance corresponds well with the ultimate strength.

Clearly, finding proper boundaries for such descriptions as "moderately" or "largely" prestressed would be difficult. Boundaries would inevitably lead to a type of classification and classifications very often infer quality or expense. In the case of "structural concrete", or the entire spectrum of concrete design, quality and expense are a result of engineering decisions in design and not on what types of

—> Problems with possible definitions of prestress reinforcing when used to imply amount of steel congestion and required constructor-controlled prestressing operations:

1) % Prestress Reinforcing by Area:

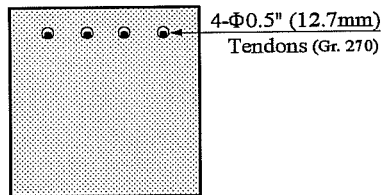


$$A_{ps} = 0.153 \text{ in.}^2 (99 \text{ mm}^2) - 16\% \text{ Prestress Reinforcing}$$

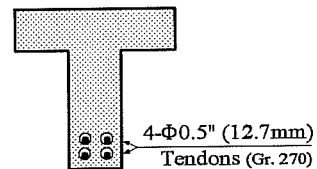
$$A_s = 0.79 \text{ in.}^2 (510 \text{ mm}^2) - 84\% \text{ Non-Prestress Reinforcing}$$

** This is not representative of required constructor-controlled prestressing operations

2) % Prestress Reinforcing by Number of Prestressed Tensile Elements:



100% Prestress Reinforcing



100% Prestress Reinforcing

** This does not accurately represent potential congestion for construction

Figure 2.3 Problems with Possible Definitions for Percentages of Prestress Reinforcing

reinforcement, if any, are used. The best way for constructors to understand the degree of constructor-controlled prestressing operations or potential problems with congestion is to simply study the design plans.

Therefore the only new terminology needed for clarifying types of design is a term for the ultimate limit state; the percentage of nominal resistance provided by any prestressing reinforcement. In no way does this new terminology change the fact that strength and serviceability must be satisfied. Instead, the ambiguity of "partial" prestressing and the implications of the present "full" prestressing will no longer exist.

As it stands today, full prestressing implies a design based on certain limiting tensile stresses to satisfy serviceability requirements. With the new terminology, a member that is 100% (similar to a current "fully prestressed" member) or 80% Prestress Reinforcement based on the ultimate limit state will not necessarily imply satisfaction of the familiar limited tensile stresses at service loads. Serviceability will of course need to be satisfied. This will be done by satisfying performance requirements rather than by satisfying one set of somewhat arbitrary concrete tensile stress limits.

This new terminology is highly desirable for application to all types of structural concrete in order to clearly express what type of design is being used and how it is being used. It does not impose restrictions by implying quality or expense and therefore leaves room for creative and innovative engineering. It is the first step towards unifying the design methods for all types of structural concrete.

2.2.2 The Treatment of Prestress in Design and Analysis

In prestressed concrete design and analysis, the prestressing reinforcement can be considered to act in two different ways. One way which has traditionally been used for ultimate strength calculations is to consider the prestressing reinforcement as strictly providing resistance to other applied loads. Another way is to consider the prestressing force as an applied load and the capacity of the tendon above the effective prestressing level as a part of the resistance. These concepts are depicted in Figure 2.4. Both approaches lead to the same end result - the same ultimate moment. There are particular cases however, when one approach might be simpler to use than another. This can best be seen in two examples - a simply supported prestressed beam and a two-span continuous prestressed beam.

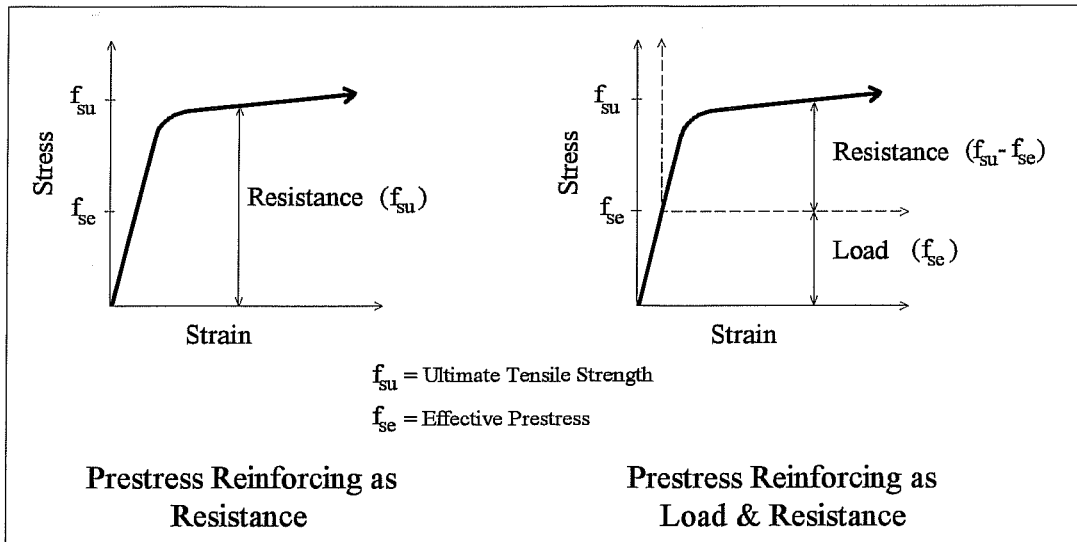


Figure 2.4 Possible Treatments of Prestress

Simply Supported Prestressed Beam

Considering the prestress as resistance only for the simply supported beam in Figure 2.5, the equilibrium equation for applied moment equalling the resisting moment at mid-span is:

$$Q^*x = A_{ps} * f_{su} * z$$

where Q^*x is the applied moment, A_{ps} is the area of the prestressed steel, f_{su} is the ultimate tensile strength of the prestressing strand, and z is the moment arm at ultimate loads.

Considering the prestress as a load first and then a resistance, the equilibrium equation for applied moment equalling the resisting moment at mid-span is:

$$\begin{aligned}
 Q^*x &= T^*z + P^*z \\
 Q^*x &= A_{ps} * (f_{su} - f_{se}) * z + A_{ps} * f_{se} * z \\
 Q^*x &= A_{ps} * f_{su} * z
 \end{aligned}$$

Where: Q^*x : applied moment
 T^* : remaining capacity of tensile force in the strand after initial stressing
 P^* : prestressing force
 z : moment arm at ultimate loads
 A_{ps} : area of the prestressed steel
 f_{su} : ultimate tensile strength of the prestressing strand
 f_{se} : effective prestress (initial stress in strand after losses)

The ultimate moment is exactly the same in both cases (see Figure 2.5).

For the case of the simply supported beam, treatment of the prestressing only as a resistance is straight-forward and much simpler than treatment of the prestressing as both a load and a resistance.

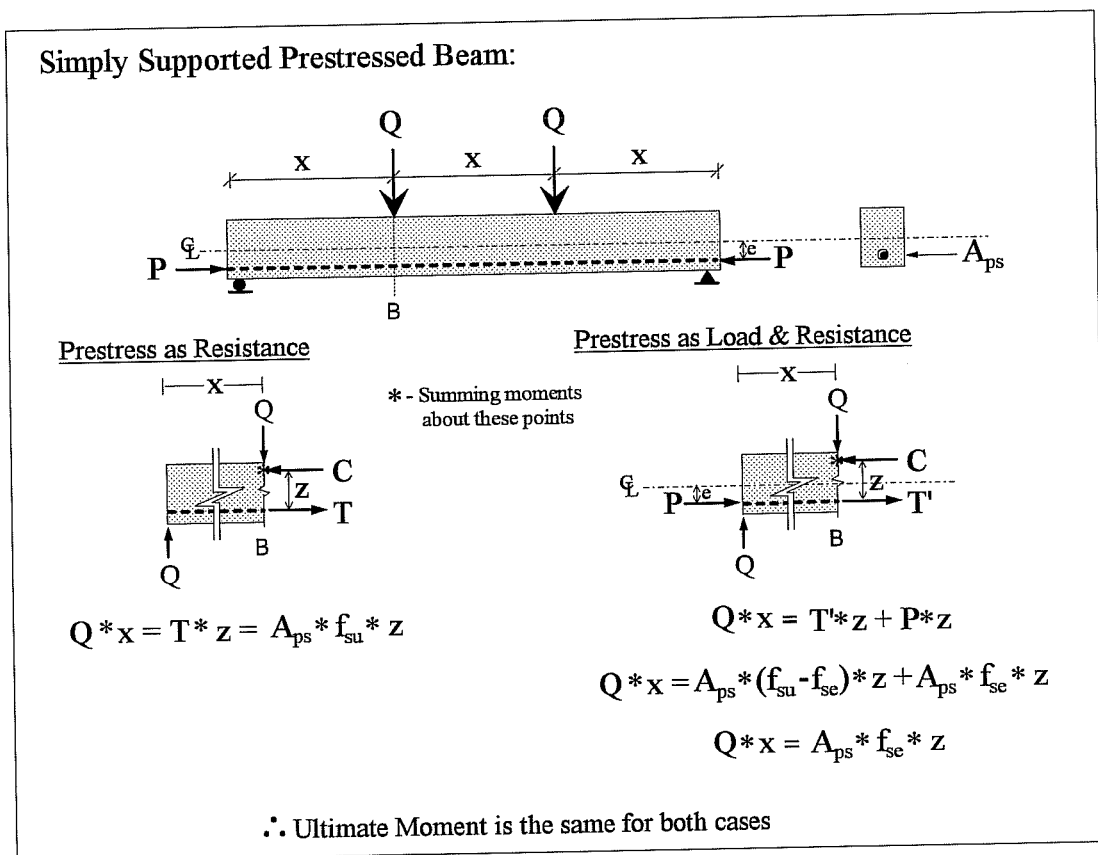


Figure 2.5 Treatment of Prestress for a Simply Supported Beam

Two-Span Continuous Prestressed Beam

Considering the prestress strictly as resistance for the indeterminate beam in Figure 2.6, the resistance side of the equilibrium equation is straight-forward - it is the same as that for the simply supported beam. However, determining the ultimate applied moment is quite complicated in part because of the secondary moments induced by the restraint of the center support. (The eccentric prestressing causes the beam to want to deflect but the center support restrains the beam from deflecting. These restraining forces then create the secondary moments in the beam.) Many methods for determining the secondary moments have been suggested including long, complicated closed-form expressions which offer no visual understanding of the solution at all. Another more common method to solve for the ultimate applied moment requires plotting moment and shear diagrams for ordinary continuous beams, applying the moment distribution method, and locating "lines of pressure" and concordancy of cables within the beam (lines along which the secondary moments would be minimized).[41] Once the secondary moments are determined, they are added to the elastic applied moments. A check is then made to ensure that this moment is less than the nominal moment provided by the prestressing strand.

The process is long and tedious by hand, primarily due to the method for determining secondary moments in an indeterminate prestressed beam. As well, the idea of designing only for concordant tendons is debatable. Secondary moments may be advantageously used leading to more efficient designs. With a thorough understanding of the behavior of prestressing, one could better judge the desirability of secondary moments.[43]

Considering the prestress as a load and then the remaining capacity of the strand that may be developed as a resistance is much more straight-forward (Figure 2.6). The ultimate applied moment can be determined by doing a simple elastic analysis of a continuous beam loaded by the applied loads, "Q" and all of the effects of the prestressing force, "P". The prestressing force is considered as both an axial force and if the tendons are eccentric, draped or harped, the transverse effects can be considered as uniform or concentrated loadings for each segment of the tendon [refer to Load Balancing Method in Reference 41]. The tedious and complicated secondary moment procedures mentioned previously are no longer necessary. Secondary moments at any section can still be determined as with the previous method by subtracting the primary moment at the section (prestressing force multiplied by the eccentricity of prestress from the center of gravity of the concrete; $P \cdot e$) from the moment calculated from the elastic analysis. However this is not necessary to determine the ultimate applied moment.

The lack of need to compute the secondary moments is an important distinction between the traditional method of treating prestressing as a resistance and treating prestressing as part load and part resistance.

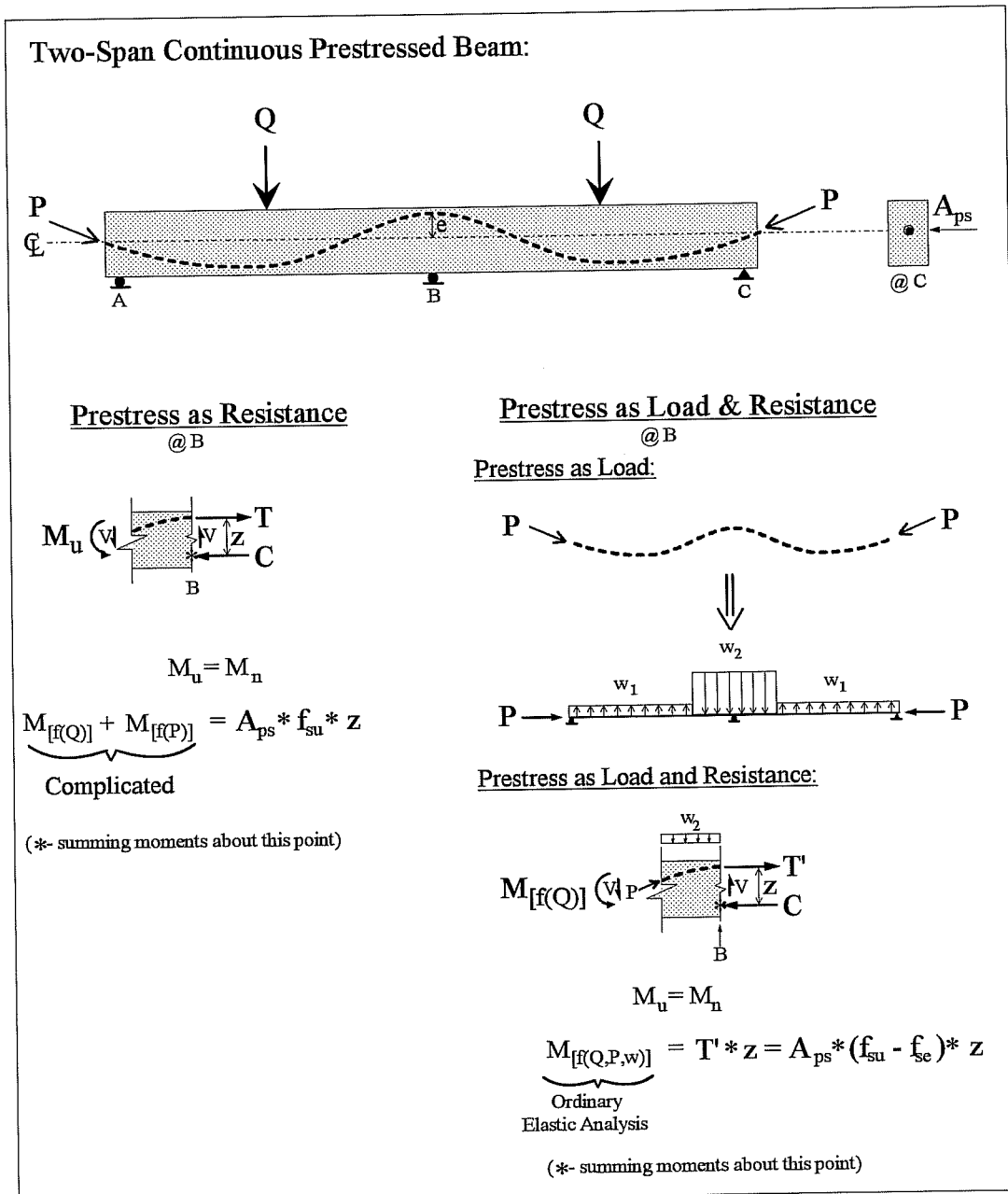


Figure 2.6 Treatment of Prestress for a Two-span Continuous Beam

In the first case, secondary moments must be determined to carry out design. In the second case, secondary moments are implicitly included in the calculations for overall prestressing effects and need not be singled out. There has been much discussion on the redistribution of these secondary moments once cracking has begun thus lessening the restraint of the indeterminate beam. With the prestress-as-load-and-resistance method, the relative stiffness of the various portions of the member or structure would need to be modified in the analysis beyond cracking to accurately determine the overall effect of the prestressing. This case can be solved if desirable by performing an ordinary elastic analysis with member stiffness modified to reflect cracking, creep, and other non-linear effects. (This is similar to stiffness modifications used in current slender column design.) The elastic method is quite simple in application due to the capabilities of current computer programs and the ease with which indeterminate systems may be analyzed elastically. With the new tools available, it is apparent that new methods of analysis and design may be employed and in this case, with more ease and clarity.

While consideration of prestressing strictly as resistance has advantages for simply-supported beams, understanding prestressing as partly an applied load and partly a form of resistance is advantageous for indeterminate members. A thorough understanding of both concepts will facilitate an engineer's ability to solve design and analysis problems.

2.3 History of Structural Concrete

2.3.1 Conventionally Reinforced Concrete

Conventionally reinforced concrete was first used in the late 19th century in many ways. A French gardener named Joseph Monier patented his idea of using wire mesh to reinforce thin concrete vessels in 1867 and continued to develop these reinforcing ideas for building and bridge design. Another frenchman, Franoise Hennebique used concrete to fireproof iron beams in 1879. From this he developed the idea of the new structural material - reinforced concrete. In Germany, the engineer G.A. Wayss developed Monier's ideas and made reinforced concrete a standard building material.[22]

As early as this time there were already different philosophies of approach to reinforced concrete design. Hennebique was an artisan by trade and this came out in his work where his designs were driven not by calculations, but by his desire for lightness and his vast field experience. This resulted in a tendency to build structures even though they could not be rationally analyzed with the theories of the day. Wayss on the other hand approached reinforced concrete much more scientifically with an emphasis on

calculations. His influence on German designers caused them to think rationally. This preoccupation with theory however, tended to inhibit them from developing designs for which they were unable to make calculations at the time. Although these early influences may not have had profound lasting effects on the designers of their respective countries, it is an example of how easy it is for the same industry (building, in this case) to be so influenced by pioneers in the field.

The United States was not immune to such influences either. By the early 20th century, reinforced concrete was being widely used in the U.S. - at first with no true standard of practice. When the first Joint Committee on Reinforced Concrete¹ was formed in 1904 to "disseminate information and experience...and to promote the best methods to be employed in the various uses of cement..."[44], their initial attempt at creating a standard (in 1908) included the use of ultimate strength design. However two years later when the next specification-type document was completed, European analytical practice seemed to be influential, and "straight-line theory" (or allowable working stress design), the common practice in Europe at the time, was adopted instead. It was not until 1956 that ultimate strength design was re-introduced into the American Concrete Institute Building Code (ACI-318) as an appendix at first and then in 1963 as part of the main body of the code. (It is believed that at this time (~1956) the U.S. was the only country using ultimate strength design except perhaps for the former U.S.S.R.)[64] European influence had apparently been quite strong, lasting almost 50 years. However, based on extensive research (particularly the introduction of Whitney's "rectangular stress block" [49]), as well as design and field experience, considerable advantages were seen in using ultimate strength design. The overseers of the codes accepted it. This is a good example of how code development is an ongoing process that requires open-minded consideration and a continual challenging of old and accepted ideas as new ideas are presented.

2.3.2 Prestressed Concrete

2.3.2.1 History

The first patented use of prestressed concrete began in the late 1800's. In San Francisco, P.H. Jackson used "tightened steel tie rods in artificial stone & concrete arches."[41] In Germany, C.E.W. Doehring used pretensioned metal in concrete for floor slabs. Both methods were unsuccessful due to the use of low strength steel. Concrete shortening due to creep and shrinkage was often comparable to the limited initial

¹ This Committee was part of the National Association of Cement Users, formed in 1904 and changed to the American Concrete Institute in 1913.

elongation of the low strength prestressed steel. With time, the concrete shortening counteracted the effect of prestressing so that beneficial effects were almost entirely lost. Other ideas included retightening or restraining the steel after creep & shrinkage occurred or using coated bars that would not bond to the concrete and tightening them after the concrete had set. Primarily for economic reasons, none of these methods caught on.

It was not until 1928 that the French engineer Eugène Freyssinet developed modern prestressing in a form that is still the basis for prestressed concrete used today. He began by using jacks to induce arch-type thrusts that would place sections under compression at service load states. He then further developed this idea by using high-strength steel wires which could be prestrained to high levels. These levels were higher than those of previous prestressing attempts so that the wires would still provide appreciable prestressing forces after creep & shrinkage losses. His idea was to create a new "wonder" material; concrete that would have no tensile stresses and therefore no cracks. This was done by calculating and controlling the longitudinal stresses in the concrete by precompressing the concrete enough so that it would stay completely in compression under working (service) loads ("full prestressing"). The method was still not economically advantageous until appropriate tensioning methods and anchorage devices were developed. Along with Freyssinet himself, E. Hoyer of Germany and G. Magnel of Belgium all developed different effective methods to accomplish this "full prestressing" [41].

Prestressing did not attract much attention in the United States until the late 1930s. As mentioned previously, Jackson had earlier experimented with prestressing as had W.S. Hewett who in 1924 used steel rods and turnbuckles to prestress water tanks.[44] In the 1930's, the Preload Company developed circular prestressing for circular concrete storage tanks.[35] However linear prestressing had yet to be introduced in the United States and in terms of being integrated into standards, it was not until 1939 that prestressing was even discussed by the ACI building code committee.

Prestressing was not initially accepted for many reasons. Practitioners were accustomed to yield stresses in conventional reinforcement of 36 ksi (248 MPa) and were very skeptical of the use of reinforcement reaching yield stresses up to 175 ksi (1207 MPa). There were also few areas where concrete manufacturers could produce concrete with a high enough strength. Concrete of 3500 psi (24.1 MPa) was considered high and prestressing typically required 5000 psi (34.5 MPa) concrete. Many were skeptical about the ability of the high-strength steel to bond well enough, both chemically and mechanically to the concrete. Another serious consideration was whether the cold-drawn steel, whose particles had been realigned in the drawing process to achieve higher tensile strength, would hold up in a fire. Some were worried that the high temperatures would ruin the advantageous particle alignment. However most of these

problems were easily addressed and the skepticism began to dissolve.[20]

With the successful construction of the Walnut Lane Bridge in Philadelphia in 1949, the first prestressed bridge built in the U.S., prestressing began to attract the attention of many bright engineers as well as entrepreneurs. The Walnut Lane Bridge was designed primarily by Magnel and had a main span of 13 post-tensioned I-girders, 160 ft. (48.8m) long and 79 in. (2m) deep.[21] Before this bridge was built, a full-scale girder was tested and loaded to failure to exhibit the capabilities of such a design. The overall success of this project led to the rapid development of the prestressed concrete industry. Over time, it was found that this pioneering bridge had limited durability. Longitudinal cracks on the two fascia girders were found as early as 1958 and were attributed primarily to freeze-thaw cycles of water that seeped into the end anchorages and the ducts. (Inadequate grouting procedures may have left voids in the ducts where water collected.) Other repairs were required over the years including removal of deck planking and repair of paving, railings, curbs and bearings. The bridge was finally replaced with pretensioned girders of similar size and shape in 1990.[31]

2.3.2.2 Formation of Committees, Organizations and Standards for Prestressed Concrete

Key events leading to a more widespread acceptance of prestressed concrete design by the American construction industry include the "First U.S. Conference on Prestressed Concrete" in 1951 at the Massachusetts Institute of Technology as well as the first "World Congress on Prestressing" held in San Francisco in 1957. As early as 1942, ACI had formed a committee on prestressed concrete, and by 1952 it had expanded and joined with ASCE to form the ACI-ASCE Joint Committee 323 on Prestressed Concrete. This Committee as well as the Bureau of Public Roads (now the Federal Highway Administration) were instrumental in developing prestressing in the United States. Leaders at the Bureau promoted the industry and set aside money each year for prestressed construction. They also developed the first guidelines for Prestressed Concrete Bridges in 1952 and 1954 with limits of allowable stresses for the full prestressing design.[35,58] They selected these limits as a result of a collaborative effort of many practitioners and researchers, each voicing their opinion on appropriate stress limits for concrete and steel based on their experiences. Fatigue was of particular concern in choosing these limits.[50,58]

While the Bureau of Public Roads wrote guidelines for bridge design, the ACI-ASCE Joint Committee first published recommendations in 1958 for both bridges and buildings. They were slower to develop their guidelines as the industry was not so open to having "rules" imposed upon it. However, the industry soon changed its mind, realizing that the acceptance of this "new" material by local building officials needed the support of nationally recognized standards.[58] Joint Committee 323 then came out with its

Recommendations for Prestressed Concrete in 1958.[16,58]

As prestressing was gaining popularity in the early 1950's, many felt the need for a new organization to meet and exchange ideas strictly related to prestressing. Initiated primarily by prestressing pioneers in Florida, the Prestressed Concrete Institute (PCI) was formed and its first convention was held in 1953. The atmosphere was vibrant. Participants were very open and excited to share their ideas and experiences. It was this general interest and excitement that has kept the industry going. [31,20]

2.3.2.3 Development of Design Philosophies and Practices of the U.S. Prestressing Industry

The prestressing industry in the U.S. has since its inception been dominated by a philosophy of "full" prestressing, stemming from Freyssinet's philosophy of "no-tension" concrete - this "no-tension" concrete being a distinct, new "wonder" material (see Figure 2.7 for a summary of design approaches taken by U.S. standards and recommendations). As well, most bridge construction has been of pretensioned structures as opposed to post-tensioned structures. There are many reasons for both of these trends.

At the time of Freyssinet's development of full prestressing, or "no tension" concrete, other notable engineers such as F. von Emperger, P. Abeles and Magnel all promoted the use of lesser amounts of prestressing, primarily for efficiency, thus allowing for some tension in concrete (discussed in Sections 2.3.3 & 2.3.4). Freyssinet's ideas however, seemed to dominate in the U.S. for many reasons. Freyssinet himself was a very innovative and powerful engineer who was highly regarded. He had many students and avid promoters of his ideas. In addition, Freyssinet had a company that developed rapidly in the U.S. and therefore also promoted his philosophy of "no-tension" prestressing. Furthermore, cracking of concrete at the time was of great concern. The idea of a "no-cracking" concrete was an excellent selling point for prestressing as a new building material.[20, 21, 58]

Although the U.S. did adopt the idea of limiting concrete tensile stresses under service load based on Freyssinet's original "no tension" philosophy, early U.S. Recommendations also acknowledged the possible presence of cracking, more along the lines of Magnel's ideas. In the original Joint Committee 323 Recommendations, the largest allowable tensile stress in the concrete under service loads was $6\sqrt{f'_c}$ ($0.5\sqrt{f'_c}$). However it is explicitly stated that "...Allowable flexural tension of $6\sqrt{f'_c}$ ($0.5\sqrt{f'_c}$)...may be exceeded provided it is shown by tests that the structure will behave properly under service conditions and meet any necessary requirement for cracking load or temporary overload." [16] This provision was included in the first draft of the ACI-318 Building Code (see Figure 2.8). The Bureau of Public Roads Design Criteria of 1954 as well added a clause essentially allowing for a certain amount of tension in the

APPROACHES TO PRESTRESSED CONCRETE DESIGN

BRIDGE DESIGN	BUILDING DESIGN
BUREAU OF PUBLIC ROADS 1954 (none stated explicitly)	
JOINT COMMITTEE 323 - 1958 The purpose of design is to define a structure that can be constructed economically, that will perform satisfactorily under service conditions, and will have an adequate ultimate load capacity.	
AASHO 1961 1.13.3 The elastic theory shall be used for the design of prestressed concrete members under design loads at working stresses. The members shall be checked by ultimate strength theory for compliance with specified load factors.	ACI 1963 2603 (a) - Stresses and ultimate strength shall be investigated at service conditions and at all load stages that may be critical during the life of the structure from the time prestress is first applied.
AASHO 1969 1.6.3 (same as AAHSO 1961)	ACI 1971 18.2.1 - Members shall meet the strength requirements specified in this Code. Design shall be based on strength and on behavior at service conditions at all load stages that may be critical during the life of the structure from the time the prestress is first applied.
AASHO 1973 1.6.3 Members shall meet the ultimate strength and allowable stress requirements as specified. Design shall be based on ultimate strength and behavior at service conditions for all load stages that may be critical during the life of the structure from the time of prestressing.	ACI 1977 18.2.1 - Prestressed members shall meet the strength requirements specified in this code. 18.2.2 - Design of prestressed members shall be based on strength and on behavior at service conditions at all load stages that may be critical during the life of the structure from the time prestress is first applied.
AASHTO 1977 1.6.3 (same as AAHSO 1973)	ACI 1983 (same as ACI 1977)
AASHTO 1983 9.13.1.1 - Members shall meet the strength requirements specified herein. 9.13.1.2 - Design shall be based on strength (Load Factor Design) and on behavior at service conditions (Allowable Stress Design) at all load stages that may be critical during the life of the structure from the time prestressing is first applied.	ACI 1989 18.2.1 - Prestressed members shall meet the strength requirements specified in this code. 18.2.2 - Design of prestressed members shall be based on strength and on behavior at service conditions at all load stages that will be critical during the life of the structure from the time prestress is first applied.
AASHTO 1992 (same as AASHTO 1983)	

Figure 2.7 Development of Design Approaches for Prestressed Concrete in the United States

concrete. This however was not included in the 1961 AASHTO Bridge Design Specifications (first edition to include prestressed concrete design). This may in part be due to the fact that the Design Criteria were essentially recommendations or, a document to impart current knowledge and understanding and to influence codes. In contrast, a standard is a legal document that must first and foremost ensure public safety. For this reason, standards tend to be more conservative than recommendations.

Provisions in the codes have slowly evolved. A series of tests, referred to as the AASHTO Road tests, were performed in the early 1960s. These tests examined full-scale pretensioned and post-tensioned girders in complete bridges under heavy traffic loads. The girders had been designed for different allowable stress levels. From these tests, came the recommendation of $3\sqrt{f'_c}$ ($0.25\sqrt{f'_c}$) as a maximum allowable concrete tensile stress limit.[5] This provision first appeared in the 1969 AASHTO Bridge Design Specifications (see Figure 2.8). It was not until 1973 that provisions implying a recognition of cracking (limit of $6\sqrt{f'_c}$ ($0.5\sqrt{f'_c}$)) were included in the AASHTO Bridge Design Specifications. While there has been a slight break from Freyssinet's "no-tension" philosophy, a related aversion to cracking has generally dominated the industry. Despite the requirement that members must also satisfy strength design criteria, most often prestressed member designs are controlled by the limits on stresses imposed under service loads. This leaves no room for the mixed reinforcement designs with cracks allowed but controlled as proposed by von Emperger, Abeles, and Magnel.

While "full" prestressing dominated in terms of design philosophies, pretensioning has historically dominated in terms of American bridge construction practice. Despite the Walnut Lane Bridge being a post-tensioned structure, pretensioning dominated the interest of early American pioneers in prestressed concrete from the start. Much of this is related to the concurrent development of the precast industry. R. Peterson and B.J. Baskin, two early precast concrete beam manufacturers of Concrete Products Company of America in Pottstown, PA, became very interested in prestressing. They saw it as a way of increasing the possible span lengths of their precast beams. At the time, spans were limited to 36 feet (11m).[31] In Florida, a consulting engineer named Harry Edwards developed the precast, pretensioned T-beam. The Florida State Bridge Engineer, Bill Dean specified precast prestressed girders for projects. Precasting pretensioned members was desirable to many at the time because of the speed with which a variety of projects could be undertaken and completed. Prestressing also eased the transport, handling, and erection of precast members. This was advantageous in the competitive building industry at the time.[20] Another promotion of pretensioning was the Interstate Highway Act of 1956 which provided federal aid for developing four-lane super highways. With its demands for longer spans for increased horizontal

LIMITING CONCRETE TENSILE STRESSES

BRIDGE DESIGN	BUILDING DESIGN
<div style="border: 1px solid black; padding: 5px; margin-bottom: 5px;"> <p style="text-align: center; margin: 0;">BUREAU OF PUBLIC ROADS 1954</p> <p>Tension in extreme fiber.....0</p> <p>Where the computations show tension in the extreme fiber, unprestressed reinforcement may be used, and designed to take the total tensile stresses, provided that the computed tension in the concrete before the unprestressed steel is added does not exceed $0.08f_c$.</p> </div>	
<div style="border: 1px solid black; padding: 5px; margin: 0 auto; width: 80%;"> <p style="text-align: center; margin: 0;">JOINT COMMITTEE 323 - 1958</p> <p>207.3.2 b. Flexural Tension in the precompressed tensile zone</p> <p>1. Single element</p> <p style="margin-left: 20px;">a. Bridge members.....0</p> <p style="margin-left: 20px;">b. Prestensioned building elements not exposed to weather or corrosive atmosphere.....$6\sqrt{f_c}$</p> <p style="margin-left: 20px;">c. Post-tensioned bonded elements not exposed to weather or corrosive atmosphere.....$3\sqrt{f_c}$</p> <p>2. Segmental elements</p> <p style="margin-left: 20px;">a. Bridge Members.....0</p> <p style="margin-left: 20px;">b. Building Members.....0</p> <p>Allowable flexural tension of $6\sqrt{f_c}$ in Section 207.3.2.b.1.b may be exceeded provided it is shown by tests that the structure will behave properly under service conditions and meet any necessary requirement for cracking load or temporary overload.</p> </div>	
<div style="border: 1px solid black; padding: 5px; margin-bottom: 5px;"> <p style="text-align: center; margin: 0;">AASHO 1961</p> <p>1.13.7 (B)</p> <p>(2) Tension (in precompressed tensile zone).....0</p> </div>	<div style="border: 1px solid black; padding: 5px; margin-bottom: 5px;"> <p style="text-align: center; margin: 0;">ACI 1963</p> <p>2605 (b)</p> <p>2. Tension stresses in the precompressed tension zone: Members, not exposed to freezing temperatures nor to a corrosive environment, which contain bonded prestressed or unprestressed reinforcement located so as to control cracking..... $6\sqrt{f_c}$</p> <p>All other members.....0</p> <p>These values may be exceeded when not detrimental to proper structural behavior as provided in Section 104</p> </div>
<div style="border: 1px solid black; padding: 5px; margin-bottom: 5px;"> <p style="text-align: center; margin: 0;">AASHO 1969</p> <p>1.6.7 (B)</p> <p>(2) Tension</p> <p>In zones initially precompressed with prestressed reinforcement or, in zones with nonprestressed reinforcement that is sufficient to resist the total tension force in the concrete computed on the assumption of an uncracked section..... $3\sqrt{f_c} < 250$ psi</p> <p>In zones without reinforcement.....0</p> </div>	
<div style="border: 1px solid black; padding: 5px; margin-bottom: 5px;"> <p style="text-align: center; margin: 0;">AASHO 1973</p> <p>1.6.6 (B)</p> <p>(2) Tension in the precompressed tensile zone</p> <p>(a) For members with bonded reinforcement..... $6\sqrt{f_c}$</p> <p style="margin-left: 20px;">For severe corrosive exposure conditions, such as coastal areas.....$3\sqrt{f_c}$</p> <p>(b) For members without bonded reinforcement.....0</p> <p>Tension in other areas is limited by the allowable temporary stresses specified in Article 1.6.6 (B) (1).</p> </div>	<div style="border: 1px solid black; padding: 5px; margin-bottom: 5px;"> <p style="text-align: center; margin: 0;">ACI 1971</p> <p>18.4.2....</p> <p>(b) Tension in precompressed tension zone..... $6\sqrt{f_c}$</p> <p>(c) Tension in precompressed tension zone in members where computations based on the transformed cracked section and on bi-linear moment-deflection relationships show that immediate and long-term deflections comply with the requirements of section 9.5..... $12\sqrt{f_c}$</p> <p>18.4.3 The permissible stresses in Sections...18.4.2 may be exceeded when it is shown experimentally or analytically that performance will not be impaired.</p> </div>
<p>(cont.)</p>	

Figure 2.8 Development of Concrete Tensile Stress Limits for Prestressed Concrete Design in the United States

AASHTO 1977 (same as AAHSO 1973)	ACI 1977 18.4.2.... (b) Extreme fiber stress in tension in pre-compressed tension zone..... $6\sqrt{f_c}$ (c) Extreme fiber stress in tension in pre-compressed tension zone of members (except two-way slab systems) where analysis based on transformed cracked sections and on bi-linear moment-deflection relationships show that immediate and long-term deflections comply with the requirements of section 9.5.4, and where cover requirements comply with Section 7.7.3.2..... $12\sqrt{f_c}$ 18.4.3 Permissible stresses in concrete of Section...18.4.2 may be exceeded if shown by test or analysis that performance will not be impaired.
AASHTO 1983 9.15.2.2 (same as AAHSO 1973 - Allowable temporary stresses in Section 9.15.2.1)	ACI 1983 (same as ACI 1977)
AASHTO 1992 (same as AASHTO 1983)	ACI 1989 (same as ACI 1977 and ACI 1983 with editorial changes in Section 18.4.3)

Figure 2.8 (cont.) Development of Concrete Tensile Stress Limits for Prestressed Concrete Design in the United States

clearances to promote safety and its implicit guarantee for large markets, this Act greatly stimulated the pretensioned girder market. The quality control and higher material strengths available in a precasting yard were desirable for pretensioned beams.[58] Prestressed concrete became the dominant bridge building material over a 40-year period, eclipsing timber, reinforced concrete and structural steel (see Figure 2.9a).[32] Although post-tensioning was employed for longer bridge spans, in general it required more sophisticated engineering. If cast-in-place construction was chosen, it required considerable shoring. For these reasons, it was often a less preferred option. Economical cast-in-place post-tensioned box girder bridges were however widely used in West Coast states.

With recent technological developments post-tensioning has gained in popularity in the U.S. for longer spans and in precast segmental span-by-span erected viaduct structures. Pretensioning however, continues to dominate the shorter span bridge industry. Other countries however, have developed post-tensioning to make it the more common and economical solution. For example in 1980, the U.S. used 0.1 lbs (0.22 kg) of post-tensioning steel per capita whereas Switzerland and the former West Germany used 0.45 lbs (1.0 kg) and 0.26 lbs (0.57 kg) per capita respectively.[63]

Prestressed concrete bridges have enjoyed an excellent service record in the United States. Initial

durability problems have been very effectively overcome and the adequacy of prestressed concrete bridges in service has been dramatically better than bridges of timber or steel and is now exceeding reinforced concrete bridges (see Fig. 2.9b).[32]

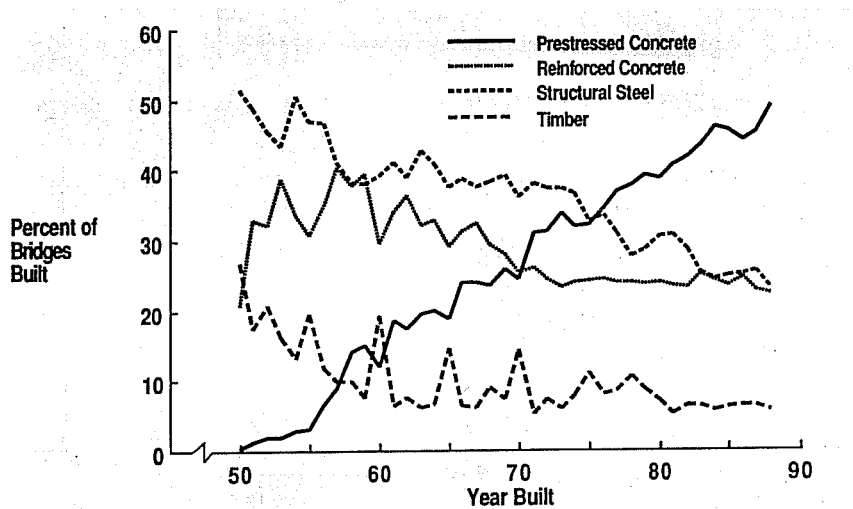


Figure 2.9a Percent of Bridge Types versus Year Built as of May 1989.[32]

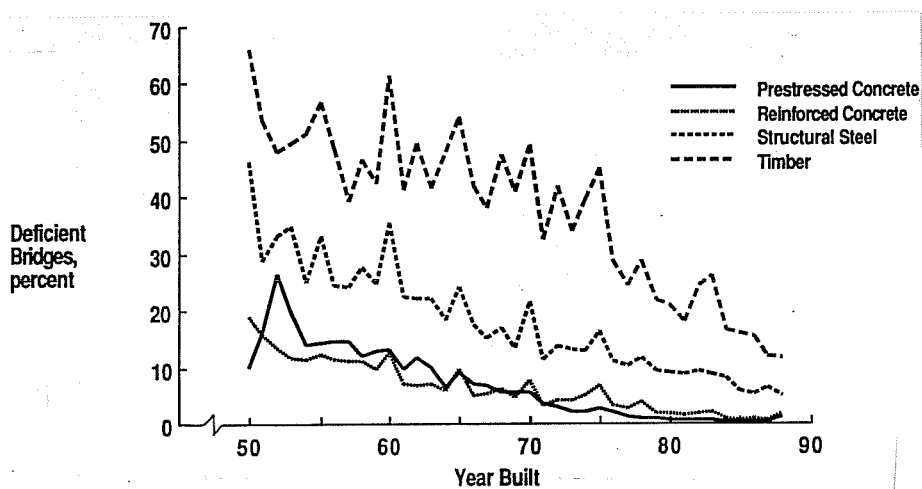


Figure 2.9b Percent of Structurally Deficient Bridge Types versus Year Built as of May 1989.[32]

2.3.2.4 Present Situation for Prestressed Concrete Design in the U.S.

The present situation of the ACI-318 Building Code and the AASHTO 1992 Bridge Specifications seem to be dominated by trends of the past. As mentioned previously, some individuals and groups saw the bright future of prestressing, yet it was at first received with much caution. Despite the numerous recommendations made by building and bridge organizations, the 1956 ACI-318 committee "explicitly excluded" prestressing from its agenda. The committee was in part wary of providing guidelines without enough research and experience to back it up. In addition, the committee did not want to stifle the industry with what it felt would have been overly conservative rules. The 1961 AASHTO Bridge Design Specifications were the first to mention prestressing in a legal standard, 12 years after it had been used by the industry. The ACI-318 Building Code followed shortly with its first chapter on prestressing appearing in the 1963 code.[64]

Even with this slow start, the ACI-318 Building Code Committee in particular made many early key decisions. It considered putting the prestressing specifications in a separate code similar to the common practice in Europe. However, many members strongly opposed this idea. They preferred to keep prestressed and reinforced concrete specifications together. This would provide more control over such things as keeping safety margins compatible between the two types of design. As well, this showed their belief that the two types of design might in fact be related, disagreeing with Freyssinet's statement that "the fields of prestressed and reinforced concrete had no common frontier." [35] (Not everyone felt that they were related however, due to the lack of research in the field of prestressed concrete.[60])

In terms of bridge design for reinforced concrete, the AASHTO Bridge Design Specifications have generally been a "follower" adopting ACI Building Code recommendations after reviewing them to suit bridge conditions. With prestressed concrete design, AASHTO has sometimes been a forerunner to ACI. AASHTO originally followed the ACI-ASCE Joint Committee 323's recommendations and as mentioned previously, it came out with a standard before ACI did (AASHTO bridge specifications, 1961). However, AASHTO has since gone on to adopt much of the ACI-318 Building Code, making revisions where necessary for applications specific to bridge design.[58] Despite the more permissive stand on cracking at service loads in AASHTO's early specifications (see Figure 2.8), it now bases the design of prestressed structures more on the "no cracking" philosophy. As will be discussed in the next section, AASHTO has recently made an effort to re-examine different philosophies, such as the use of mixed reinforcement design which would no longer be based strictly on a prescriptive set of concrete tensile stress limits.

The ACI and AASHTO prestressed concrete standards have changed very little in terms of design philosophy since the 1960s (see Figure 2.7). With the great caution exercised early came a belief that what

was eventually decided upon is forever satisfactory. The designs have proven to be conservative and therefore many see no need to change them. However, again in the words of Leonhardt, ". We have to check whether our philosophy of prestressed concrete is sound or whether it carries unwanted prejudices or ideologies." [39] This is important not only in terms of efficiency but also in terms of overall understanding of structural behavior. It is not clear to most where the limited tensile stress values came from and what exactly they represent. They are simply blindly followed as being "right", leaving little room for engineering judgement. They have taken on the character of divine rules, immutable and too sacred to be questioned. The initial conservatism was warranted due to the lack of experience in prestressed concrete design and construction. However, there has since been extensive research carried out and particularly in countries like Switzerland and Austria, substantial experience in construction of mixed reinforcement designs, not designed according to prescriptive concrete tensile stress limits. Particularly in the area of mixed reinforcement design, these ideas have often led to more efficient designs in terms of strength, economy, and constructability while still satisfying serviceability. Many feel such designs should be considered more seriously by the prestressing industry. [1,26,29,36,39,40,42,46,47,55,61,62,63]

2.3.3 Mixed Design

The use of both prestressed and non-prestressed reinforcement in design is an evolving alternative. It is an ideal way to economically satisfy both strength and serviceability requirements. It is already successfully employed by codes and standards in such countries as Switzerland, Austria and Germany. It has been researched experimentally and analytically as well as used in construction since the first widespread introduction of prestressed concrete in the late 1920s.

In the 1930s, vonEmperger of Austria was one of the first engineers to propose using a mixture of both conventional or non-prestressed reinforcement and prestressed reinforcement in the same member. His ideas were extensively developed beginning in 1933 by Paul Abeles who coined the phrase "partial prestressing". Abeles proposed a mixed reinforcement design solution in which the design is based on ultimate load² and micro or temporary cracking is permitted under working (service) loads. He used this

²Abeles noted that full compression in the elastic state under working loads used by Freyssinet does not necessarily ensure adequate safety at ultimate loads [1].

type of design successfully in 1945 when designing concrete railway ties for British Railways. Many other design philosophies have since been proposed by prominent engineers and are discussed in Sections 2.3.3.1 and 2.3.4. There has also been extensive research as well as conferences devoted entirely to mixed design. Two significant conferences were the International Symposium on "Nonlinearity and Continuity in Prestressed Concrete" in Waterloo, Ontario, Canada in July of 1983 and the NATO Advanced Research Workshop on "Partial Prestressing , From Theory to Practice", in Paris, France in June of 1984. [29,47]

Despite the successful uses of mixed reinforcement design in the past there is usually little emphasis on mixed reinforcement design in text books and in classrooms. As well, many American code-writing organizations, ACI and AASHTO in particular, are reluctant to abandon the Freyssinet school of thought on "full prestressing" (see Section 2.3.2). Both the 1992 AASHTO Bridge Specifications and ACI-318-89 briefly mention the use of non-prestressed reinforcement with prestressed reinforcement. However, they offer little guidance or coherent design models for designers to follow. More recently however, AASHTO has funded a large project (NCHRP Project 12-33) to develop an LRFD (Load and Resistance Factor Design) Standard to facilitate the use of composite construction. In this proposed standard they have introduced the idea of mixed reinforcement design (under the title of "partial prestressing") and explicitly state that "...complete freedom from cracking may or may not be necessary at any particular loading stage." [48] - counter to Freyssinet's philosophy and recalling the ACI-ASCE Joint Committee 323's first Recommendations for Prestressed Concrete Design. This project is a positive step towards a more unified approach to design. AASHTO also has an improved specification for segmental bridge design. [6] This standard includes clearer behavioral models, following Strut & Tie methods. Although an improvement, there remains a concern for dry and epoxy joints which is resolved by requiring "full prestressing". As well, mixed reinforcement is more difficult to provide across the joints.

The acceptance of mixed reinforcement design in general has been difficult in the U.S.. This may in part be due to Freyssinet's strong influence on early American design standards and his adamant belief that anything that "was not fully prestressed was worse than both reinforced concrete or prestressed concrete." [1] There has since been an ongoing debate as to which philosophy is "better".

2.3.3.1 The Debate between Full Prestressing and Mixed Reinforcement Design

There is no doubt that Freyssinet's idea of prestressing was revolutionary. He in fact titled his first paper on the subject "Une révolution dans l'art de bâtir" (A revolution in the art of building). [39] However there are many flaws and disadvantages to his "no tension" philosophy and also numerous strong arguments for the use of degrees of prestressing less than "full" prestressing. To look fairly at both design

strategies one must first consider what the purpose is for using any prestressing.

A primary goal of prestressing is to improve structural or member behavior so as to economically fulfill serviceability requirements. In terms of serviceability, this includes decreasing both instantaneous and time-dependent deformations, avoiding cracks or limiting crack widths for corrosion protection and improved visual appearance, and decreasing steel tensile stress variations to keep them within allowable ranges for the fatigue strength of both the concrete and the steel. These serviceability requirements are judged on performance and it therefore seems logical that they should be regulated or enforced by performance standards. This points to one of the first problems of full prestressing in that it is primarily governed in U.S. codes by the "prescriptive" standard of limiting concrete tensile stresses in the direction of the prestressed steel.

A second goal of prestressing is to allow for the safe and serviceable use of very high strength steels. Modern steel technology has developed economic strands with ultimate tensile capacities of 270-300 ksi (1860-2070 MPa). The use of such steels without prestressing would result in huge crack widths and deflections at service load levels. Prestressing may be seen as a clever sales technique for very high strength reinforcement. High initial strains are needed to effectively develop the required steel stresses. This high amount of initial strain, or elongation, is thus essentially removed during prestressing before major loads are applied. This allows for efficient use of these high strength steels to satisfy strength and serviceability limit state conditions.

Along with the prescriptive rule of limiting concrete tensile stresses come many other disadvantages and misconceptions about fully prestressed concrete:

1. With full prestressing, new factors of safety are implicitly established by fixing values of allowable concrete tensile stress at service loads. In the absence of ultimate strength criteria, this could lead to unsafe designs, as noted by Abeles [1], as well as extremely conservative and therefore inefficient designs.[42]
2. Practical experience has shown that service limit state allowable stresses dominate the determination of the required prestressing force. This often results in substantially more of the higher priced prestressing steel than would be required were the strength limit state to dominate as it does for non-prestressed members.
3. The "no tension" philosophy is deceptive in that it only applies to longitudinal stresses. There are numerous other tensile stresses present such as bond stresses, stresses in anchor zones and stresses due to restraint from shrinkage, creep and temperature differentials [40].

4. It is a common misconception that there are no cracks in fully prestressed beams. Not only might they occur as a result of the stresses listed in 3, but they may also appear from repeated loadings and relatively slight overloads above the design service loads.
5. Full prestressing can be harmful in that it often creates such large compressive stresses in the most highly compressed fibers that excessive creep deflections ("hogging") can occur.
6. In the case of post-tensioning, large compressive stresses often require the need for staged loading during construction (for example to prevent too much uplift before superimposed dead load is applied). This can be both expensive and inconvenient.
7. Large compressive stresses may require larger concrete sections than originally desired.
8. Control of tensile stresses may require large amounts of prestressing steel which can be expensive in both material cost as well as construction cost.

In light of these problems, the use of varying amounts of prestressing can be immediately recognized as having certain advantages:

1. Mixed reinforcement design can be primarily based on the ultimate limit state leading to more efficient designs. The amount of prestressing can vary and is therefore problem dependent (no one stress limitation for all types).
2. Mixed reinforcement design, when properly employed, directly considers the limitation of crack widths.
3. The generally lesser amount of prestressing tendons implies less prestressing force and induced stress. This leads to fewer creep & shrinkage problems, less elastic shortening, less camber and often lower material and construction costs. The fewer tendons also mean that sections will less likely need to be increased to handle large compressive forces.
4. The increased ductility of less than "fully" prestressed beams implies higher energy absorption (this is particularly advantageous in seismic regions).

The major arguments against mixed reinforcement design include the increased susceptibility to cracking, corrosion and fatigue failure.

In terms of cracking, using varying amounts of prestressed reinforcement has possible visual disadvantages in that there will likely be more cracks in a mixed reinforcement element than in a similar fully prestressed element. The visibility of such cracks will depend on the effectiveness of the non-

prestressed reinforcement in controlling crack widths.

There are many methods for predicting crack widths with mixed reinforcement. Most are based on simple principles as well as on ".highly empirical data such as creep factor, free-shrinkage strains, degree of cracking within a member and bond characteristics." [56] There are two major categories of formulas used to predict crack widths. The first involves relating the crack width to the fictitious stress which would exist in the concrete were it not to crack under service loads (advocated by Abeles). The second type involves relating the crack width to the tensile stress in the reinforcement. [46] An example of the first approach is the "hypothetical tension stress method" used in the British Code (BS8110). Here it is assumed that the tension force in the uncracked, unreinforced section must be carried by the bonded prestressed and non-prestressed reinforcement after cracking. An example of the second approach is in the Gergely-Lutz equation employed by ACI and AASHTO. Although the Gergely-Lutz equation is based on research with reinforced concrete, it has been adequate for predicting crack widths of members with mixed reinforcement as well. [56]

The concern for corrosion of prestressing is due to the stress in a prestressed strand being much greater than that in a non-prestressed bar, yet the area of the strand is typically less than that of a bar. A similar amount or depth of corrosion on a prestressed strand as on a non-prestressed bar would therefore have a more damaging effect on overall capacity. In addition, the higher strength prestressing steel seems to have higher susceptibility to corrosion. Even in "full prestressing" the strand must have special corrosion protection during storage and handling.

The idea of cracking leading to increased corrosion activity is however a more controversial subject. There has been much research in the past focused on trying to determine maximum crack widths as a function of corrosion protection. Yet there has been very little consensus on what these limits should be. A study of the durability of bridge decks using transverse prestressing in the early 1980's by R. Poston at the University of Texas at Austin supported the theory of cracking leading to corrosion. In this study, Poston concluded that corrosion of non-prestressed steel in transversely post-tensioned bridge decks is initiated where flexural cracks occur. He found that virtually no corrosion occurred in the non-prestressed steel where crack widths were limited to 0.002 in. (0.051 mm). This limit also greatly reduced the penetration of chloride ions. Corrosion was also found to be independent of concrete cover between 2 and 3 in. (50.8 and 76.2 mm). Finally, Poston concluded that for increased durability, ".the main benefit of prestressing is to eliminate and to greatly control cracking." [51]

Other recent studies involving exposure tests have shown little correlation between crack widths and increased rates of corrosion (perhaps corrosion will begin sooner with the larger crack width but the rate

of corrosion will not necessarily be greater).[18] There are also numerous other more likely ways for corrosion to begin such as poor materials or sloppy construction practices. In any case, researchers are now tending more towards the idea of providing adequate concrete cover and the use of low-permeability concrete to result in better corrosion protection.[18]

Further research is certainly needed in this area. However, in light of past research on mixed reinforcement design as well as state-of-the-art theories on corrosion and serviceability, the use of mixed reinforcement design allowing for cracks should not be dismissed strictly because of potential corrosive activity. Rather, current thought on the subject tends to suggest that proper mixed reinforcement design may easily provide adequate corrosion protection.

Fatigue strength is another concern. Fatigue strength is a function of such things as stress range, penetration and width of cracks, cyclic load repetitions, bonded or unbonded tendons, and contact with deviators or ducts. It is well understood that cracks in bonded prestressed members cause sharply increased stress ranges at the location of the cracks.[65] "Full prestressing" is not necessarily advantageous over mixed reinforcement design in that fully prestressed elements may also experience cracking with repeated loadings or overloads.[50] The resultant stress increase in the tendons would occur despite the closing of the crack at service loads thus making the element still susceptible to fatigue failure (closing is primarily advantageous for corrosion protection and appearance). It has also been studied and determined that the presence of bonded non-prestressed reinforcement reduces stress ranges in the prestressed reinforcement and is therefore advantageous.[50]

There are many cases where using various amounts of prestressed and non-prestressed reinforcement is a logical solution to a design difficulty with reinforced or "fully prestressed" concrete. With conventionally reinforced concrete, deflections under sustained loadings can be a problem. This could easily be controlled by adding a limited amount of prestressed tendons. In the case of fully prestressed tendons experiencing cyclic loading, fatigue resistance can be reduced significantly if crack widths are limited through the addition of non-prestressed reinforcement (This is of course admitting that preventing cracks in fully prestressed beams is unrealistic). In both cases, all of the steel should be included in determining ultimate resistance.

As seen from these examples alone, there should clearly be a smooth transition between these different types of designs. A unified design method covering all degrees of prestressing would do this. It would greatly simplify structural design and clear up misconceptions that now arise due to the current separation of reinforced concrete and fully prestressed concrete as well as the general lack of acceptance of mixed

reinforcement design. There has already been much discussion regarding removal of artificial barriers which has led to the call for unifying all types of concrete design under the title Structural Concrete.

2.3.4 Unified Design for Structural Concrete

Many prominent engineers have proposed the idea of a unified design method. One of the first was A.S.G. Bruggeling of the Netherlands. He understood that partial prestressing was not widely accepted for many reasons. These include:

- 1) The existing methods for analyzing cracked sections were long and complicated.
- 2) Partial prestressing was not encouraged by most country's codes and standards of practice.
- 3) There was little experience with the construction of such structures.

In his unified design proposal he emphasizes the fact that the amount or degree of prestressing to be used is problem dependent and can be determined after the section is initially designed. This allows for simplification in the design of the reinforcement and the shapes of members. It also allows for better control of deflections and crack widths.[26]

F. Leonhardt of Germany firmly believes in the advantages of allowing for different amounts or degrees of prestressed steel. He emphasizes that many negative effects of full prestressing such as excessive creep and camber are overcome by using less prestressed steel but in combination with non-prestressed steel. He advocates performance requirements for codes which would permit use of any percentage of prestressing reinforcement, from 0% to 100% of the main longitudinal reinforcement [see Reference 40 for possible definitions of percentages of prestressing reinforcement]. He also believes that full service load may not always be appropriate for design and suggests ranges of "frequent" live load.[40]

T.Y. Lin points out that most prestressed concrete in fact has non-prestressed reinforcement so that it is in fact already a mixed reinforcement design. Non-prestressed reinforcement is often required as "cage" steel to hold up stirrups. Non-prestressed reinforcement may also be needed in areas of high stress concentrations. He sees a natural progression occurring within structural concrete design in that reinforced concrete design standards went from initially following Allowable Stress Design to Ultimate Strength Design and so too should prestressed concrete design. With all types of concrete designed similarly the combination of prestressed steel with non-prestressed steel and thus a unified design method should be easier. Lin feels as does Leonhardt, that performance should control design, not an arbitrary set of limiting concrete tensile stresses.

Thürlimann reinforces the appropriateness of a unified design approach for the simple reason that "...At

ultimate load reinforced concrete, prestressed concrete and partially prestressed concrete reach their limit at strains in the concrete and the ordinary steel which are equal for all cases." [63] In Reference 63, he presents a very clear picture of this in a comparison of behavior of a series of beams that range from 0% to 100% prestressing reinforcement (Equation 2-2 in Section 2.2.1 gives Thürlimann's definition of percentage of prestressing reinforcement).

J. Schlaich of Germany as well believes in the need for and value of a unified design method. He emphasizes the importance of all parts of a structure noting how current codes and standards often require highly accurate and in-depth calculations for some parts while other parts are designed based on judgement and past experience. He presents a very convincing argument and one possible solution to this problem in the paper "Towards a Consistent Design of Structural Concrete" written in conjunction with K. Schäfer and M. Jennewein. The authors reintroduce the Strut & Tie Modelling Method (developed as the "Truss Analogy" at the turn of the century) with clear, realistic examples of modelling. [55]

Drawing upon these ideas as well as others, the single most important push for a unified design method for structural concrete came in 1991. At this time IABSE and ACI co-sponsored a Colloquium on Structural Concrete in Stuttgart, Germany. [61] One of the major concerns of the IABSE Working Commission III was that:

...the overall goal of designing and constructing high quality concrete structures [is] being impeded by increasingly fragmented, inconsistent, and complex structural codes and standards... Innovation and skillful conceptual design, which are such important contributions of the structural designer, have been deemphasized. [61]

Some of the major conclusions drawn at the Colloquium were:

1. Performance requirements should be emphasized in codes and standards. Clear statements and behavior models should be presented for designers to follow.
2. Both the Ultimate Limit State and Service Limit State should be considered for design. The design approach should be consistent and unified for all types of structural concrete.
3. The focus for designers should be oriented towards understanding global structural behavior. This includes attention to overall conceptual design, economics, aesthetics and structural integrity.

Unfortunately, the current American codes such as ACI-318 and the AASHTO Bridge Design Specifications remain compartmentalized. As they stand now, reinforced and prestressed concrete design follow very different guidelines. This prevents an easy transition to a more desirable unified design method. It also creates confusion for designers when faced with unusual designs such as for large-scale stocky beams (discussed in Section 2.4). To overcome these problems, the use of various combinations of active and passive reinforcement must be accepted before a unified design method will be possible. Only then will clearer design models be available for engineers to follow. At the Stuttgart Colloquium, Swiss engineer René Walther supported the call for a unified code eloquently:

If we wish to improve the reputation of our profession again, then we must have the courage to pursue it in a more progressive way and to place more emphasis on innovative conceptual design rather than on mere dimensioning of structures according to codes. One little step in the right direction would certainly be to raise the scientific standard of our codes, specifying essentially only basic principles and goals while leaving it to the creativity and experience of the engineers to translate this into innovative conceptual design. A concise unified code for structural concrete could undoubtedly be helpful in this respect.[61]

2.3.5 Comparison with European Codes

The idea of a unified code for structural concrete is not new. The British code CP110 has been unified since 1972. Text books covering unified design of structural concrete have been written in Great Britain as well.[52]

More specifically, the CEB-FIP Model Code 90 (MC 90) is an excellent example of a clear unified code. One of the major goals of the Code Committee was to emphasize the understanding of structural behavior through models rather than "arbitrary equations". [52] MC 90 recognizes that prestressed concrete design can follow the two methods described earlier in Section 2.2.2; one in which prestressing is strictly a form of resistance, and one in which the prestressing force is considered an external load along with a resistance equal to the capacity of the tendon above the effective prestressing force. Although MC 90 recommends the "prestressing as a loading" method in almost all cases, the designer is free to choose which method to use. As discussed in Section 2.2.2, the first method may be easier for simply supported beams. The loading method is recommended by CEB however, simply because most engineers are accustomed to designing for loads. This loading method is reminiscent of T. Y. Lin's load-balancing method. Lin however, only uses his

method to apply to the service limit state (with a follow-up check of the ultimate limit state) while MC 90 applies it to both the service and ultimate limit states in design.

The Swiss code for concrete structures (SIA 162) is another example of a clear unified code.[57] Analysis is based on structural models. Prestressing may be considered as a resistance or as a load with the remaining capacity able to be developed as a resistance. Many different methods are permitted for checking safety of different types of structural elements. The use of mixed reinforcement design is not singled out. Rather, it is accepted as a normal form of design. The provisions cover combinations of non-prestressed and prestressed reinforcement. For instance, in controlling crack widths, it is stated that "Cracking behaviour can be favourably influenced by prestressing. In special cases, full prestressing can be used to achieve desired cracking behaviour." [Section 3 33 33, Reference 57] Full prestressing is one of many ways to use prestressing. As well, it is stated that water-tightness can be "improved by.. limiting crack width, e.g. by prestressing, sufficient mild reinforcement, or an appropriate choice of construction operations." [Section 3 36 1, Reference 57] Unlike many American standards, SIA 162 makes no distinction between design methods for different types of reinforcement nor does it emphasize prescriptive rules for design. Rather, it proposes the applicability of both non-prestressed and prestressed reinforcement in different areas of design to satisfy performance standards.

The open approach that MC 90 and SIA 162 present is an excellent spur for innovative design. These codes emphasize behavioral models and performance standards rather than prescriptive guidelines. The type of design whether reinforced, prestressed or with mixed reinforcement is left up to the discretion and ingenuity of the engineer. This freedom leaves room for more truly creative and potentially artistic designs.

2.4 Structural Concrete in the 1992 AASHTO Bridge Design Specifications

2.4.1 Reinforced Concrete Design

The design of reinforced concrete members is covered in Chapter 8 of the 1992 AASHTO Bridge Design Specifications. This standard allows for both Service Load Design (Allowable Stress Design) and Ultimate Strength Design. The reinforced concrete continuous beam design modelled in an experiment of this thesis was designed primarily using Ultimate Strength Design. Therefore this method will be described further. Section references all refer to section numberings in Reference 9.

The design assumptions for using this method include an assumed elastic-perfectly-plastic stress-strain

curve for the mild reinforcement and the tensile strength of the concrete is neglected. As well, the maximum useable concrete compressive strain is taken as 0.003 and a rectangular compressive stress distribution (Whitney stress block) is assumed (Section 8.16.2). Load factors are outlined in Chapter 3 of the AASHTO Bridge Design Specification and the applicable reduction factors for this method are 0.9 for flexure and 0.85 for shear.

The amount of flexural steel is that which will provide sufficient resistance to the applied factored loads. Sectional analysis is performed wherein it is assumed that the applied, factored moment must be balanced by an internal resisting moment. This resisting moment at ultimate is the result of the steel being fully yielded and balanced by the rectangular compressive stress block. Moment redistribution for continuous members is not permitted. There are limits for maximum percentages of steel to ensure ductility as well as minimum amounts of steel based on the predicted cracking load (Sections 8.16.3 and 8.17.1 respectively).

Shear strength contribution of the concrete is assumed to be equal to the amount of shear required to cause significant inclined cracking. If this amount is enough to carry the maximum factored applied shear, only minimum shear reinforcement is required as per Section 8.19. If the concrete shear strength is not enough, shear reinforcement in the form of stirrups is required. Limits are given for the amount of shear that can be carried by this reinforcement as well as spacing requirements for the stirrups. When it is necessary to consider shear transfer across a certain plane, shear friction theory may be applied to determine the additional amount of shear steel needed to develop the clamping force required to properly transfer the shear force.

In terms of serviceability, appropriate checks must be made of the distribution of the flexural reinforcement to satisfy equations that are based on the Gergely-Lutz crack width control equations. Deflections must be checked as well as reinforcement fatigue stress range limits (Sections 8.9 and 8.16.8.3). For members with a depth greater than 3-ft. (914mm), additional side face crack control steel must be provided (Section 8.17.2.1.3). Shrinkage and temperature steel is required and adequate concrete cover must be provided for corrosion protection (Sections 8.20 and 8.22).

For detailing, spacing limitations for reinforcement are given primarily to ensure enough room for aggregate to fit between the reinforcing bars (Section 8.21). Guidelines for development for all types of reinforcement are outlined in Sections 8.24 to 8.30. (This is the only place mentioning deep flexural members in terms of requiring adequate anchorage, but deep has not been defined under the strength design method.) These guidelines are based primarily on empirical evidence and practical experience.

2.4.2 Prestressed Concrete Design

Prestressed concrete design is covered in Chapter 9 of the 1992 AASHTO Bridge Design Specifications. Section references refer to the section numberings of Reference 9.

The beginning of the specifications for prestressed design state that "...prestressed members shall be proportioned for adequate strength using (the) specifications as minimum guidelines." (Section 9.4). For continuous members, appropriate strength must be accompanied by adequate behavior accounting for any moment, shear or axial forces due to prestressing, effects of creep, shrinkage, temperature, axial deformation, restraint of attachments, or foundation settlement (Section 9.4). In particular, for post-tensioned cast-in-place construction, secondary moments must be included in both service load calculations and ultimate load calculations with a load factor of 1.0 (Section 9.7.1).

All designs are based on Load Factor (strength) Design as well as behavior at service loads. The load factors must be in compliance with Chapter 3 of the Specifications and the resistance factors are 0.95 for post-tensioned members and 0.9 for shear.

There are numerous stress limitation checks that must be made at various load stages. For post-tensioned members they include maximum allowable temporary steel stresses before losses due to creep and shrinkage as well as maximum allowable steel stresses at service loads after losses. There are also concrete compressive stress limits before losses as well as both concrete tensile and compressive stress limits at service loads after losses. The tensile stress limits at service loads lie below the code assumed cracking stress of $7.5\sqrt{f'_c}$ ($0.62\sqrt{f'_c}$), the largest allowable concrete tensile stress being $6\sqrt{f'_c}$ ($0.5\sqrt{f'_c}$). A maximum bearing stress for anchorages is also specified (Section 9.15).

Provisions are given in Section 9.16 for calculating prestress losses including friction losses, shrinkage, elastic shortening, creep and relaxation of steel.

Although the allowable stress limits often control design, a check for adequate flexural strength must also be made. Strength is calculated assuming a rectangular compressive stress block as with reinforced concrete design (Section 9.17). As mentioned previously, a factor of 1.0 on the secondary moments due to prestressing is added to the actions of the applied factored loads (Section 9.7.1). Maximum prestressing steel ratios are given to ensure ductility and minimum ratios are given as a function of the cracking moment to ensure sufficient resistance so that the structure will not collapse immediately upon cracking. Non-prestressed reinforcement may be included for ultimate strength calculations provided that the overall reinforcement ratio is below a prescribed limit (Section 9.17.2, 9.19).

Shear strength is calculated including the effects of prestressing and taking into account concrete strength (Section 9.20). Two types of concrete contributions must be checked, V_c and V_{cw} . V_c represents the strength based on flexure-shear crack failure and V_{cw} represents the strength based on web-shear crack failure. The lesser of the two is taken as the concrete shear contribution. The effective depth may be taken as 0.8 times the height of the section. Determining the shear strength contribution of the web reinforcement is similar to the methods for reinforced concrete design and is outlined in Section 9.20.3.

Anchor zone details include requiring end blocks for post-tensioned construction. Details may be left to the supplier of the post-tensioning hardware, or must follow the prescriptive guidelines outlined in Section 9.21. Revisions to these provisions have recently been approved for the 1994 edition of the AASHTO Bridge Design Specifications based on the results of a recent NCHRP sponsored research project wherein clear models of anchor zone behavior are outlined to aid the engineer in efficient anchor zone design.[24]

Required cover for adequate corrosion protection is given in Section 9.25.11 along with spacing requirements of ducts for construction ease and adequate concrete distribution around the ducts. Crack control and fatigue resistance are assumed to be inherently taken care of with the allowable stress limits at service loads.

2.4.3 Problems with Current ACI and AASHTO Specifications

The separation of reinforced and prestressed concrete design is perhaps the worst problem now facing designers in terms of designing two-span continuous large-scale stocky substructures. According to the 1992 AASHTO Bridge Design Specifications (as well as the ACI-318 Building Code), if any prestressing is used, enough must be provided to limit the concrete compressive and tensile stresses at service loads. Limiting the concrete tensile stress typically governs design. With such large members, this amount of prestressing is high and problems with congestion and placing of concrete are common. This occurs as there are no specific provisions for skin reinforcement with mixed reinforcement construction. As a result, contributions of the prestressing force to control cracking are neglected and the large amount of skin reinforcement required is based on needs for reinforced concrete design alone. This can substantially add to the congestion of the reinforcing "cage". This also results in an excessive "over"-strength of the member, which is inefficient and often uneconomical.

In addition, the inclusion of a load factor of 1.0 on the secondary moments due to prestressing in calculating ultimate strength can lead to either conservative or unconservative design. In a two-span continuous beam for instance, secondary moments are present due to the inability of the member to rotate

at the center support. However, once the beam is cracked at this location and begins to rotate, this restraint is "weakened" and the secondary moments begin to decrease. The amount by which they decrease is related to how much the member may rotate at the "restrained" support before failure. Because secondary moments could either increase or decrease the primary moment due to prestressing (or the resistance provided by the prestress reinforcement) depending on the design, the ultimate strength calculations may be conservative or unconservative by not recognizing that the secondary moments will have begun to redistribute when the ultimate state is reached.[43]

2.5 Proposed Integrated Design Methodology

In light of the problems of compartmentalized standards and the potential for having a unified design code, the following integrated design method was developed and investigated in this study. The particular method presented is geared towards the design of large-scale stocky members although the principles can be applied to other types of design. (An experimental investigation using this method is presented in Chapters 3 through 6.)

Flexure Design - Flexure design will be based on providing combinations of prestressed and non-prestressed reinforcement proportioned on a strength basis with a total nominal strength capable of resisting factored loads.

Shear Design - Shear design will be based on Strut & Tie modelling. Minimum shear steel provisions in AASHTO may still apply (where it is determined by modelling that concrete contribution to shear strength alone is adequate).

Tensile Chord Crack Control - Two methods of crack control are suggested as possibilities:

- 1) Perform an elastic finite element analysis at service loads including the prestressing force as a load. Provide "crack control" steel to carry amount of tensile stress in excess of $2\sqrt{f'_c}$ psi ($0.17\sqrt{f'_c}$ MPa), assuming service load stress in the steel ($f_s = 0.6*f_y$).

$$A_c * f_c = A_s * f_s = A_s * (0.6 * f_y) \quad (2-3)$$

Where A_c : tensile concrete area
 f_c : tensile stress in the concrete
 A_s : area of crack control steel (to be determined)
 f_s : the stress in the steel at service loads.
 f_y : the yield stress for the steel

- 2) Use conventional reinforcement distribution methods as described in AASHTO 8.16.8.4 which are derived from the Gergely-Lutz crack equation with possible modifications to include prestressed reinforcement effects.[54]

Side Face Crack Control - Side face cracking steel should be provided in accordance with AASHTO provision 8.17.2.1.3. This is the result of a research project studying crack control of non-prestressed deep members carried out at the University of Texas at Austin. [25] Again these provisions should be restudied for possible modifications to include prestressed reinforcement effects.

Anchor Zone Design - Anchor zone design will be in accordance to proposed revisions to AASHTO as reported in NCHRP Report No. 356.[48]

Stress Range Check for Fatigue

Stress ranges in both the prestressed and non-prestressed steel must be checked between dead load (plus superimposed dead load where applicable) and full live load plus impact. The range must be kept below 14.5 ksi (124 MPa) for prestressed steel³ and the following equation from AASHTO provision 8.16.8.3 for non-prestressed steel:

$$f_f = 21 - 0.33f_{min} + 8 \left(\frac{r}{h} \right) \quad (2-4)$$

³This value is taken from recommendations from Wollmann [65]. This also corresponds with the limit used by the Swiss code, SIA 162, for bonded tendons in corrugated steel duct.

Where: f_r : stress range in k/in^2
 f_{\min} : algebraic minimum stress level in k/in^2
 r/h : ratio of base radius to height of rolled-on transverse deformations
 (0.3 if unknown)

Each critical section must be checked in terms of both prestressed and non-prestressed steel. Where the stress range for the prestressed steel is excessively conservative, the non-prestressed steel need not be checked. An example of a stress range check involving cracked section analysis is given in Appendix A.

2.6 Related Research - Literature Review

There is an extensive amount of literature related to the ideas presented thus far and the experiments to be presented.

Mixed Reinforcement Design - general

As previously discussed, Abeles, Bruggeling, Leonhardt and Lin have researched and written extensively on this type of design. [1,26,39,40,42] As well, the proceedings from the International Symposium on "Nonlinearity and Continuity in Prestressed Concrete" in Waterloo, Canada in 1983 and the NATO Advanced Workshop on "Partial Prestressing, From Theory to Practice" provide extensive information on more recent developments and understanding. [29,47]

Other Integrated Design Methods

Perhaps most importantly, R Mast presents his ideas for unified design provisions that have been adopted for the 1995 ACI-318 Building Code. Mast points to the numerous inconsistencies and unnecessary complications in current code guidelines. He proposes new concepts for design that unify the current code by giving provisions that apply to flexural and compressive members, all types of structural concrete with any mix of prestressed and non-prestressed reinforcement, sections of any shape or with any location of steel, and composite sections made up of more than one type of concrete. [45]

Bruggeling discusses an integrated design method at length in Reference 26. A brief summary of this method is given in Section 2.2.4.

Thürlimann gives guidelines for a unified design method in his paper "Considerations to the Design of Prestressed Concrete Bridges" mentioned also in Section 2.2.4. [63] In general he emphasizes that the use and amount of prestress for a design should not be chosen at first. Rather, the necessary yield forces for tension, shear, torsion etc. at the ultimate limit state should be determined first. Then, to determine how to proportion the reinforcement between prestressed and nonprestressed, such things should be considered as deflection control, amount of space available for reinforcement, the need to improve certain local stress concentrations, amount of desired corrosion protection and fatigue life considerations.

In Reference 36, Inomata proposes designing for ultimate and for certain allowable stress ranges with two simultaneous equations to get an optimum design. The stress range equation would be based on a given stress range or crack width. If an optimum solution is not possible, one equation should be solved and the potential cost of the second be minimized. Steel stress limits and allowable crack widths are suggested. However, Inomata emphasizes using ACI reinforcing detailing rather than crack width computation.

Naaman proposes an integrated design method that he feels can be easily accommodated to the ACI Building Code. In Reference 46 he gives the background of his procedure and discusses various ways to define different levels or amounts of prestressing in an element. In his design method, flexure is based on ultimate loads and guidance is given on the calculation of camber. Naaman does not believe that the ACI-318 Gergely-Lutz crack equation can be applied to partially prestressed beams and therefore proposes his own crack width estimation equation.

Crack control / Corrosion protection investigations

Scholz presents simple rules for determining the deflection and crack widths of partially prestressed beams. He advocates using simplified methods due to the variability in properties of both concrete and steel. Most importantly, Scholz presents a comparison of various crack-width prediction equations such as the ACI Gergely-Lutz equation, and the CEB/FIP 1978 Calculated Crack Spacing Method. [56]

Naaman as well presents crack control investigations in Reference 46, summarized under *Other Integrated Design Methods* above.

The write-up of a 1984 ACI Debate between Darwin, Manning, Hogenstad, Beeby, Rice, and Ghowrwal is found in Reference 19. The debate covered current standards regarding crack control. In particular, such ideas were discussed as the limiting of crack widths by reducing the amount of concrete cover which may lead to an undesirable increase in corrosion. The debate covers many sides of such issues from the perspectives of these six experienced engineers. The write-up includes a lively discussion following a

background to the problems of crack widths, cover and corrosion, a background of current provisions, and design considerations and crack control of sanitary engineering structures.

Fatigue life investigations

Many studies have been carried out on the subject of fatigue. T. Overman's Thesis work presents an extensive literature review discussing investigations and concerns about fatigue since the introduction of prestressing to the construction industry. This includes pioneering work by Abeles, Naaman, Thürlimann and J. Hanson.[50]

A report on fretting fatigue in post-tensioned concrete by G. Wollmann, D. Yates, J. Breen, and M. Kreger also presents a comprehensive overview of past research and thought on fatigue in general. The report contains an excellent source of references covering fatigue problems for many types of structural concrete design.[65]

Strut & Tie Modelling

In Reference 55, the authors present a very comprehensive explanation of strut & tie modelling and its applications to a unified design method. They point out the present situation in design where certain parts of a structure are designed to much more accuracy and precision than others. The applicability of strut & tie modelling to all parts of structures with both prestressed and non-prestressed reinforcement is given through numerous design examples and explanations.

Deep beams

Along with the text of Reference 38, a report by D. Ricketts and J. MacGregor on continuous deep reinforced concrete beams explores their behavior using "plastic truss models". In particular they investigate the effects of changes in shear strength due to changes in shear span-to-depth ratios, the ability of members to fully develop the stress fields assumed in modelling, and the flexibility of truss models by varying distributions of steel.[53]

Tan & Mansur investigated the accuracy of shear friction theory as well as cracking moment equations and strut & tie analysis for a series of corbels and deep beams using various amounts of prestressing. They determined that the ACI-318 shear strength assumption as per shear friction theory greatly underestimates the shear capacity of partially prestressed members. Truss or strut & tie methods however estimated ultimate shear capacity quite well, to within 20% of tested values. Other observations were that stiffness and cracking moments increased with an increase in degree of prestressing, and that ultimate shear capacity increased

when the shear span-to-effective depth ratio (a/d) decreased in combination with an increase in amount of prestress and/or concrete compressive strength. [62]

Two-span Continuous Prestressed Beams

One of the most comprehensive summaries of continuity in prestressed concrete is given by M.Z. Cohn in Reference 28. Cohn discusses many relevant debates about the behavior of continuous prestressed beams and reviews many test results and literature related to such controversial topics as inelastic behavior and moment redistribution of these elements. He also discussed different methods and approaches to design and their particular implications.

T.Y. Lin and K. Thornton investigate the importance of secondary moment and moment redistribution in continuous prestressed beams in Reference 43. They point out the necessity of including secondary moments if full moment redistribution is not permitted. Ignoring these secondary moments can lead to either conservative or unconservative results.

CHAPTER 3

EXPERIMENTAL PROGRAM

3.1 Introduction

In an effort to properly examine the advantages and disadvantages of the integrated design method discussed in Section 2.5 as it would apply to designs typical of the San Antonio Y-Project straddle bent caps, four different model specimens were built and tested to failure. Their designs are discussed in Section 3.3. All construction and testing of models was carried out at the Ferguson Structural Engineering Laboratory of the University of Texas at Austin.

3.2 Modelling

A number of prototypical TxDOT substructures of the San Antonio Y-Project were examined to determine appropriate dimensions to be modelled for a laboratory investigation. Due to the large size of the element to be modelled, an appropriate scale factor was chosen to facilitate construction and testing. Dimensions of the model such as span length, depth and shear span as well as the materials such as concrete aggregate size, steel area, and post-tensioning duct size needed to be reduced as did the applied loads. Reducing the scale of the prototypical beam and loads had many consequences that required attention to ensure accurate modelling.

3.2.1 Prototype and Model Dimensions

Upon investigating many of the TxDOT-designed straddle bent caps of the San Antonio Y-Project, a prototypical specimen was chosen to be modelled. The straddle bent caps found in San Antonio are primarily on two supports often with an overhang comparable to the span length. However because an investigation of moment and secondary moment redistribution was desired, a two-span continuous model was chosen for this study. Notable similarities between these two members are the use of draped tendons and both positive and negative bending moment regions. Considerations that were kept consistent with the prototype and the model included span-to-depth ratios (l/h) and shear span-to-effective depth ratios

(a/d). These ratios for the prototypical member were:

$$\begin{aligned}l/h &= 5.33 \\ a_1/d &= 0.83 \\ a_2/d &= 2.60\end{aligned}$$

where: a_1 = shorter of the two shear spans from one pair of point loads.
 a_2 = longer of the two shear spans from one pair of point loads.

As further discussed in Section 3.2.2, each pair of point loads represent the loads from a box girder superstructure.

A scale factor of 1/4 was then chosen based on the capacities of the available laboratory equipment and facilities. The resulting model had two 8-ft. (2.44m) spans with a 1.5-ft. x 1.5-ft. (460mm x 460mm) cross section. An additional 1-ft. (305mm) in length was added to provide a 6-in. (150mm) overhang on each end for proper bearing above roller supports. The resulting model was then 17' x 1.5' x 1.5' (5.2m x 0.46m x 0.46m). Figures 3.1 & 3.2 and Table 3.1 summarize this selection process.

Scaling down the overall dimensions of the model then required the scaling down of the different materials.

3.2.1.1 Modelling of Concrete

The important concrete component to be scaled down was the aggregate size. The San Antonio Y-Project used 1-1/2" (38mm) uniform aggregate. The models therefore used 3/8" (9.5mm) uniform aggregate. (Concrete mix details can be found in Section 3.4.1.)

3.2.1.2 Modelling of Reinforcement

The scale factor of 1/4 required the ideal area of modelled reinforcement to be 1/16 that of the prototype. Due to the restricted availability of small bar sizes not all of the model dimensions were exactly at 1/4-scale. Table 3.2 presents a list of prototype and corresponding model bar sizes with the scale factor in terms of area. Where bar areas were not directly at 1/16-scale, the total area of steel required was adjusted so that the provided area would be at 1/16-scale. In cases where the yield strengths differed, total ultimate tension forces were made to be at the proper scale. Prestressing strand areas as well were 1/16 the area of that needed in the prototype. The area of strand was dependent on each design (see Section 3.3). For shear design, double stirrups were used for modelling as they were typically used in the San Antonio Y-Project designs.

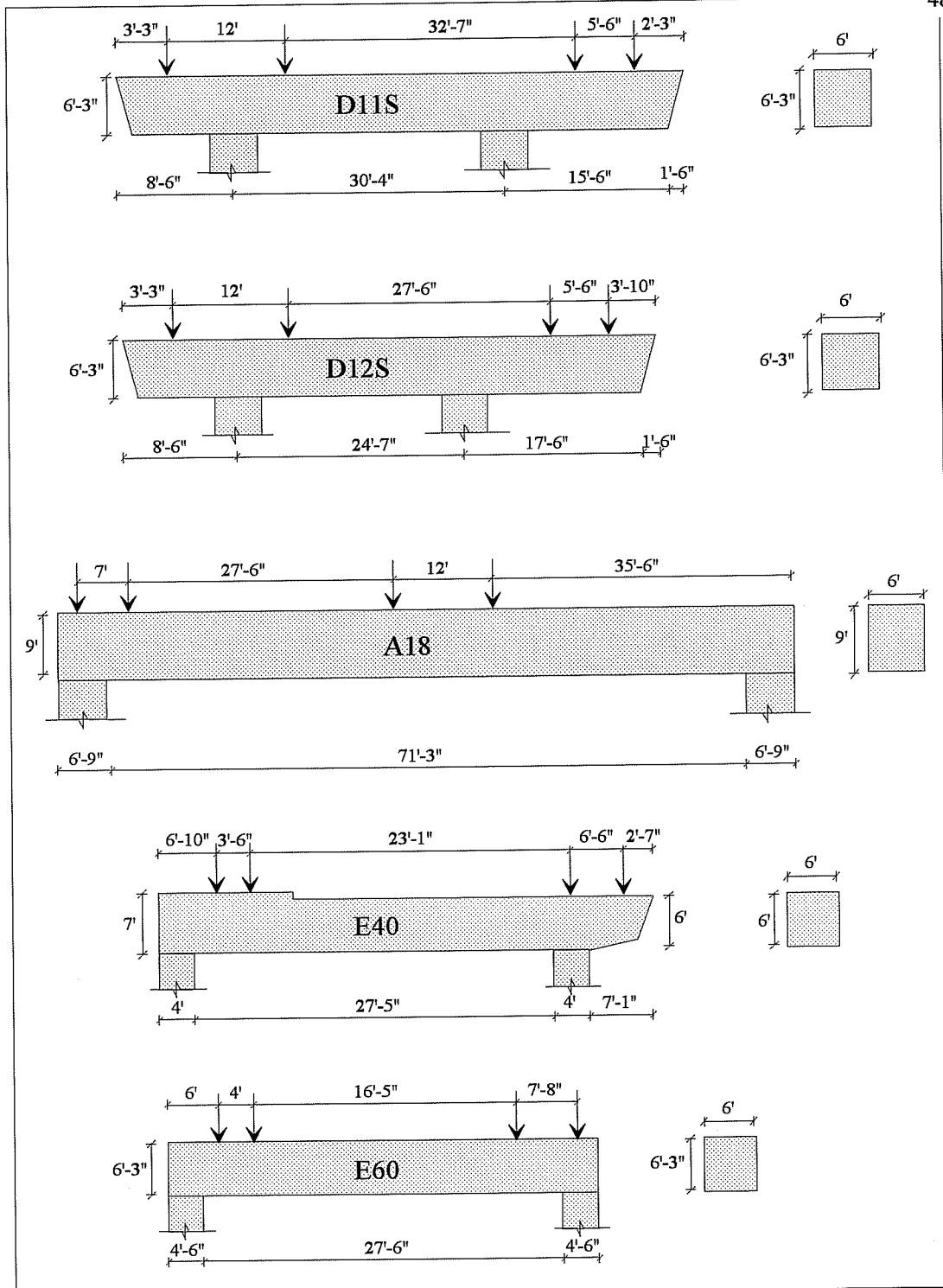


Figure 3.1a Prototypical Designs from San Antonio "Y" Project, English units

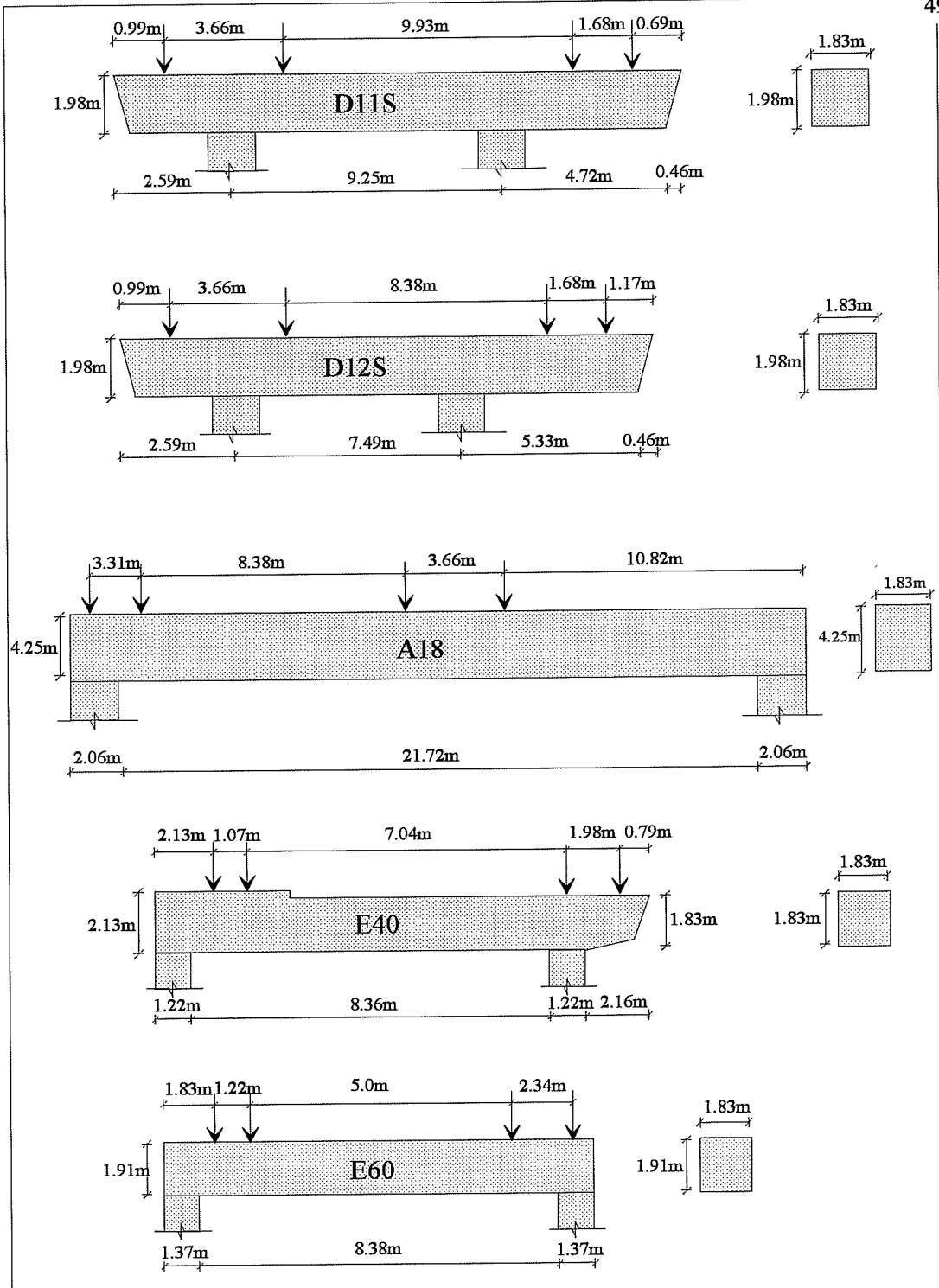


Figure 3.1b Prototypical Designs from San Antonio "Y" Project, S.I. units

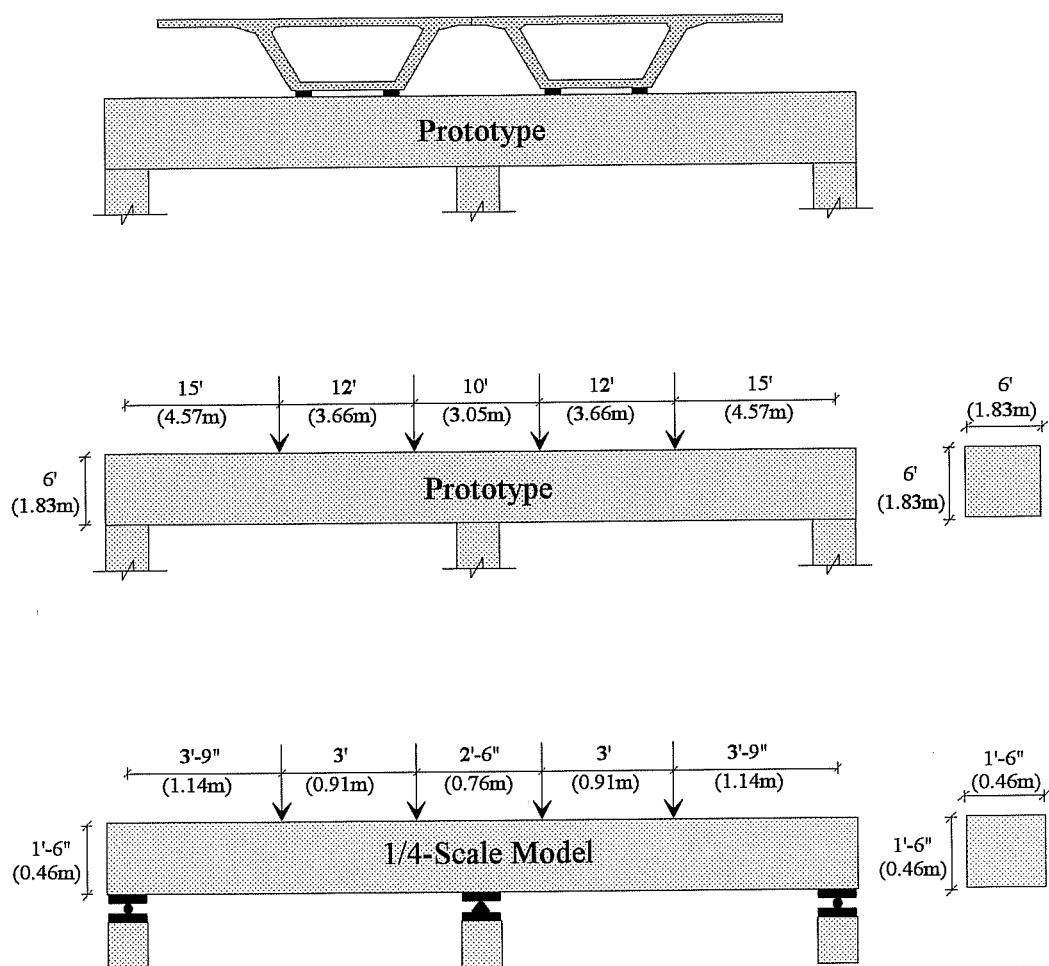


Figure 3.2 Modelling of Prototype

BENT	l/h	a ₁ /d*	a ₂ /d	a ₃ /d	a ₄ /d
D11S	4.86	0.91	0.84	1.47	-
D12S	3.94	0.91	0.84	1.62	-
A18	8.67	-	0.56	3.59	3.38
E40S	5.23	0.68	-	-	0.98
E60S	5.82	0.45	-	1.35	-
MODEL	5.33	2.61	0.83	0.83	2.61

* "a₁₋₄" refers to shear spans for the loads pictured from left to right on each bent in Figure 3.1 and the model in Figure 3.2.

Table 3.1 Typical Span Length-to-Height and Shear Span-to-Effective Depth Ratios for San Antonio Y-project Straddle Bents

Prototype	Model	Scale Factor
#11 bars A _s =1.56 in ² (1006 mm ²)	#3 bars A _s =0.11 in ² (71 mm ²)	1/14
# 8 bars A _s =0.79 in ² (510 mm ²)	#2 bars A _s =0.044 in ² (28 mm ²)	1/18
# 5 bars A _s =0.31 in ² (200 mm ²)	5/32" wire A _s =0.019 in ² (12.4 mm ²)	1/16
# 3 bars A _s =0.11 in ² (71 mm ²)	12-ga. wire A _s =0.0087 in ² (5.6 mm ²)	1/12.6

Table 3.2 Modelling of Reinforcement

3.2.2 Prototype and Model Loads

3.2.2.1 Dead Load

The model was designed so that every dimension of the prototype was reduced by 1/4. Therefore, the volume of the concrete was 1/64 of the prototype volume. As volume is directly related to the self-weight or dead load (DL), the model dead load was 1/64 that of the prototype. The modelling problem this creates with respect to the prestressed models is discussed in Section 3.2.3. The prototype chosen weighed 365 kips (1624 kN). Each model weighed 5.7 kips (25.8 kN).

3.2.2.2 Applied Loads

Applied loads included superimposed dead load (SDL) and live load (LL). The superimposed dead load is the dead load of the box girder superstructure and the live loads were considered to be the truck loadings on the superstructure. The applied loads are proportional to the area of steel required in the straddle bent to provide adequate resistance. This can be seen in the following equation for flexural resistance of a conventionally reinforced beam:

$$M_u = \Phi M_n = \Phi A_s f_y \left(d - \frac{a}{2} \right) \quad ; \quad a = \frac{A_s f_y}{0.85 f'_c b} \quad (3-1)$$

In the straddle bent model, the moment due to the point loads is approximately linear. Assuming for a simple example that the moment is the load times a distance one can represent the previous equation's variables with their respective reduction factors in terms of the scale factor "S" (which is equal to 4 for a 1/4-scale model) and the unknown scale factor for the load, Q as "X":

$$M = \frac{Q}{X} * \frac{e}{S} = \frac{A_s}{S^2} * f_y * \left[\frac{d}{S} - \frac{\frac{A_s}{S^2} * f_y}{0.85 * f'_c * \frac{b}{S}} \right] \quad (3.2)$$

$$\frac{1}{SX} * (Qe) = \frac{1}{S^3} * [A_s f_y (d - \frac{a}{2})]$$

$$\therefore X = S^2$$

and the scale factor for Q needs to be $1/(S^2) = 1/16$.

Superimposed Dead Load - The superimposed dead load consisted of a segmental box girder superstructure. For simplicity in modelling and analysis, two box girders were modelled symmetrically about the middle support on the model. They represent a box superstructure resting on bearing pads 12-ft.

(3.66m) apart. The resulting four point loads for the prototype loads were taken as 350 kips (1558 kN). Therefore the model superimposed dead load was 22 kips (97 kN).

Live Load - The live load consisted of individual and lane loadings of trucks. A typical live load carried by the support structures from the San Antonio Y-Project designs was 120 kips (534 kN). Therefore the modelled live load was 7.5 kips (33.4 kN). This resulted in a dead-to-(dead+live) load ratio of 0.79.

3.2.2.3 Construction Loads

Construction loads (CL) controlled some section designs. This loading assumed only one span being loaded with the superstructure (superimposed dead load) with an additional 180-kip (800 kN) crane. This corresponds to an 11.25 kip (50 kN) crane load at 1/4-scale. The crane load was assumed to distribute evenly from the box girder to the pier cap resulting in two point loads of 5.6 k (25 kN) each.

3.2.2.4 Service and Factored Loads

Following the loading criteria of Chapter 3 of the AASHTO Bridge Specifications [9], service loads were unfactored, and factored loads were taken according to Load Case I for Factored Loads with no impact and no centrifugal force:

$$\text{Factored Load} = 1.3 * [DL + 1.67 * LL] \quad (3-3)$$

Construction loads were factored with the dead load factor of 1.3 from Factored Load Case I.

Service Loads:

$$\begin{aligned} \text{Point Loads} = Q &= \text{SDL} + \text{LL} = 22\text{k} + 7.5\text{k} = \underline{29.5\text{k}} \\ & \quad (97\text{kN} + 33\text{kN} = 130\text{kN}) \end{aligned}$$

$$\text{Distributed Load} = w = \text{DL} = \underline{1.35 \text{ k/ft}} \quad (19.7 \text{ kN/m})$$

Factored Loads:

$$\begin{aligned} Q &= 1.3 * \text{SDL} + 1.3 * (1.67 * \text{LL}) = 28.6\text{k} + 16.3\text{k} = 44.9\text{k}, \text{ use } \underline{45\text{k}} \\ & \quad (127\text{kN} + 72\text{kN} = 199\text{kN}, \text{ use } 200\text{kN}) \end{aligned}$$

$$w = 1.3 * \text{DL} = \underline{1.76 \text{ k/ft}} \quad (25.6 \text{ kN/m})$$

Construction Loads:

$$Q = 1.3*SDL + 1.3*CL = 28.6k + 7.3k = 35.9k, \text{ use } \underline{36k}$$

$$(127.3 \text{ kN} + 32.5\text{kN} = 159.8 \text{ kN, use } 160\text{kN})$$

$$w = 1.3*DL = \underline{1.76 \text{ k/ft.}} \quad (25.6 \text{ kN/m})$$

Although the models were designed at the ultimate limit state for factored dead load, factoring the dead load was not included in the experimental program.

3.2.3 Dead Load Blocks

As mentioned in Section 3.2.2.1, the weight of the model was 1/64 that of the prototype. This presented a problem with the design of the prestressed models as dead load is counted on to control excessive camber due to the eccentricity of the prestressed reinforcement. As the area of the reinforcing steel was reduced from the prototype by 1/16, so too was the prestressing force. To properly model the prototype's behavior a corresponding dead load of 1/16 was required of the model. To achieve this, extra dead load (3/64 more) was hung from the beam. The application of this dead load is described in Section 3.5.4.

3.3 Test Models

The first two models were designed according to the 1992 AASHTO Bridge Specifications; one conventionally reinforced and one fully prestressed. Both of these designs were first made for the full-scale prototype member. Model designs were then made and dimensions were compared to check the accuracy of the scale modelling. The third and fourth models were designed using the integrated design method presented in Section 2.4. These designs were carried out for the model only. Because of the general accuracy in scale modelling of the first two models, the dimensions and areas for the third and fourth models were simply scaled up to give prototypical dimensions and areas for these designs.

The model designs are presented first followed by the corresponding prototype designs for each specimen. For simplicity, only forces and resulting steel areas required are presented here. Equations used are presented in Appendix A. In determining the areas of steel required, a resistance factor of 1.0 was used throughout under the traditional assumption that material properties and construction practices would be well controlled in a laboratory experiment.

There were many items of design that were consistent throughout all of the models or all of the post-tensioned models. The concrete cover requirement for the non-prestressed steel was the same for all models and the cover requirement for the center of the post-tensioning duct was the same for all of the post-tensioned strands. Side face cracking steel requirements and the anchor zone design used were similar as well for all of the post-tensioned models. (Similar anchor zone design was not required. For simplicity however, the most conservative design was used for all models.) These design items are discussed the first time they are applicable. Reference to the original design is then made for the remaining models.

Fatigue resistance was examined for each model as well, concentrating on the two critical sections; the maximum positive moment region and the maximum negative moment region. When determining the amount of stress in the strand at various load levels, an elastic distribution of loads was assumed. Performing the analysis assuming elastic behavior simplifies calculations and provides the required information - whether fatigue resistance is a potential problem in the design or not. A sample fatigue calculation for a post-tensioned model is presented in Appendix B.

A similar approach is taken in determining first yielding. A strain compatibility analysis was used to determine first yielding of both the non-prestressed and prestressed steel for the post-tensioned models. A cracked transformed section analysis was used for the non-prestressed model. In some cases, the non-prestressed steel was expected to yield and fracture before the prestressed steel would yield. The non-prestressed reinforcement was then not included in the yield analysis of the prestressed reinforcement. However when the nonprestressed steel was not included in the analysis the prestressed steel would in some cases theoretically yield before fracture of the non-prestressed steel occurred. In these cases, it is assumed that fracture of the non-prestressed reinforcement would lead directly to yielding of the prestressed reinforcement.

This analysis to predict yielding did not consider the effects of cracking which, effectively softening the beam in some regions, could change the yield point.

After designing the prestressed models it was determined that the secondary moments were relatively small for these stocky beams. The change in reactions induced by redistribution of the secondary moments upon cracking could not be recorded with sufficient accuracy.

3.3.1 Designs According to 1992 AASHTO Bridge Design Specifications

The designs presented here follow provisions outlined in the 1992 AASHTO Bridge Specifications.[9] Specific references to this standard not be made here are found in Appendix A.

3.3.1.1 Conventionally Reinforced - CB-RU

The first model is referred to as CB-RU. This stands for the Continuous Beam conventionally Reinforced based on Ultimate loads.

Flexure Design - CB-RU - Flexure design was based on the maximum positive and negative moments due to factored loads. The maximum negative moment occurred over the center support due to full factored loads. The maximum positive moment occurred under factored construction loads (see Section 3.1.2.4) Figure 3.3 shows the critical moment diagrams (The moment diagrams are represented as linear for simplicity. They are in fact slightly parabolic due to the uniform dead load. This does not effect the peak values used in design.) Continuing cage steel as well as developed steel in the compression regions of the critical sections was not considered as compressive steel for doubly reinforced sections.

The critical sections for flexure were therefore the negative moment region over the center support ("B" on Figure 3.3) as well as the positive moment region ("D" on Figure 3.3) under the point load near the mid-spans. The required area of steel over the center support was 1.49 in.^2 (961 mm^2). An initial design of 14-#3 bars with $A_s = 1.54 \text{ in.}^2$ (994 mm^2) was chosen. In checking steel distribution requirements for crack control, it was found that 14 bars were adequate.

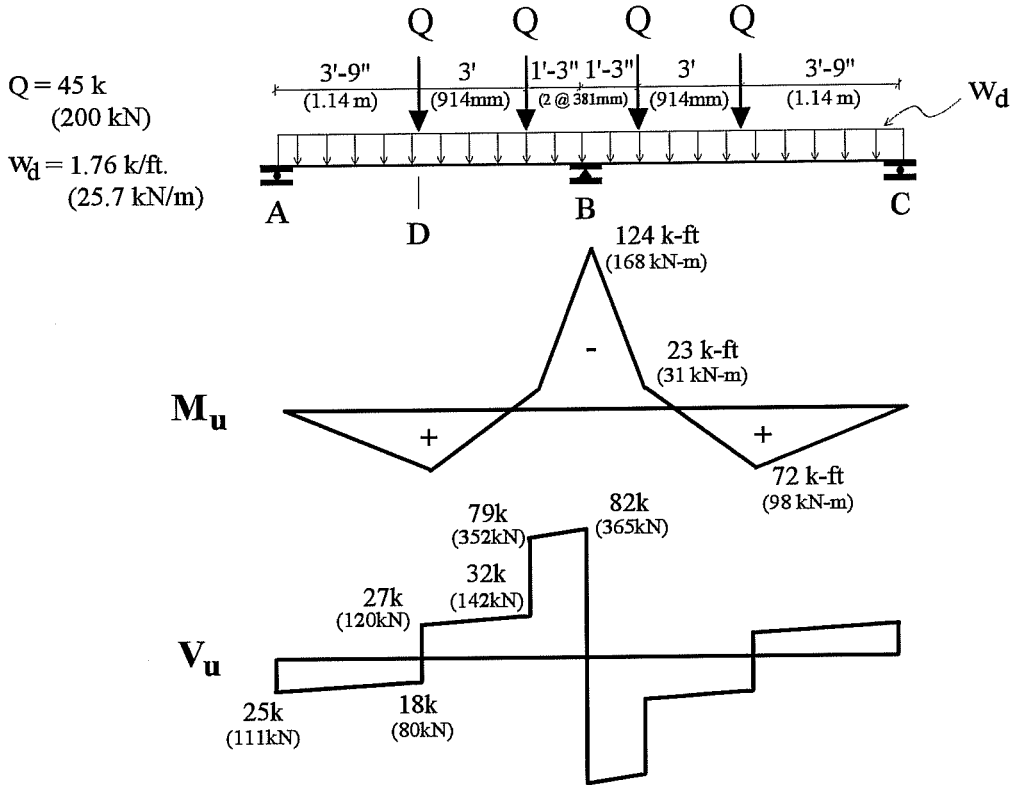
Use 14-#3 bars; $A_s = 1.54 \text{ in.}^2$ (994 mm^2)

In terms of spacing of bars, the controlling limit was a minimum spacing of 1.5 times the maximum aggregate size (or bar size, which was the same in this case). With the 3/8" (9.5mm) aggregate and bar diameter, a minimum spacing of 0.56 in. (14.3mm) was required which was satisfied by using 14-#3 bars (see Figure 3.4).

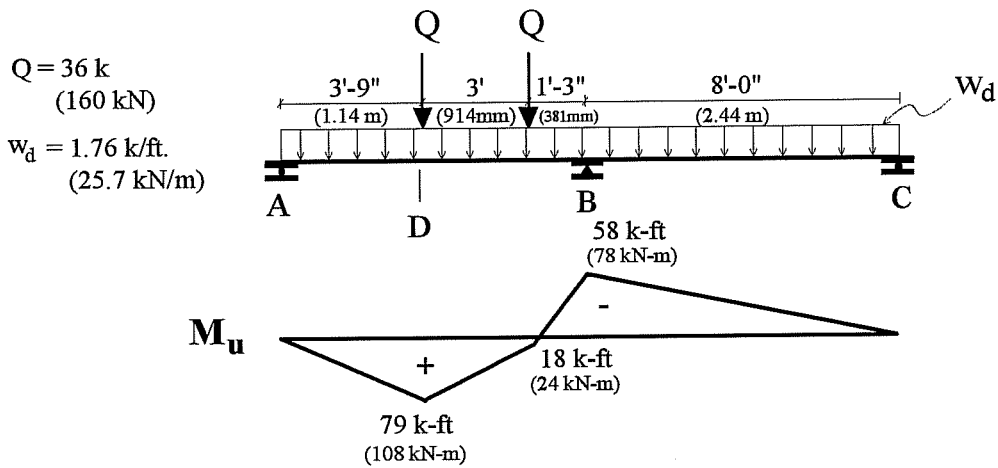
The reinforcement required for the positive moment region, D, was computed in the same way as that for the negative moment region. Assuming the use of #2 bars with a yield strength of 75 ksi (517 MPa), the required area of steel was 0.74 in.^2 (477 mm^2). An initial design of 16-#2 bars where $A_s = 0.78 \text{ in.}^2$ (506 mm^2) was chosen. In checking the crack width control criterion, the use of 16 bars in this location was inadequate. The number of bars needed to be increased to 24 bars.

Use 24-#2 bars; $A_s = 1.18 \text{ in.}^2$ (759 mm^2)

Factored Dead + Live Load



Factored Construction Load



*Note: Moment diagrams are simplified here, being represented as linear. The parabolic curve from the uniform dead load is neglected.

Figure 3.3 Critical Moment and Shear Diagrams for Designs

Shear Design - CB-RU - Shear design was based on full factored loads. The shear diagrams used for design are given in Figure 3.3. (The beam was conservatively designed for 90k (400kN) of shear as that was the calculated shear at ultimate for the beam already designed for flexure.) The concrete shear strength and the required steel shear strength at this section were:

$$V_c = 44 \text{ k (196 kN)}$$

$$V_s = 46 \text{ k (205 kN)}$$

Using a design yield strength of 60 ksi (414 MPa) for 5/32 in. (4 mm) diameter double stirrups, the required spacing was 1.5 in. (38.1 mm). This spacing was continued from the center support out to the applied loads closest to the support or, 1.25 ft. (381 mm) in each direction (see Figure 3.11).

Use 5/32" (4mm) double stirrups @ 1.5" (38mm), symmetrically out 15" (381mm) from center

The remainder of the section required only minimum shear reinforcement in accordance with AASHTO Specifications.

Use Φ 5/32" (Φ 4mm) double stirrups @ 5" (127mm), over remainder of beam

Side Face Crack Control - CB-RU - Side face crack control steel, or "skin" steel for this deep member required a total area of 0.05 in.² (32.3 mm²) on each face distributed up 8.5 in. (210 mm) from the bottom of the tension zone. This was best satisfied by 12-gauge wire. For simplicity in construction, this skin reinforcement was placed along the entire side face at 1.5 in. (38.1mm) on the inside of the stirrups. This provided 0.052 in.² (33.7 mm²) in the critical tension zone (bottom 5.5 in. (140mm) of tension zone).

Use 12-gauge wires (Φ 2.7mm) @ 1.5 in. (38.1mm) along entire sides

Development - CB-RU - Development lengths were provided for the steel in accordance with the AASHTO provisions and are described in Appendix A. Of particular importance to the ultimate capacity of this beam was the allowance in design to cut off a portion of the positive moment reinforcement within the positive moment region (AASHTO 8.24.1.4.3) (see Figure 3.4). Although generally not a good detailing practice, this is permitted by the specifications.

Concrete Cover - CB-RU - In terms of cover, the cover dimensions typical of the TxDOT San Antonio Y-Project substructure designs were adopted and used at 1/4-scale. The 2.5 in. (63.5mm) side cover was modeled as a 0.63 in. (15.9mm) side cover and the 2.25 in. (57.2mm) top and bottom cover was modeled as a 0.56 in. (14.3mm) top and bottom cover. The effective depth, "d" is therefore 17.17 in. (438mm) as opposed to the 17.25 in. (438mm) assumed for the designs above. This however makes virtually no difference in the overall design.

Fatigue - CB-RU - Finally, the problem of fatigue was checked for this design. The stress range for the steel was examined between full dead load (dead + superimposed dead load) and full service loads plus impact (dead + superimposed dead + live load x impact factor). An impact factor of 1.3 in accordance with AASHTO provision 3.8.2.1 was used. The loads between which steel stress ranges were checked for susceptibility to fatigue failure were from $P = 22\text{k}$ (98 kN) to $P = 31.8\text{k}$ (141kN). The stress ranges at the critical sections, B and D were 9.2 ksi (63.4 MPa) and 10.3 ksi (71 MPa) respectively. The allowable stress ranges in accordance with AASHTO 8.16.8.3 (Equation 2-4 in this thesis) are 15.4 ksi (106 MPa) at B and 13.8 ksi (95MPa) at D.

Comparison to prototype - CB-RU - In summary, the model design provisions are listed in Table 3.3 with the corresponding full scale prototype designs. As the prototype was designed separately, a comparison of the accuracy of the scale modeling is made.

Prediction of Cracking, Yield and Ultimate Moments - CB-RU - Recognizing the actual concrete strength at testing, first cracking was predicted to occur over the center support with applied point loads of 11.3k (50.3kN). This corresponds to an applied dead plus live load moment of -38.3 k-ft. (-52 kN-m). This first cracking prediction is based on assuming a concrete tensile strength of $6\sqrt{f'_c}$. First yielding was predicted to occur over the center support with moment of -131 k-ft (-178 kN-m) ($Q_{\text{elastic}} = 49\text{k}$, 220kN), and at mid-spans with a moment of 119.4 k-ft. (162 kN-m) ($Q_{\text{elastic}} = 79\text{k}$, 351kN). The formation of a full mechanism, with hinges formed over the center support and at the two mid-spans, was predicted to occur under applied point loads of 72k (320kN) (lower-bound equilibrium solution).

CB-RU Conventional Reinforcement

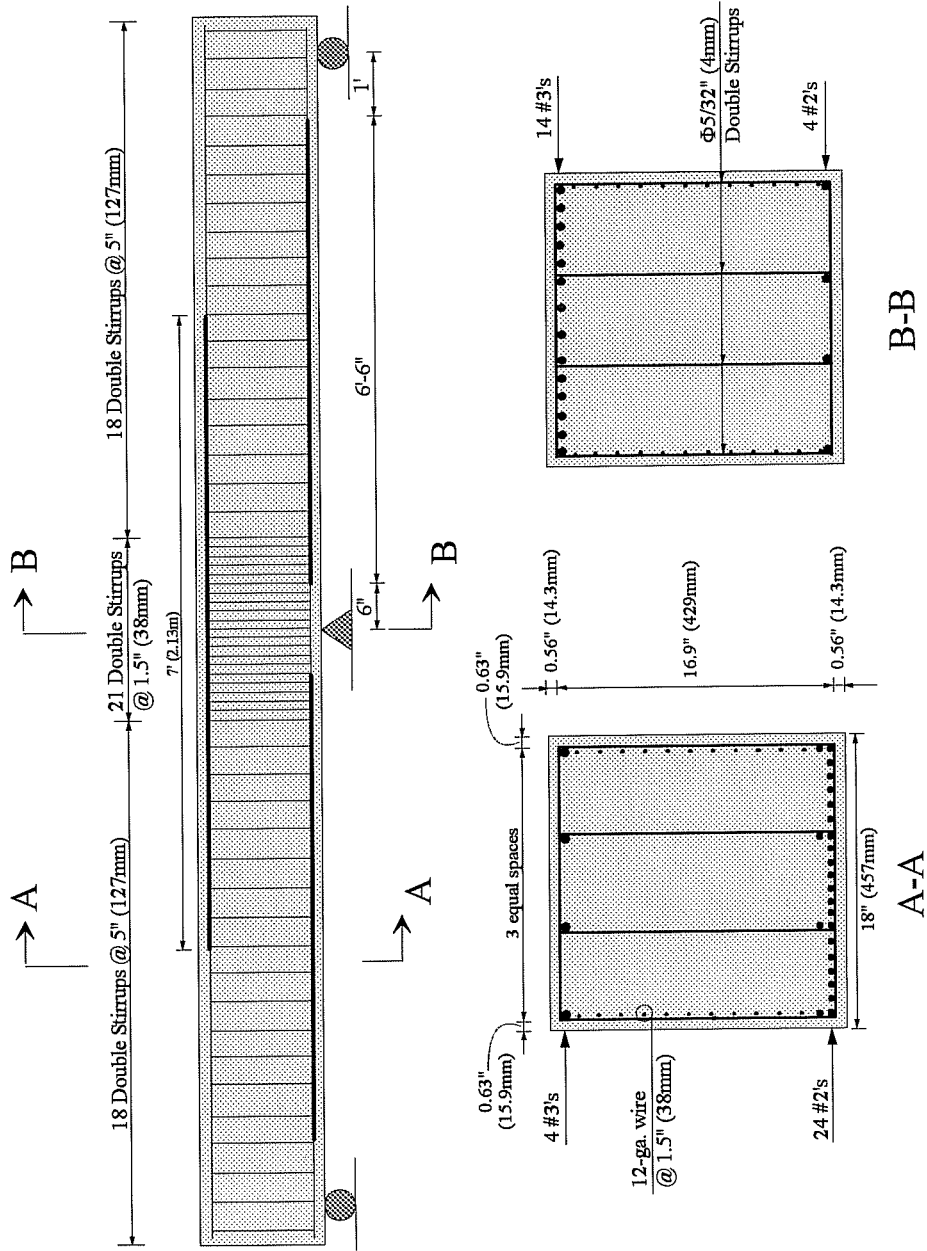


Figure 3.4 Design of CB-RU - Conventionally Reinforced based on AASHTO

Provisions For ↓	MODEL CB-RU	PROTOTYPE	SCALE FACTOR
M-	14-#3 bars $A_s = 1.54 \text{ in}^2$, $T = 92.4 \text{ k}$ (994 mm ² , 411kN)	16-#11 bars $A_s = 25.0 \text{ in}^2$, $T = 1500 \text{ k}$ (16130 mm ² , 6675kN)	1:16.2, 1:16.2
M+	24-#2 bars $A_s = 1.18 \text{ in}^2$, $T = 88.3 \text{ k}$ (761 mm ² , 393kN)	15-#9 bars $A_s = 15.0 \text{ in}^2$, $T = 900 \text{ k}$ (9677 mm ² , 4005kN)	n.a.*, 1:10.2
Vs-symmetrically 15" (381mm) out from center	5/32" dbl. stirrups @ 1.5" $A_v = 0.62 \text{ in}^2/\text{ft}$ (1310 mm ² /m)	#5 dbl. stirrups @ 6" $A_v = 2.48 \text{ in}^2/\text{ft}$ (5250 mm ² /m)	1:4
Vs - else	5/32" dbl. stirrups @ 5" $A_v = 0.19 \text{ in}^2/\text{ft}$ (390 mm ² /m)	#5 dbl. stirrups @ 20" $A_v = 0.74 \text{ in}^2/\text{ft}$ (1565 mm ² /m)	1:4
Side Face Crack Control (per face)	6-12-ga. wires over 8.5" $A_s = 0.052 \text{ in}^2$ (33.5 mm ² over 216 mm)	7-#3 bars over 33" $A_s = 0.77 \text{ in}^2$ (497 mm ² over 838 mm)	1:14.8 over 1:3.9
cover - sides	0.63" (15.9 mm)	2.5" (63.5 mm)	1:4
cover top & bottom	0.56 in. (14.3 mm)	2.25 in. (57.2 mm)	1:4

* Scaling the areas is not appropriate as the reinforcement has a different yield strength. Comparison must be made with the tensile strength, T , provided at ultimate (assuming elastic-perfectly-plastic steel behavior).

Table 3.3 Comparison of Model and Prototype Designs for CB-RU

3.3.1.2 Fully Prestressed - CB-PS-100S

The second model is referred to as CB-PS-100S. This stands for the **C**ontinuous **B**eam **P**restressed based on **S**ervice loads where **100%** of the serviceability requirements are satisfied by use of prestressed **S**trand.

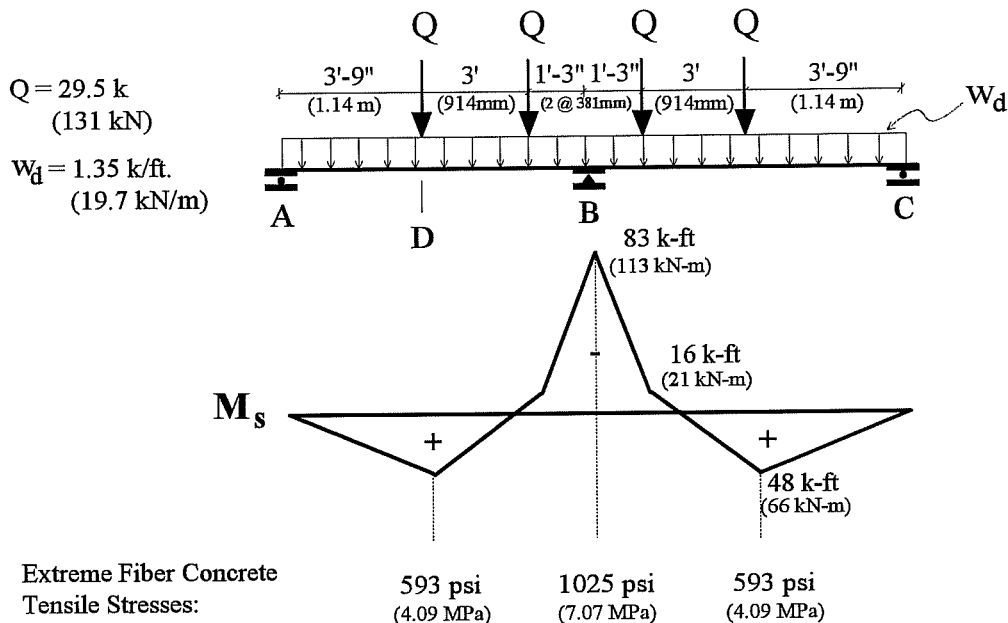
Flexure Design - CB-PS-100S - Flexure design was based on first satisfying serviceability requirements at service loads, and then providing adequate strength for factored loads. The amount of prestress required was therefore dimensioned to satisfy the serviceability criteria and an ultimate strength check followed.

The maximum moments under service loads and construction loads and their corresponding extreme fiber stresses at the critical sections, B and D, are depicted in Figure 3.5. The maximum stress at section B was produced under service loads while the maximum stress at section D was created under construction loads. (It was later determined that this model would need to be stage loaded. This construction load case would not occur with stage loading. The design however was then slightly conservative and not remodified.) In accordance with the prototype, i.e. San Antonio "Y" requirements, the maximum allowable concrete tensile stress was $3\sqrt{f'_c}$ ($0.25\sqrt{f'_c}$). The prestressing force was required to resist the maximum (critical) applied stresses by an amount that would keep the overall extreme fiber concrete tensile stress below the allowable limit:

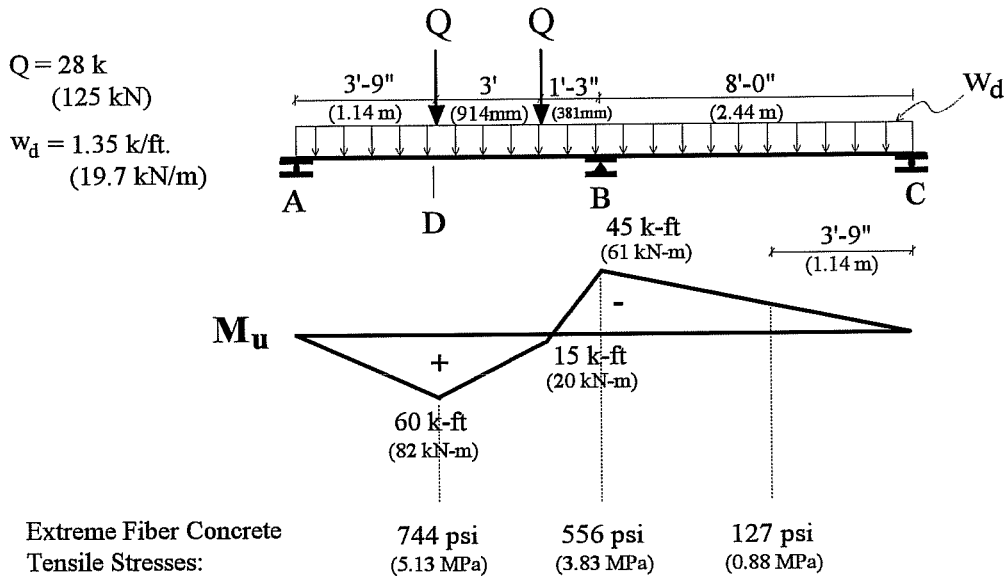
$$\sigma_{critical} - \sigma_{prestress} \leq \sigma_{allowable} \quad (3-5)$$

To determine the appropriate amount of prestressing and its eccentricity at the critical sections, equations for the required $\sigma_{prestress}$ to satisfy Equation (3-5) at the two critical sections were set up based on three variables; the prestressing force and the eccentricities over the center support and under the applied load near the mid-spans. These equations were developed using closed form expressions which determine the amount of moment (primary and secondary) due to prestressing in a member based on the geometry and prestressing force of the tendons. Both eccentricities had an upper bound of 7.5 in. (191mm) due to a cover requirement of 1.5 in. (38mm) measured from the center of the strand (modelling 6 in. (152mm) cover of San Antonio designs). These two simultaneous equations with three unknowns were then solved iteratively to determine an ideal layout and prestressing force. Stresses were then re-checked under construction loads as well as service loads. The resulting layout consisted of a draped tendon with a 7.5" eccentricity over the support and a 3.6" eccentricity under the applied load near the mid-spans (see Figure 3.8). The prestressing force required was 90k (400kN). An effective prestress of $0.56f_{pu}$ was

Service Loads (Unfactored Dead + Live)



Unfactored Construction Loads



*Note: Moment diagrams are simplified here, being represented as linear. The parabolic curve from the uniform dead load is neglected.

Figure 3.5 Moment Diagrams for Service and Unfactored Construction Loads

assumed. This was to account for losses that would occur in the prototype but not necessarily in the model as the model was loaded for testing within days of stressing. This effective prestress for Grade 270 prestressing strand required the following amount of prestressing strand:

$$f_{se} = 0.56f_{pu} = 151 \text{ ksi (1041 MPa)}$$

$$F = A_p f_{se} \quad \therefore \quad A_p = 90/151 = 0.609 \text{ in.}^2 \text{ (393 mm}^2\text{)}$$

Use 4- Φ 1/2" (Φ 12.7mm) Gr 270 mono-strands; $A_p = 0.612 \text{ in.}^2 \text{ (395 mm}^2\text{)}$

Stresses were re-checked with this slightly larger area of prestress than required and were satisfactory. Ultimate strength at the critical sections was checked, including the prestressed and non-prestressed steel in the tension zone, and in all cases the nominal resisting moment provided by the prestressing strand substantially exceeded the applied factored moment:

$$\textcircled{B}: M_n = 236 \text{ k-ft (320 kN-m)} > M_u = 124 \text{ k-ft. (168 kN-m)}$$

$$\textcircled{D}: M_n = 180 \text{ k-ft. (244 kN-m)} > M_u = 72 \text{ k-ft. (98 kN-m)}$$

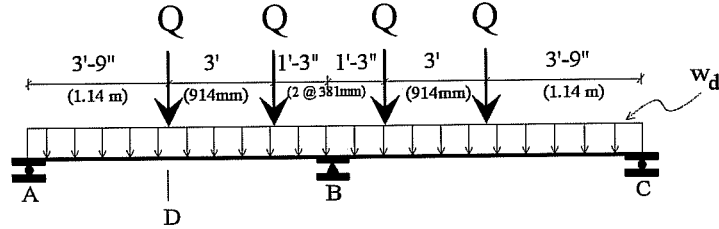
Therefore, the reinforcement required was proportioned based on satisfying concrete tensile stress limits rather than on ultimate loads. Both limit states are of course satisfied.

Construction errors - CB-PS-100S - With the construction of this member, described more fully in Section 3.5, the tendon profile was cast in place incorrectly. The error is shown in Figure 3.9. The result was that the point of inflection on the strand, near the area where the moment changes from positive to negative, was pushed in closer to the center than it was in the design. The radius of curvature of the tendon was therefore smaller. The resulting equivalent load was larger and over a smaller area. A check of the new stresses resulting from this tendon layout showed that the serviceability and strength limit states were still satisfied. The design in general became more conservative for the service limit state and the expected amount of friction loss over the center support was increased. While this did change the effect of prestressing on shear, it did not effect the outcome of the shear design. The original shear design calculations are summarized here.

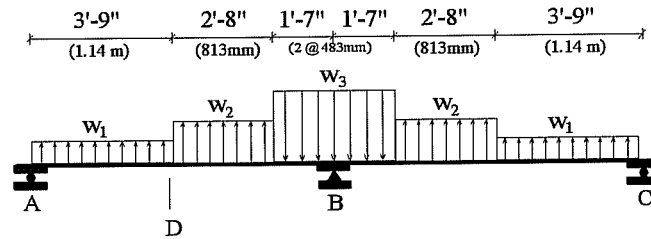
Shear Design - CB-PS-100S - Shear design was based on full factored loads including the effects of prestressing. The factored shear load used for design can be found in the shear diagrams of Figure 3.6. The concrete shear strength was taken as the lesser of V_{ci} and V_{cw} , (the concrete shear strength against

Factored Dead + Live Load

Q = 45 k
(200 kN)
w_d = 1.76 k/ft.
(25.7 kN/m)

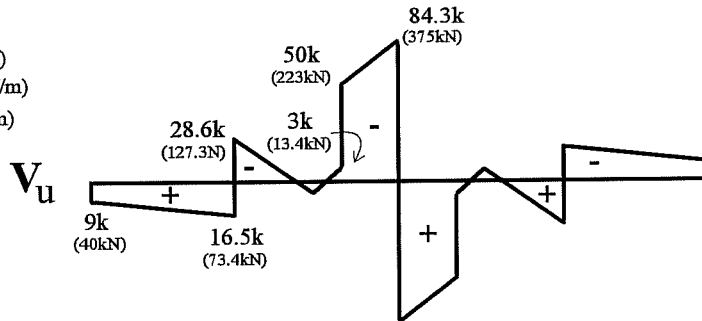


Transverse Effects of Prestress as Load:



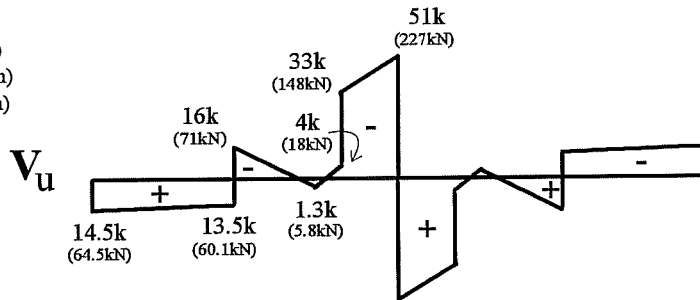
CB-PS-100S

w₁ = -3.8 k/ft. (-55.5 kN/m)
w₂ = -14.8 k/ft. (-216.1 kN/m)
w₃ = 24.6 k/ft. (359.2 kN/m)



CB-PU-100S

w₁ = -1.1 k/ft. (-16.1 kN/m)
w₂ = -7.1 k/ft. (-103.7 kN/m)
w₃ = 13.0 k/ft. (189.8 kN/m)



CB-PU-71S

w₁ = -0.7 k/ft. (-10.2 kN/m)
w₂ = -5.1 k/ft. (-74.5 kN/m)
w₃ = 8.4 k/ft. (122.6 kN/m)

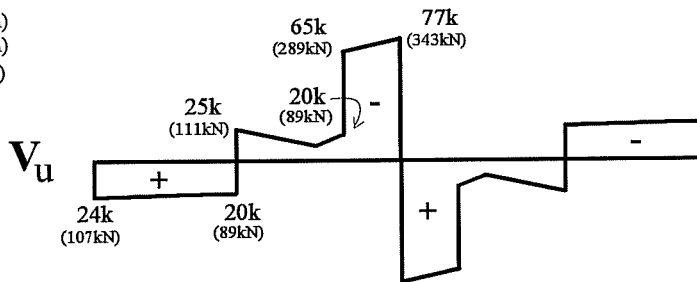


Figure 3.6 Factored Shear for Design of Post-tensioned Specimens

inclined-shear crack and web-shear crack failure respectively, AASHTO 9.20.2 [9]) calculated at 10 points along each span. At critical sections, where the applied shear was greatest, the concrete strength was taken as the underlined value:

$$\text{Near center: } V_d = 150 \text{ k (668 kN)}, \underline{V_{cw} = 98 \text{ k (436 kN)}}$$

$$\text{Remainder of beam: } \underline{V_d = 45 \text{ k (200 kN)}}, V_{cw} = 91 \text{ k (405 kN)}$$

As the concrete shear strength exceeded the full factored shear force at all sections, only minimum shear stirrups were required. Using the tested design yield strength of 71 ksi (490 MPa) for 5/32 in. (4 mm) diameter double stirrups, the required spacing was 6 in. (152 mm).

Use Φ 5/32" double stirrups @ 6", throughout
(Φ 4mm double stirrups @ 152 mm)

Side Face Crack Control - CB-PS-100S - Side face crack control steel, or "skin" steel for this deep member required a total area of 0.045 in.² (29 mm²) on each face distributed up 8.5 in. (210 mm) from the bottom of the tension zone. A maximum spacing of 1.5 in. (38.1 mm) was required. This was best satisfied by 12-gauge wire. For simplicity in construction, this skin reinforcement was placed along the entire side face at 1.5 in. (38.1 mm) on the inside of the stirrups. This provided 0.052 in.² (33.7 mm²) in the critical tension zone.

Use 12-gauge wires (Φ 2.7mm) @ 1.5 in. (38.1mm) over entire sides

Concrete Cover - CB-PS-100S - The same cover requirements for CB-RU were used here for the mild reinforcement; a 0.63 in. (15.9 mm) side cover and a 0.56 in. (14.3 mm) top and bottom cover. In addition, a minimum distance of 1.5 in. (38.1 mm) from the center of the strand to the extreme concrete fiber was required. This was only restrictive over the center support.

Anchor Zones - CB-PS-100S - Anchor zone reinforcement as well as bearing plate sizes were designed according to NCHRP Report 356.[24, Appendix A] Bearing plates of 4.25"x3"x1" (108mm x 76 mm x 25.4 mm) with a 15/16" (23.8mm) diameter hole in the center were chosen so as to fit four plates together in one row across the 18"-wide (457 mm) beam. Bearing strength on the concrete as well as bearing plate

stiffness requirements were met. Bursting forces were checked in two directions; spreading within the depth and within the width of the beam as shown in Figure 3.7. The largest bursting force occurred in the spreading within the depth of the beam. This was carried by 10 double stirrups of 5/32" (4 mm) diameter wire spaced at 2 in. (51 mm) over 18 in. (457 mm).

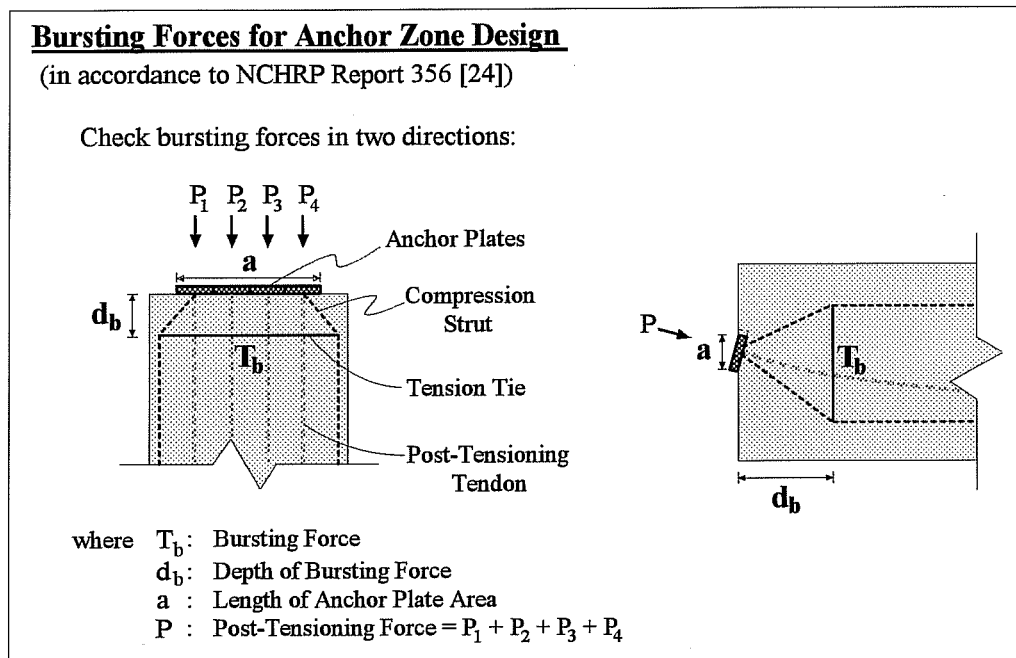


Figure 3.7 Anchor Zone Design Method for CB-PS-100S

Fatigue - CB-PS-100S - Finally, the problem of fatigue was checked for this design. As the dead and live loads were the same here as for the previous model, the same loading range was used to examine the steel stress ranges. The stress ranges at B and D were 3 ksi (20.7 MPa) and 1 ksi (6.9 MPa) respectively. This check is in fact not required by the 1992 AASHTO Bridge Design Specifications. Due to the limitation of concrete tensile stresses in design, fatigue resistance is assumed not to be a problem. The recommended maximum stress range for bonded post-tensioned strand according to Wollmann [65] is 14.5 ksi. The stress range that this prestressing reinforcement is expected to experience is therefore not a problem according to Wollmann either.

Comparison to prototype - CB-PS-100S - In summary, the model design provisions are listed in Table 3.4 with the corresponding full scale prototype designs. As the prototype was designed separately, a comparison of the accuracy of the scale modeling is made.

Prediction of Cracking, Yield and Ultimate Moments - CB-PS-100S - Recognizing the actual concrete strength at testing, first cracking was predicted to occur in the negative moment region with applied point loads of 44.5k (198kN), or an applied dead plus live load moment of -120.1 k-ft. (-163 kN-m). First yielding was predicted to occur in the non-prestressed cage steel at the mid-spans with an applied moment of 110 k-ft. (149 kN-m) ($Q_{elastic}=73k, 325 \text{ kN}$). The non-prestressed cage steel over the center support was then expected to yield with an applied moment of -201 k-ft (-273 kN-m) ($Q_{elastic}=78k, 347 \text{ kN}$) followed by yielding of the prestressed strand over the center support with an applied moment of -215 k-ft. (-292 kN-m) ($Q_{elastic} = 84k, 373kN$). The formation of a full mechanism, with hinges formed over the center support and at the two mid-spans, was predicted to occur at applied point loads of 120k (534kN) (lower bound equilibrium solution).

3.3.2 Designs According to Presented Integrated Design Method

The third and fourth models of the test series were designed according to the integrated design method presented in Section 2.5. A summary of relevant equations used for design is found in Appendix A.

3.3.2.1 100% Prestress for Factored Loads - CB-PU-100S

The third model is referred to as CB-PU-100S. This stands for the Continuous Beam Prestressed based on Ultimate loads where 100% of the ultimate tensile force is carried by the prestressing Strand.

Flexure Design - CB-PU-100S - Flexure design was based on the factored moment diagrams used for the conventionally reinforced beam (Figure 3.3). The amount of prestressing steel to be used was that required to resist the maximum factored moment at the critical sections - over the center support and near the mid-spans. An ideal layout of the tendon was determined so that the ultimate moment would be carried 100% by the prestressing reinforcement at both critical moment sections. This was done by iteration using a spreadsheet. No moment redistribution was considered in this design. Using prestressing strand with $f_{su} = 270 \text{ ksi (1860 MPa)}$, $0.36 \text{ in.}^2 (9.1 \text{ mm}^2)$ of this strand were required. This corresponds to a required ultimate tensile force of 97.2 k (433 kN). Considering available strand sizes with $f_{su} = 270 \text{ ksi (1860 MPa)}$, $2-\Phi 0.5" (12.7\text{mm})$ strands and $1-\Phi 0.375" (9.5\text{mm})$ strand were used having a total area of $0.391 \text{ in.}^2 (246 \text{ mm}^2)$. This provided an ultimate tensile force of 106 k (470 kN). This is only 59% of the ultimate tensile

CB-PS-100S
"Fully" Prestressed based on AASHTO

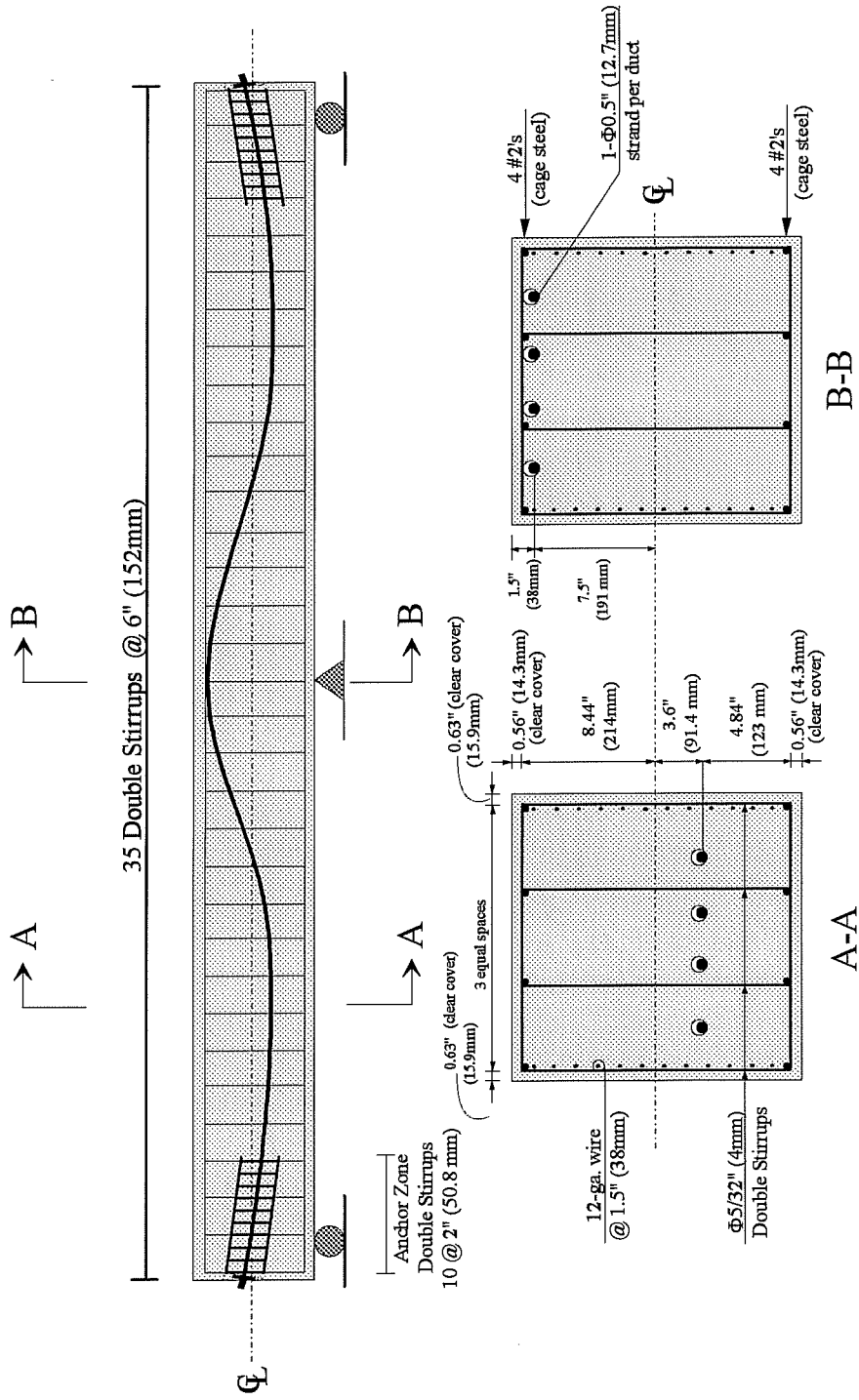
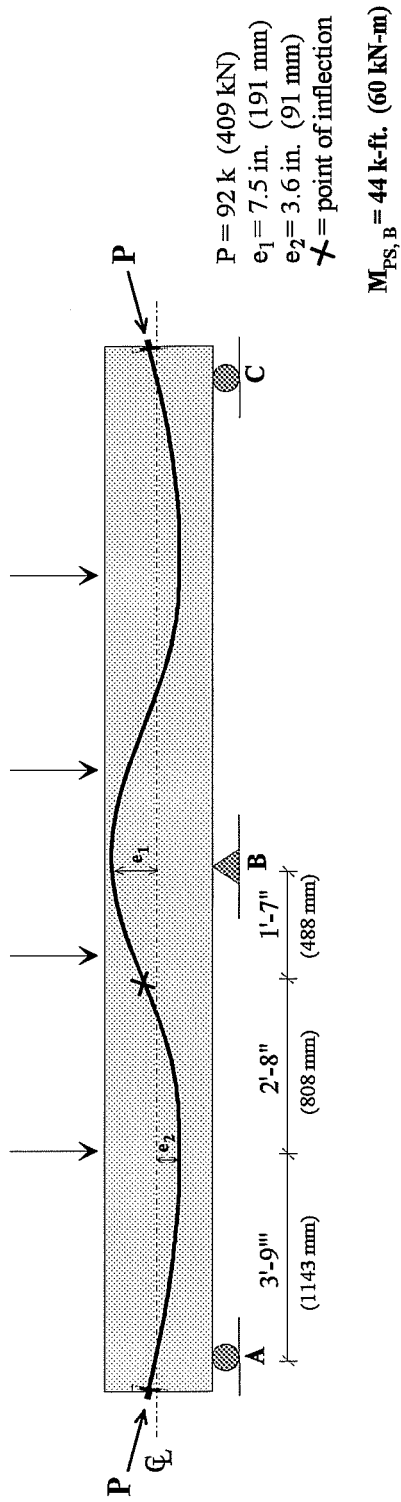


Figure 3.8 Design of CB-PS-100S - "Fully" Prestressed based on AASHTO

DESIGNED:



BUILT:

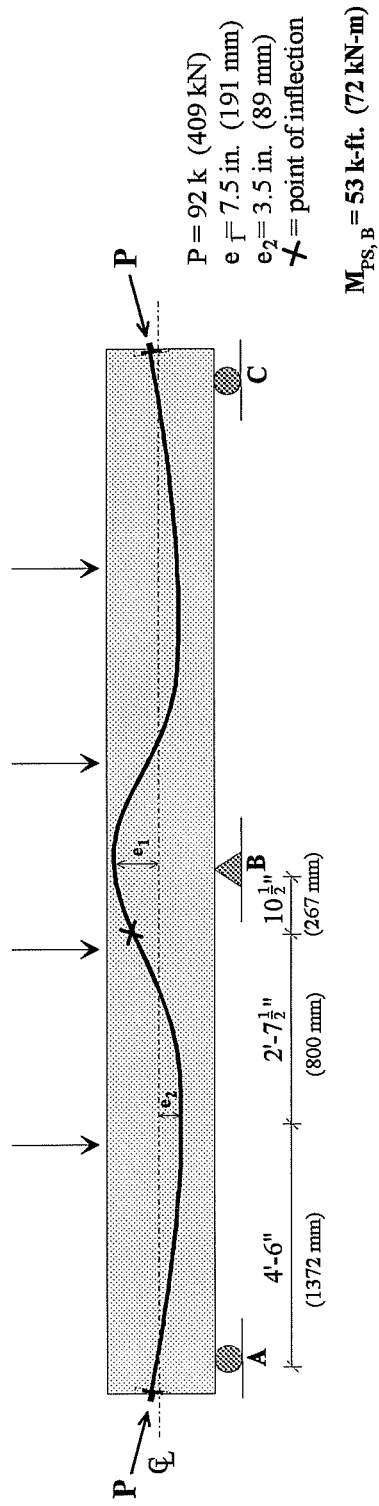


Figure 3.9 Designed vs. Built Tendon Profile for CB-PS-100S

Provisions For ↓	MODEL CB-PS-100S	PROTOTYPE	SCALE FACTOR
M+, M- & Serviceability	4- Φ 0.5" (12.7mm) strands $A_{ps} = 0.61 \text{ in.}^2$, $T = 92 \text{ k}$ (395 mm^2 , 409 kN)	4-12 Φ 0.6" (15.2mm) tendons $A_{ps} = 10.3 \text{ in.}^2$, $T = 1545 \text{ k}$ (6645 mm^2 , 6875 kN)	1:16.8, 1:16.8
V_s	5/32" dbl. stirrups @ 6" $A_v = 0.15 \text{ in.}^2/\text{ft.}$, $T_v = 10.9 \text{ k/ft.}$ (326 mm^2/m , 159 kN/m)	#5 dbl. stirrups @ 20" $A_v = 0.74 \text{ in.}^2/\text{ft.}$, $T_v = 44.6 \text{ k/ft.}$ (1575 mm^2/m , 652 kN/m)	n.a.*, 1:4.1
Side Face Crack Control (per face)	6-12-ga. wires over 8.5" $A_s = 0.052 \text{ in.}^2$ (33.5 mm^2 over 216 mm)	7-#3 bars over 33" $A_s = 0.77 \text{ in.}^2$ (497 mm^2 over 838 mm)	1:14.8 over 1:3.9
cover - sides	0.63" (15.9 mm)	2.5" (63.5 mm)	1:4
cover top & bottom	non-PS: 0.56 in. (14.3 mm) PS: 1.5 in. (38.1 mm)	non-PS: 2.25 in. (57.2 mm) PS: 6.0 in. (152 mm)	1:4 1:4

* Scaling the areas is not appropriate as the reinforcement has a different yield strength. Comparison must be made with the tensile strength, T , provided at ultimate (assuming elastic-perfectly-plastic steel behavior).

Table 3.4 Comparison of Model and Prototype Designs for CB-PS-100S

force provided in CB-PS-100S where the service limit state governed in determining required amounts of prestressing steel. The layout for CB-PU-100S is pictured in Figure 3.12.

Use 2- Φ 0.5" (12.7mm) and 1- Φ 0.375" (9.5mm) strands, $A_{ps} = 0.391 \text{ in.}^2$ (246 mm²)

Shear Design - CB-PU-100S - Shear design using the integrated design method of Section 2.5 proposes using strut & tie modelling to determine the amount of shear reinforcement required. A preliminary finite element analysis was performed and stress concentrations and patterns were plotted (Figure 3.10). From this preliminary investigation there appeared not to be considerable shear forces in the beam. It can be seen from the shear diagram in Figure 3.6 that the vertical force along the beam is minimal. In all areas except near the center support, the vertical (shear) force was less than the nominal concrete shear contribution. In these areas, minimum shear reinforcement was provided in accordance with AASHTO 9.20.3.3. The amount of shear resistance provided by this steel was then enough to carry the amount of shear force in excess of the concrete shear strength contribution near the center support. Therefore minimum shear reinforcement was used throughout.

Use Φ 5/32-in. (Φ 4.0 mm) double stirrups @ 6 in. (152 mm) throughout.

Tensile Chord Crack Control - CB-PU-100S - For this model, tensile chord crack control was provided based on the results of an elastic finite element analysis at service loads. Figure 3-11a shows the orientation of the tensile stresses in one half of the continuous beam (i.e. one span). Stresses throughout the beam were plotted in terms of $\sqrt{f'_c}$ (see Figure 3.11b). The line of the tendon is visible in this tension plot. Six elements were used above and below the tendon along the length of the span, resulting in varying sizes of elements. The stresses however, are plotted in a regular grid not according to their actual location on the member. Therefore it is necessary to refer to the finite element model to see where the stresses are actually located within the member.

It was assumed that the concrete could carry $2\sqrt{f'_c}$ ($0.17\sqrt{f'_c}$) alone. Wherever this value was exceeded, crack control steel was provided. In this case, the tensile stresses according to the finite element analysis exceeded $2\sqrt{f'_c}$ ($0.17\sqrt{f'_c}$) only over the center support. For this design, the area of steel required to control cracking was determined based on equating the tensile force in the steel under service loads to the tensile force in the concrete under service loads (Equation 2-3). Assuming that crack control steel was necessary

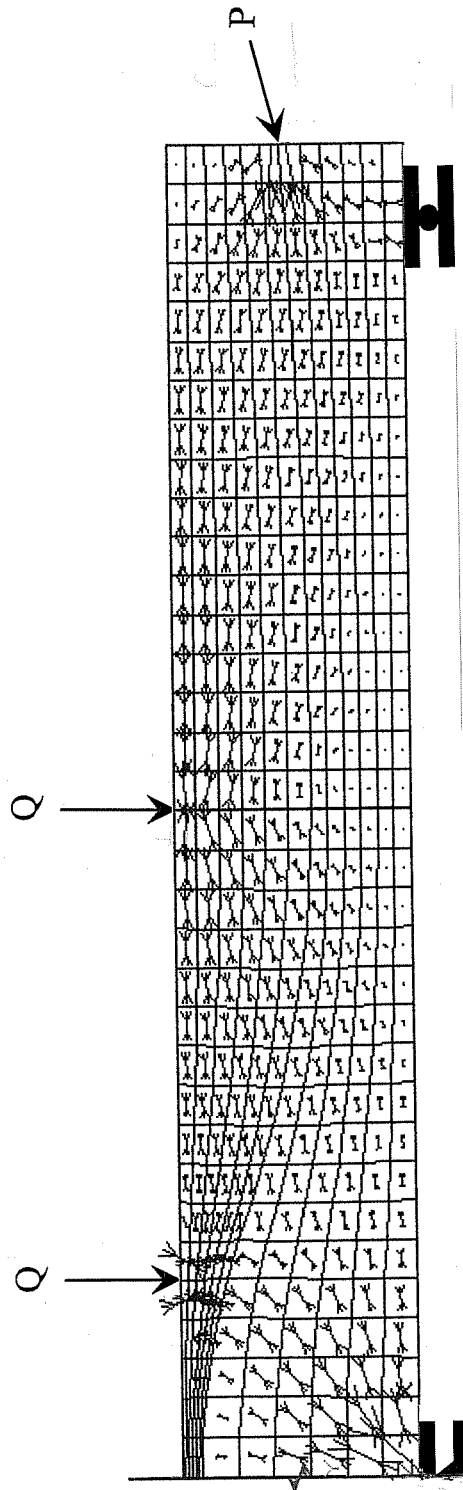


Figure 3.10 Compressive Stress Orientation in CB-PU-100S under Factored Loads for Shear Design

in elements with stresses exceeding $2\sqrt{f'_c}$ ($0.17\sqrt{f'_c}$), and assuming a service load steel stress of 36 ksi, the amount of tensile chord crack control steel required was 0.236 in.² (152 mm²). This required 6-#2 bars. 4-#2 bars were used as "cage" steel for the stirrups. For better distribution of the steel area, the rest of the required steel area was provided by 4 wires of 5/32-in. (4.0mm) diameter (rather than 2-#2 bars).

Use 4-#2 bars and 4 - Φ 5/32-in. (Φ 4.0mm) wires, $A_s = 0.253$ in.², distributed evenly

Side Face Crack Control - CB-PU-100S - Side face crack control steel was provided in the same way as for CB-PS-100S (Section 3.4.1.2) as the depth of the beam and the concrete cover were the same.

Use 12-gauge wires (Φ 2.7mm) @ 1.5 in. (38.1mm) over entire sides

Concrete Cover - CB-PU-100S - The concrete cover is the same for this model as it was for CB-PS-100S in Section 3.4.1.2. There was a 0.63 in. (15.9 mm) side cover and a 0.56 in. (14.3 mm) cover top and bottom. In addition, a minimum distance of 1.5 in. (38.1 mm) from the center of the strand to the extreme concrete fiber was required. This was only restrictive over the center support.

Anchor Zones - CB-PU-100S - Anchor zone design followed the guidelines of NCHRP Report No. 356.[24] Seven 5/32 in. (4.0mm) diameter double stirrups spaced at 3 in. (76 mm) were required. For simplicity however, the same anchor zone design was used here as for model CB-PS-100S. Conservative design for this area should have no effect on the overall behavior of the beam.

Use 10 Φ 5/32" (Φ 4.0mm) wire double stirrups @ 2 in. (50.8mm)

Fatigue - CB-PU-100S - The problem of fatigue was checked for this design in the same manner as it was checked for CB-PS-100S. The stress ranges at B and D were 7 ksi (48.3 MPa) and 1 ksi (6.9 MPa) respectively. Wollmann's recommendation of a maximum allowable stress range of 14.5 ksi was satisfied. As the stress range was well below the recommended allowable limit, the non-prestressed steel was assumed to have adequate fatigue resistance as well.

Comparison to prototype - CB-PU-100S - In summary, the model design provisions are listed in Table 3.5 with the corresponding full scale prototype designs.

CB-PU-100S

100% Prestress for Ultimate Tensile Force

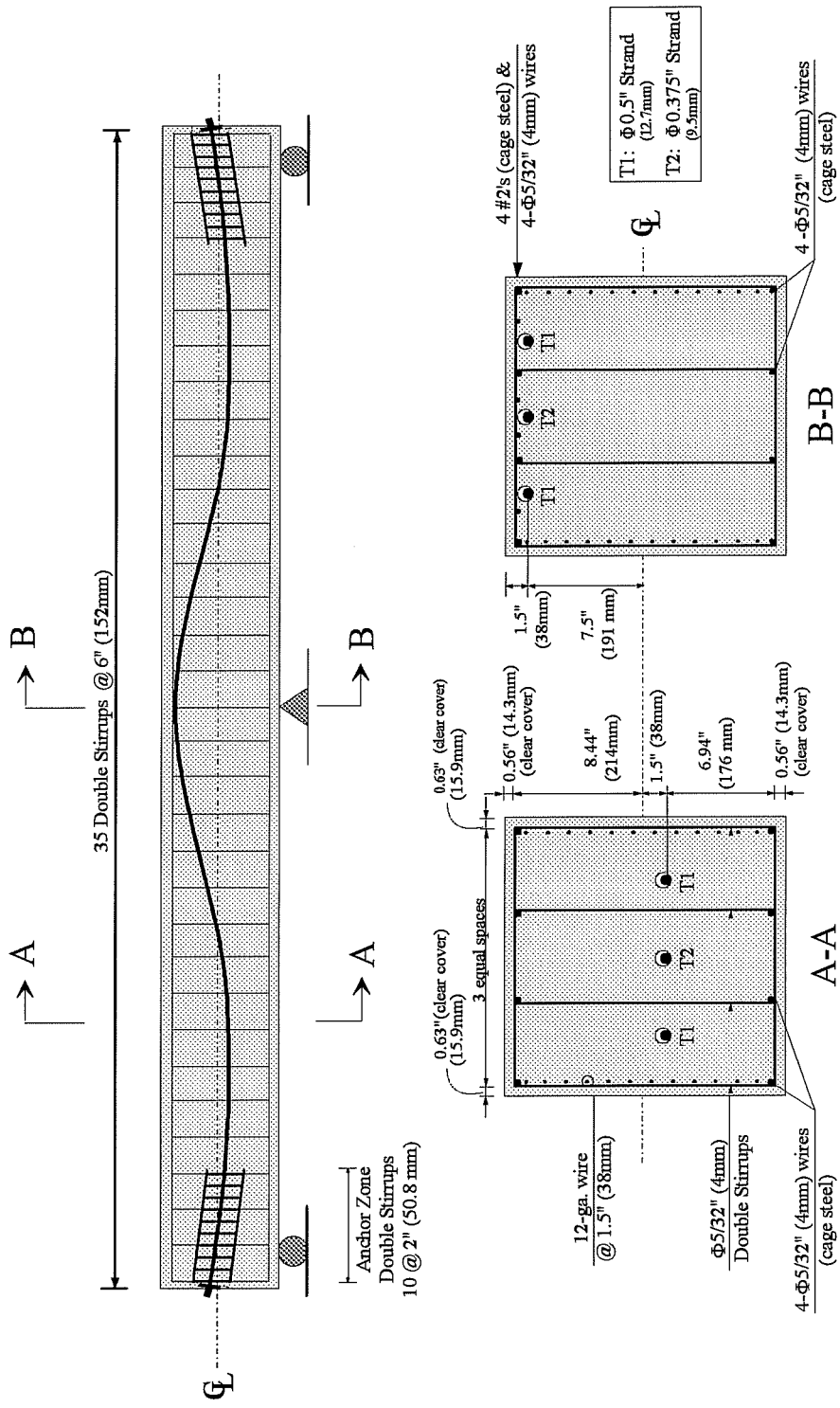


Figure 3.12 Design for CB-PU-100S - 100% Prestress for Ultimate Tensile Force

Provisions For ↓	MODEL CB-PU-100S	PROTOTYPE*
M+, M-	2- Φ 0.5" & 1- Φ 0.375" Strands $A_{ps} = 0.391 \text{ in.}^2$, T = 59 k (252 mm ² , 261 kN)	2-12 Φ 0.6" and 1-7 Φ 0.6" Tendons $A_{ps} = 6.7 \text{ in.}^2$, T = 100 k (4300 mm ² , 4450 kN)
V _s	5/32" dbl. stirrups @ 6" $A_v = 0.15 \text{ in.}^2/\text{ft.}$, T _v = 10.9 k/ft. (326 mm ² /m, 159 kN/m)	#5 dbl. stirrups @ 20" $A_v = 0.74 \text{ in.}^2/\text{ft.}$, T = 44.6 k/ft. (1575 mm ² /m, 652 kN/m)
Tensile Chord Crack Control M- Region	4-#2 bars & 4- Φ 5/32" wires evenly distributed $A_s = 0.253 \text{ in.}^2$ (163 mm ²)	4-#8 bars and 4-#5 bars evenly distributed $A_s = 4.4 \text{ in.}^2$ (2839 mm ²)
Tensile Chord Crack Control M+ Region	no supplementary steel required	no supplementary steel required
Side Face Crack Control (per face)	6-12-ga. wires over 8.5" $A_s = 0.052 \text{ in.}^2$ (33.5 mm ² over 216 mm)	7-#3 bars over 33" $A_s = 0.77 \text{ in.}^2$ (497 mm ² over 838 mm)
cover - sides	0.63" (15.9 mm)	2.5" (63.5 mm)
cover top & bottom	non-PS: 0.56 in. (14.3 mm) PS: 1.5 in. (38.1 mm)	non-PS: 2.25 in. (57.2 mm) PS: 6.0 in. (152 mm)

* Full scale assuming $f'_c = 60 \text{ ksi}$ (414 MPa) and $f'_{ps} = 270 \text{ ksi}$ (1862 MPa)

Table 3.5 Model and Corresponding Prototype Designs for CB-PU-100S

Prediction of Cracking, Yield and Ultimate Moments - CB-PU-100S - Recognizing the actual concrete strength at testing, first cracking was predicted to occur with applied point loads of 26.9k (119.7kN), or an applied dead plus live load moment of -92.7 k-ft. (-126 kN-m). First yielding was predicted to occur in the non-prestressed steel at mid-span with an applied moment of 71 k-ft (96 kN-m) ($Q_{elastic} = 45\text{k}$, 200kN). A simultaneous yielding of the non-prestressed and prestressed reinforcement over the center support and of the prestressed reinforcement at the mid-spans was predicted to occur shortly after with moments of -147 k-ft. (-199 kN-m) and 89 k-ft. (121 kN-m), respectively ($Q_{elastic} = 56\text{k}$, 249kN). The formation of a full mechanism, with hinges formed over the center support and at the two mid-spans, was predicted to occur at applied point loads of 70k (312kN) (lower bound equilibrium solution).

3.3.2.2 71% Prestress for Factored Loads - CB-PU-71S

The fourth model is referred to as CB-PU-71S. This stands for the **C**ontinuous **B**eam **P**restressed based on **U**ltimate loads where **71%** of the ultimate tensile force is carried by the prestressing **S**trand. The remaining 29% of the ultimate tensile force is carried by the non-prestressed reinforcement.

Flexure Design - CB-PU-71S - Flexure design was based on the factored moment diagrams used for the conventionally reinforced beam (Figure 3.3). The amount of prestressing steel to be used was that required to resist the maximum factored moment at the critical sections, over the center support and near the mid spans. An ideal layout of the tendon was determined so that approximately 70% of the ultimate moment would be carried (resisted) by prestressing steel and 30% of the ultimate load would be carried (resisted) by non-prestressed steel. This layout was determined by iteration using a spreadsheet. No moment redistribution was considered in this design. Using prestressing strand with $f_{su} = 270$ ksi (1860 MPa), 0.252 in.² (6.4 mm²) of this strand were required. This corresponds to a required ultimate tensile force of 68k (303kN) for the prestressing reinforcement. Considering available strand sizes with $f_{su} = 270$ ksi (1860 MPa), 3- Φ 0.375" (9.5mm) strands were used having a total area of 0.255 in.² (165 mm²). This provided an ultimate tensile force of 69k (307kN). This is only 42% of the ultimate tensile force provided in CB-PS-100S where the service limit state governed in determining required amounts of prestressing steel. The layout is shown in Figure 3.15.

Use 3- Φ 0.375" (Φ 9.52mm) strands, $A_{ps} = 0.255$ in.² (165 mm²)

An amount of non-prestressed reinforcement to carry the remaining 30% of the ultimate moment was then calculated. Considering the contribution of the side face crack control steel to the section's ultimate strength, 0.32 in.² (206 mm²) of non-prestressed reinforcement was required over the center support. The #2 bars for this design had been assumed to have a yield strength of 73 ksi (503 Mpa). The actual yield strength was 75ksi. This requirement was satisfied by using 4-#2 bars and 7- Φ 5/32" (4.0 mm) wires in addition to accounting for the tensile strength contribution of 3-12 gage side face crack control wires on each face.

Use 4-#2 bars and 7- Φ 5/32" (Φ 4.0 mm) wires in negative moment region

$A_s = 0.31$ in.² (200 mm²)

In the positive moment region, 0.21 in.^2 (135 mm^2) steel was required. Again considering the contribution of 3 side face crack control wires on each face to the ultimate strength, an additional 10- $\Phi 5/32$ " (4.0 mm) wires were required.

Use 10- $\Phi 5/32$ " ($\Phi 4.0 \text{ mm}$) wires in positive moment regions

$$\underline{A_s = 0.21 \text{ in.}^2 (135 \text{ mm}^2)}$$

Shear Design - CB-PU-71S - A preliminary finite element analysis was performed and stress concentrations and patterns were plotted (Figure 3.13) to determine the usefulness of strut & tie modelling for this design. From this preliminary investigation there appeared not to be considerable shear forces in the beam. From the shear diagram in Figure 3.6, one can see the only appreciable shear force is near the center support. Strut & tie modelling did not appear to be advantageous in this design. Therefore shear reinforcement was determined in a traditional manner. In all areas except near the center support, the vertical (shear) force was less than the concrete shear strength of 46k (205kN). In these areas, minimum shear reinforcement was provided. A slightly closer spacing of the same size stirrups was then required to carry the larger shear force of 65k (289kN) near the center support (Appendix A).

Use $\Phi 5/32$ -in. ($\Phi 4\text{mm}$) double stirrups @ 4.5 in. (114mm)

symmetrically out 15 in. (381mm) from center

Use $\Phi 5/32$ -in. ($\Phi 4\text{mm}$) double stirrups @ 6 in. (152mm) elsewhere

Tensile Chord Crack Control - CB-PU-71S - Tensile chord crack control was provided based on the results of an elastic finite element analysis at service loads in a similar manner to that of CB-PU-100S (Section 3.3.2.1). Figures 3.14a & b show the tensile stress vectors and concrete tensile stresses in each element, respectively. In this case, the tensile stresses according to the finite element analysis exceeded $2\sqrt{f'_c}$ ($0.17\sqrt{f'_c}$) over the center support ($7\sqrt{f'_c}$ ($0.58\sqrt{f'_c}$)) as well as under the point loads near the mid-spans ($4\sqrt{f'_c}$ ($0.33\sqrt{f'_c}$)). Assuming a crack covering the area of the elements with stresses exceeding $2\sqrt{f'_c}$ ($0.17\sqrt{f'_c}$), and assuming a service load steel stress of 36 ksi, the amount of tensile chord crack control steel required over the center support was 0.291 in.^2 (188 mm^2). However from the flexure design of 29% non-prestressed reinforcement for ultimate loads, 0.362 in.^2 (227 mm^2) was provided over the center support, 0.33 in.^2 (213 mm^2) of which was in the "cracked" area. Therefore no supplementary tensile chord crack control steel was added. Under the point load near mid-span, the excess stress of $2\sqrt{f'_c}$ ($0.17\sqrt{f'_c}$) required

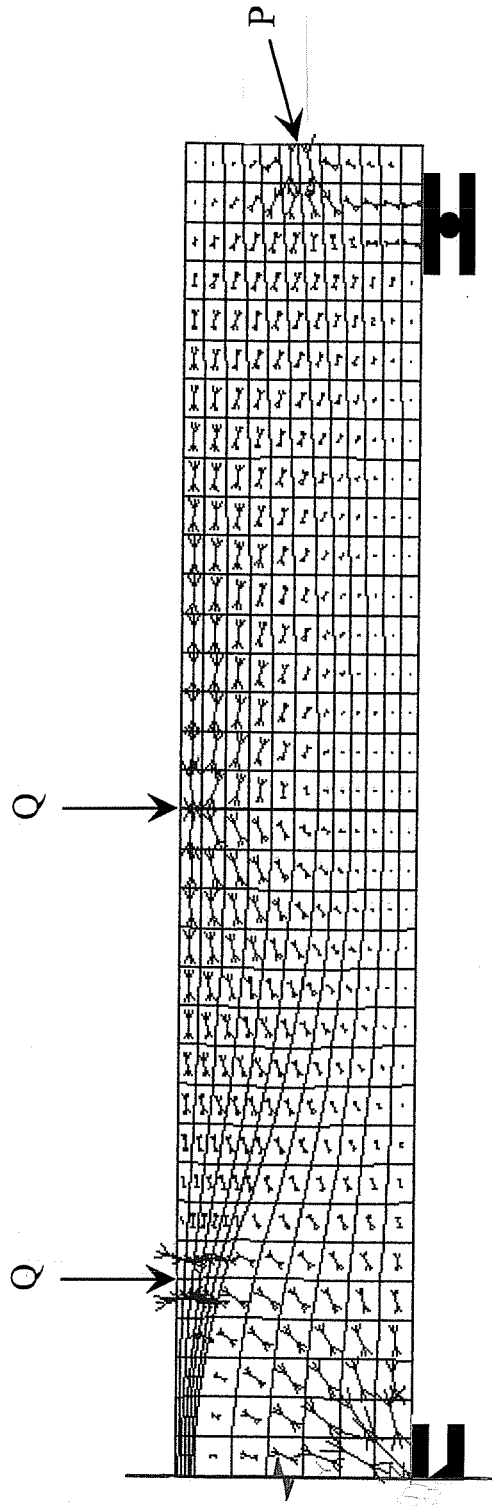


Figure 3.13 Compressive Stress Orientation in CB-PU-71S under Factored Loads for Shear Design

0.19 in.² (125 mm²) of crack control steel. This section was reinforced with 0.244 in.² (135 mm²) of non-prestressed steel to carry 29% of the ultimate tensile force. There existed 0.21 in.² (135 mm²) of this steel in the assumed "cracked" section. Therefore no supplementary crack control steel was necessary.

Side Face Crack Control - CB-PU-71S - Side face crack control steel was provided in the same way as for CB-PS-100S (Section 3.4.1.2). The depth of the beam and the concrete cover were the same.

Use 12-gauge wires (Φ 2.7mm) @ 1.5 in. (38mm) over entire sides

Concrete Cover - CB-PU-71S - The concrete cover is the same for this model as it was for CB-PS-100S in Section 3.3.1.2.

Anchor Zones - CB-PU-71S - Anchor zone design followed the guidelines of NCHRP Report No. 356.[24] As the prestressing force was reduced in comparison to the last model, the maximum bursting force was less and therefore the bursting force was less. Rather than designing exactly for the loads expected, a conservative design similar to that for CB-PS-100S and CB-PU-100S was used. Conservative design for this area should have no effect on the overall behavior of the beam.

Use 10- Φ 5/32 in. (Φ 4.0mm) wire double stirrups @ 2 in. (50.8mm)

Fatigue - CB-PU-71S - The problem of fatigue was checked for this design in the same manner as it was checked for CB-PS-100S and CB-PU-100S. The stress ranges at B and D were 27 ksi (186 MPa) and 1 ksi (6.9 MPa) respectively. Over the center support (at B), this design does not satisfy Wollmann's recommendation of a maximum allowable stress range of 14.5 ksi for bonded post-tensioned strand.[65] The calculated stress range for the non-prestressed steel at B was 28 ksi (193 MPa). According to AASHTO provision 8.16.8.3 (Equation 2-4 in this thesis), the maximum allowable stress range is 20.1 ksi (139 MPa).

In order to satisfy design criteria, either more non-prestressed steel would need to be added or the design would need to be changed. As CB-PU-100S satisfied fatigue resistance criteria, a design between 71% and 100% prestress reinforcing based on ultimate tensile force might be an efficient and sufficient design.

Comparison to prototype - CB-PU-71S - In summary, the model design provisions are listed in Table 3.6 with the corresponding full scale prototype designs.

CB-PU-71S

71% Prestress, 29% Non-prestress for Ultimate Tensile Force

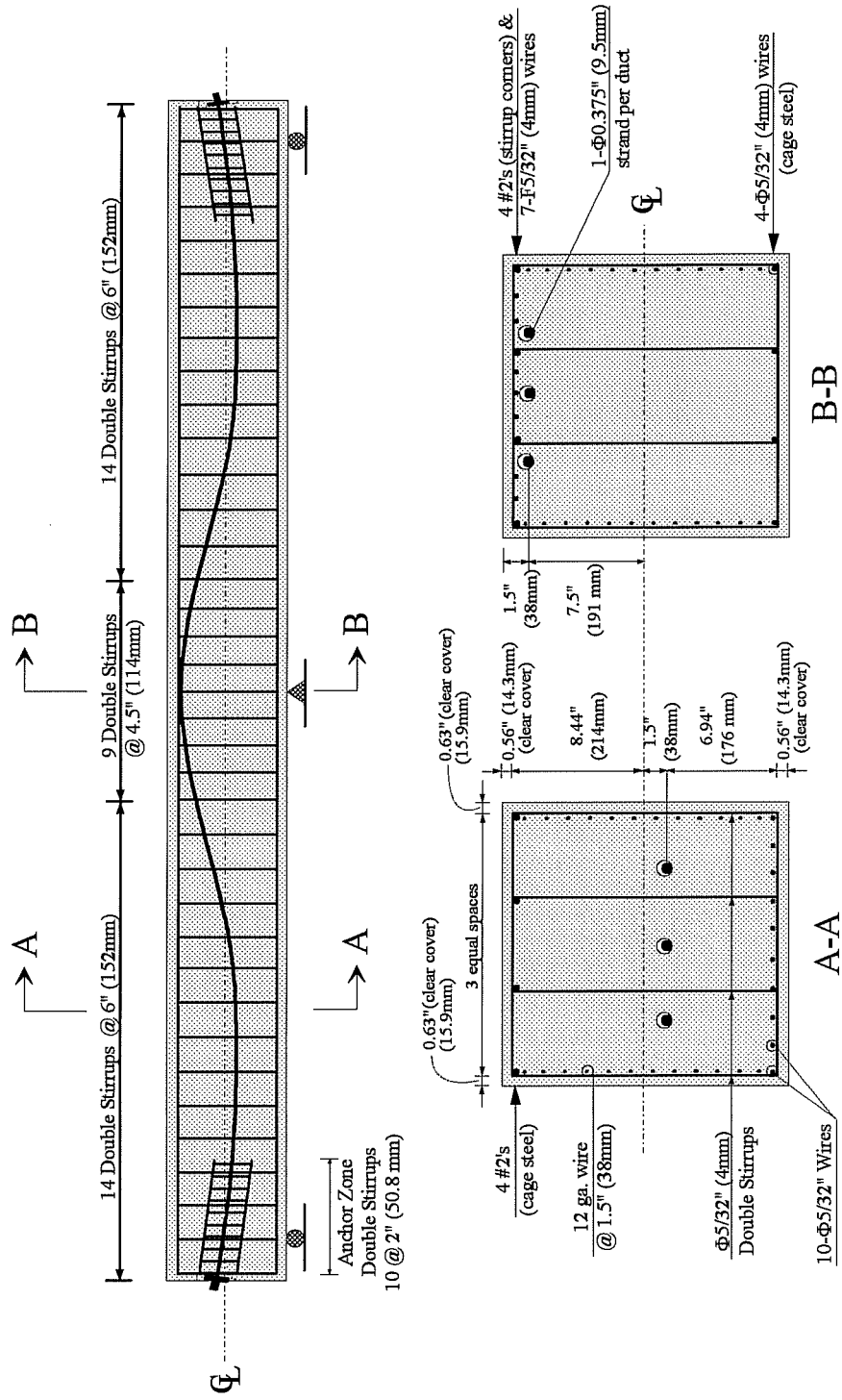


Figure 3.15 Design for CB-PU-71S - 71% Prestress for Ultimate Tensile Force

Provisions For ↓	MODEL CB-PU-71S	PROTOTYPE*
M+, M-	3- Φ 0.375" Strands $A_{ps} = 0.255 \text{ in.}^2$, $T = 38 \text{ k}$ (165 mm ² , 170 kN)	3-7 Φ 0.6" Tendons $A_{ps} = 4.5 \text{ in.}^2$, $T = 677 \text{ k}$ (2913 mm ² , 3014 kN)
Vs symmetrically 15" (381mm) out from center	5/32" dbl. stirrups @ 4.5" $A_v = 0.20 \text{ in.}^2/\text{ft.}$, $T_v = 14.5 \text{ k/ft.}$ (433 mm ² /m, 212 kN/m)	#5 dbl. stirrups @ 15" $A_v = 0.99 \text{ in.}^2/\text{ft.}$, $T_v = 59.5 \text{ k/ft.}$ (2096 mm ² /m, 869 kN/m)
V _v - else	5/32" dbl. stirrups @ 6" $A_v = 0.15 \text{ in.}^2/\text{ft.}$, $T_v = 10.9 \text{ k/ft.}$ (326 mm ² /m, 159 kN/m)	#5 dbl. stirrups @ 20" $A_v = 0.74 \text{ in.}^2/\text{ft.}$, $T_v = 44.6 \text{ k/ft.}$ (1575 mm ² /m, 652 kN/m)
Tensile Chord Crack Control M- Region	4-#2 bars and 7- Φ 5/32" wires evenly distributed $A_s = 0.31 \text{ in.}^2$ (200 mm ²)	4-#8 bars and 7-#5 bars evenly distributed $A_s = 5.33 \text{ in.}^2$ (3439 mm ²)
Tensile Chord Crack Control M+ Region	10- Φ 5/32" wires evenly distributed $A_s = 0.19 \text{ in.}^2$ (124 mm ²)	10-#5 bars evenly distributed $A_s = 3.1 \text{ in.}^2$ (2000 mm ²)
Side Face Crack Control (per face)	6 12-ga. wires over 8.5" $A_s = 0.052 \text{ in.}^2$ (33.5 mm ² over 216 mm)	7-#3 bars over 33" $A_s = 0.77 \text{ in.}^2$ (497 mm ² over 838 mm)
cover - sides	0.63" (15.9 mm)	2.5" (63.5 mm)
cover top & bottom	non-PS: 0.56 in. (14.3 mm) PS: 1.5 in. (38.1 mm)	non-PS: 2.25 in. (57.2 mm) PS: 6.0 in. (152 mm)

* Full Scale assuming $f_y = 60 \text{ ksi}$ (414 MPa) and $f_{ps} = 270 \text{ ksi}$ (1862 MPa)

Table 3.6 Model and Corresponding Prototype Designs for CB-PU-71S

Prediction of Cracking, Yield and Ultimate Moments - CB-PU-71S - Recognizing the actual concrete strength at testing, first cracking was predicted to occur with applied point loads of 21.9k (97.5kN), or an applied dead plus live load moment of -74.8 k-ft. (-101 kN-m). First yielding was predicted to occur simultaneously in the non-prestressed steel in both critical regions with applied moments of -116 k-ft. (-157 kN-m) over the center support and 67 k-ft. (91 kN-m) at the mid-spans ($Q_{elastic} = 43\text{k}, 191\text{kN}$).

Yielding of the prestressed steel was predicted to begin at applied moments of -122 k-ft. (-165 kN-m) over the center support and 70 k-ft. (95 kN-m) at the mid-spans ($Q_{elastic} = 45k, 200 \text{ kN}$). The formation of a full mechanism, with hinges formed over the center support and at the two mid-spans, was predicted to occur at applied point loads of 56k (249kN) (lower bound equilibrium solution).

3.4 Materials

3.4.1 Concrete

A modified standard 5000 psi (34.47 MPa) concrete mix from Capitol Aggregate in Austin, TX was used for the construction of the test models (Standard mix 207R - Modified). This mix was a "high early strength" mix so as to decrease the wait between casting and testing. The mix proportions per cubic yard were:

Cement (Type II)	465 lbs	(827 kg*)
3/8" Uniform Aggregate	1463 lbs	(2601 kg)
Sand	1631 lbs	(2900 kg)
Water	200 lbs +	(356 kg)
Retarder (300R)	25 oz.	(2.78 kg)
Super Plasticizer (Rheobuild)	45 oz.	(5.00 kg)
		(* these units are per cubic meter)

A slump of 5" was requested upon delivery. Additional super plasticizer was added on site to improve the workability and ease the placement of the concrete. Cylinders were cast with each model and 2-3 cylinders were typically tested on days 1, 3, 5, 7, 14, 21, and 28. Concrete properties including the strengths on days of stressing and testing as well as the 28-day strengths for each model are reported in Table 3.7.

3.4.2 Non-prestressed Reinforcement

Four sizes of non-prestressed reinforcement, mentioned in Section 3.2.1.2 were used in the fabrication of the test models. The #3 bars (9.5 mm dia.) from a local manufacturer were standard Grade 60 deformed reinforcing bars and had an average yield stress of 64.5 ksi (445 MPa) as shown in Figure 3.16. The

deformed #2 bars (Φ -6mm) were from a manufacturer in Sweden. They had a typical yield strength of 75 ksi (517 MPa) shown in Figure 3.17. The 5/32" (4.0mm) diameter wire was not deformed and had been straightened and annealed. It had a typical yield strength of 71 ksi (490 MPa) (see Figure 3.18). The last type of non-prestressed reinforcement used was 12 ga. wire (Φ -2.7mm). This undeformed wire was straightened in the laboratory and had a typical yield strength of 38 ksi (262 MPa) as shown in Figure 3.19.

SPECIMEN	SLUMP	WATER-CEMENT RATIO	STRENGTH AT STRESSING	STRENGTH AT TESTING	28-DAY STRENGTH
CB-RU	4.5 in. (114 mm)	0.37	n.a.	6235 psi (43.00 MPa)	5570* psi (38.41 MPa)
CB-PS-100S	5 in. (127 mm)	0.41	7000 psi (48.28 MPa)	7000 psi (48.28 MPa)	6160 psi (42.48 MPa)
CB-PU-100S	2 in. (50.8 mm)	0.42	7150 psi (49.31 MPa)	7170** psi (49.45 MPa)	6830** psi (47.10 MPa)
CB-PU-71S	4.5 in. (114 mm)	0.35	6990** psi (48.21 MPa)	7190 psi (49.59 MPa)	7300 psi (50.34 MPa)

* 29-day Strength

** Interpolation

Table 3.7 Concrete Properties

3.4.3 Prestressing Strand

The prestressing strand used was seven-wire Grade 270 strand. The 1/2" (12.7 mm) diameter strand was from Florida Wire & Cable and had an ultimate tensile strength of 276.1 ksi (1904 MPa) (Figure 3.20). The 3/8" (9.5 mm) diameter strand was from Austin Prestress and had an ultimate tensile strength of 281.1 ksi (1939 MPa) (Figure 3.21).

3.4.4 Post-tensioning Duct

According to provision 9.25.4.2 of the AASHTO Bridge Specifications, a post tensioning duct for a single strand must have a diameter at least 1/4" larger than the nominal diameter of the strand. For the models, single strands were used and largest diameter strand used was 1/2" (12.7mm). Therefore a 3/4" (19mm) diameter duct was required. Rigid duct was unattainable in this small size and therefore flexible electrical conduit was used.

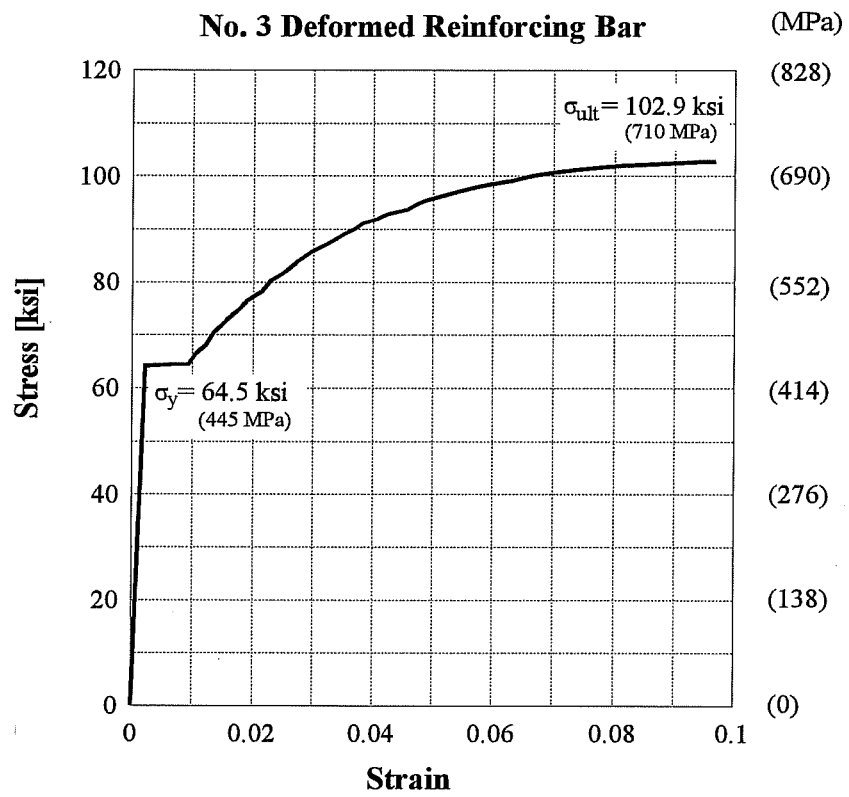


Figure 3.16 Stress-Strain Curve for No. 3 Deformed Reinforcement

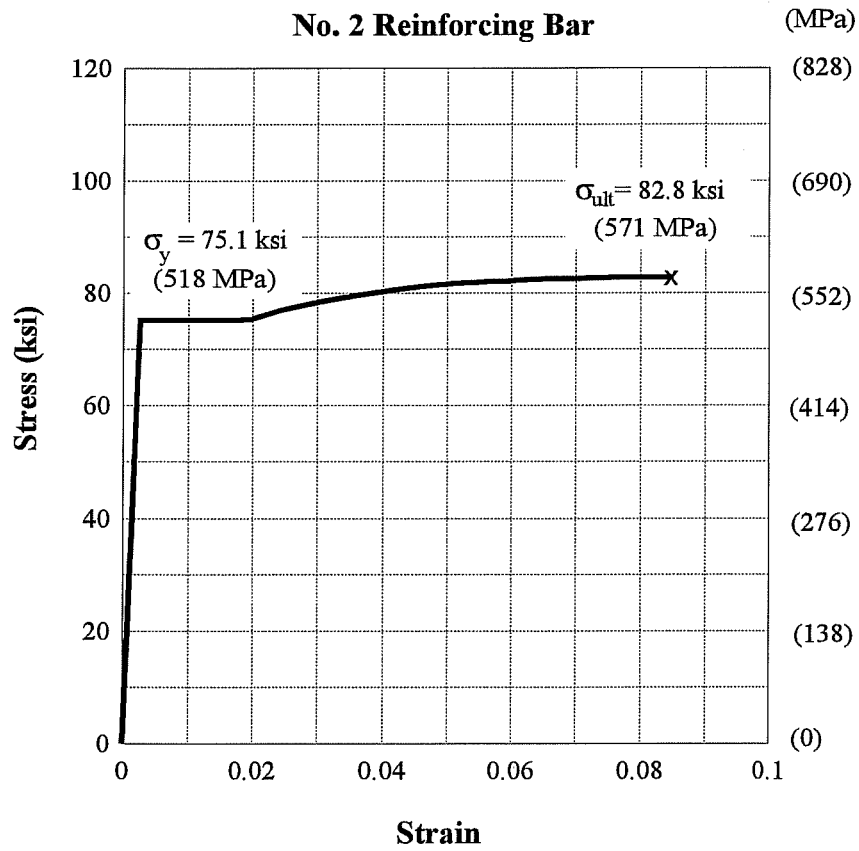


Figure 3.17 Stress-Strain Curve for No. 2 Deformed Reinforcement from Sweden.

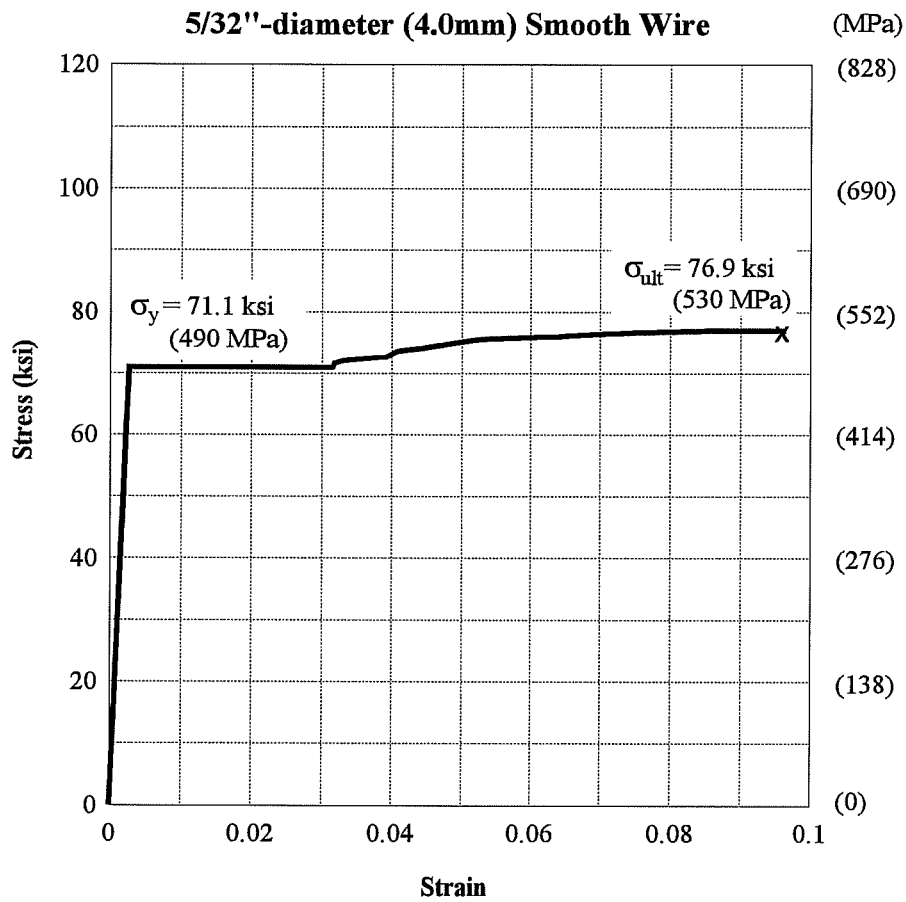


Figure 3.18 Stress-Strain Curve for the Φ 5/32" (4.0 mm) Smooth Wire Reinforcement

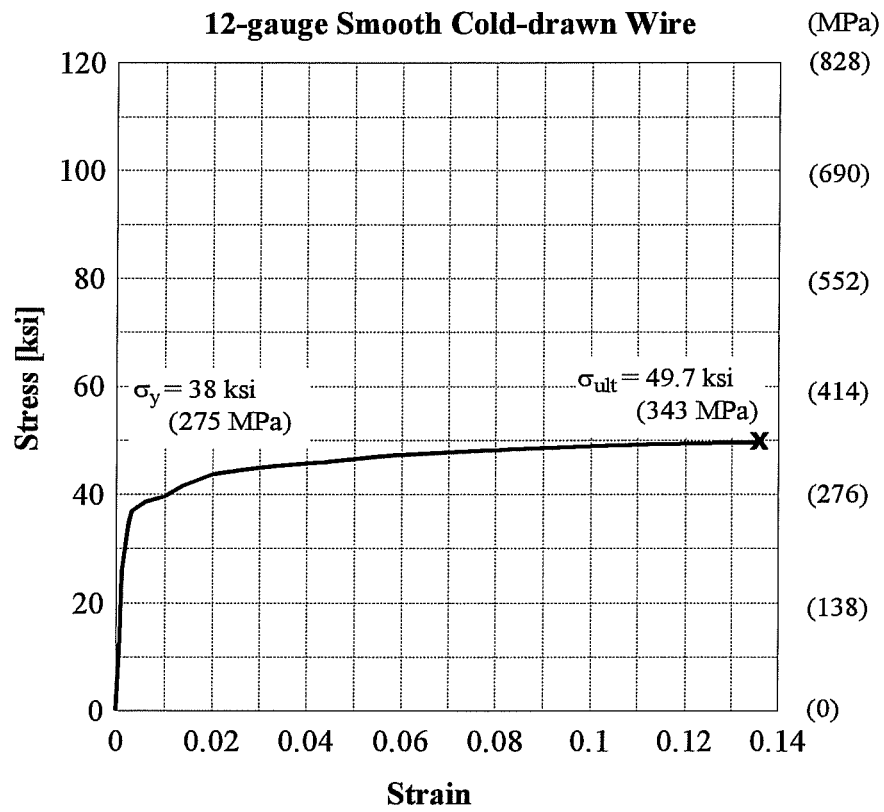


Figure 3.19 Stress-Strain Curve for 12-gauge Smooth Cold-drawn Wire

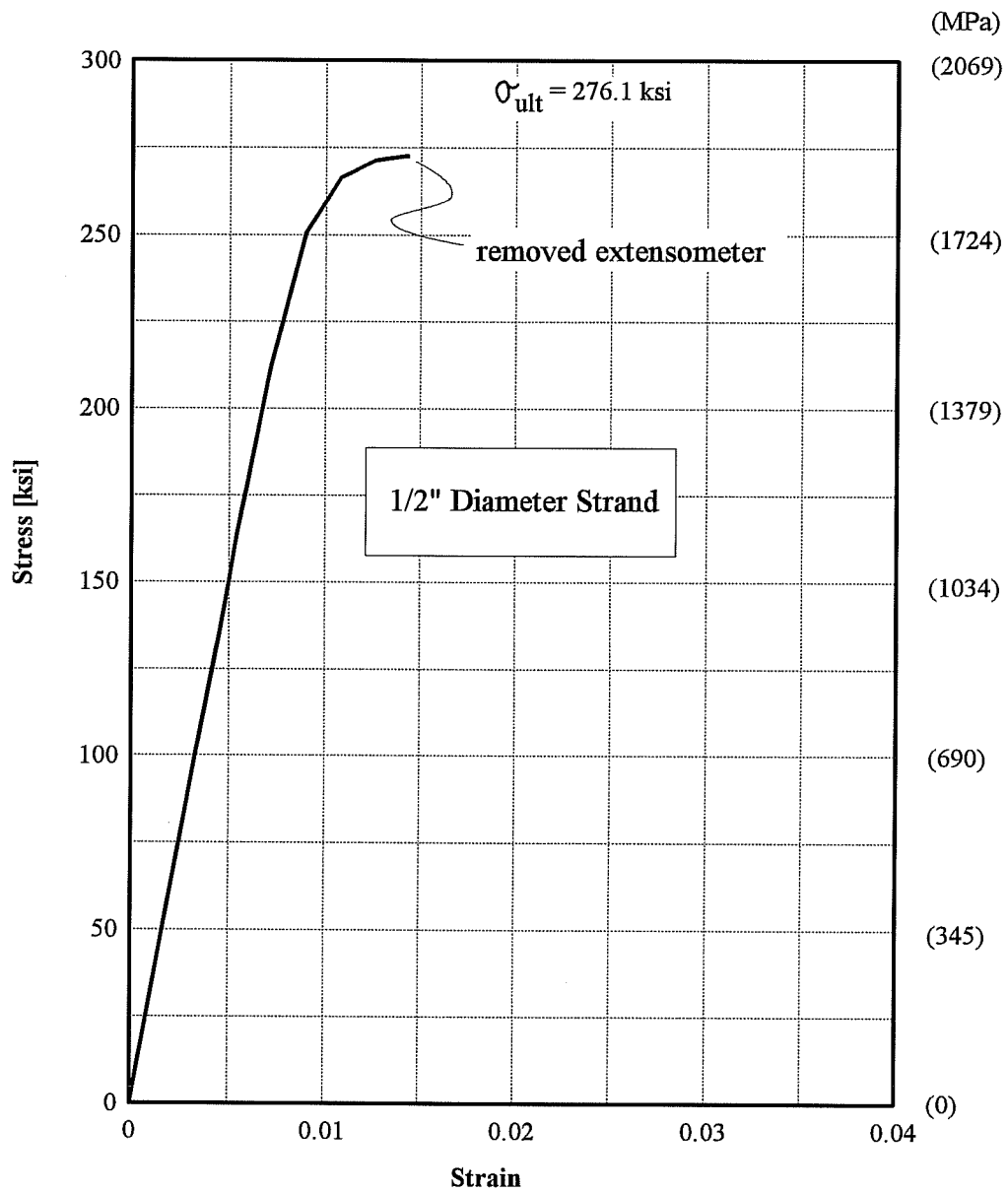


Figure 3.20 Stress-Strain Curve for 1/2 in. (12.7 mm) Diameter Prestressing Strand. [17]

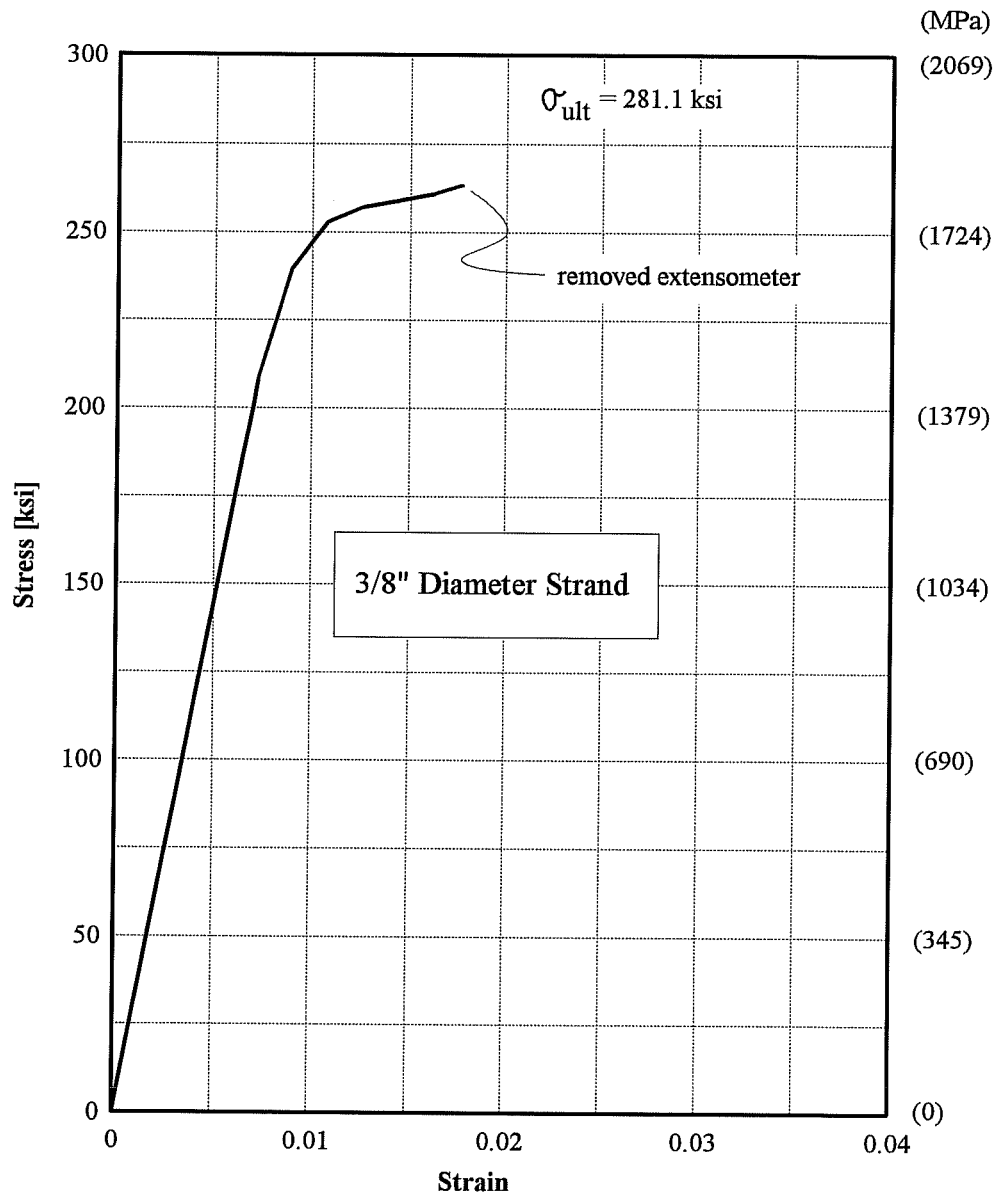


Figure 3.21 Stress-Strain Curve for 3/8 in. (9.5 mm) Prestressing Strand [17]

3.4.5 Grout

The grout used for bonding the post-tensioned strand was in compliance with AASHTO Bridge Specifications.[9] It had an expansion of 2-4% and a water-cement ratio of 0.44. For a typical batch of 0.42 ft³ (0.012 m³), the mix proportions were:

Type I Portland Cement	34.3 lbs	(15.6 kg)
Water	1.8 gal.	(6.8 L)
Interplast	0.31 lbs	(0.14 kg)

To determine cube strength, 6-2" (50.8 mm) cubes were made with each batch and were tested on the first day of testing. These values are reported in Table 3.8.

SPECIMEN	GROUT STRENGTH AT TESTING	
	Batch 1	Batch 2
CB-PS-100S	2600 psi (17.93 MPa)	2725 psi (18.79 MPa)
CB-PU-100S	3070 psi (21.17 MPa)	(no 2nd batch)
CB-PU-71S	1950 psi * (13.45 MPa)	2240 psi * (15.45 MPa)

Table 3.8 Grout Compressive Strengths

3.4.6 Anchorage Hardware

Anchorage hardware consisted of individual anchor plates and threaded chucks with wedges for each strand at each end. The plates were 1" (25.4mm) thick and 3" x 4.25" (76.2mm x 108mm) in area. Calculations for these dimensions are found in Appendix A. Threaded chucks were used to minimize seating losses and help in determining accurate stressing levels (see stressing procedure in Section 3.4.5).

3.5 Fabrication

3.5.1 Reinforcing Cage and Strain Gages

All reinforcing steel was received as straight bars or wires with the exception of the 12-gauge wire, which was purchased in a coil and straightened by hand at the laboratory. Stirrups were bent by hand around small studs welded to a steel plate at appropriate distances. Before tying reinforcing cages together, strain gages were applied to a number of straight bars and wires, stirrups, and prestressing strand (see Section 3.6.3.2). The gages were applied to a smoothed surface on the steel and were appropriately covered with waterproofing material. Resting on sawhorses, the reinforcing cages were then securely tied together with nylon cable ties (Figure 3.22). When placed in the formwork, the cage was supported by chair lifts providing the 0.63 in. (15.9mm) cover for the bottom. Proper side cover was ensured by tying 0.56 in. (14.2mm) thick sections of PVC pipe (0.75"-1.5"-diameter, 19.1mm-38.1mm) to the sides of the cage.



Figure 3.22 Fabrication of Reinforcing Cage

3.5.2 Post-tensioning Duct

For the models requiring post-tensioning, the post-tensioning duct was placed after the cage was in place in the formwork. First the strand was placed in the ducts. The ducts were then secured in the proper profile by tying them to the cage steel as well as tying them to braces across the top of the forms. Strand was placed in the ducts before casting in an effort to preserve the gages placed on the strand as well as avoid any difficulties in threading the strand through once the duct profile was cast (see Figure 3.23). For grouting, holes were pre-drilled in the duct at the ends and at the center and 0.5 in. (12.7mm) diameter polyethylene tubing was secured around these holes.

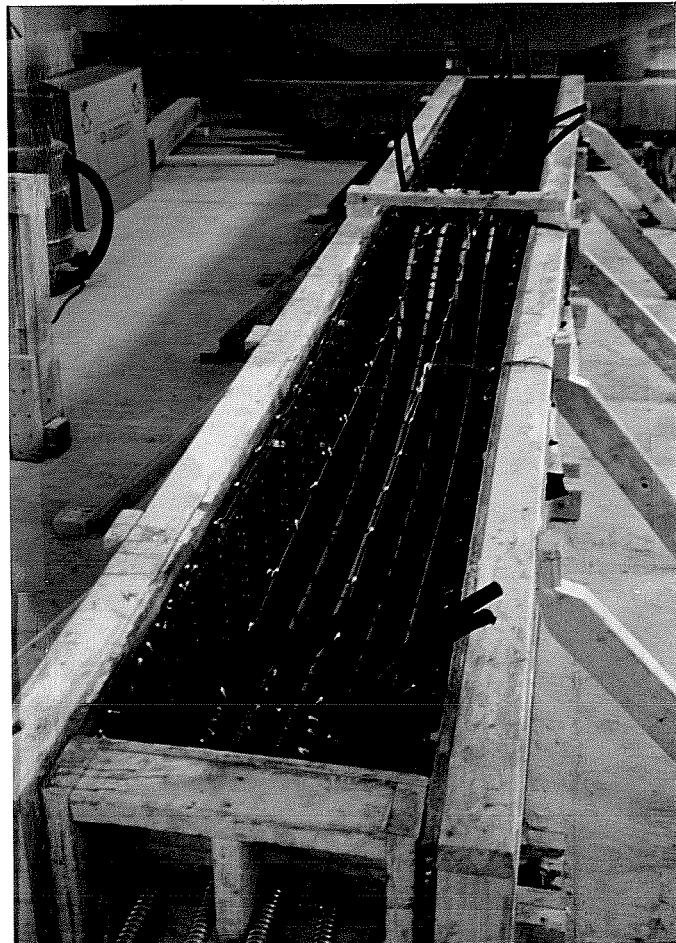


Figure 3.23 Post-Tensioning Duct Secured in Formwork before Placement of Concrete

3.5.3 Concrete Placing and Curing

The models were cast upright. Concrete was placed for each model over a one hour period in an afternoon. The concrete was placed in three layers using a hopper suspended on a crane from above (Figure 3.24). Each layer was well consolidated with internal vibrators. Concrete cylinders were cast simultaneously. The models were screeded and then finished with hand trowels. When the surface had set (typically 5 hours after placement), wet burlap was placed on top of the beam and the entire beam was then covered with plastic. The burlap and sides of the forms were then re-wetted when necessary to keep the burlap moist. Forms were typically stripped after 3-4 days and curing was continued for an additional 3-4 days.

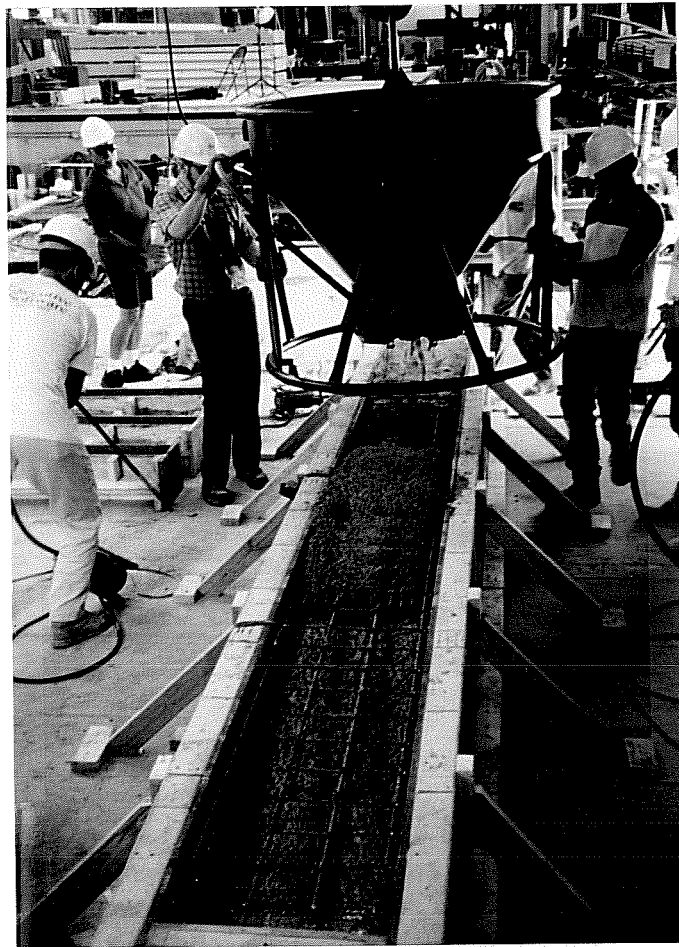


Figure 3.24 Placement of Concrete

3.5.4 Placement of Model in Testing Frame

The models were then ready to be placed in the testing frame on the supports. The models were placed on hydrostone on top of plates on a pin or roller. The strain gages as well as load cells and pressure transducers for the loading rams were then attached to a data acquisition system (see Test Set-up, Section 3.6).

3.5.5 Application of Dead Load Blocks

Dead load blocks amounting to three times the weight of the model being tested (see Section 3.2.3) were applied. In an effort to distribute the extra dead load evenly over the beam, to represent a uniform dead load, three blocks each weighing ~380 lbs (173 kg) were hung from 6 points on each span, ~13 in. (330mm) apart (Figure 3.25). At each spot, two blocks were balanced hanging on a wire cable passing over the top of the beam and one block was hung from underneath the beam on an eye-hook screwed into a cast-in-place lift insert (Figure 3.26). Steel blocks were then distributed evenly over each pair of balanced blocks to bring the total dead load up to the required 1/16 of the prototype for accurate modelling.

3.5.6 Post-tensioning Procedure

With the dead load in place, post-tensioning was performed. Each strand was tensioned using a hydraulic ram (Figures 3.27 and 3.28). Each strand was initially stressed to an amount 15% higher than the amount desired for service load stresses (150 ksi, 1034 MPa). This was in order to reduce the friction losses along the draped tendon and account for seating losses. The initial tensioning of each strand was determined based on a voltage reading from a pressure transducer. After the overstressing was completed, pressure was lowered to the service load stress. The bearing plate and chuck were then pushed into place against the model and the pressure was released to allow the wedge to seat. All strands were tensioned from both sides, to further reduce friction losses.

After the initial overstressing and seating at service loads, "lift-offs" were performed for each strand to more accurately reach the proper tension in each strand. A linear potentiometer was placed on the stressing ram measuring the movement of the piston of the stressing ram (see Figure 3.27). The ram pressure transducer and this linear potentiometer were connected to a plotter to give a load vs. displacement curve. In this way, the amount of stress in the strand could be determined by where the displacement



Figure 3.25 Dead Load Blocks Hanging from Model

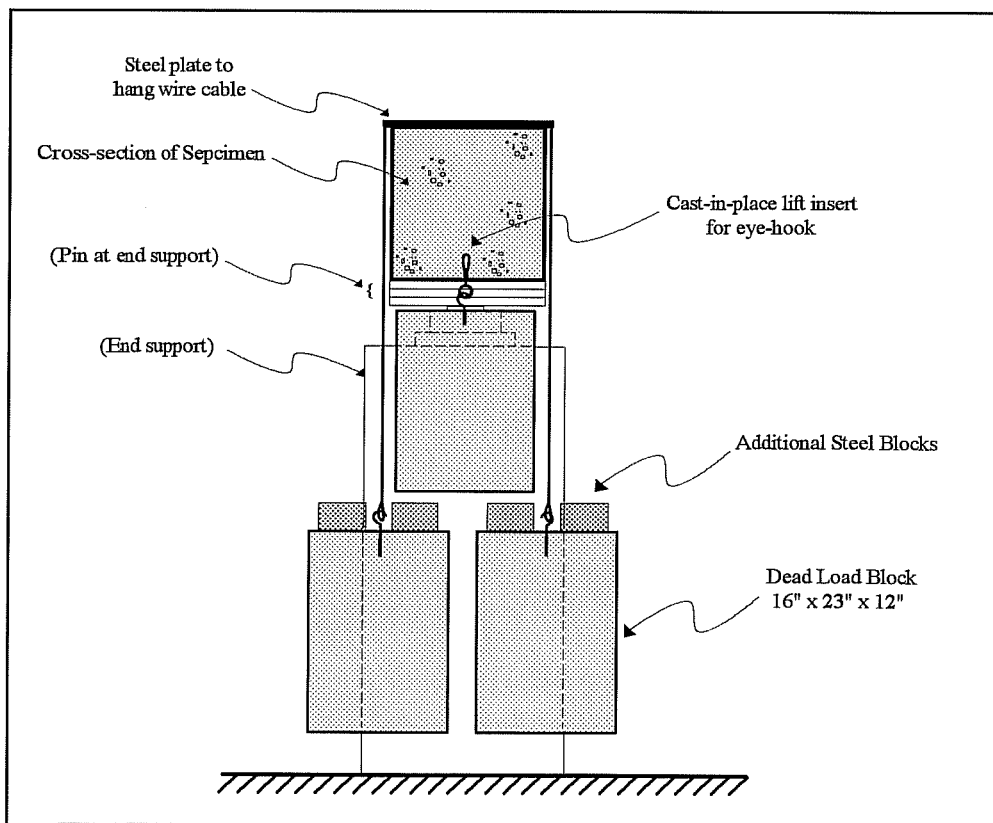


Figure 3.26 Cross Section of Dead Load Blocks Hanging from Model

began to increase more rapidly with respect to the load (loss of stiffness). This marked when the amount of stress already present in the strand was overcome and more stress was being applied. As a result, the wedge would "lift off". Depending on whether the lifting off occurred too soon (not enough stress in the strand) or too late (too much stress in the strand), the threaded chuck could be brought out or in respectively, to compensate for the error. Lift-offs were performed for each strand until a reasonable accuracy was achieved. This typically required 3-4 lift-offs per strand.

As a second check to see if the strands were appropriately stressed, the elongations were measured (only for model CB-PU-100S). The measured elongations matched quite accurately the elongations expected for each strand once stressed to their "service load" stress. Ideally, elongations should have been measured for each test. However, from the close agreement of the assumed stresses and the calculated elongations for the desired stresses, it is felt that the lift-offs alone can be assumed to have been an adequate measure for determining appropriate stress levels in models CB-PS-100S and CB-PU-71S.

In the case of post-tensioning model CB-PS-100S, stage loading was required. The drape of the tendon in combination with the high prestressing force would have caused cracking in the model during post-tensioning operations. To prevent this, load was applied through the hydraulic loading rams. Once grouting was complete, temporary screw jacks were placed between the loading blocks and the loading rams to maintain the necessary load in case the hydraulic rams lost pressure.

3.5.7 Grouting Procedure

Each tendon was grouted immediately following the completion of the lift-offs for prestressing. One or two batches of grout were mixed per model. The grout was hand-pumped through a grouting tube at one end of the duct until an even flow of grout (no air bubbles) exited the center grouting tube, at the highest point on the draped tendon. Grout was then pumped from the other end of the same duct until again an even flow of grout left the center grouting tube. This procedure was performed for each duct in an effort to provide adequate bond by reducing the possibility of air bubbles forming at the highest point in the duct (the negative moment region over the center support).

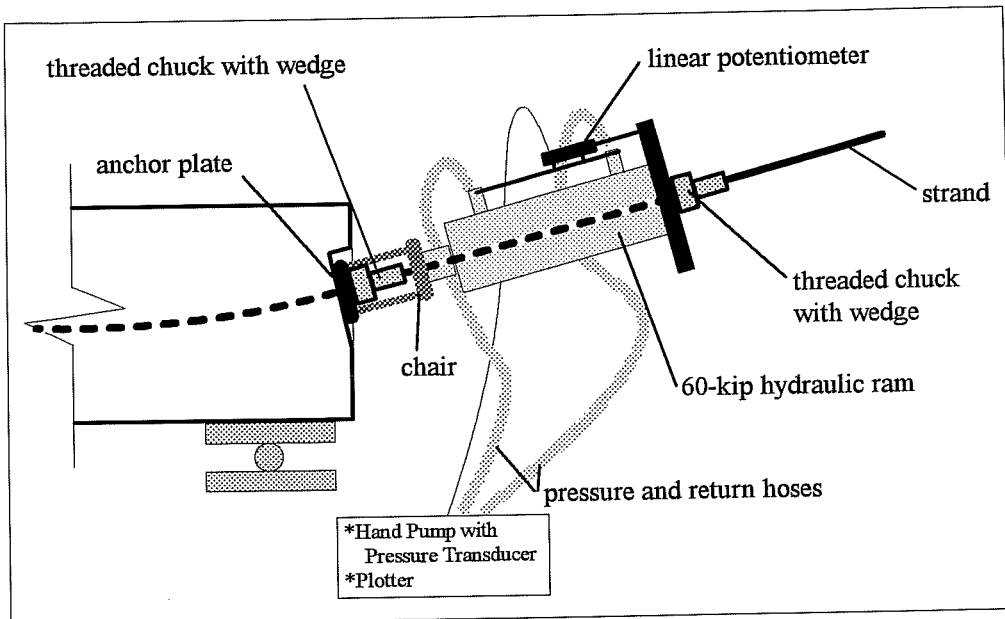


Figure 3.27 Set-up for Post-tensioning Operations

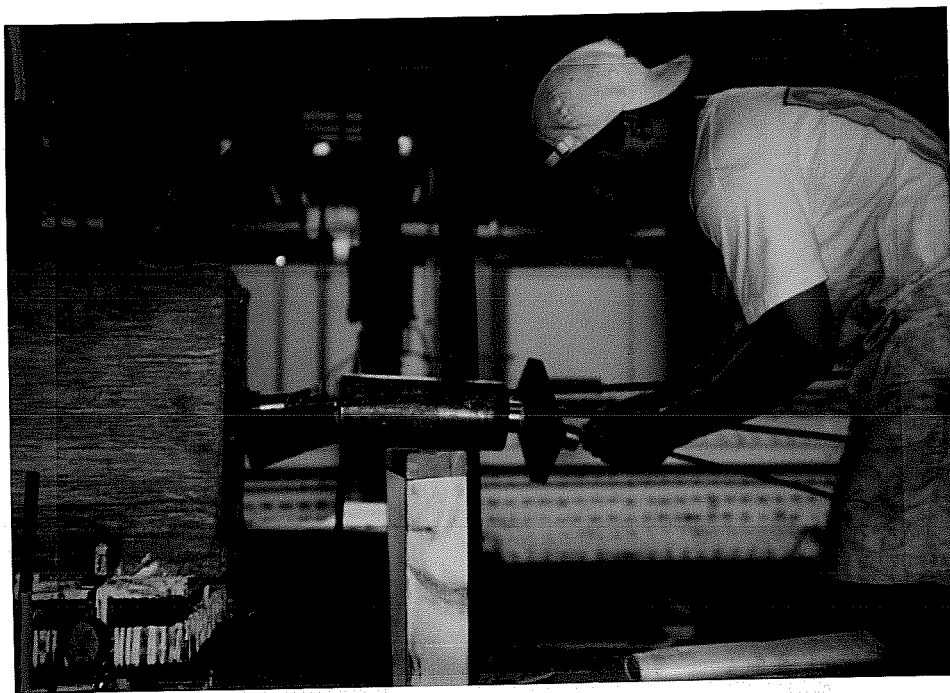


Figure 3.28 Preparing for Post-tensioning Procedures

3.6 Test Set-up

3.6.1 Support System

Each model was supported on three supports, two "rollers" and one "pin". The original test set-up is pictured in Figure 3.29. From the bottom up, each support consisted of a reinforced concrete block, four 1.5 in. (38.2mm) diameter adjustable bolts between two 2 in. (50.8mm) steel plates, one or two load cells, and a pin (for the center support) or a roller (for the end supports). The adjustable bolts were gaged and the system was originally intended to act as a second "load cell" reading as well as be able to move the supports up and down. The supports would be adjusted at the beginning of the test to where the load cell readings corresponded to predicted initial reactions including the reactions due to secondary moments in the prestressed models.

This set-up was used for the initial testing of the first model, CB-RU (Conventionally reinforced as per AASHTO). It was quickly determined that the gaged bolts were not able to measure load with sufficient accuracy. The area of the bolts was too large to accurately measure strain due to the expected reactions.

When testing began it was also found that the loads were not distributing to the supports as expected by elastic theory. It was determined, by monitoring support displacements as well as mid-span displacements, that the supports were of approximately the same stiffness as the beam being tested. This caused secondary moments to be induced in the beam, thus changing the reactions from what ordinary elastic theory predicted. The center support was the least stiff and it is believed that the 150k (668kN) load cells used here were a primary cause for the lack of stiffness. Testing was temporarily stopped and a new support system was designed.

A much simpler, "cleaner" system was then constructed (see Figure 3.30). As the bolt groups were not acting as secondary load cells and were also very difficult to adjust, they were removed from the set up. As well, the 150k (668kN) load cells under the center support were removed. Additional concrete was cast on top of the original blocks so that the resulting height of the supports would be the same (this height was needed in order to hang the dead load blocks). Load cells were placed only under the end supports as the center support needed to carry the greatest amount of load and therefore needed to be the stiffest support.

To prevent or counteract any secondary moments due to support settlements, the beam needed to be held in a straight line. Therefore, a hydraulic ram with an adjustable screw jack was placed under one

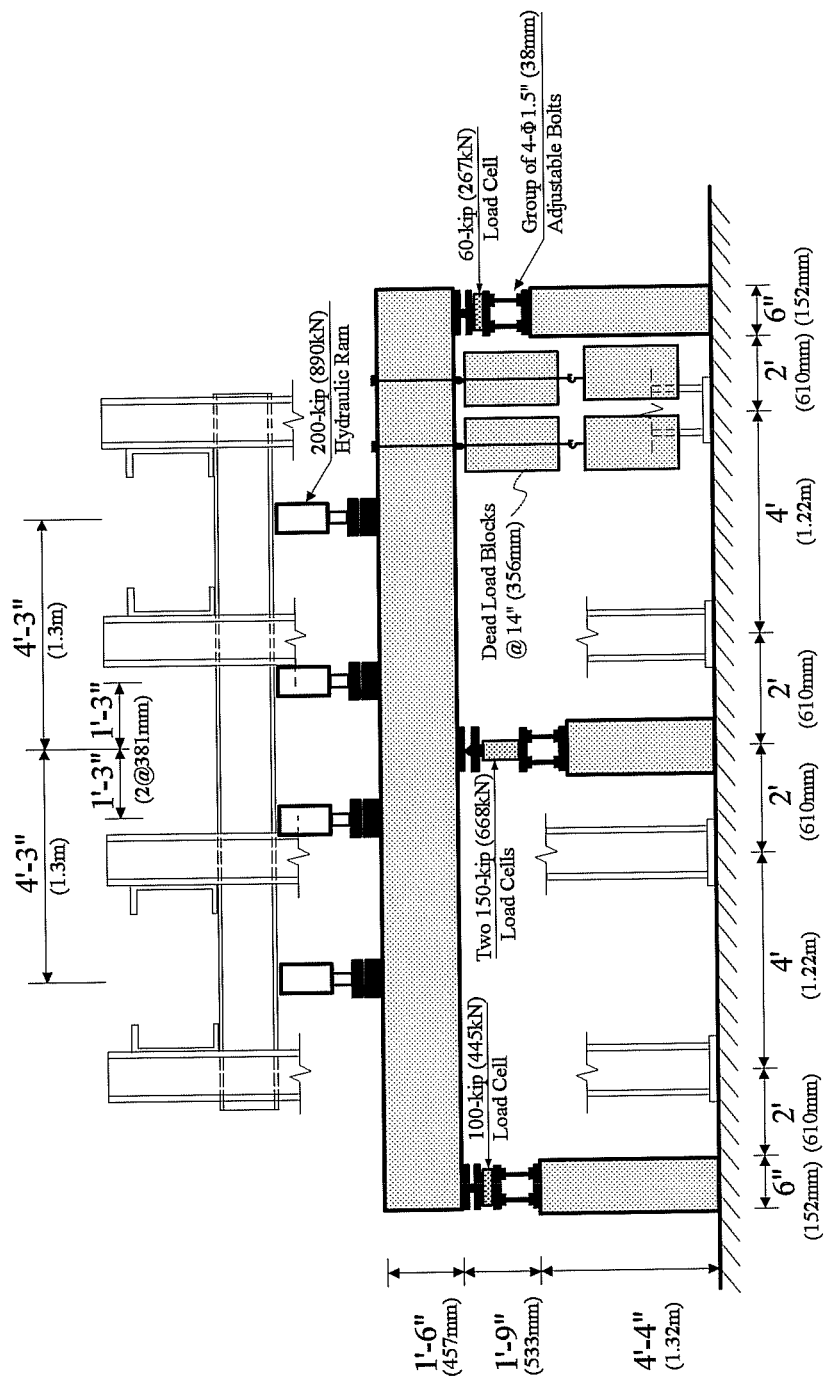


Figure 3.29 Original Test Set-up

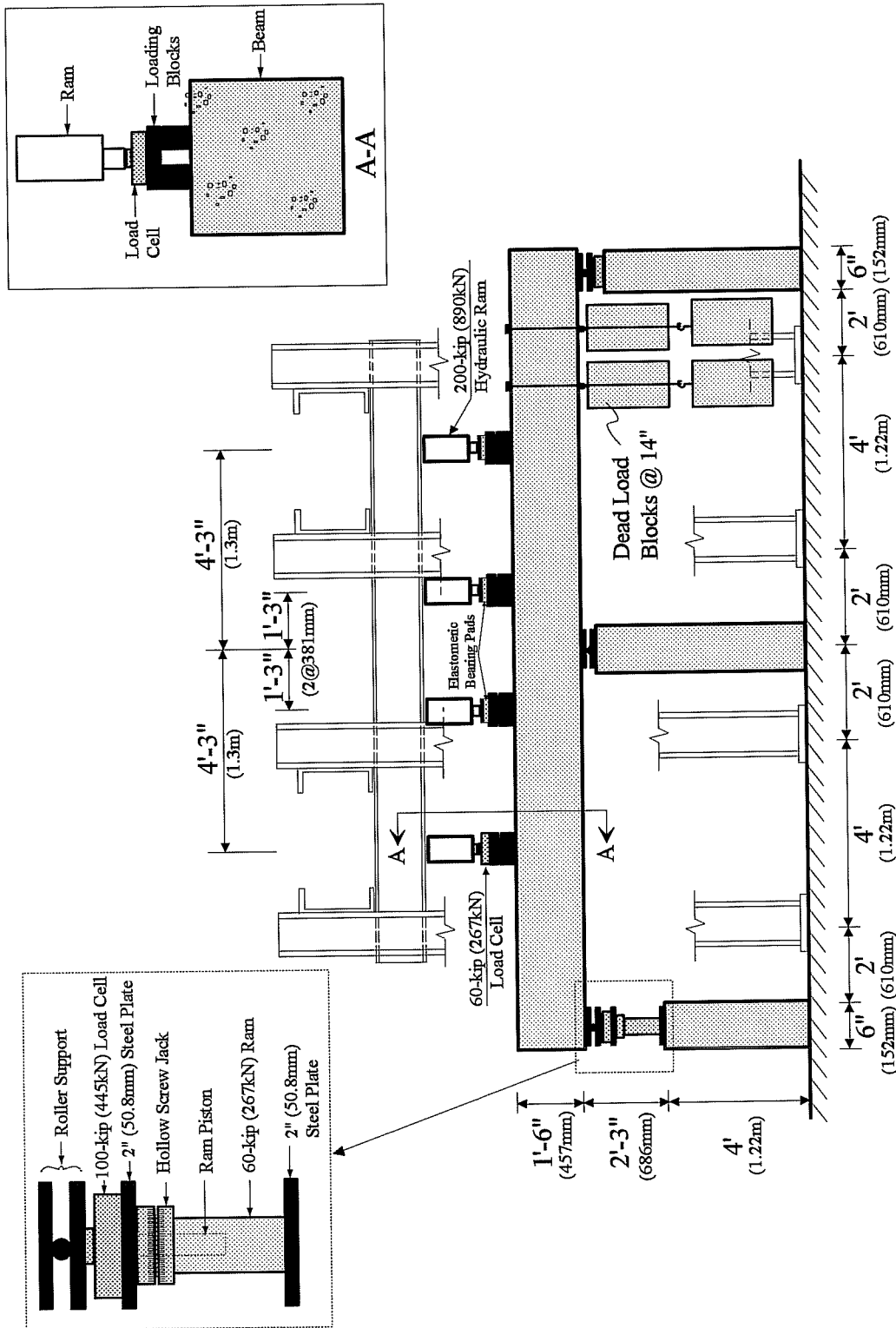


Figure 3.30 Final Test Set-up

support (Figure 3.30). By monitoring the support settlements, this one end could be raised or lowered to keep that end in line with the elevations of the other two supports. This was done by raising the beam up off of the screw jack. The jack was then adjusted accordingly (to an accuracy of ± 0.0005 in. (± 0.013 mm)) and the beam was lowered back down onto the jack. This system worked very well.

3.6.2 Loading System

Each model was loaded using four 200-kip (890-kN) hydraulic rams reacting off of a testing frame that was bolted to a reinforced "loading" (or "reaction") floor (Figure 3.30). The load from each ram was to be equal. The rams were therefore connected to a manifold which was in turn connected to a single hand pump.

3.6.3 Instrumentation

3.6.3.1 Pressure Transducers and Load Cells

A pressure transducer and a pressure dial gage was connected to the hydraulic ram system. The dial gage was read visually and the pressure transducer was connected to a voltmeter to be read visually as well. The voltmeter could be read more accurately than the dial gage. The pressure transducer was also connected to the data acquisition system to be recorded.

Before each model was set on its supports, the load cells under the end supports were connected to a manually read strain indicator. Once the beam was in place and adjusted to a level position line (based on the predicted reactions), the strain indicators were removed and the load cells were connected to the data acquisition system.

A load cell was also placed under a loading ram for the first two models (CB-RU and CB-PS-100S) to serve as a check for the pressure transducer readings. It was determined that the pressure readings were ~ 700 lbs (~ 3.1 kN) too high. This was attributed to friction in the rams. From the consistency of the load cell readings under the ram and the pressure transducer readings, the load cell was not put in place for the last two models (CB-PU-100S and CB-PU-71S). They were not used here primarily for convenience as the lower capacity of the available load cells required them to be removed during testing.

3.6.3.2 Strain Gages

Strain gages were applied to a number of straight bars and wires, stirrups, and prestressing strand for each model. The gages used were 5mm and 2mm strain gages with 33 ft (10m) lead wires. They were placed on flexural reinforcement where maximum positive and negative moments were expected. They were placed on both tensile chord and side face crack control steel at these same expected maximum moment sections. Gages on shear stirrups were placed on stirrups under each point load and over the center support. Prestressing strand was gaged as well at points of expected maximum moment. Exact locations of these gages for each model are shown in Figure 3.31a-d.

The gages were connected to the data acquisition system once each beam was set on the supports and before dead load blocks were applied. The strains due to the self-weight of the beam were not measured since they should be negligible.

3.6.3.3 Deflection Readings

Deflections of the beam and support settlements were originally to be measured using linear potentiometers attached to a frame above the beam. To record accurate measurements, this frame was attached to the ground. However due to the necessary height of the frame (~ 9 ft. (2.7m) from the ground), a sufficiently stiff attachment would have been unreasonable. An effort was made to not disturb the attachment used however this too was unreasonable. Therefore a different system of measuring deflections was employed.

Deflections were instead measured relative to a 2 in. (50.8mm) steel channel spanning the support blocks approximately 1 ft. (305mm) below the bottom of the beam. Mechanical as well as digital dial gages were set up so as to measure deflections of the beam at the supports and the mid spans. Gages with an accuracy of at least 0.001 in. (0.025mm) were used. Figure 3.32 shows the locations of the gages with respect to the rest of the test set-up.

An additional deflection measuring system was used for measuring large deflections. A piano wire was strung across the centerline of one side of the beam. It was tied to a bolt coming out of the end of the beam over one support and hung with a weight over a pulley on the other end. Strips of mirror with a millimeter ruler next to them were attached to the beam behind the wire over the supports and under the point loads (no deflection was to exist over the end supports). The measured deflections would be relative to the two end supports.

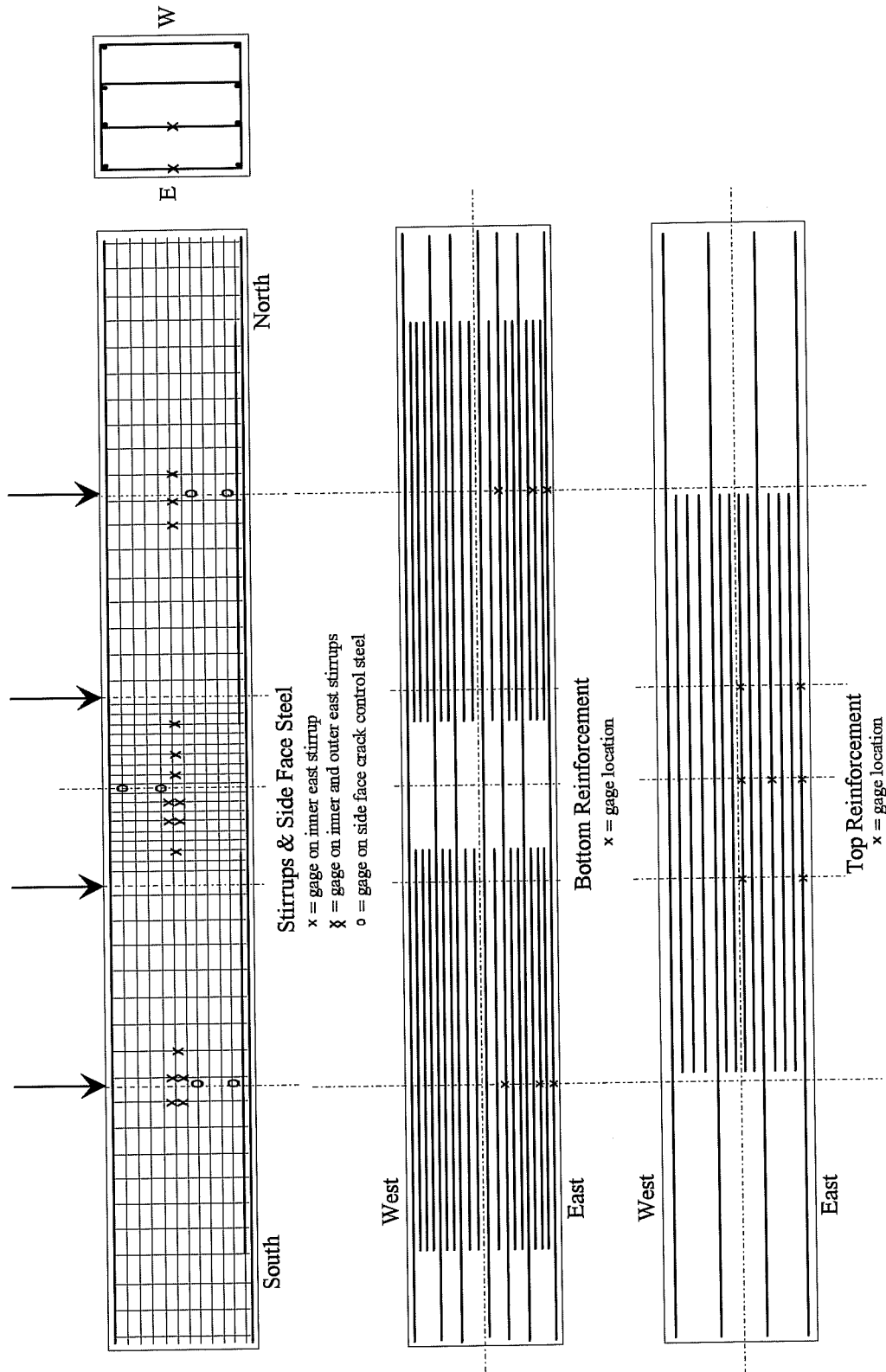


Figure 3.31a Strain Gage Locations for CB-RU

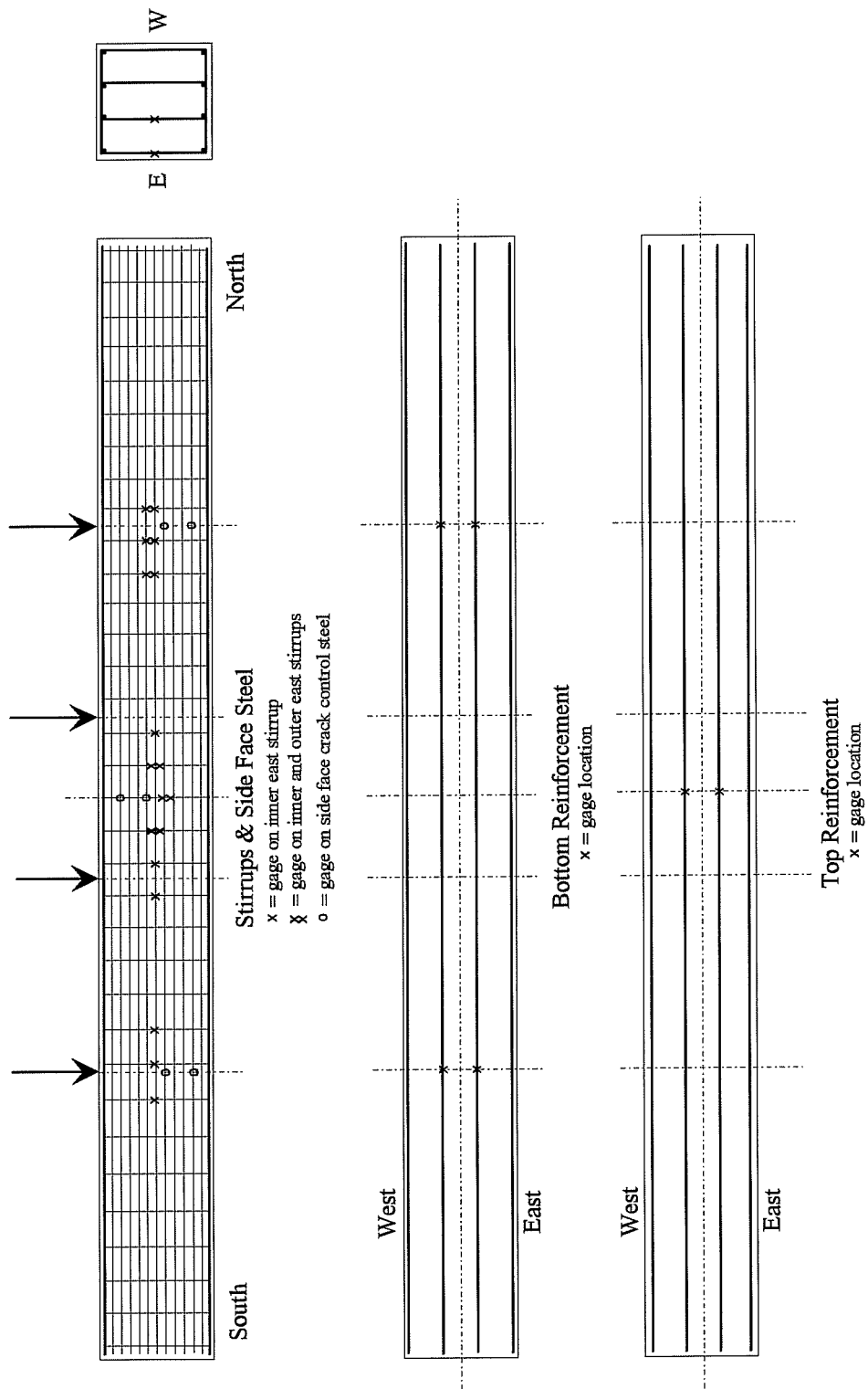


Figure 3.31b Strain Gage Locations for CB-PS-100S

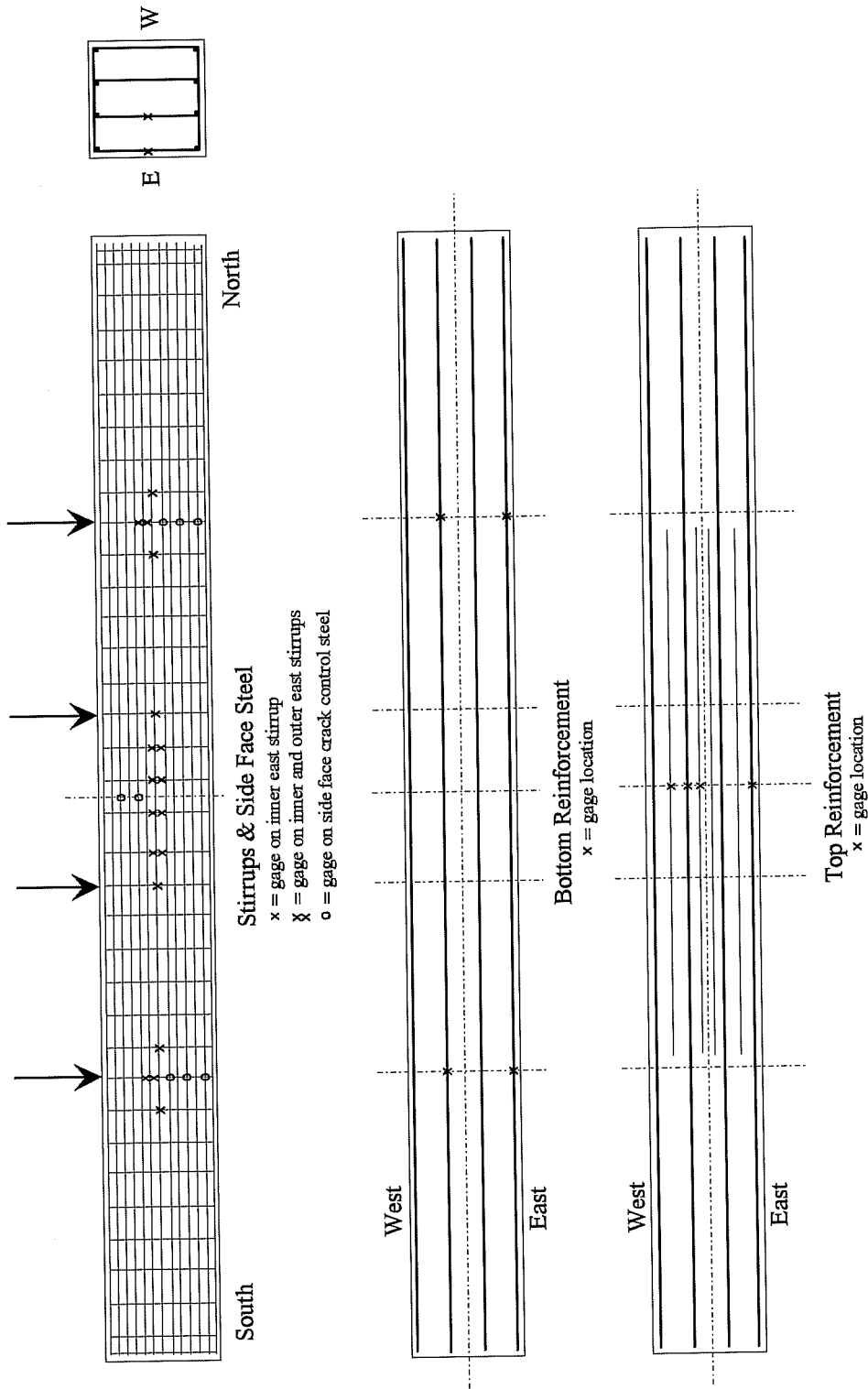


Figure 3.31c Strain Gage Locations for CB-PU-100S

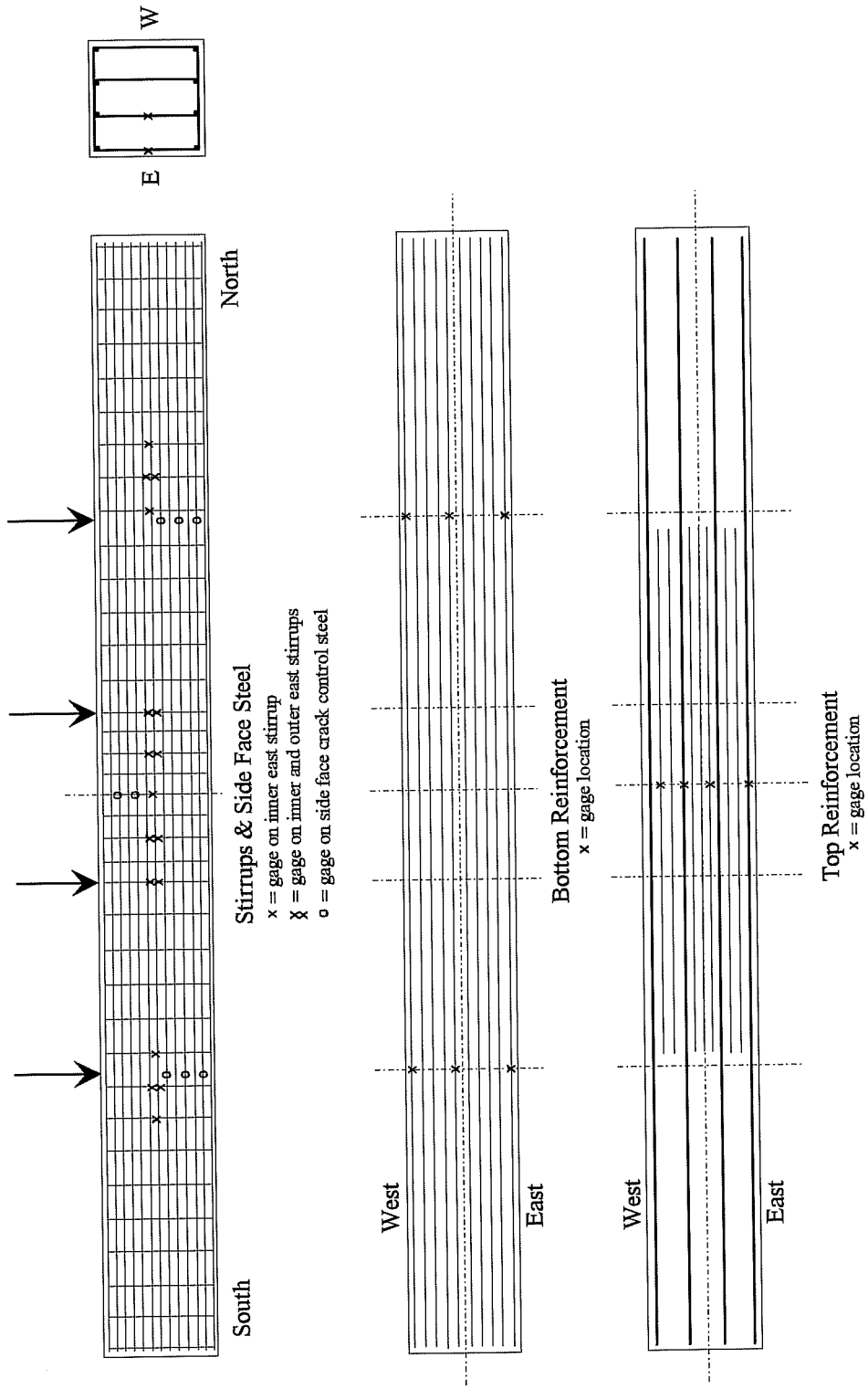


Figure 3.31d Strain Gage Locations for CB-PU-71S

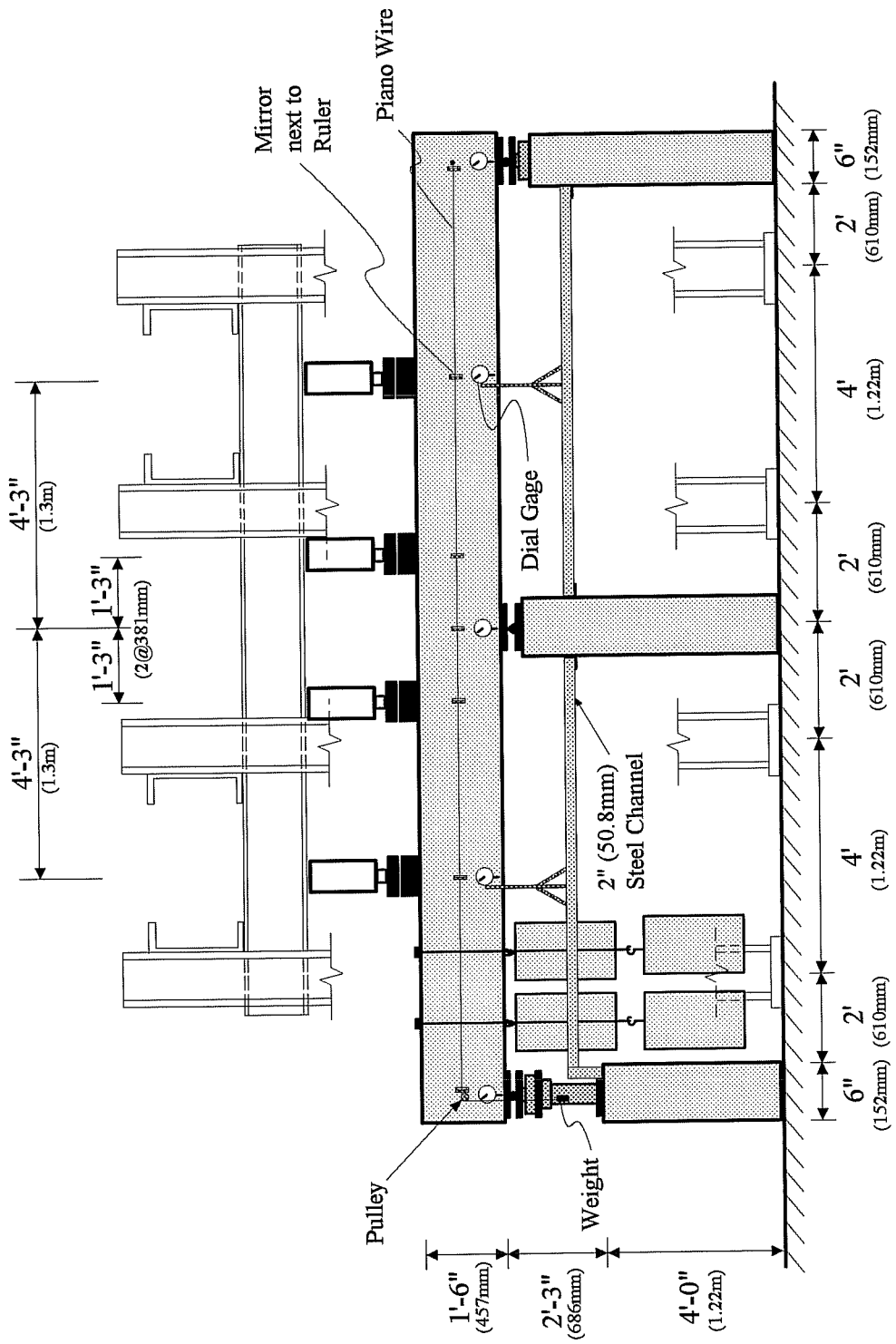


Figure 3.32 Deflection Measuring Systems for Final Set-up

3.7 Testing Procedure

3.7.1 Static Loading

Load was applied to the beam for testing once the dead load blocks were in place and the grout for the post-tensioned models reached at least 2000 psi (13.8 MPa). Each model was loaded by 2-3k (9-13kN) increments up to service loads and then factored loads. This usually took one day. The next day, the models were reloaded by 10k (44.5kN) increments up to factored loads and then continued to be loaded with 2-3k (9-13kN) increments up to failure. The smaller 2k increments were typically used when the predicted cracking load was being neared, as well as between service and factored loads and once yielding had occurred (where relatively small load increments resulted in large displacements).

When the failure load was being reached, as noted by very large deflections with small load increments, testing was continued using displacement control. Loading was continued until a given increment of displacement at one mid-span was reached. Measurements with the data acquisition system as well as mid-span deflections were then recorded. Another static reading was then made and loading was continued up to the next increment of displacement. This displacement control procedure continued until the model failed.

3.7.2 Data Collection

3.7.2.1 Data Acquisition System.

The strain gages on the reinforcement as well as the load cells and pressure transducer were all connected to a scanner as part of an HP Data Acquisition System. Measurements or "scans" were taken at each load step or, as failure was being reached, a dynamic and static reading was taken with each displacement increment. A conversion program developed at Ferguson Laboratory named CPROF7 was then used to convert the measurements into engineering units of loads and strains.

3.7.2.2 Deflection measurements

Dial gage readings for support and mid-span deflections were recorded by hand at every load step. A load-deflection plot accounting for support displacements, was recorded by hand throughout testing. With incipient failure all but two dial gages, one at each mid-span region, were removed and displacement-controlled testing continued.

Deflection readings using the wire and mirror set-up were recorded at service loads, factored loads and upon failure in all cases. In the case of CB-PS-100S, all dial gages were removed as failure was being reached, and displacement control continued with wire and mirror readings.

3.7.2.3 Crack Width Measurements

Crack widths were measured using an optical crack monitor as well as crack comparator cards (see Figure 3.33). The accuracy of these measurements was within ± 0.0005 in. (± 0.013 mm). Measurements were recorded upon the first appearance of each crack and at even intervals up to service & factored loads and beyond, including service loads if cracks formed before they were reached. Crack width measurements were taken at the extreme fibers as well as at grid lines drawn on the side of the beam at even intervals of 0.75", 4.25", 9", 13.25" and 17.25" (19.1mm, 108mm, 229mm, 337mm, and 438mm) from the top. The first and last lines corresponded to the level of the non-prestressed steel. From the top these points for measuring were labelled A-G.

Crack widths as well as maps of crack locations were recorded during testing. At loads above factored loads, maximum crack widths of major cracks only were recorded.



Figure 3.33 Measuring of Crack Widths with an Optical Crack Monitor

3.7.3 Post-mortem Investigation

After failure had been reached for each model, they were removed from the testing frame and transported outside. The post-tensioned models were opened up with a jackhammer at failure locations including the center in the negative moment region and/or one of the positive moment regions near mid-span (see Figure 3.34). Bars and strand were checked for signs of yielding or fracture and measurements were made to determine actual locations of the strand in the cross section (to determine if the ducts were moved during construction). Some of the smaller wires were damaged due to jack hammering. However, the difference in damage from yielding to fracture and jack hammering was discernable. The fully reinforced model was not opened as the condition of the reinforcement in the failed region was evident at the time of failure.



Figure 3.34 Failed Test Specimen Opened for Post-Mortem Investigations

CHAPTER 4

TEST RESULTS

4.1 Introduction

The test results for the models designed according to the 1992 AASHTO Bridge Design Specifications are presented first. These are followed by the results of the models designed using the proposed integrated design method.

For each test, five major types of results are presented:

- 1) *Cracking Behavior* - including first cracking, crack widths emphasizing serviceability considerations and crack distribution.
- 2) *Moment-Strain Behavior* - to show yielding of sections as well as section ductility (also includes shear vs. strain behavior)
- 3) *Moment vs. Applied Load* - to show moment redistribution behavior.
- 4) *Load-Deflection Behavior* - to show overall member behavior as well as moment redistribution behavior.
- 5) *Moment-Deflection Behavior* - to show section ductility as well as moment redistribution behavior.
- 6) *Post-mortem Investigation* - to determine where yielding and fracturing of steel occurred and to determine actual location of strands.

A brief discussion follows each set of test results.

For all models, the regions under the point loads nearest to the mid-spans, station 1 and station 4 (see Figure 4.2) will be referred to as "mid-span". For better comparison of results of the different models, similar scales are used for presentation of each type of result (i.e. moment-deflection behavior or moment-vs.-applied load behavior). In the case of moment-strain behavior, a different scale is used for the mid-span results than for the center support results, due to the different range of moments reached at these sections.

For moment-strain behavior, all working gage results are presented for various sections. Data points for obviously malfunctioning gages are not included. Where gage results for two sections are very similar, results from only one section are presented.

Initial yielding of the non-prestressed steel at the mid-span regions as indicated by the moment-strain

behavior results are marked on both the load-deflection and the moment-deflection figures. The average yielding moment for the north and south spans is shown on the figures.

4.2 Designs According to AASHTO Bridge Specifications - 1992 edition

The first model was the reinforced concrete design and was tested using two different test set-ups. Each set of tests are presented separately. The first is referred to as CB-RU-initial and the second as CB-RU-final. Results for the second model CB-PS-100S, the fully prestressed design based on AASHTO (Service Load Design), are presented as well.

4.2.1 CB-RU-initial - Conventionally Reinforced

Experimentation began on this model using the original test set-up described in Section 3.6.1. The model was tested on four separate days with variations made in the test set-up and testing procedure. It was then determined that the supports were too flexible and that a new test set-up was required. Descriptions of the first four test days follow and are referred to in the results presented later.

Day 1 - On the first day of testing, the model was loaded up to service loads. The distribution of the loads to the supports of the uncracked beam did not correspond well with the expected elastic distribution. Another unexpected result was that the first crack in the beam appeared at station 1 near mid-span of the south span. From an elastic analysis, the applied moment over the center support should have been approximately 70% higher than the moment at mid-span (before cracking) (see Figure 3.3). Therefore first cracking was expected to occur over the center support, not at mid-span. Due to the unexpected load distribution and first cracking location, testing was temporarily halted. Uneven support settlement was suspected to be causing these unexpected results. It was determined as well that the initial deflection reading system (Section 3.6.3.3) was inadequate and not dependable.

Day 2 - Once the new deflection system was in place (Section 3.6.3.3), testing was resumed. The model was again loaded up to service loads. Cracks were marked and measured and a new, smaller crack formed near station 1 at mid-span of the south span. The support reactions remained significantly different than elastic analysis predictions. However, since the beam was already cracked, the predicted elastic distributions could no longer be used accurately for comparison. Of primary concern however, was that

the stiffness of the model and that of the supports were roughly the same. This was apparent as the center support settlement relative to the end support settlements was of the same order of magnitude as the mid-span deflections of the beam.

The amount of relative deflection of the center support was examined. The effects of this deflection were considered using the compatibility method. The beam was modelled as simply supported on the end supports with a point load where the center support would be. The amount of this point load required to produce the measured deflection at the center was determined. This "point load" corresponding to the relative displacement, created a positive moment throughout the beam. This decreased the negative moment over the center support and increased the positive moments at the mid-spans (see Figure 4.1). According to an elastic analysis, the amount of relative deflection measured on Day 2 was not enough to cause cracking to first occur near mid-span. However, these deflection measurements were made during the testing of a pre-cracked beam. The loss of stiffness near mid-span may have resulted in less center support deflection. As well, the relative displacement of the beam when initially placed on the supports was unknown. As seen from the experiment, very small deflections (less than 0.005 in., 0.127mm) changed moments by up to 10%.

Day 3 - In an effort to better understand and try to correct the support displacement problem, a third test was run. Additional measurements were made of any deflection in the support base blocks. The model was tested to service loads again. No settlement of the support base blocks occurred and the overall settlement of the center support was similar to that of the second day of testing and of the same order of magnitude as the mid-span deflection. No new visible cracks appeared and crack widths were not re-measured for this test.

Day 4 - It was noted that the support settlements from Days 2 & 3 of testing seemed to stabilize near service loads. Therefore one last effort was made to solve the support displacement problem before revising the test set-up. On the fourth day of testing, the ends were lowered (this approach was easier than raising the center support) using the screw-jack/bolt system. They were lowered by a fraction of the expected deflection at first so as not to induce prematurely a crack over the center support. The deflections were monitored throughout the test and the ends were lowered periodically in an attempt to keep the beam supports linear (free of relative displacements). Cracks did form over the center support. All cracks were marked and crack widths were measured. With this test, it did not appear that the support settlements were stabilizing near service loads.

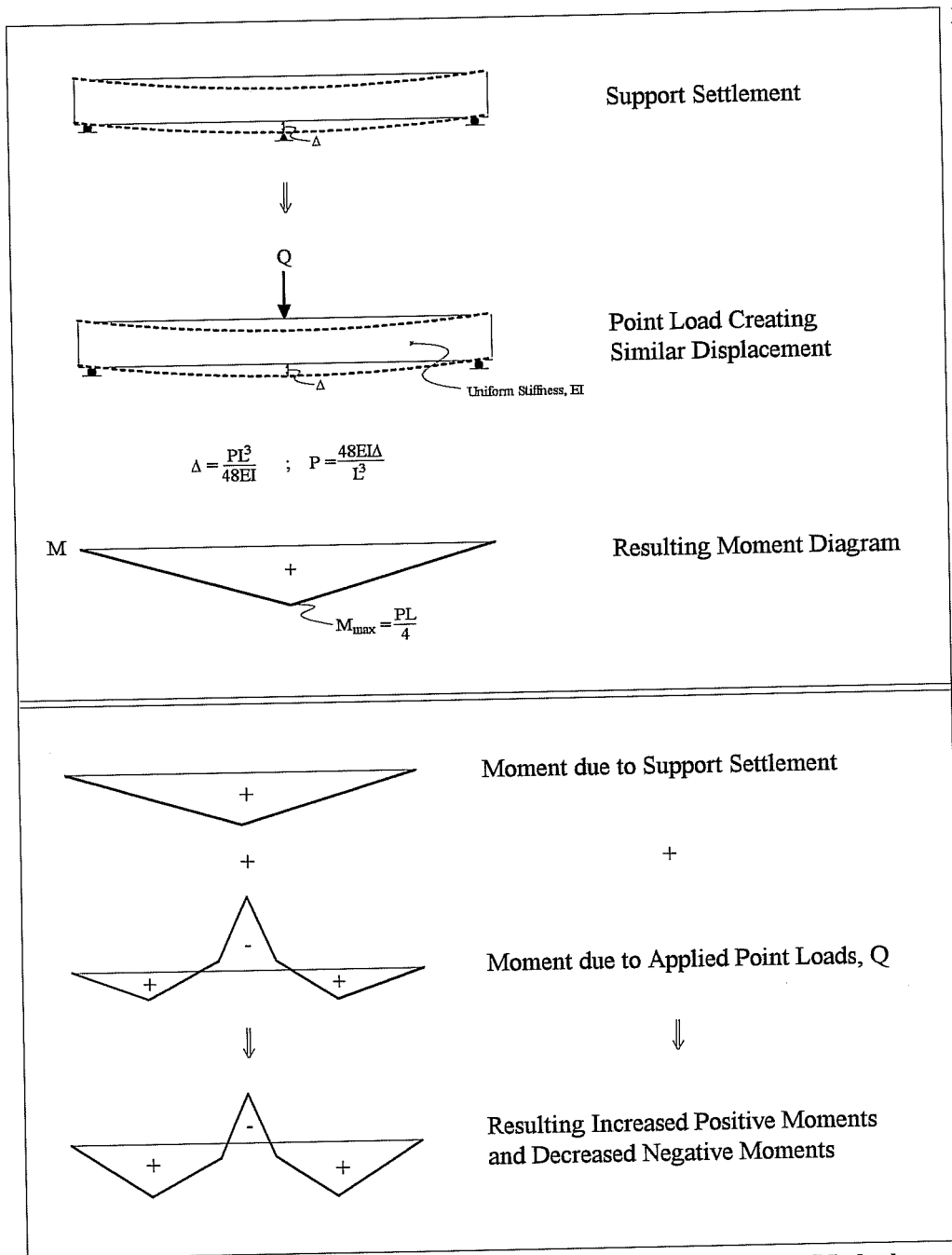


Figure 4.1 Analysis of Support Settlements using the Compatibility Method

In general, it was decided that the test results using this test set-up would not be reliable as the beam and supports were of similar stiffness. The settlements were not stabilizing and continual adjusting of the support elevations was difficult and imprecise. The model was completely unloaded, a new test set-up was designed and assembled, and testing resumed at a later date.

The results of the initial test follow.

4.2.1.1 Cracking Behavior - CB-RU-initial

First Cracking - Cracking distribution under service loads as well as location of initial cracks are depicted in Figure 4.2. The first crack appeared at station 1 near mid-span of the south span on Day 1 of testing under an applied load of 24k (107kN). Based on the reaction at the south support and the dead load of the beam and dead load blocks, the calculated applied moment at this section was 51.1 k-ft (69.3 kN-m). This corresponds to a cracking tensile stress of:

$$\sigma_{cr} = \frac{M_{cr} * y}{I} = \frac{51.1 * 9}{8748} * 12000 = 631 \text{ psi} = 8.4 \sqrt{f'_c} \quad (4-1)$$

$$(\sigma_{cr} = \frac{M_{cr} * y}{I} = \frac{69.3 * 229}{3641 * 10^6} * 10^6 = 4.36 \text{ MPa} = 0.67 \sqrt{f'_c})$$

where σ_{cr} : cracking stress, psi (MPa)
 M_{cr} : cracking moment, k-ft (kN-m)
 y : distance from the neutral axis to the extreme tensile fiber, in. (mm)
 I_g : gross moment of inertia, in.⁴ (mm⁴)
 f'_c : compressive strength of the concrete, psi (MPa)

The first crack to appear over the center support became visible with point loads of 6k (27kN) on Day 4 of testing. The calculated applied moment at this section was 23 k-ft (31 kN-m). This corresponds to a cracking stress of $3.8 \sqrt{f'_c}$ ($0.3 \sqrt{f'_c}$). The lower cracking stress for the center support may have been due to micro-cracking from earlier tests. In particular, a concrete tensile stress of $7.4 \sqrt{f'_c}$ ($0.59 \sqrt{f'_c}$) was reached over the center support on Day 1 of testing. This may have caused cracks that were not yet visible on the surface. The pre-cracked concrete would then be weaker and the cracks would widen at stress levels lower than the concrete tensile strength. As well, the exact amount of center support deflection under no load was unknown before the end supports were lowered for this test. Lowering the supports induced an

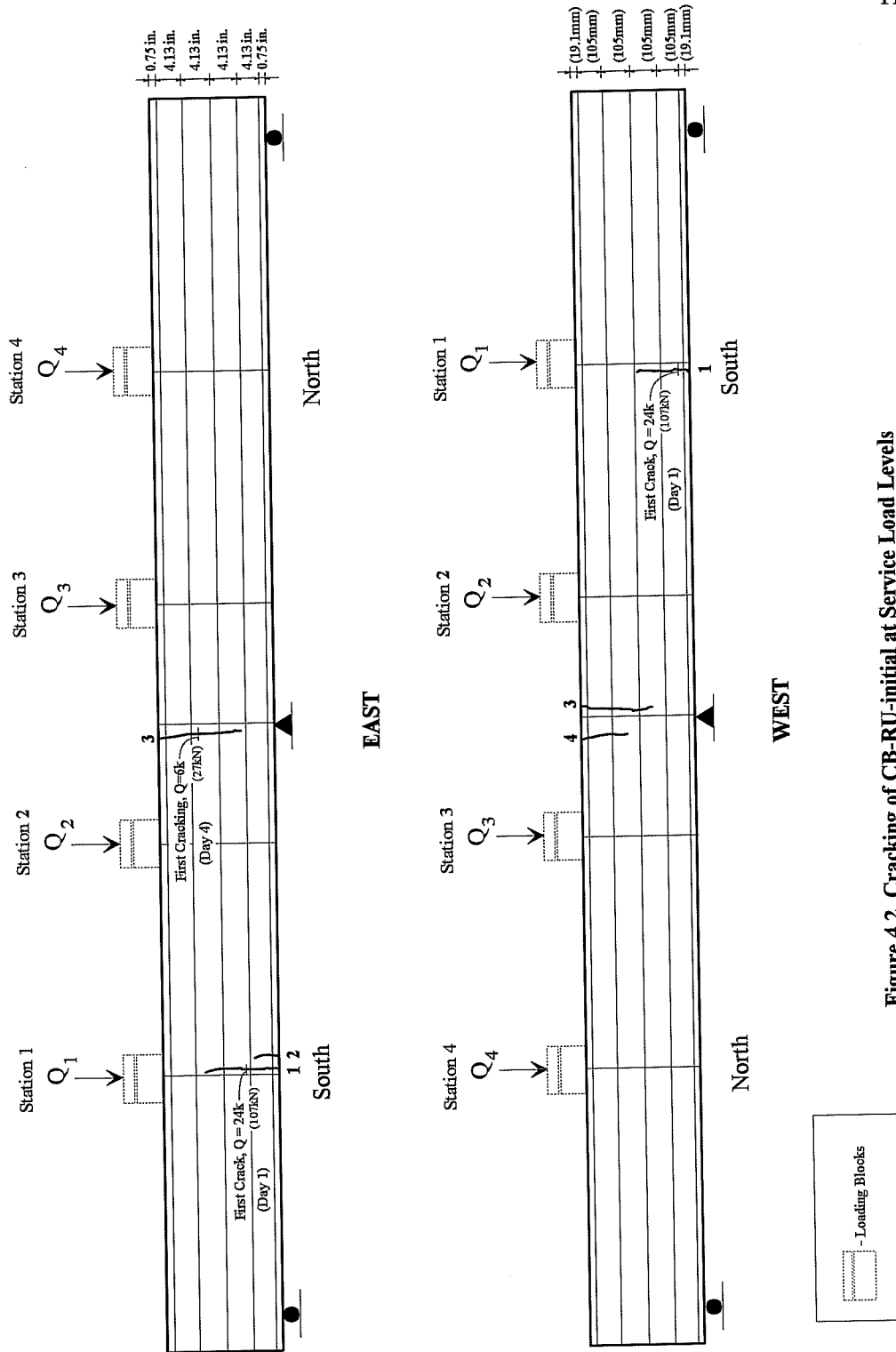


Figure 4.2 Cracking of CB-RU-initial at Service Load Levels

additional negative moment over the center support, adding to the moment determined from the measured point loads and reactions.

Crack Widths & Serviceability - Cracking behavior is particularly important for serviceability considerations. Of most importance are the crack widths under service loads. The beam was cracked on the first day of testing just before service loads. Beam loading was continued up to service loads where cracks were measured for the first time. The applied point loads were then completely removed. Cracks were remeasured at service loads on Days 2 and 4 of testing.

Figure 4.2 shows the crack locations under service loads. Maximum crack widths for certain load steps are recorded in Table 4.1.

The first crack had an initial maximum width of 0.0015 in. (.038mm) on the east side. At service loads, this same crack extended further up the beam and had a maximum crack width of 0.004 in. (0.102mm) on the west side on Day 4 of testing (see Figure 4.2). Crack widths are assumed to be scalable.[23] Therefore the maximum crack width of 0.0044 in. (0.102mm) in the 1/4-scale model corresponds to a crack width of 0.016 in. (0.106mm) for the prototype. The 1992 AASHTO Bridge Design Specification serviceability criterion for crack width control is indirect, using a reinforcement distribution factor, z , based on the Gergely-Lutz equation.[9,34] Using this provision, crack widths are essentially limited to 0.0155 in. for moderate exposure and 0.012 in. for severe exposure. Model CB-RU was designed for moderate exposure and the prototype crack width of 0.016 in. (0.406mm) therefore slightly exceeds the crack width serviceability criterion.

Distribution of Cracking - Up to service loads, only a few flexural cracks appeared (see Figure 4.2). No cracks had formed in the north span.

4.2.1.2 Moment-Strain Behavior - CB-RU-initial

Moment-strain data for the tensile steel is presented in Figures 4.3-4.5. On Day 1 of testing, Figure 4.4a shows a sudden increase in strain in the south mid-span data when the first crack formed at this section. The bottom of Figure 4.3 shows the crack patterns at first cracking for the south mid-span and center support regions. The corresponding moments at which these cracks appear are then indicated on the plots of Figures 4.3-4.5 with numbered circles. As expected, the increase in strain with increasing moment in Figure 4.4b is linear for the uncracked north mid-span. Over the center support, Figure 4.3 shows a larger increase in strain once the first crack formed at the south mid-span on Day 1 of testing. On

(a) CB-RU-initial - East

TEST DAY	LOAD, Q kips	CRACK WIDTH, in.		
		1	2	3
1	25	0.0015		
1	27	0.002		
1	29.5 - Service	0.002		
2	29.5 - Service	0.003	0.001	
4	9	0.001	<.001	0.003
4	12	0.0015	<.001	0.003
4	20	0.0015	<.001	0.0035
4	25	0.002	<.001	0.0035
4	29.5 - Service	0.0025	0.001	0.004

(b) CB-RU-initial - West

TEST DAY	LOAD, Q kips	CRACK WIDTH, in.		
		1	3	4
1	25	0.001		
1	27	0.002		
1	29.5 - Service	0.003		
2	29.5 - Service	0.003		
4	9	<.001	0.003	
4	12	0.001	0.003	
4	20	0.0015	0.0035	
4	25	n.m.	0.0035	0.002
4	29.5 - Service	0.003	0.004	0.0025

Table 4.1E Maximum Crack Widths for CB-RU-initial, English Units

(a) CB-RU-initial - East

TEST DAY	LOAD, Q kN	CRACK WIDTH, mm		
		1	2	3
1	111	0.038		
1	120	0.051		
1	131 - Service	0.051		
2	131 - Service	0.076	0.025	
4	40	0.025	<.025	0.076
4	53	0.038	<.025	0.076
4	89	0.038	<.025	0.089
4	111	0.051	<.025	0.089
4	131 - Service	0.064	0.025	0.102

(b) CB-RU-initial - West

TEST DAY	LOAD, Q kN	CRACK WIDTH, mm		
		1	3	4
1	111	0.025		
1	120	0.051		
1	131 - Service	0.076		
2	131 - Service	0.076		
4	40	<.025	0.076	
4	53	0.025	0.076	
4	89	0.038	0.089	
4	111	n.m.	0.089	0.051
4	131 - Service	0.076	0.102	0.064

Table 4.1S Maximum Crack Widths for CB-RU-initial, S.I. Units

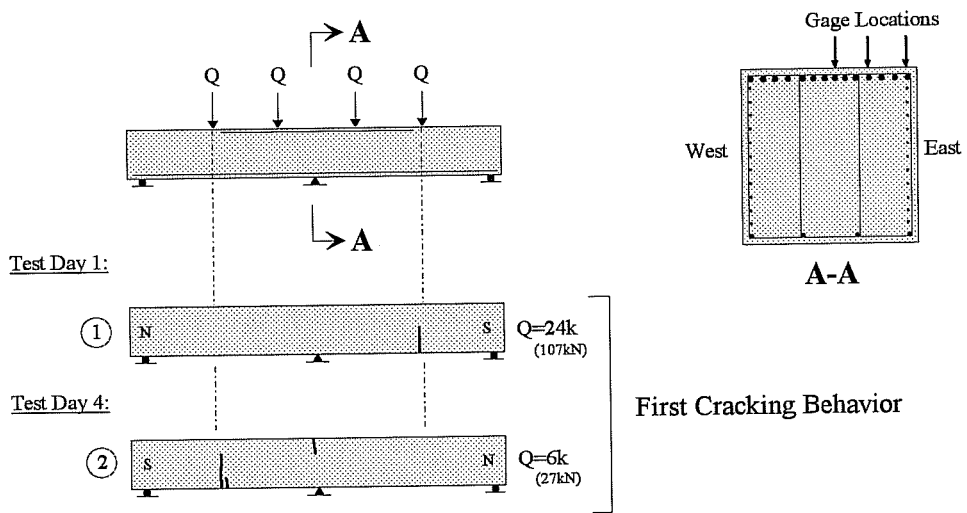
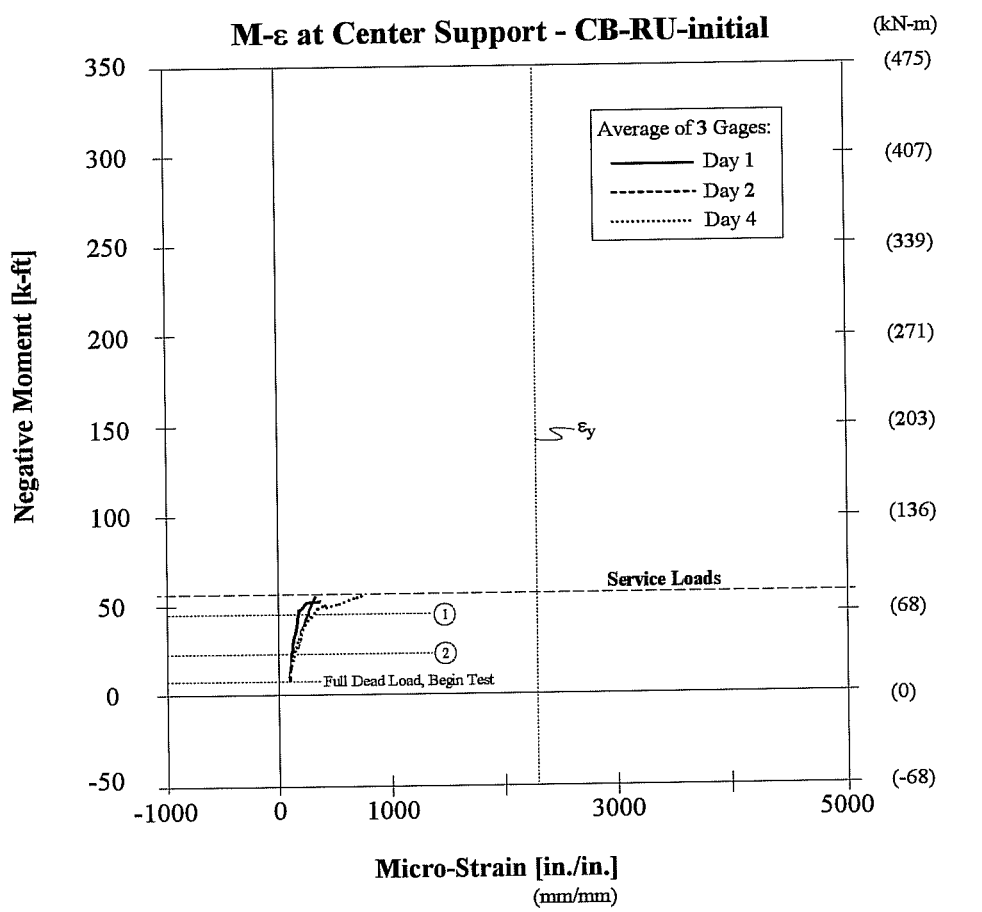


Figure 4.3 Moment-Strain Behavior in the Negative Moment Region CB-RU-initial

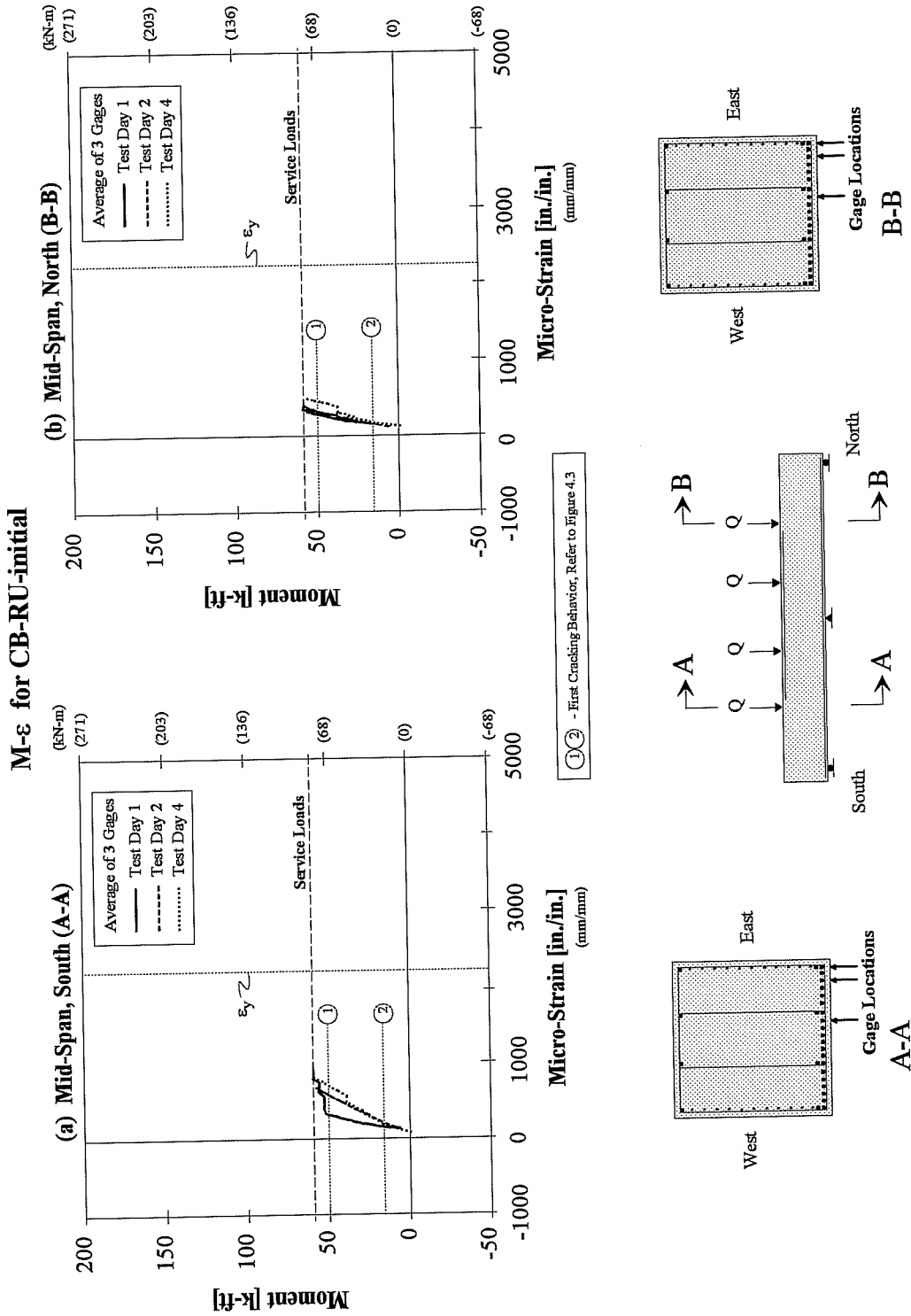


Figure 4.4 Moment-Strain Behavior of Mid-Span Tensile Steel - CB-RU-initial

the second day of testing the decreased slope indicates that the section was "softer". Although no cracking was visible to the eye, these results indicate that micro-cracking may have occurred. This is supported by the appearance of the first crack over the center support on Day 4 of testing under the unexpectedly low extreme tensile fiber stress of $3.8\sqrt{f'_c}$ ($0.31\sqrt{f'_c}$).

The tensile steel in all sections remained elastic up to service loads. This can be seen in Figures 4.3-4.4 where the maximum strains are substantially less than the yield strain $\epsilon_{y,s}$ of the steel.

Shear Force-Strain behavior was elastic up to service loads. The shear force is assumed to be the center support reaction. The results were similar to those presented for the final testing of this model in Figure 4.12 (see CB-RU-final, Section 4.2.2.2).

In looking at the side face crack control steel shown in Figure 4.5, first cracking behavior for the east face is presented and indicated on the plots with numbered circles (note that these numbered circles refer to the first cracking drawings presented on this figure and are different than those presented on Figure 4.3). On Day 1 of testing, Figure 4.5a shows linear increases in strain with increasing moment up to first cracking on this face. At this point the plot shows a quick increase in strain with no increase in moment. On Day 2, similar behavior resulted with the elastic portion being "softer" (smaller slope of the plot). Day 4 shows increases in strain and softening once the crack formed over the center support. On the north span, Figure 4.5b shows elastic behavior of the side face crack control steel with a general softening as the beam was being re-tested over the four different test days. This points to the presence of micro-cracking as no cracks were visible on the exterior. As with the southern span crack control steel, a small sudden increase in strain was measured on Day 4 shortly after the first appearance of a crack over the center support.

At the center support, Figure 4.5c shows the crack control steel behaving elastically on all three test days presented. Softening is particularly noticeable on Day 4 after a crack had formed in this region. The softening from Day 1 to Day 2 again points to the possible presence of micro-cracking.

M-ε for CB-RU-initial

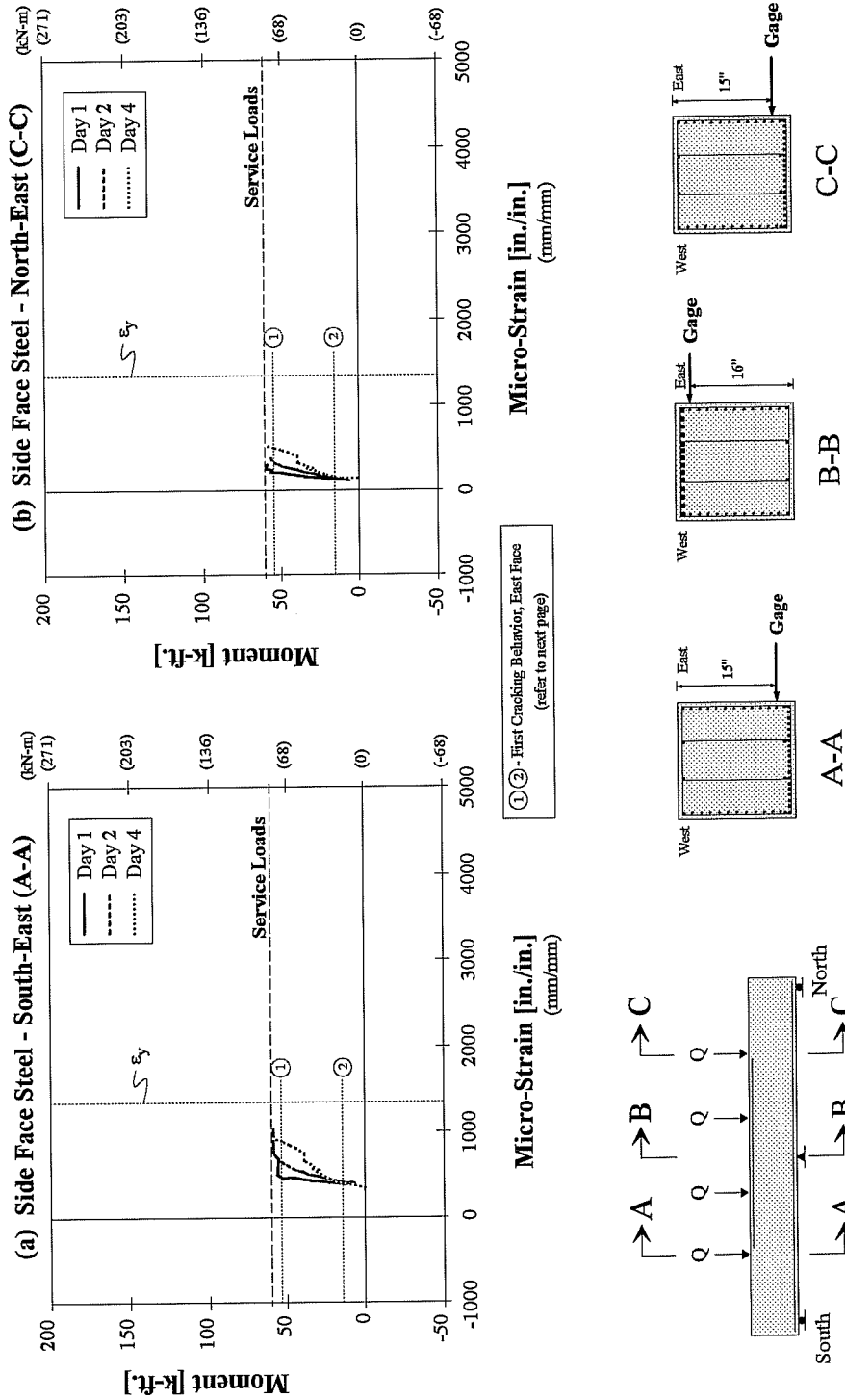


Figure 4.5 Moment-Strain Behavior of Side Face Crack Control Steel for CB-RU-initial (continued on next page)

M-ε for CB-RU-initial

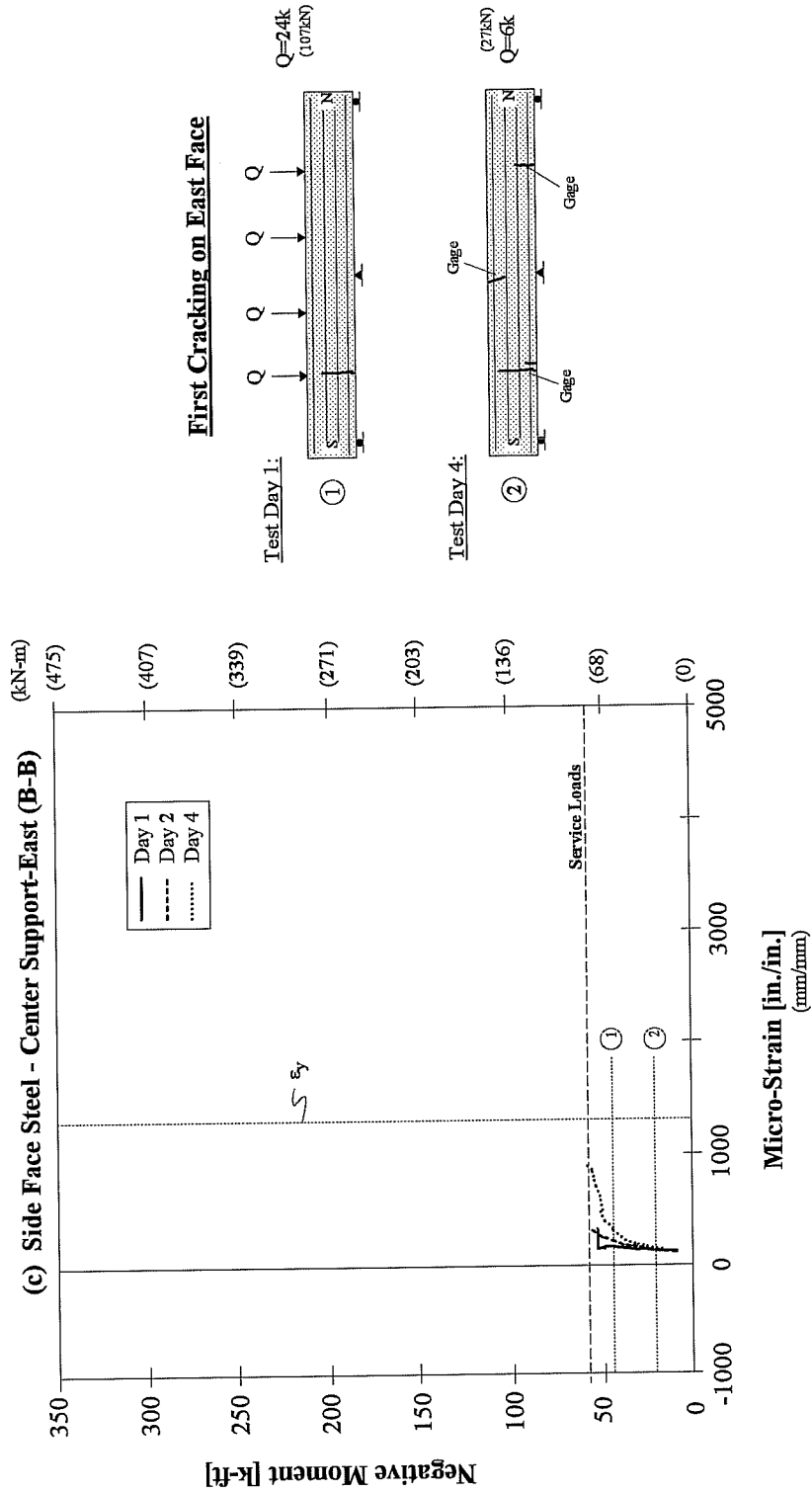


Figure 4.5 (cont.) Moment-Strain Behavior of Side Face Crack Control Steel for CB-RU-initial

4.2.1.3 Load-Deflection and Moment-Deflection Behavior - CB-RU-initial

Load-deflection behavior is not presented for the initial tests but is shown for the final test, CB-RU-final (refer to Section 4.2.2.3).

The moment-deflection behavior was similar for all three tests. The results from Day 1 of testing are shown in Figure 4.6. Deflection downwards is measured as positive. First cracking of the south span occurred on Day 1 of testing and is indicated on the plot with a numbered circle. This numbered circle refers to the first cracking drawing found in Figure 4.3. The north span results are more linear and show the north span to be stiffer than the south span.

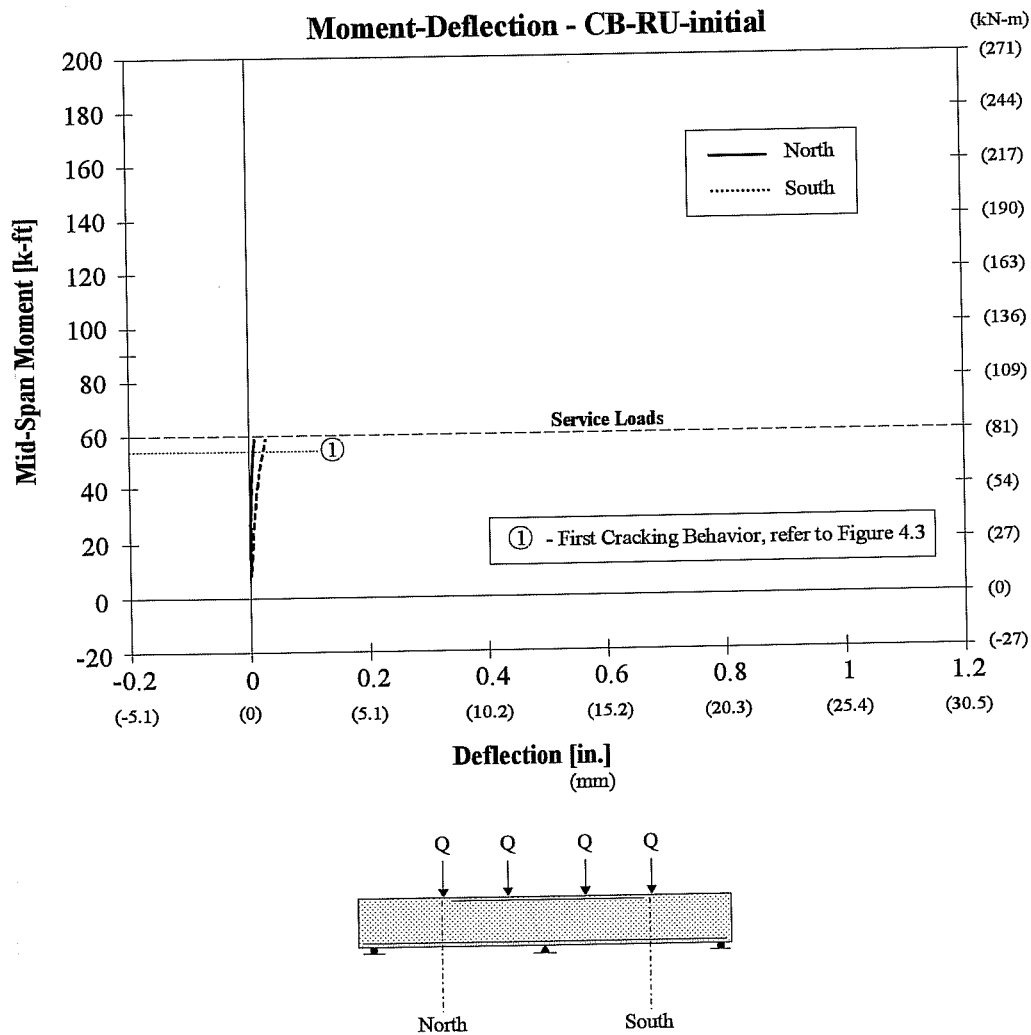


Figure 4.6 Mid-Span Moment-Deflection Behavior for CB-RU-initial

4.2.2 CB-RU-final - Conventionally Reinforced

After the test set-up was modified (see Section 3.6), the model was retested over the course of three days. Testing went smoothly. The first day the model was tested up to service loads only. The second day the model was tested past factored loads until a flexure-shear crack appeared in a sudden manner near the south support. The beam was then tested to failure on the third day.

The maximum measured moment over the center support was 207 k-ft. (281kN-m) which was greater than the 141 k-ft (191kN-m) predicted ultimate moment capacity of this section. This is attributed to restraining forces set up in the loading rams and is further discussed in Section 5.7.

4.2.2.1 Cracking Behavior - CB-RU-final

First Cracking - This model was pre-cracked over the center support and at the south mid-span. The first crack to appear near station 4 at the north mid-span occurred under point loads of 21k (93kN) (see Figure 4.7). This corresponds to a calculated cracking stress of $6.6\sqrt{f'_c}$ ($0.53\sqrt{f'_c}$).

Crack Widths & Serviceability - The distribution and lengths of cracks at service and factored loads as well as at ultimate are shown in Figure 4.7. Maximum crack widths for this test are listed in Table 4.2. The maximum crack width at service load was 0.005 in. (0.127mm) on a re-opened crack. At full scale this would correspond to a crack width of 0.020 in. (0.508mm). This does not satisfy the 1992 AASHTO indirect criterion of a maximum crack width of 0.0155 in. (0.039mm) for moderate exposure. The readings are accurate to within 0.0005 in. (0.013mm) which could put the experimental crack width somewhat closer to or further from the Specification limit.

Figure 4.8 shows a crack width envelope for this model. Here, maximum crack widths at service loads are plotted with respect to the load step at which they were measured. Again it can be seen that at service load levels the measured results lie slightly outside the allowable limits on which the 1992 AASHTO Bridge Design Specifications are based.

Side face crack control steel was placed in the tension zone to specifically control crack widths at levels where there was no flexural steel. As seen in Figure 4.9, the crack widths did tend to be larger above the level of the primary flexural steel in the positive moment region and below the flexural steel in the negative moment region. The side face crack control steel was therefore contributing to control of these crack widths.

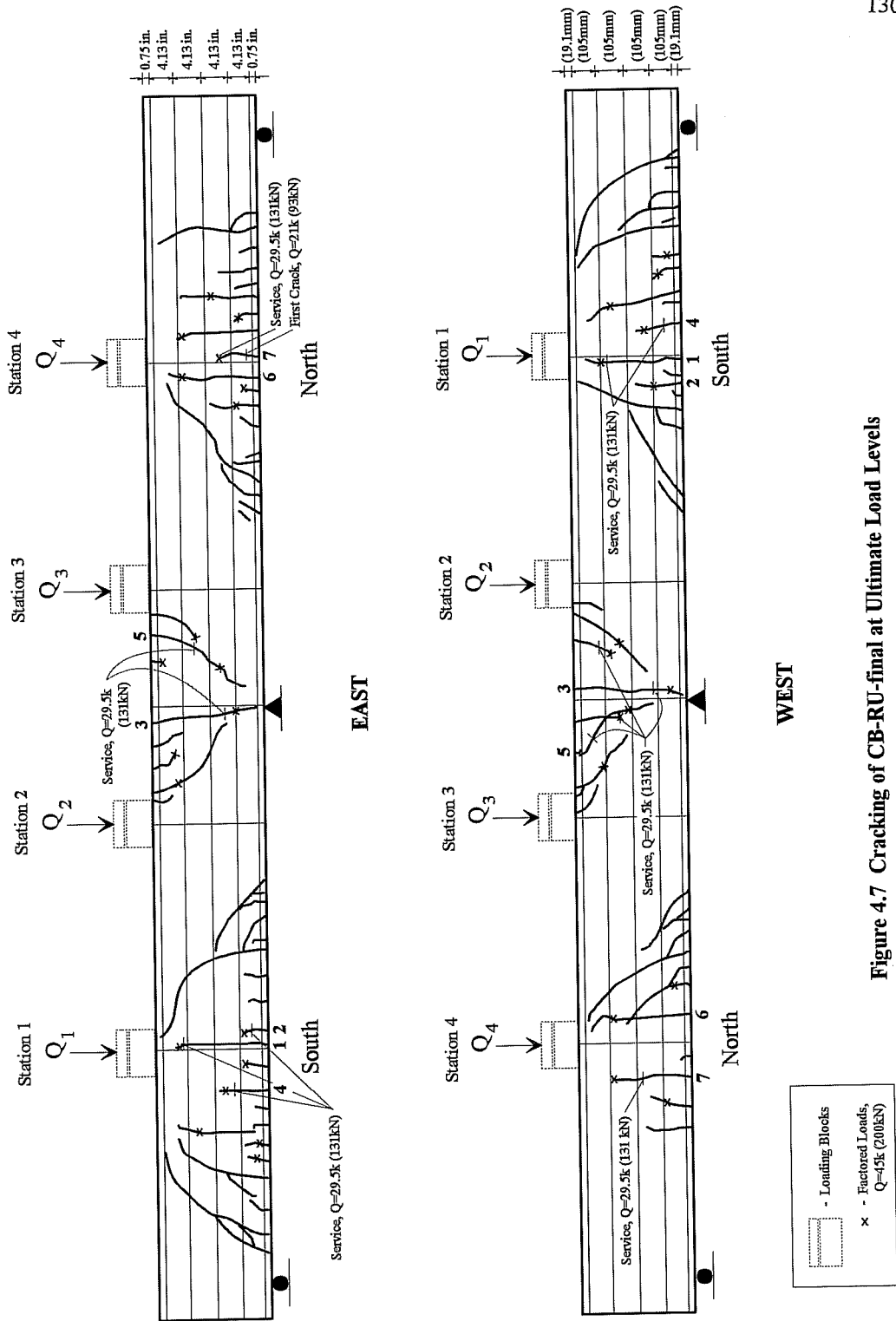


Figure 4.7 Cracking of CB-RU-final at Ultimate Load Levels

(a) CB-RU-final - East

TEST DAY	LOAD, Q Kips	CRACK WIDTH, in.						
		1	2	3	4	5	6	7
1	O (Full Dead)	0.0015		0.003				
1	29.5 - Service	0.004	0.0015	0.004		0.002		0.002
2	29.5 - Service	0.004	0.001	0.005	0.0015	0.0025		0.001
2	33	0.005	0.001	0.005	0.0015	0.004		0.003
2	39	0.006	0.0015	0.008	0.003	0.0045	0.003	0.003
2	45	0.01	0.003	0.01	0.003	0.005	0.004	0.003
3	45	0.009	n.m.	0.01	0.0025	0.004	0.005	n.m.
3	57	0.01	n.m.	0.012	n.m.	0.009	0.006	n.m.
3	69	0.01	n.m.	0.015	n.m.	0.012	0.006	n.m.

(b) CB-RU-final - West

TEST DAY	LOAD, Q Kips	CRACK WIDTH, in.						
		1	2	3	4	5	6	7
1	O (Full Dead)	0.002		0.001				
1	29.5 - Service	0.004		0.003		0.001		0.0015
2	29.5 - Service	0.003		0.003	0.0015	0.002		0.0015
2	33	0.0045		0.003	0.002	0.002		0.0025
2	39	0.0055	0.0015	0.0055	0.0025	0.0035	0.003	0.003
2	45	0.006	0.0025	0.01	n.m.	0.004	0.006	0.0045
3	45	0.007	0.002	0.01	n.m.	0.006	0.004	0.004
3	57	n.m.	n.m.	0.01	n.m.	0.008	0.003	0.006
3	69	0.01	n.m.	0.016	n.m.	0.008	0.005	0.005

Table 4.2E Maximum Crack Widths for CB-RU-final, English Units

(a) CB-RU-final - East

TEST DAY	LOAD, Q kN	CRACK WIDTH, mm						
		1	2	3	4	5	6	7
1	O (Full Dead)	0.038		0.076				
1	131 - Service	0.102	0.038	0.102		0.051		0.051
2	131 - Service	0.102	0.025	0.127	0.038	0.064		0.025
2	147	0.127	0.025	0.127	0.038	0.102		0.076
2	174	0.254	0.038	0.203	0.076	0.114	0.076	0.076
2	200	0.254	0.076	0.254	0.076	0.127	0.102	0.076
3	200	0.229	n.m.	0.254	0.064	0.102	0.127	n.m.
3	254	0.254	n.m.	0.305	n.m.	0.229	0.152	n.m.
3	307	0.254	n.m.	0.381	n.m.	0.305	0.152	n.m.

(b) CB-RU-final - West

TEST DAY	LOAD, Q kN	CRACK WIDTH, mm						
		1	2	3	4	5	6	7
1	O (Full Dead)	0.051		0.025				
1	131 - Service	0.102		0.076		0.025		0.038
2	131 - Service	0.076		0.076	0.038	0.051		0.038
2	147	0.114		0.076	0.051	0.051		0.064
2	174	0.14	0.038	0.14	0.064	0.089	0.076	0.076
2	200	0.152	0.064	0.254	n.m.	0.102	0.152	0.114
3	200	0.178	0.051	0.254	n.m.	0.152	0.102	0.102
3	254	n.m.	n.m.	0.254	n.m.	0.203	0.076	0.152
3	307	0.254	n.m.	0.406	n.m.	0.203	0.127	0.127

Table 4.2S Maximum Crack Widths for CB-RU-final, S.I. Units

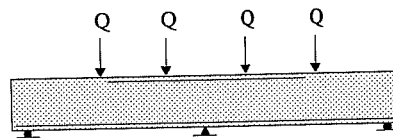
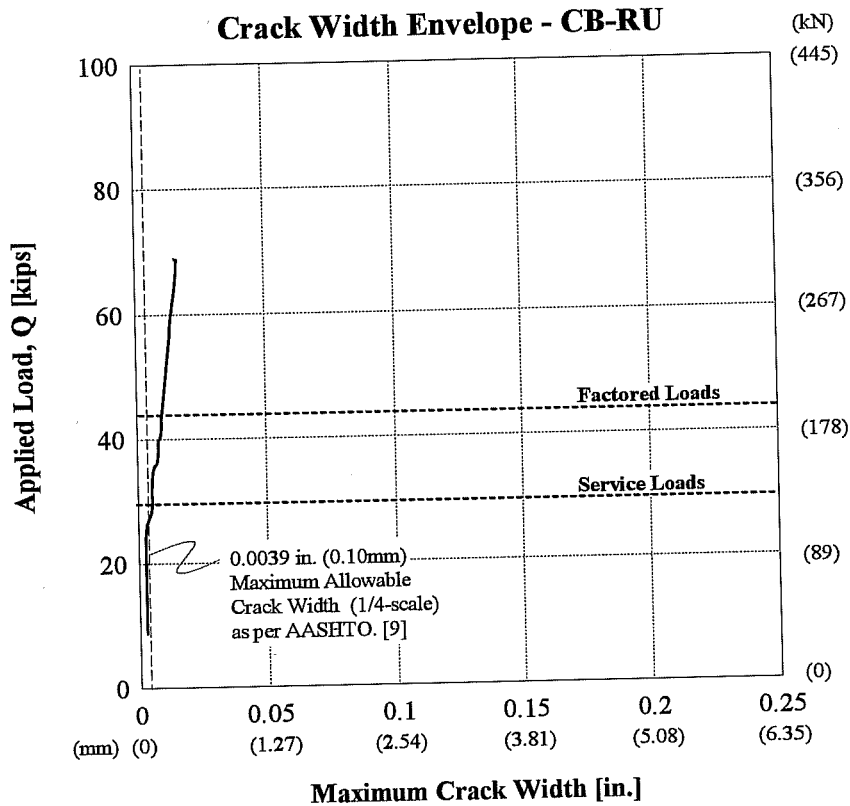


Figure 4.8 Maximum Crack Width Envelope - CB-RU

Distribution of Cracking - Cracking was initially dominated by flexural cracking as can be seen with the service load cracks shown in Figure 4.7. At factored loads, cracks continued to be well distributed and flexure-shear cracks began to appear over the center support. Both flexure and flexure-shear cracks continued to form until failure. A large flexure-shear crack between the southern support and station 1 led to sudden failure of this beam (see Figures 4.7, 4.17, and Moment-Deflection Behavior, Section 4.2.2.4).

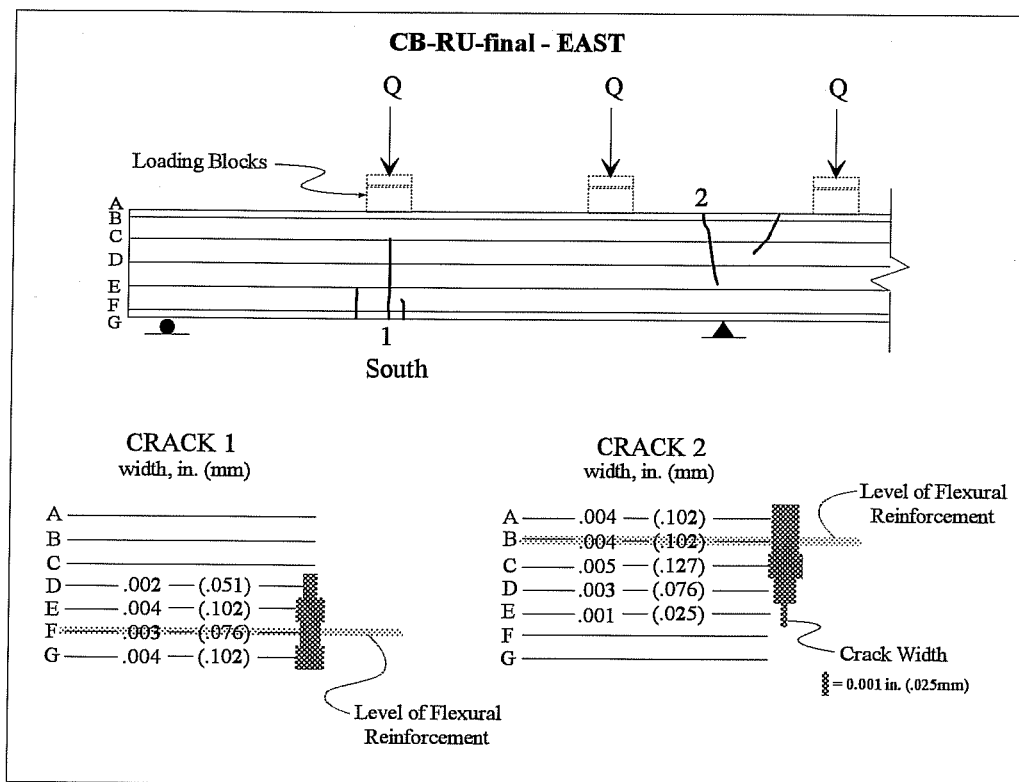


Figure 4.9 Behavior of Side Face Crack Control Steel at Service Loads for Model CB-RU-final

4.2.2.2 Moment-Strain Behavior - CB-RU-final

Moment-strain data for the tensile steel is presented in Figures 4.10-4.13. First cracking of the north span is presented in Figure 4.10 and is indicated on the plots of Figures 4.10-4.13 with a numbered circle. Figure 4.10 shows that over the center support, the steel behaved elastically up to a negative moment of approximately 180 k-ft. (245 kN-m). At this point the steel clearly yielded.

Figure 4.11a shows that the tensile steel in the south span behaved fairly linearly up to factored loads. Here, the section seemed to soften and then continue to strain linearly until failure. This steel had just yielded when failure occurred. The relatively constant linear behavior similar to that over the center support is due to the section being pre-cracked.

Figure 4.11b shows that at the north span a more abrupt change in stiffness is apparent. This occurred around service loads, shortly after the first crack in the region appeared. The change in slope most likely occurred after the initial crack was seen because the gages were not located right at the crack. The gages

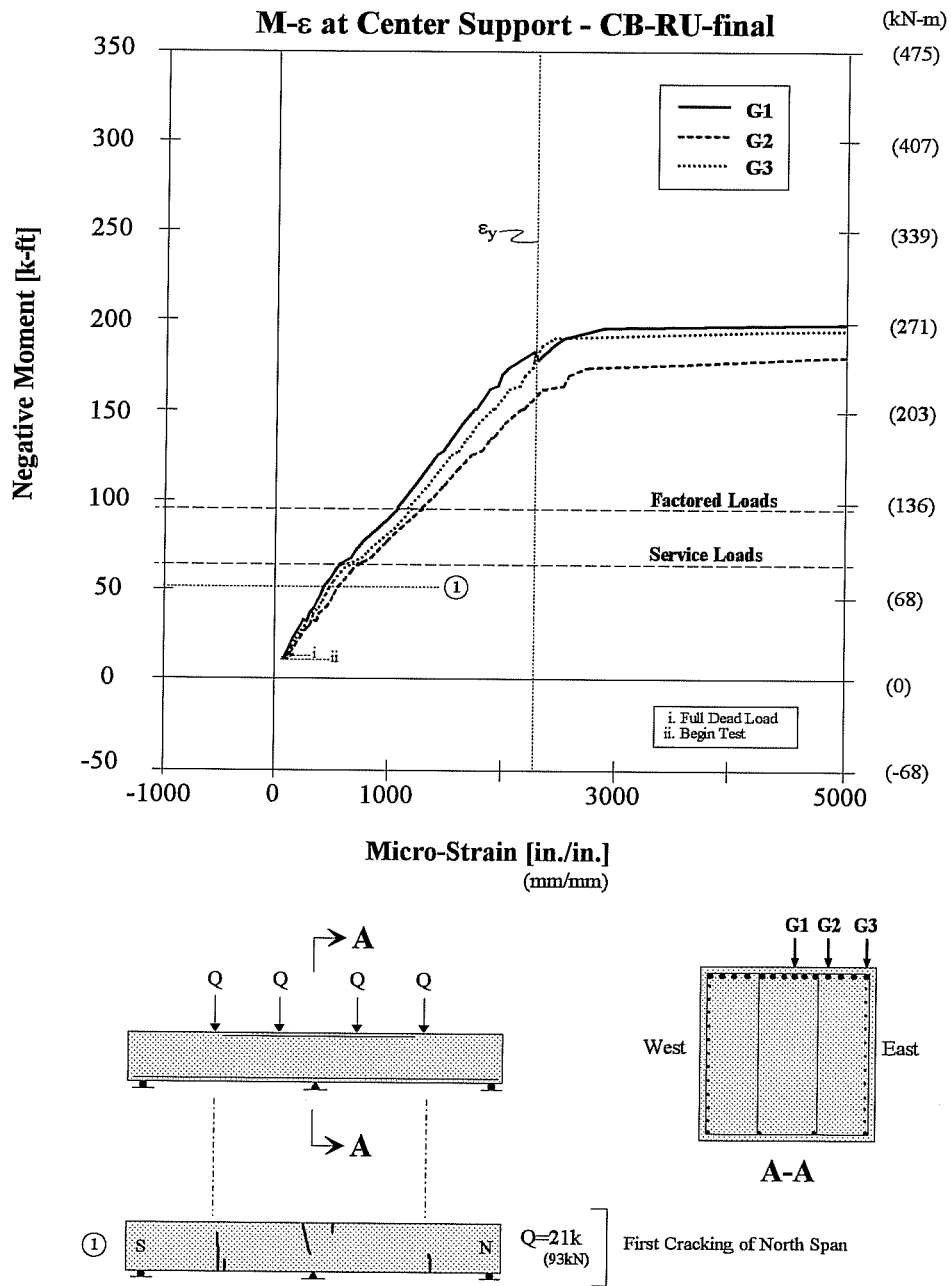


**Figure 4.10 Moment-Strain Behavior in the Negative Moment Region
 CB-RU-final**

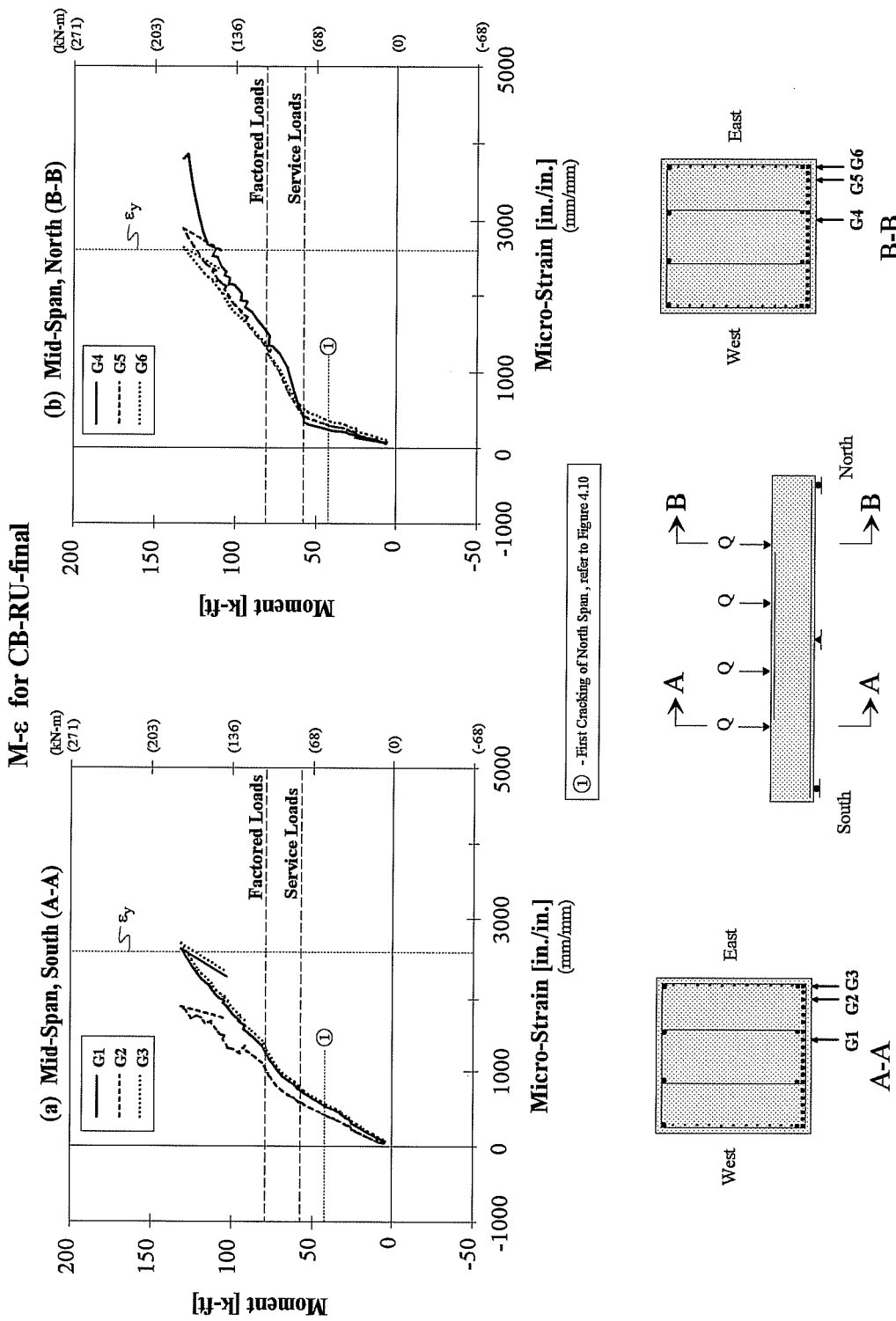


Figure 4.11 Moment-Strain Behavior of Mid-Span Tensile Steel - CB-RU-final

would not register the increased stress in the steel until the force was developed back from the crack to the location of the gage. One of the gages in this span showed the steel markedly yielding when failure occurred (Gage 4 of Figure 4.11b).

The shear force vs. stirrup strain behavior in the negative moment region is presented in Figure 4.12. The shear force is assumed to be the center support reaction. Behavior for the gaged inner stirrup was elastic up to service loads where a quick increase in strain occurred. Behavior then continued to be elastic until a shear force of approximately 185k (823kN) was reached. At this point, the gage appears to have malfunctioned. The outer stirrup measured very little change in strain throughout the test. Shear force-stirrup strain results for the other gaged stirrups showed very little change in strain throughout testing.

Moment-strain behavior for the side face crack control steel is shown in Figure 4.13. First cracking behavior for the east face is presented and indicated on the plots with numbered circles (note that these numbered circles refer to the first cracking drawings presented on this figure and are different than those presented on Figure 4.10). Figure 4.13a shows that both of the gaged side face crack control steel elements behaved elastically up to service loads. The results for the steel closer to the extreme tensile fiber near the south mid-span followed a smaller slope. This was to be expected as the section was pre-cracked and therefore "softened". At factored loads this steel yielded while the steel further from the extreme tensile fiber continued to strain elastically. At a mid-span moment of 90 k-ft (122 kN-m), the gage appears to have malfunctioned. On the north span, Figure 4.13b shows that both crack control steel elements behaved elastically until a moment of approximately 70 k-ft (95 kN-m) was reached. This corresponded to loads half-way between service and factored loads. Up to this point, there were no considerable increases in strain measured near the load that induced first cracking of this section. Most likely, the crack control gages were not located where the crack was located. Beyond this point, strains increased at a higher rate until yielding began shortly after factored loads were applied. The crack control steel at the north span therefore did not appear to be controlling cracks until after service loads. At the south span that was pre-cracked, the crack control steel was controlling cracks from the beginning of the test.

At the center support, the crack control steel behaved elastically up to and slightly beyond service loads. The shallow slope seems to be a result of the section having been pre-cracked and the steel did seem to be controlling cracks at service loads. The gages appear to have malfunctioned before factored loads were reached.

Due to the sudden failure of this model, the contribution of the side face crack control steel to nominal resistance is unclear.

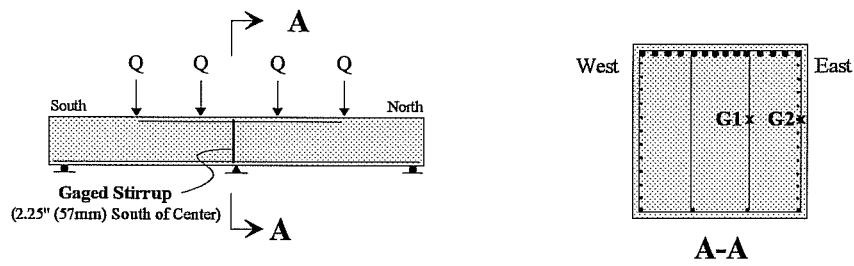
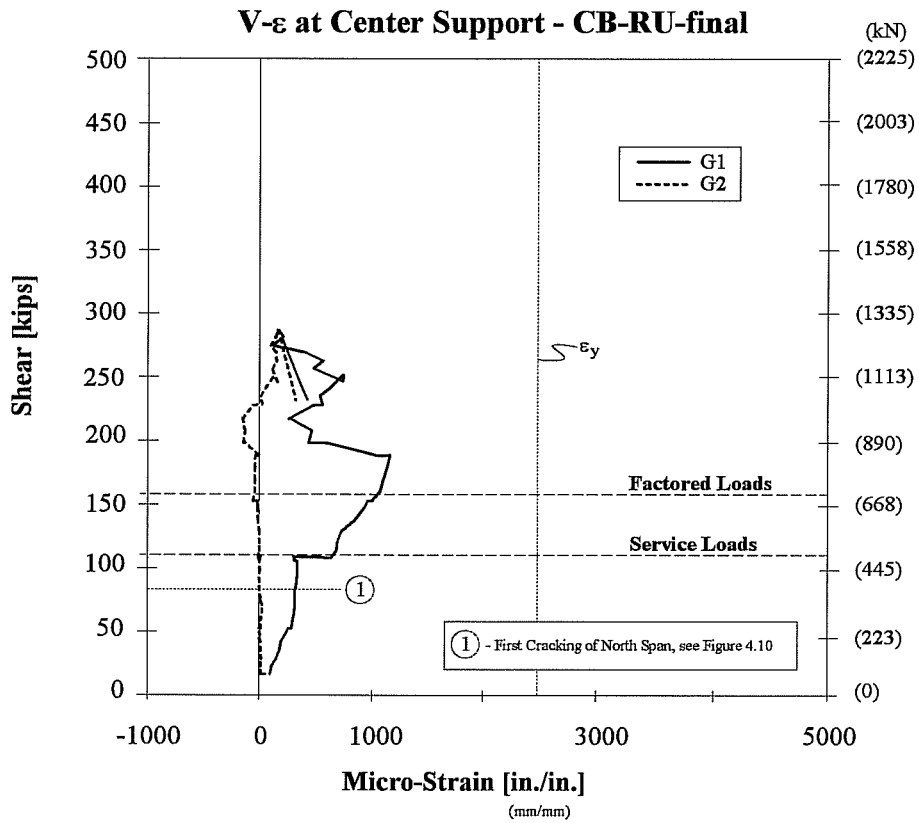


Figure 4.12 Center Support - Strain Behavior for Shear Stirrups - CB-RU-final

M-ε for CB-RU-final

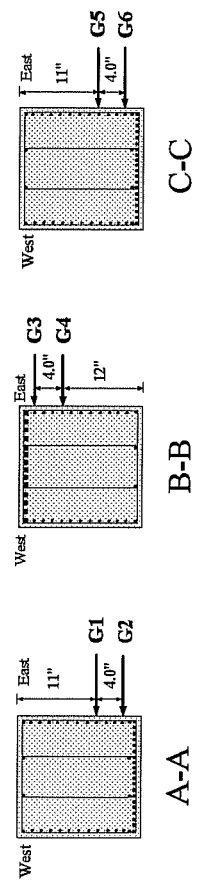
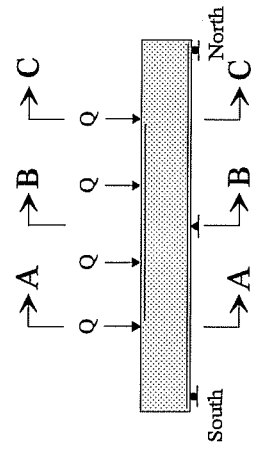
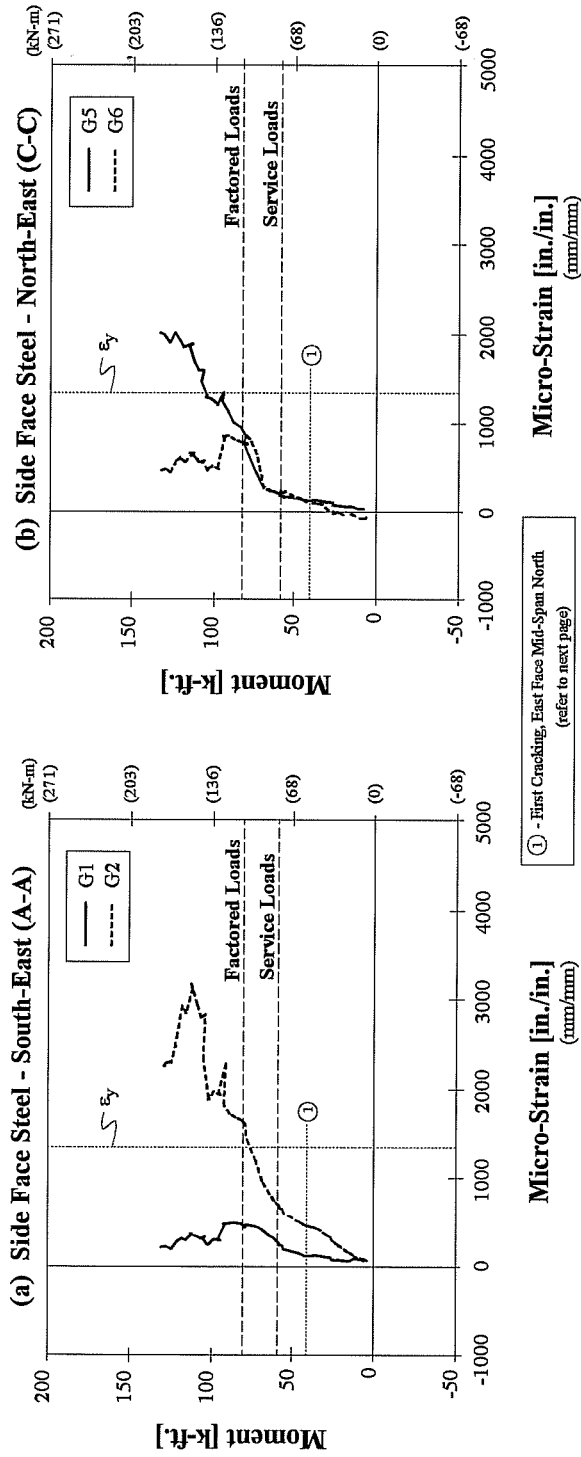
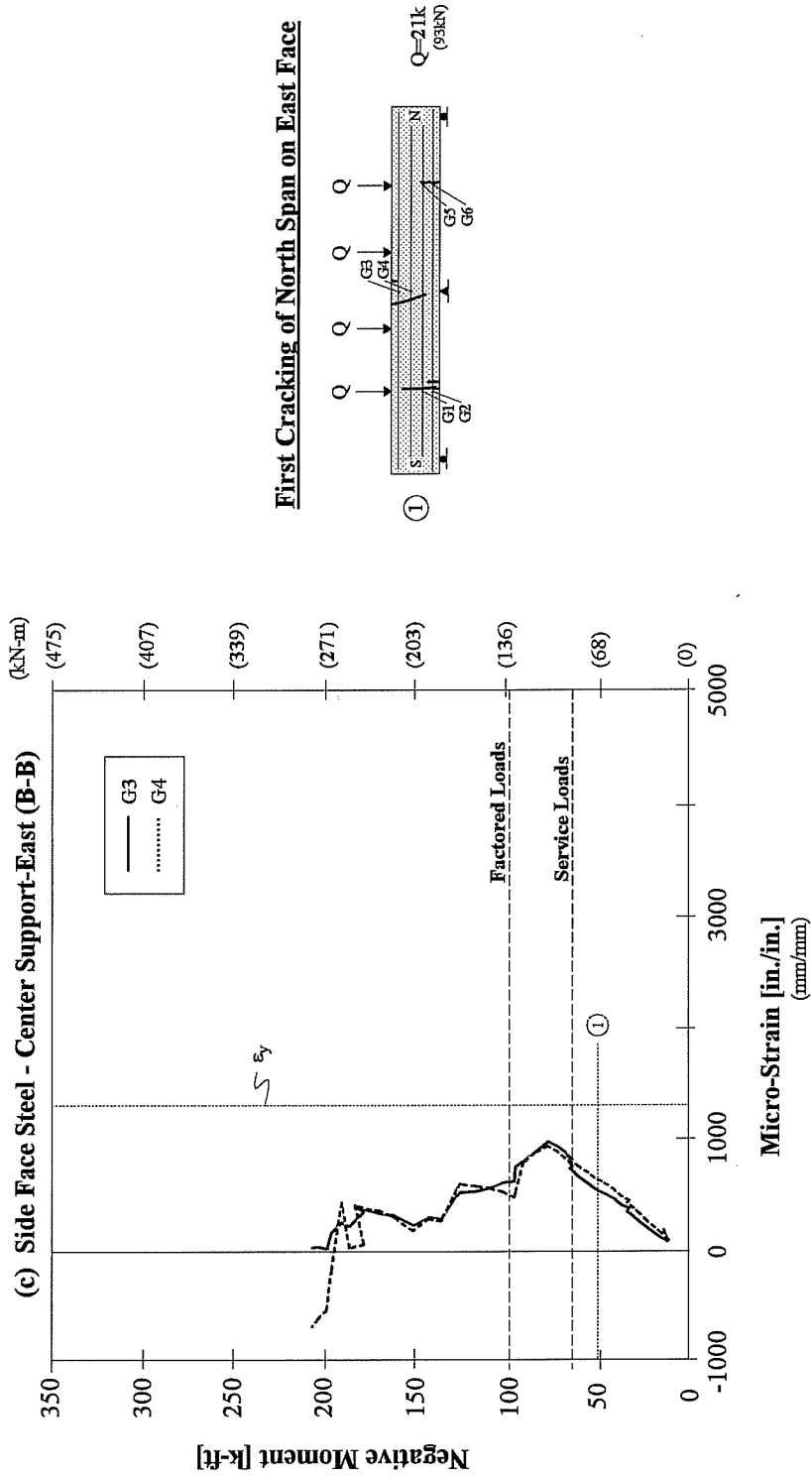


Figure 4.13 Moment-Strain Behavior of Side Face Crack Control Steel for CB-RU-final (continued on next page)

M-ε for CB-RU-final



First Cracking of North Span on East Face

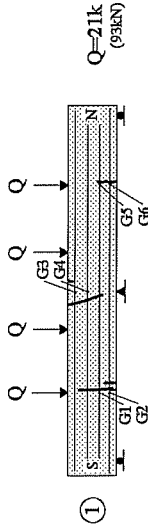


Figure 4.13 (cont.) Moment-Strain Behavior of Side Face Crack Control Steel for CB-RU-final

4.2.2.3 Applied Load vs. Moment Behavior - CB-RU-final

Figure 4.14 is a plot of the applied point loads, Q , versus the moment at the mid-spans and over the center support. Moment redistribution behavior can be seen in this figure where the linearity of the plots change. (This is best seen by looking down the x-axis with the figure held horizontally at eye-level.)

The beginning of the plot shows the moment corresponding to an equivalent point load, $Q_{\text{equivalent}}$. This equivalent point load represents the loading before the point loads are applied for testing. The equivalent load corresponds to a point load that would produce the same negative moment over the center support that the dead load creates. While this is not representing the behavior of the mid-spans exactly numerically, the behavior is well-represented by the linearity and slope changes of the plot.

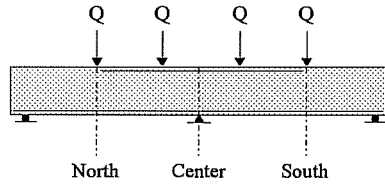
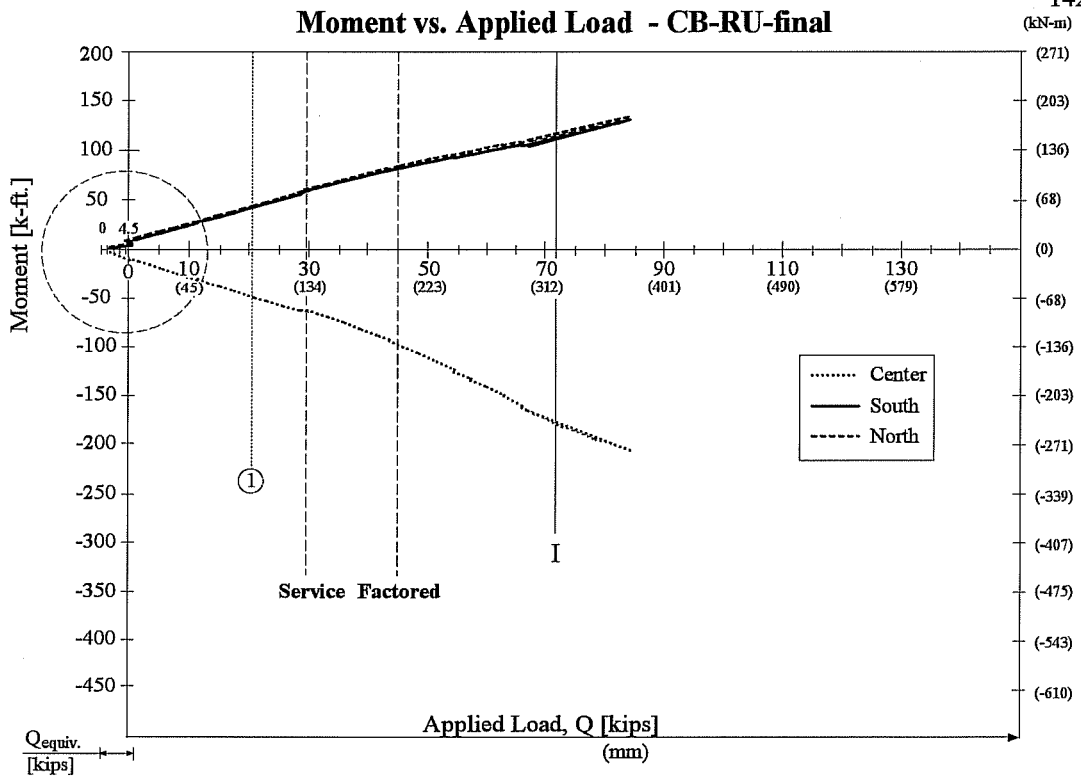
First cracking of the north span is indicated with a numbered circle corresponding to the first cracking drawing presented in Figure 4.10. First yielding is indicated with the roman numeral I, and corresponds to the yield moment found from the moment-strain results of Section 4.2.2.2.

The first evidence of moment redistribution occurs around service loads where there is a shift in the slope of the plots. The mid-span moments begin to increase more rapidly while the moment over the center support increases less rapidly. Moment seems to be redistributing from the center support to the mid-span regions. Around factored loads however, this begins to reverse as moment is distributed back from the mid-spans towards the center support. When yielding of the center support occurs (marked with "I" on Figure 4.14), the moment over the center support continues to attract more moment from the mid-spans. The plot ends at the point where the large-flexure shear crack near the southern support formed.

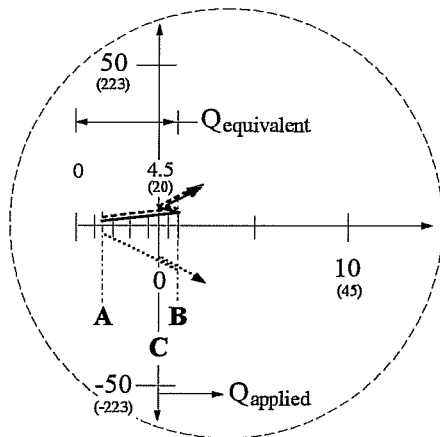
4.2.2.4 Load-Deflection Behavior - CB-RU-final

Load-deflection behavior for this model is shown in Figure 4.15. Service load deflection criteria in accordance with AASHTO 1992 and ACI-318-89 were satisfied. The maximum service load deflection corresponded to $L/2900$.

Stiffness changes are not apparent in this pre-cracked beam until near factored loads where a general softening of the beam occurs. This beam exhibited very little ductility due to the sudden failure resulting from the formation of the flexure-shear crack near the southern support. Despite this early failure, the beam clearly exhibits overstrength. A load of 1.9 times factored loads was carried at the time of failure.



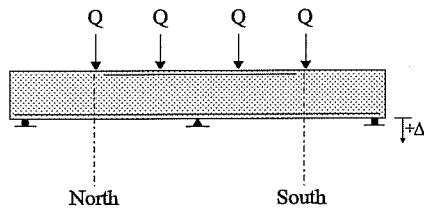
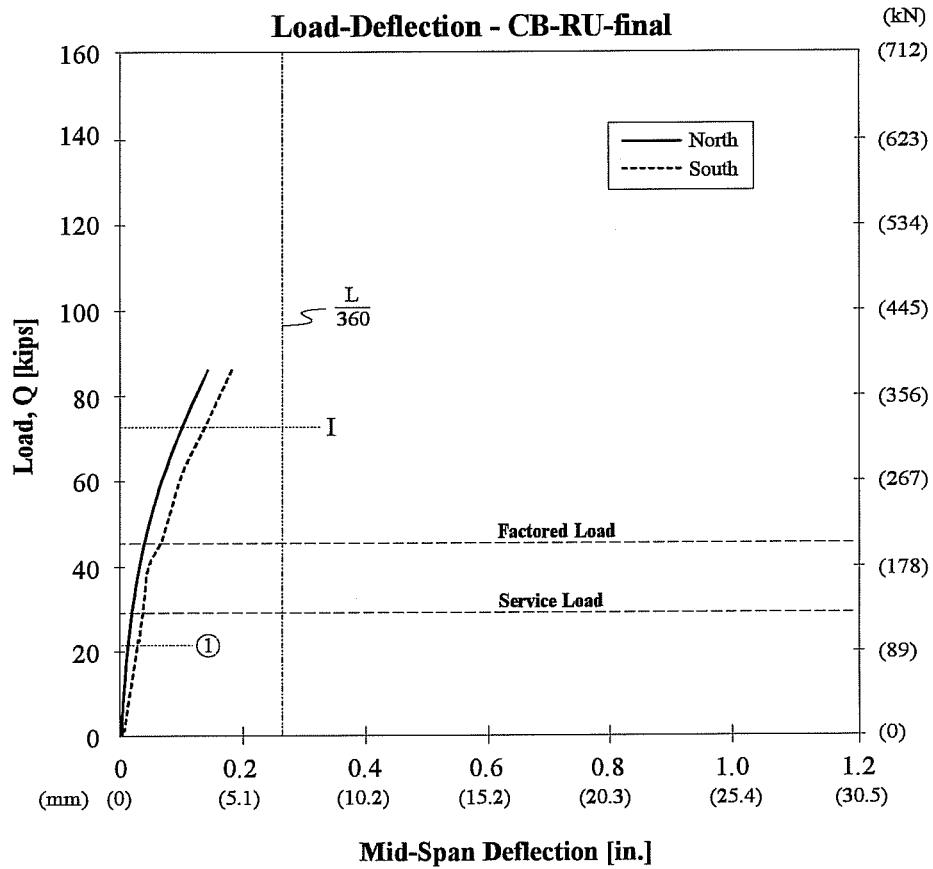
① First Cracking of North Span, see to Figure 4.10
 I. Yield of Tensile Steel at Center



Where $Q_{equivalent}$ is the force corresponding to loads Q , that would produce the negative moment over the center support resulting from the dead load. Both negative and positive moments are plotted using the same $Q_{equivalent}$.

- A** - Beam Only
- B** - Full Dead Load
- C** - Begin Test

Figure 4.14 Moment vs. Applied Load - CB-RU-final



① - First Cracking of North Span, refer to Figure 4.10
 I. Yield of Non-prestressed Steel, Mid-Span Center

Figure 4.15 Load-Deflection Behavior - CB-RU-final

4.2.2.5 Moment-Deflection Behavior - CB-RU-final

The moment-deflection plot for CB-RU-final is shown in Figure 4.16. The plotted curve represents the response of a model pre-cracked at two of the critical moment regions - the southern mid-span and over the center support. Deflection downwards is measured as positive. The deflection scale reaches 1.2 in. (30.5mm) as this is the largest deflection recorded for all four of the test models. Plotting the curve with a reduced x-axis would accentuate changes in the slope of the curve. This would be misleading in that the slope changes may be interpreted as yielding points when in fact they are slight changes in stiffness due to increased cracking.

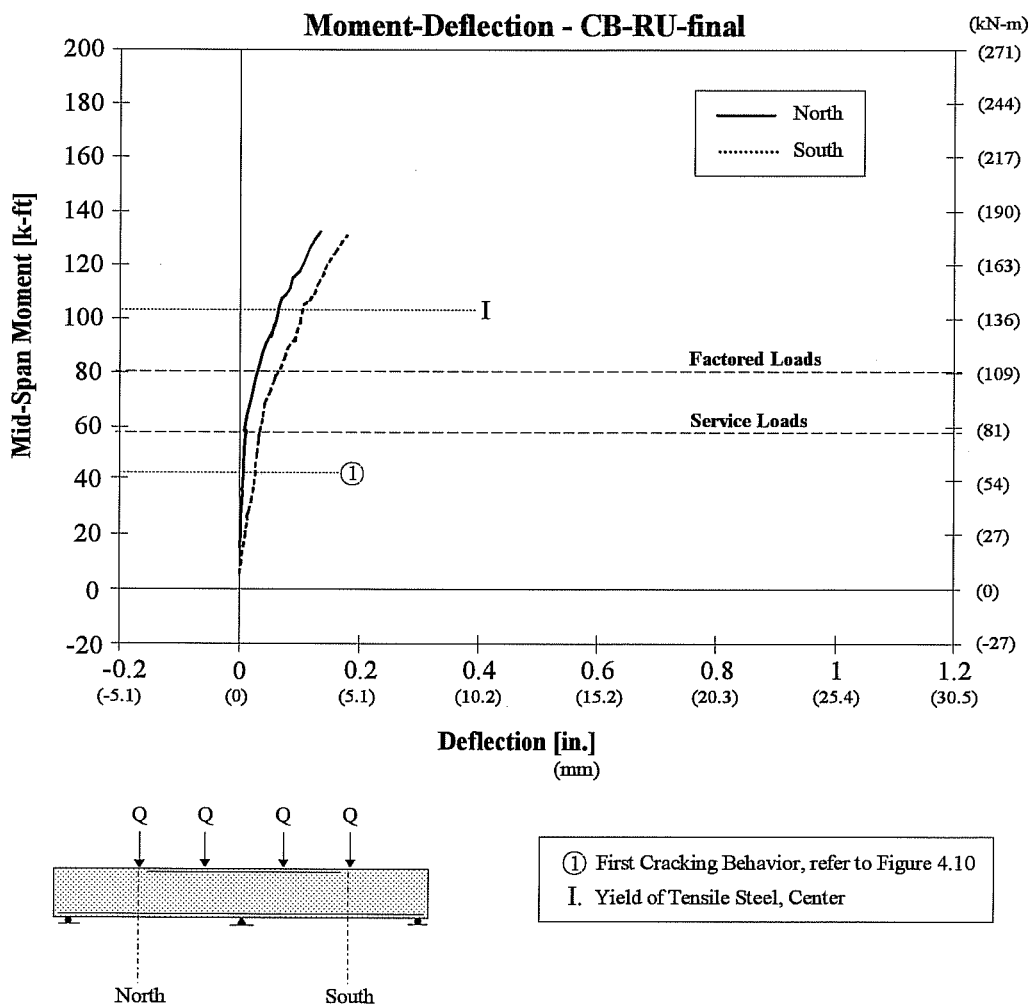


Figure 4.16 Mid-Span Moment-Deflection Behavior for CB-RU-final

First cracking of the north span is indicated by the numbered circle and refers to the first cracking drawing of Figure 4.10, and first yielding as indicated by the moment strain results of Section 4.2.2.2 is represented with the roman numeral, I.

Up to the point of failure, there are no distinct points at which yielding seems to have occurred. The moments at the critical sections at failure were -207 k-ft (-281 kN-m) over the center support and 132 k-ft (179 kN-m) at the mid-spans. This occurred under point loads of 84k (374kN). Little ductility is evidenced by the sudden failure.

4.2.2.6 Post-mortem Investigation - CB-RU-final

This model was not opened after testing was completed. However, at failure, the large flexure-shear crack shown in Figure 4.17 and 4.18 was 1.25 in. (32mm) wide and it was observed that all seven flexural bars that continued beyond the support had fractured. There was no evidence of debonding and a number of the bars that had been cut off were visible as well.

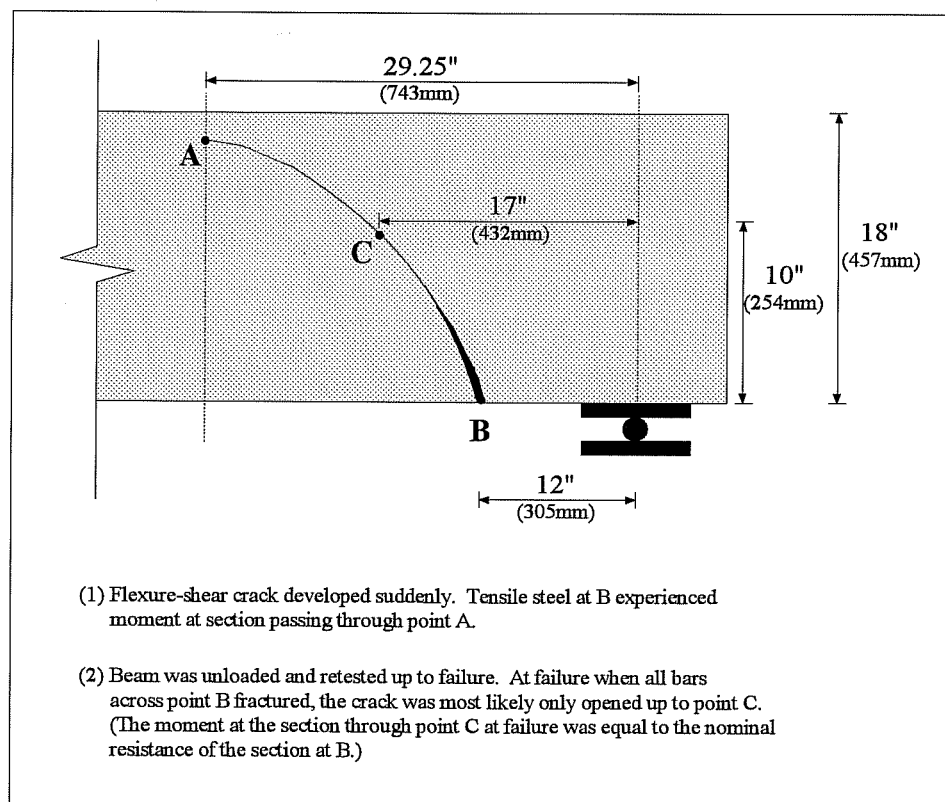


Figure 4.17 Failure Condition for CB-RU-final

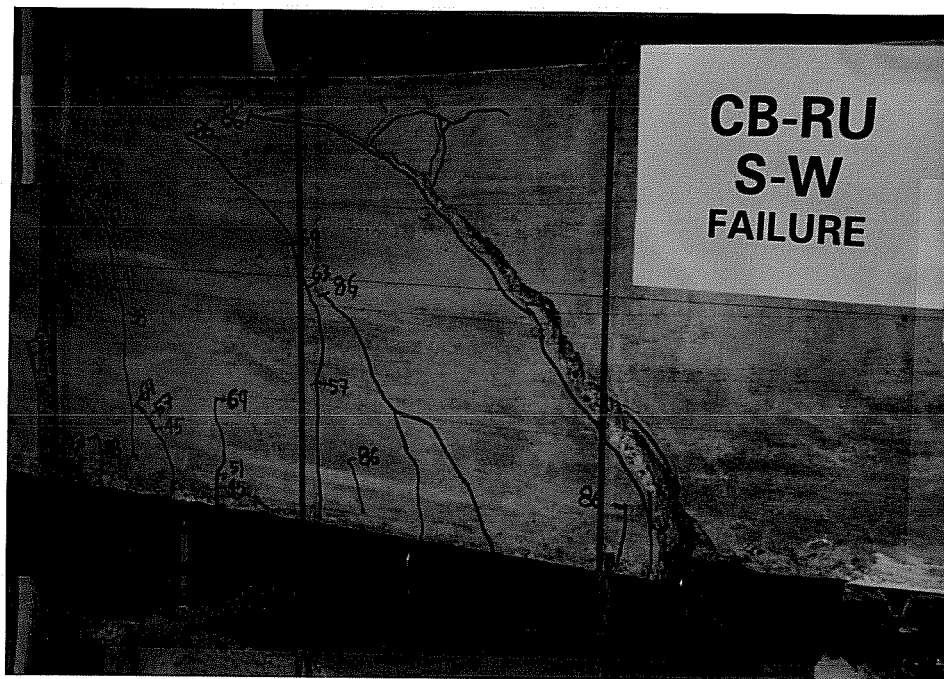


Figure 4.18 Failure Condition for CB-RU-final - South Support, West Side

4.2.2.7 Further Discussion - CB-RU-final

Even though a poor detail led to a sudden failure, the beam appeared to be continuing to carry load well until that point. The deflections were small and the majority of the mid-span tensile steel had not yet yielded. With this failure at a load of 84k (374kN), the beam was already carrying 1.9 times the factored loads for which it was designed. While the negative moment region had been designed for ultimate loads, the positive moment region was in effect substantially over-designed in order to satisfy crack control criteria for the AASHTO Bridge Design Specifications. This probably caused some of the excessive over-capacity of the beam. Restraining forces in the loading rams, as discussed in Section 5.7, may also have contributed to this experimental over-strength.

Failure - Failure occurred suddenly with the fracturing of all of the reinforcement across a section 1 ft. (305mm) from the southern support (see Figures 4.17 & 4.18). This occurred as the result of a flexure-shear crack that first appeared under applied point loads of 84k (374kN), a level 90% higher than factored loads. Testing was stopped upon the formation of this crack. The model was unloaded and reloaded up to point loads of 77k (343kN) when all of the bars fractured.

The formation of a flexure crack in this region occurred due to a reinforcement detail in which all but 7 of the positive moment reinforcing bars were cut off. The moment at the location of the initial flexure crack was 35 k-ft. (47 kN-m). The predicted cracking moment of the beam was 38 k-ft. (typical provision of minimum nominal resistance of 1.2 times the predicted cracking moment, M_{cr} , was not necessary in design as per Article 8.17.1.2 in the AASHTO Bridge Design Specifications).

At fracture of all the reinforcement at this section, the moment in the steel was equivalent to that at the top of the crack, or the compression zone. This point was 29.25 in. (743mm) from the end support which would have resulted in a moment of 66 k-ft at the fractured section (see Figures 4.17 and 4.18). The nominal resistance of this section however, was calculated as being approximately 39 k-ft. Most likely, the crack did not re-open all the way out to 29.25 in. (743mm) from the support. Based on the southern support reaction and considering dead load (which was not part of the reactions here), a moment of 39 k-ft would occur 17 in. (434mm) from the southern support. In looking at the crack diagrams, the crack would have been reopened approximately 10 in. into the depth of the section.

4.2.3 CB-PS-100S - Prestressed based on AASHTO (Service Load Design)

This model was post-tensioned and grouted 5 days before it was first tested. On the first day of testing, the model was loaded to three times factored loads ($Q=135k$, 600kN). Two days later the beam was loaded to failure.

Due to the draped tendon and high prestressing force, staged loading was required. Point loads of 11k (49kN) were applied when the post-tensioning was half complete. This load was then maintained for the remainder of the post-tensioning operations and through completion of testing.

As with model CB-RU, the maximum measured moment over the center support for model CB-PS-100S exceeded the predicted ultimate capacity of this section. A moment of 417 k-ft. (566kN-m) was measured and 236 k-ft (320kN-m) was the predicted ultimate moment capacity of this section. This is again attributed to restraining forces set up in the loading rams and is further discussed in Section 5.7.

4.2.3.1 Cracking Behavior - CB-PS-100S

First Cracking - First cracking occurred over the center support under point loads of 43k (191kN) (see Figure 4.19). This corresponds to an extreme concrete tensile fiber stress of $4.6\sqrt{f'_c}$ ($0.37\sqrt{f'_c}$) assuming full effective prestress.

The first crack in the mid-span region of the north and south spans (stations 4 and 1, respectively) appeared under point loads of 58k (258kN) where the moments at these sections were 92 k-ft. (125 kN-m) and 88 k-ft (119 kN-m) respectively. These correspond to calculated cracking tensile stresses of $6.5\sqrt{f'_c}$ ($0.52\sqrt{f'_c}$) and $5.9\sqrt{f'_c}$ ($0.47\sqrt{f'_c}$) respectively, assuming full effective prestress.

Crack Widths & Serviceability - Figure 4.19 shows the crack locations under service and factored loads as well as at failure. Maximum crack widths for certain load steps are recorded in Table 4.3. These maximum crack widths are then plotted versus each load step in Figure 4.20 to give a maximum crack width "envelope".

This beam did not crack under service loads and therefore satisfied serviceability criteria in terms of crack control.

By factored loads one crack had formed over the center support and it measured 0.002 in. (0.051mm) wide, corresponding to a crack width of 0.008 in. (0.203mm) for a full-scale prototype.

Distribution of Cracking - Three major cracks formed at each critical moment region and they were relatively evenly spaced. Near station 4 at mid-span of the north span, the cracks appeared to be flexure cracks up to failure. Near station 1 at mid-span of the south span, the flexure cracks developed into flexure-shear cracks at point loads of approximately 77k (343kN). Of the three flexure cracks over the center support, one was directly above the pin support and the other two began away from the center and developed as flexure-shear cracks, moving closer to the center as they propagated more deeply into the section. This was most likely the result of high shear forces at this location. The 1" (25.4mm) steel plate which supported the beam above the pin may also have affected the beam at this location, forcing the cracks to form further away from the center.

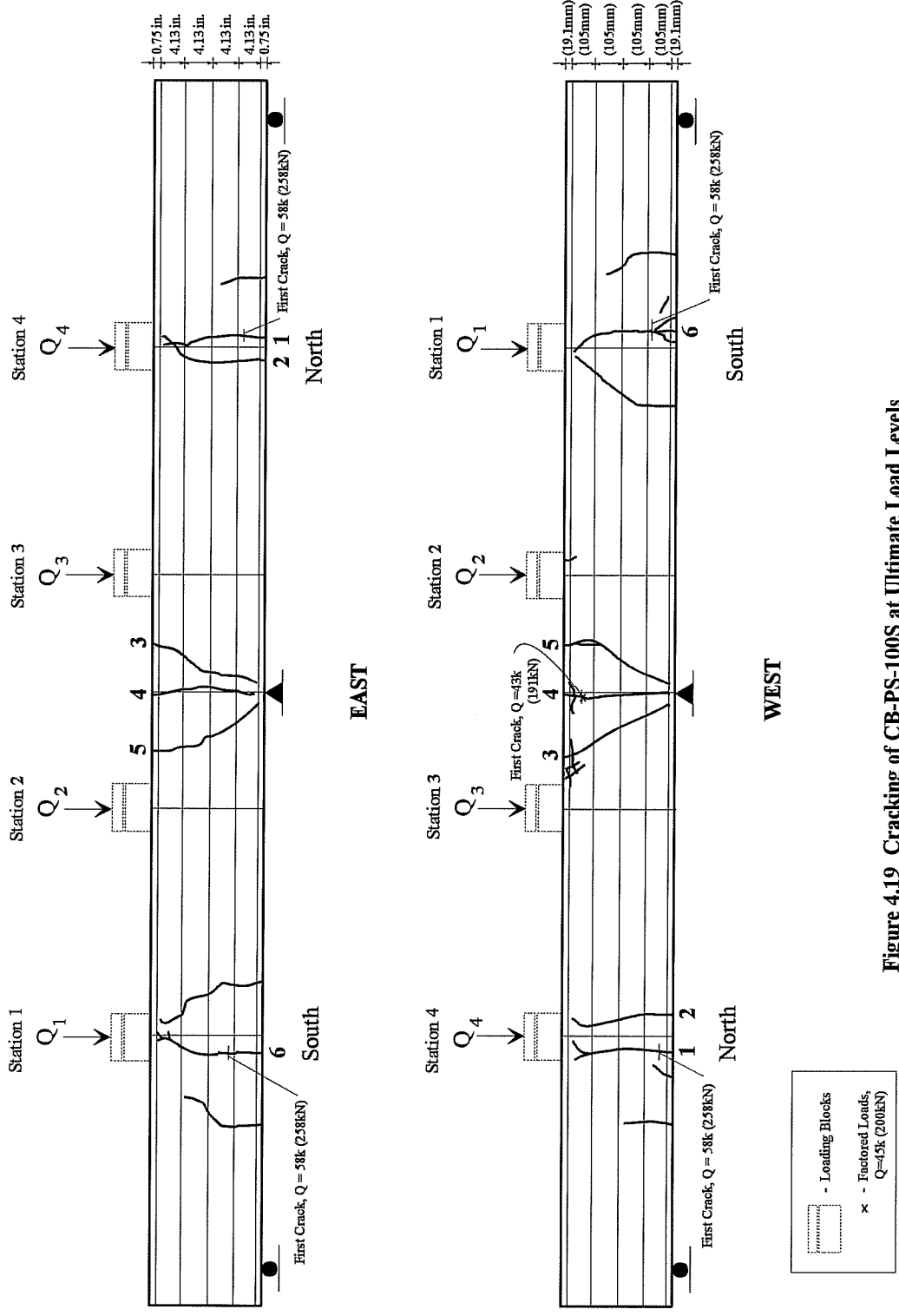


Figure 4.19 Cracking of CB-PS-100S at Ultimate Load Levels

(a) CB-PS-100S - East

LOAD, Q Kips	CRACK WIDTH, in.					
	1	2	3	4	5	6
29.5 - Service	-	-	-	-	-	-
43	-	-	-	-	-	-
45 - Factored	-	-	-	-	-	-
51	-	-	-	0.0025	-	-
58	0.0015	-	-	0.002	-	0.0015
64	0.003	-	-	0.003	0.002	0.005
70	0.004	-	0.0025	0.006	0.003	0.0075
91	0.021	n.m.	0.016	0.009	n.m.	0.038

(b) CB-PS-100S - West

LOAD, Q Kips	CRACK WIDTH, in.					
	1	2	3	4	5	6
29.5 - Service	-	-	-	-	-	-
43	-	-	-	0.002	-	-
45 - Factored	-	-	-	0.002	-	-
51	-	-	-	0.002	-	-
58	0.002	-	-	0.002	-	0.003
64	0.004	-	-	0.003	0.0035	0.004
70	0.007	-	0.003	0.006	0.005	0.007
91	0.02	0.018	0.018	0.016	n.m.	0.03

Table 4.3E Maximum Crack Widths for CB-PS-100S, English Units

(a) CB-PS-100S - East

LOAD, Q kN	CRACK WIDTH, mm					
	1	2	3	4	5	6
131 - Service	-	-	-	-	-	-
191	-	-	-	-	-	-
200 - Factored	-	-	-	-	-	-
227	-	-	-	0.064	-	-
258	0.038	-	-	0.051	-	0.038
285	0.076	-	-	0.076	0.051	0.127
312	0.102	-	0.064	0.152	0.076	0.191
405	0.533	n.m.	0.406	0.229	n.m.	0.965

(b) CB-PS-100S - West

LOAD, Q kN	CRACK WIDTH, mm					
	1	2	3	4	5	6
131 - Service	-	-	-	-	-	-
191	-	-	-	0.051	-	-
200 - Factored	-	-	-	0.051	-	-
227	-	-	-	0.051	-	-
258	0.051	-	-	0.051	-	0.076
285	0.102	-	-	0.076	0.089	0.102
312	0.178	-	0.076	0.152	0.127	0.178
405	0.51	0.457	0.457	0.406	n.m.	0.762

Table 4.3S Maximum Crack Widths for CB-PS-100S, S.I. Units

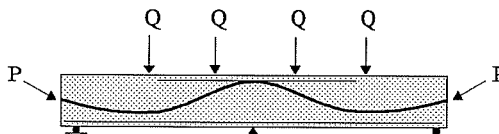
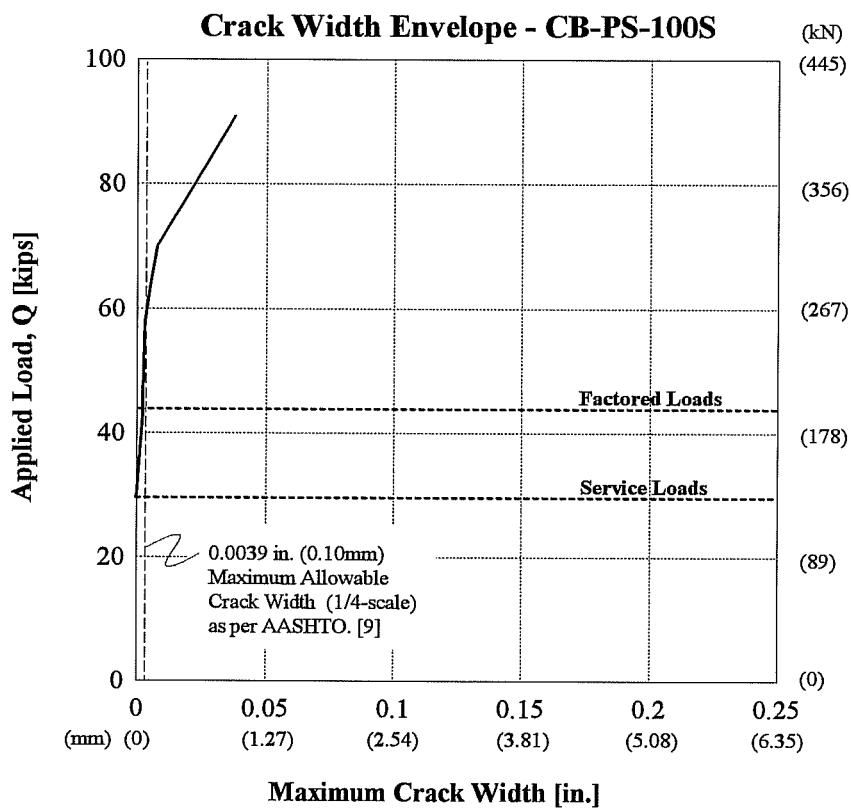


Figure 4.20 Maximum Crack Width Envelope - CB-PS-100S

4.2.3.2 Moment-Strain Behavior - CB-PS-100S

Moment-strain data for the non-prestressed cage steel in the tension zone of the critical moment regions is presented in Figures 4.21-4.24. First cracking behavior is presented in Figure 4.21 and is indicated on the plots of Figures 4.21-4.23 with numbered circles.

Figure 4.21 shows that over the center support, the steel behaves elastically up to a negative moment of approximately 150 k-ft. (203 kN-m). At this point where the curve begins to bend, the stiffness of the section is decreasing. This occurs directly after the mid-span regions cracked. The softening of the mid-span regions most likely caused an increase in the negative moment over the center support which brought on yielding of the non-prestressed steel. The jump in strain around 180 k-ft (244 kN-m) is most likely due to a gage registering the effects of a crack opening near-by. This negative moment steel continued to strain well beyond its yield strain.

Figure 4.22a shows that the non-prestressed cage steel in the tensile zone of the south mid-span responded linearly up to first cracking over the center support. A jump in strain shortly after the first crack appeared led to a considerable stiffness drop in this section. This occurred before the first crack in this region was visible. Micro-cracking, invisible to the eye was most likely the cause of the increased strain. Yielding and strain hardening began with an external moment of approximately 120 k-ft. (163kN-m). Full yielding most likely led to the gage failure at a moment of 160 k-ft (217kN-m). Figure 4.22b shows that in the north span, the cage steel picked up increases in strain after both the north and south mid-span regions had cracked. The steel appears to have begun to yield almost immediately after an increased rate of strain began.

Shear force vs. stirrup strain behavior for the negative moment region is shown in Figure 4.23. The shear force is assumed to be the center support reaction. Both the gaged inner and outer stirrup measured very little strain throughout the test. Shear force-stirrup strain results for the other gaged stirrups similarly showed very little change in strain throughout testing, with the exception of one gaged stirrup near the north mid-span, shown in Figure 4.24. At this location, the inner stirrup began to strain considerably with small increases in load. The stirrup however, did not appear to yield before failure occurred.

In looking at the side face crack control steel shown in Figure 4.25, first cracking behavior for the east face is again presented and indicated on the plots with numbered circles (note that these numbered circles refer to the first cracking drawings presented on this figure and are different than those presented on Figure 4.21). Figure 4.25a shows that the steel closer to the extreme tensile fiber near the south mid-span began to strain considerably just before the first crack over the center support appeared. Again this points to the presence of micro-cracking. In the north span, Figure 4.25b shows that the crack control steel closest to

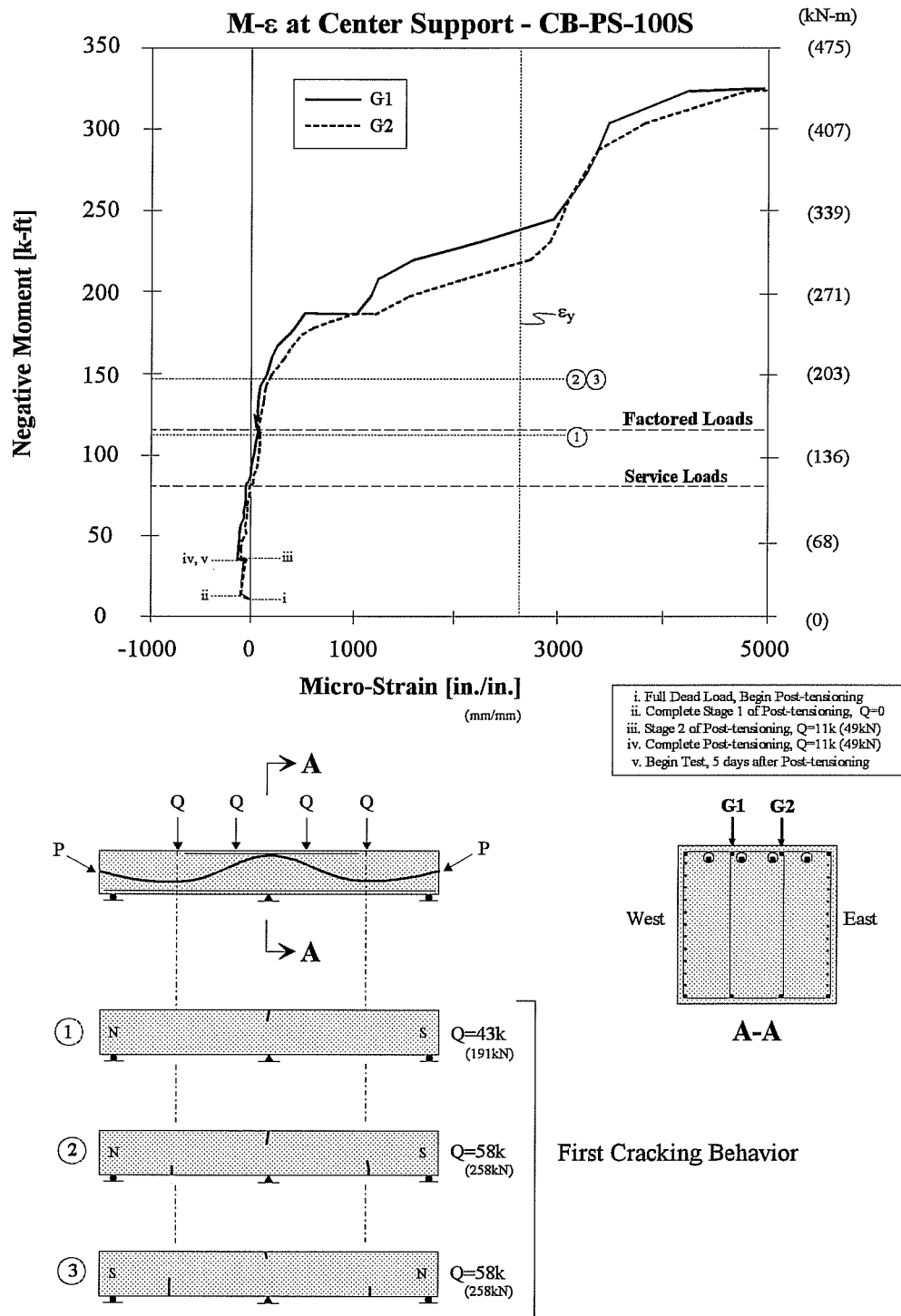
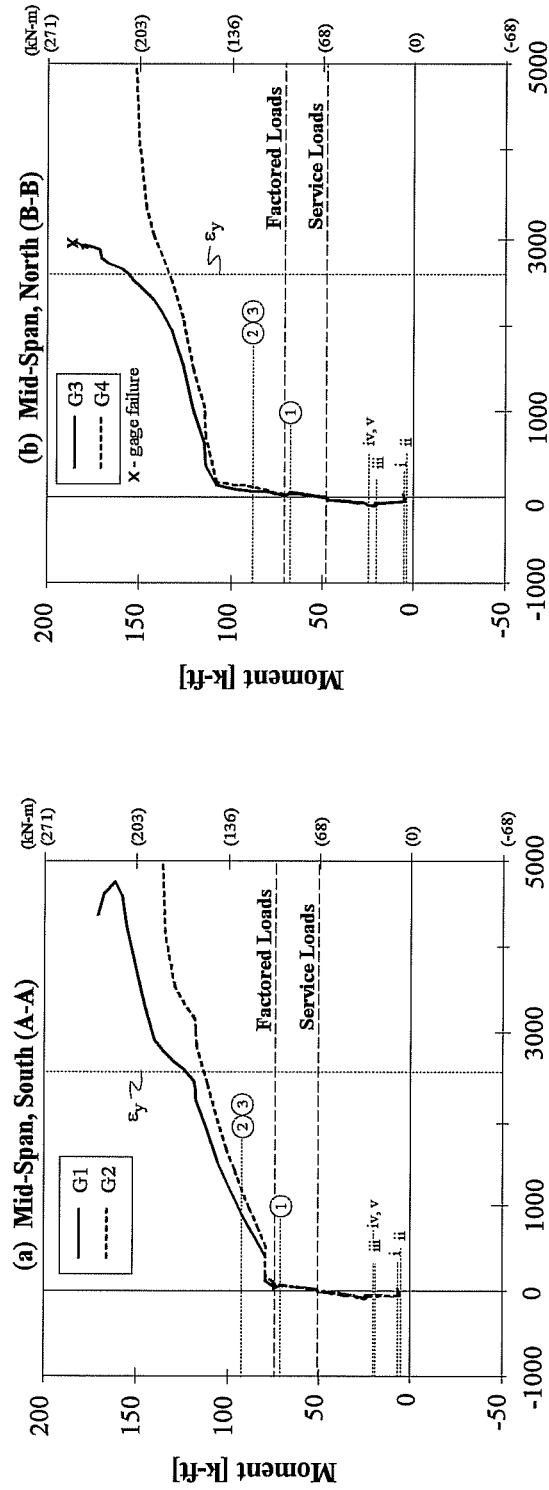


Figure 4.21 Moment-Strain Behavior for Non-Prestressed Steel in the Negative Moment Region - CB-PS-100S

M-ε for CB-PS-100S



Micro-Strain [in./in.] (mm/mm)

- i. Full Dead Load, Begin Post-tensioning
 - ii. Complete Stage 1 of Post-tensioning, Q=0
 - iii. Stage 2 of Post-tensioning, Q=11k (49kN)
 - iv. Complete Post-tensioning, Q=11k (49kN)
 - v. Begin Test, 5 days after Post-tensioning
- ①②③ - First Cracking Behavior, Refer to Figure 4.21

Micro-Strain [in./in.] (mm/mm)

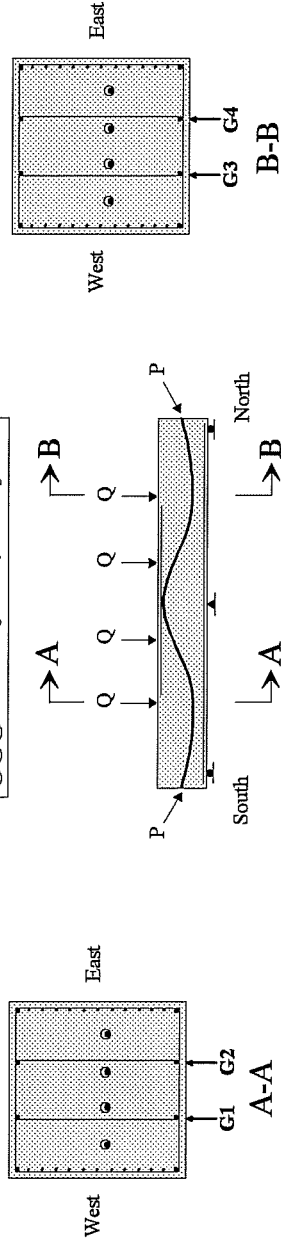


Figure 4.22 Moment-Strain Behavior of Mid-Span Non-pressed Tensile Steel - CB-PS-100S

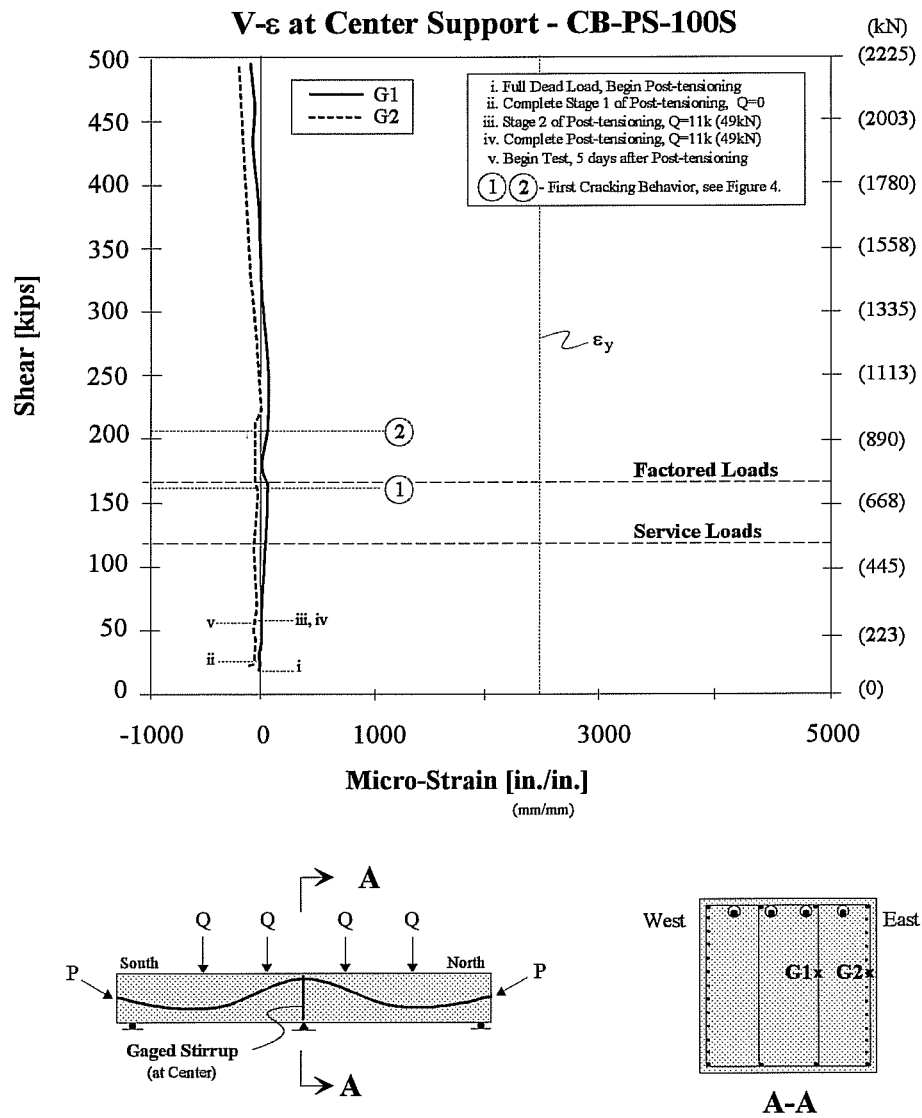


Figure 4.23 Center Support - Strain Behavior for Shear Stirrups - CB-PS-100S

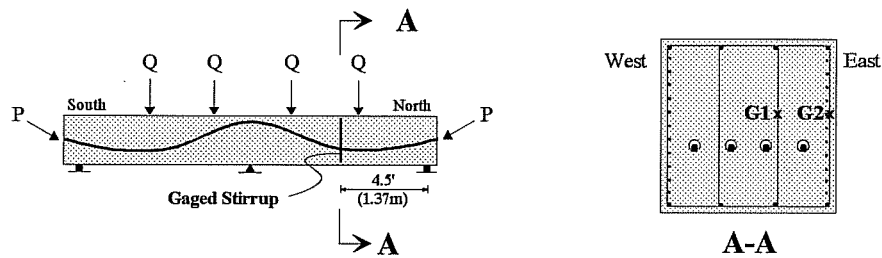
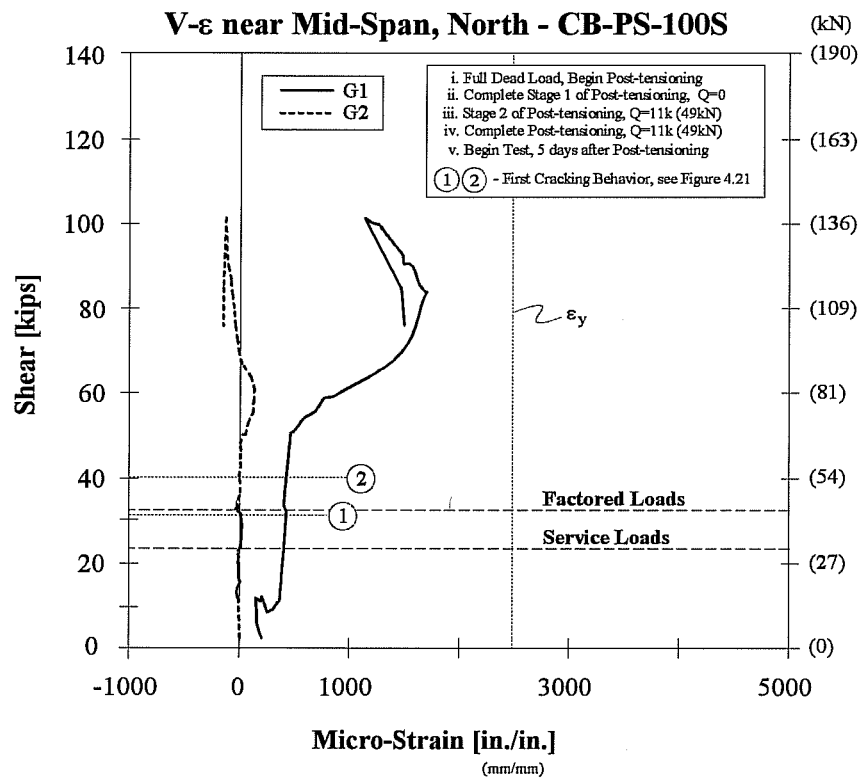
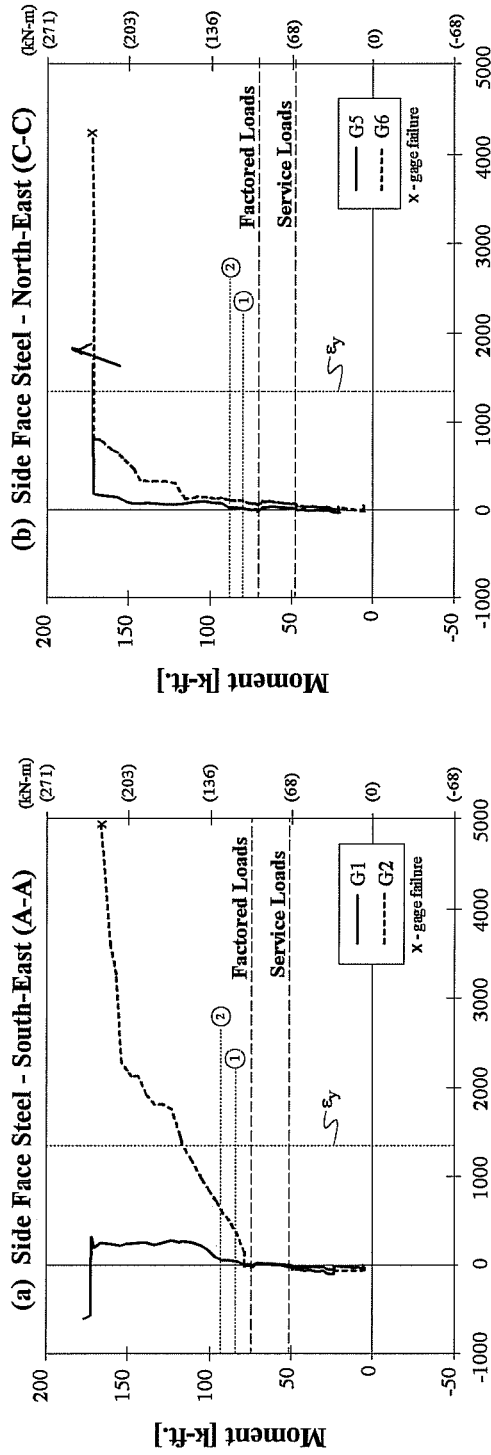


Figure 4.24 Shear-Stirrup Strain Behavior near North Mid-Span - CB-PS-100S

M-ε for CB-PS-100S



Micro-Strain [in./in.]
(mm/mm)

Micro-Strain [in./in.]
(mm/mm)

①② - First Cracking on East Face
see next page

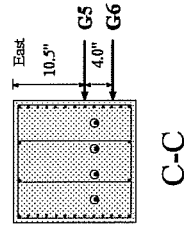
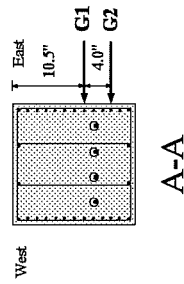
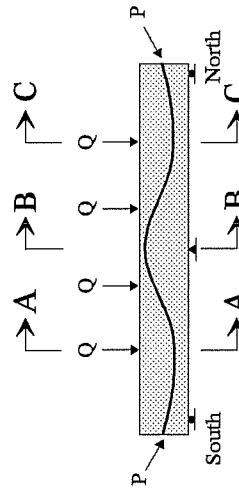
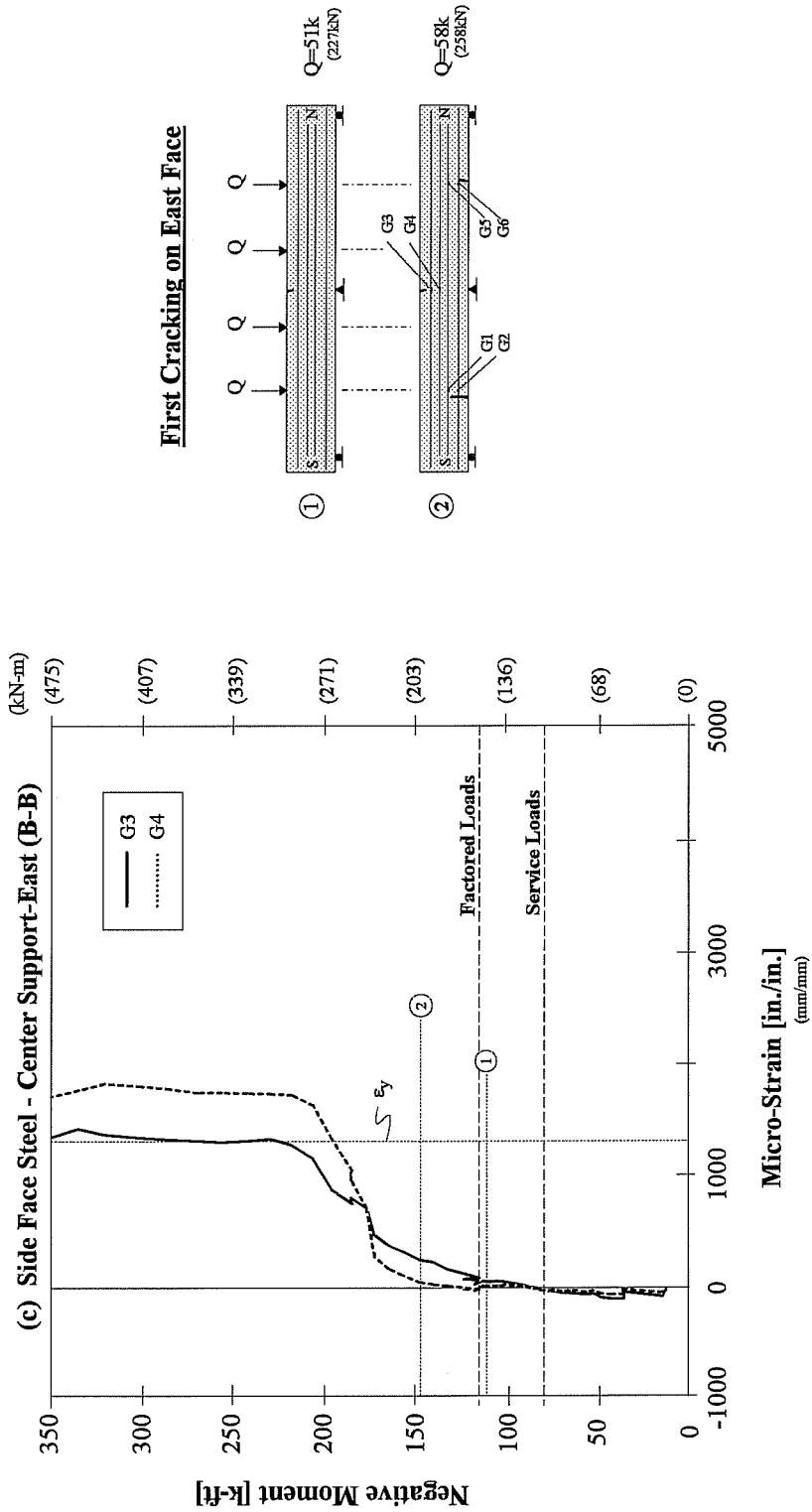


Figure 4.25 Moment-Strain Behavior of Side Face Crack Control Steel for CB-PS-100S
(continued on next page)

M-ε for CB-PS-100S



First Cracking on East Face

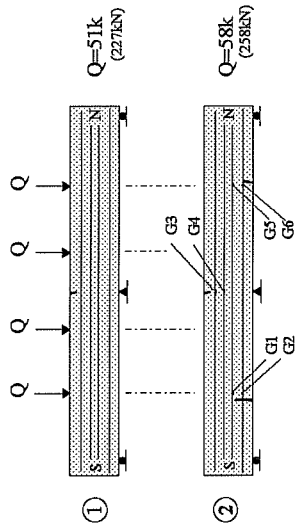


Figure 4.25 (cont.) Moment-Strain Behavior of Side Face Crack Control Steel for CB-PS-100S

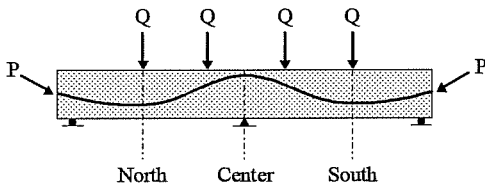
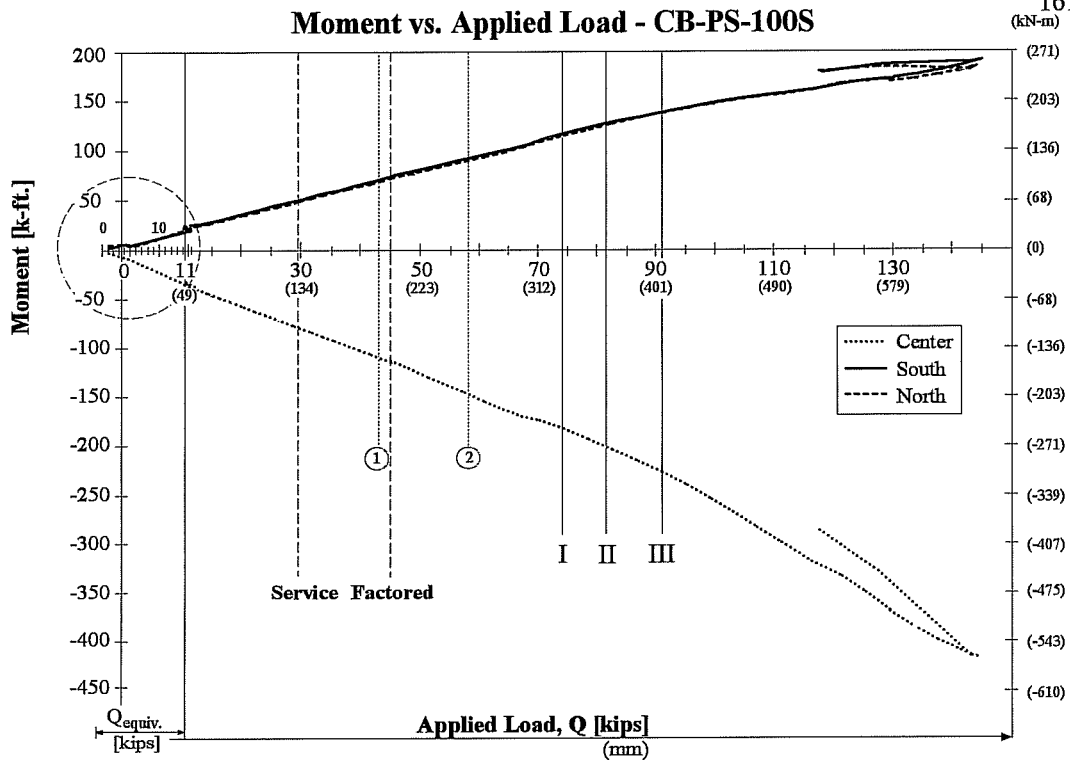
the extreme tensile fiber began to strain more under a moment of 140 k-ft. (190 kN-m). The crack control steel closer to the centroid of the section strained and yielded at a moment of 175 k-ft. (237kN-m). The crack control steel was not controlling cracks at service loads (there were no cracks) nor was it contributing significantly to the moment capacity of the beam at factored loads. Crack control was effective above factored loads at both spans (south mid-span in particular).

At the center support as well, the crack control steel was not contributing significantly to crack control or resistance at service and factored loads respectively as only a single crack formed just before factored loads were reached (see Figure 4.25c). Beyond cracking at all critical sections, the crack control steel did begin to have a more considerable increase in strain and appeared to have yielded at a negative moment of 200 k-ft. (271 kN-m). The extreme increase in load with no additional strain in the crack control steel indicates that the gage was not located at the actual crack opening.

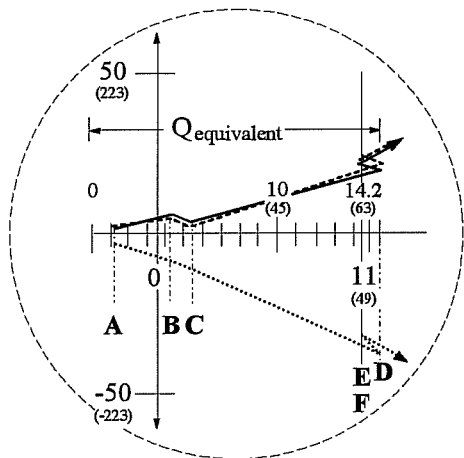
4.2.3.3 *Moment vs. Applied Load - CB-PS-100S*

Figure 4.26 is a plot of the applied point loads, Q , versus the moment at the mid-spans and over the center support. First cracking behavior over the center support and near the mid-spans is indicated with numbered circles corresponding to the first cracking drawings presented in Figure 4.21. First yielding is indicated with the roman numerals I-III, and correspond to the yield moments of the non-prestressed steel at these same sections found from the moment-strain results of Section 4.2.3.2.

The beginning of the plot shows the moment corresponding to an equivalent point load $Q_{\text{equivalent}}$. This equivalent point load is similar to that explained in Section 4.2.2.3 but it also includes the effects of prestressing. The equivalent load corresponds to a point load that would produce the same negative moment over the center support that the dead load and the prestressing forces create. While this is not representing the behavior of the mid-spans exactly numerically, the behavior is still well-represented. The moments in the positive and negative moment zones increased under the effects of the dead load. In the first stage of post-tensioning where no applied load was required, the positive moments decreased and the negative moment increased. This exhibits the beginning of the action of secondary moments. The overall secondary moment was predicted to be negative and this is supported by the behavior shown in Figure 4.26. With the application of the point load for the second stage of post-tensioning, the moments increased. After three days, creep or temperature changes may have caused the resulting slight decrease in negative moment over the center support and increase in positive moments at the mid-spans. At this point testing began.



- ① ② ③ - First Cracking Behavior - Refer to Figure 4.21
- I. Yield of Non-prestressed Steel at Center
 - II. Yield of Non-prestressed Steel at Mid-span, North
 - III. Yield of Non-prestressed Steel at Mid-span, South



Where $Q_{equivalent}$ is the force corresponding to loads Q , that would produce the negative moment over the center support resulting from the dead load and prestressing forces. Both negative and positive moments are plotted using the same $Q_{equivalent}$.

- A - Beam Only
- B - Full Dead Load, Begin Post-tensioning
- C - Complete Stage 1 of Post-tensioning, $Q=0$
- D - Stage 2 of Post-tensioning, $Q=11k$ (49kN)
- E - Complete Post-tensioning, $Q=11k$ (49kN)
- F - Begin Test (5 days after post-tensioning)

Figure 4.26 Moment vs. Applied Load - CB-PS-100S

The first evidence of moment redistribution occurred around the point load of 70k (312kN) where there is a shift in the slope of the plots. The mid-span moments increased more rapidly while the moment over the center support increased less rapidly. After this initial shift, the behavior reversed (negative moment increased more rapidly). Moment seems to have redistributed from the mid-span regions to the center support. This occurred while the non-prestressed steel in all three critical moment regions was yielding. Another shift occurred under point loads of 120k (534kN) after which some redistribution back to the mid-spans was visible when the loud bang was heard and the load dropped off considerably. The moment at the center support decreased rapidly while the mid-span moments decreased only slightly. Testing was then stopped.

4.2.3.4 Load-Deflection Behavior - CB-PS-100S

Load-deflection behavior for this model is shown in Figure 4.27. Service load deflection criteria in accordance with AASHTO 1992 and ACI-318-89 were satisfied. The maximum service load deflection corresponded to $L/8000$.

Stiffness changes were first apparent with the onset of yielding of the non-prestressed reinforcement in the north and south spans. The beam exhibited some ductility before failure, particularly in the south span. This beam clearly exhibited excessive over-strength. A load of 3.2 times factored loads was carried at the time of failure.

4.2.3.5 Moment-Deflection Behavior - CB-PS-100S

The moment-deflection plot for CB-PS-100S is shown in Figure 4.28. Deflection downwards is measured as positive. The numbered circles and the roman numerals correspond to first cracking behavior and first yield of non-prestressed steel respectively, as explained in Section 4.2.3.3.

The beginning of the plot is shown underneath to a larger scale in an effort to show deflection behavior during post-tensioning operations and to determine where decompression of the sections occurred. During the first stage of post-tensioning, mid-span deflections were negative meaning the beam was cambering upward. Under the applied load for the second stage of loading, the deflection increased positively (downward). During the three days between post-tensioning and testing, the mid-span deflection increased positively. This corresponds with the apparent increase in positive moment seen in the close-up of Figure 4.28. The decompression values shown do not correspond well with the predicted decompression moment. At these loads, the deflections were quite small and it was noticed that the deflections recorded could change 100% over the course of a day due to temperature changes. The observed behavior is therefore not

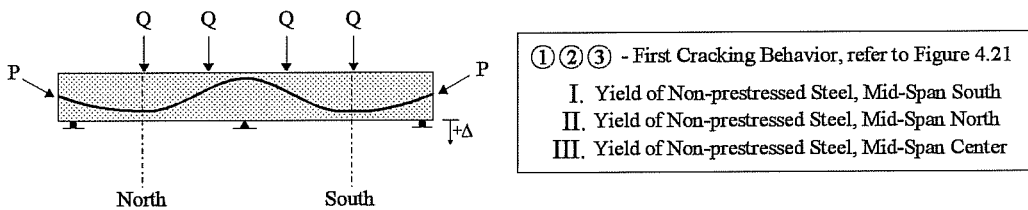
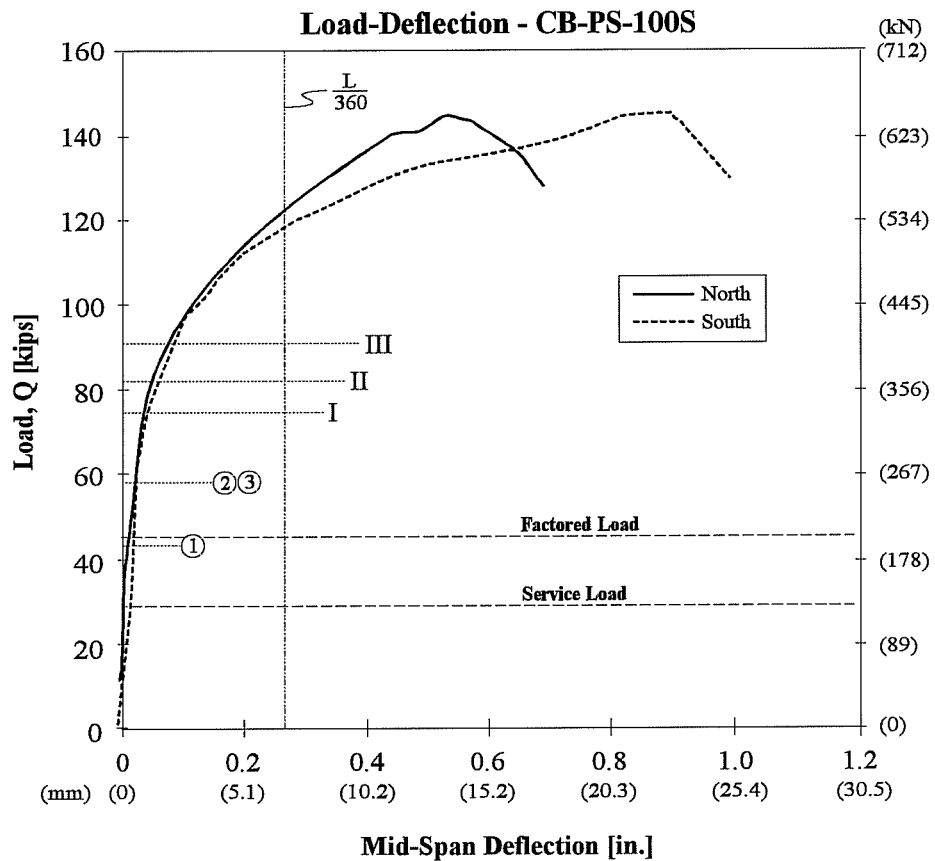
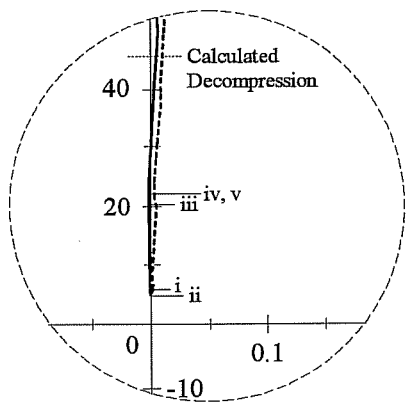
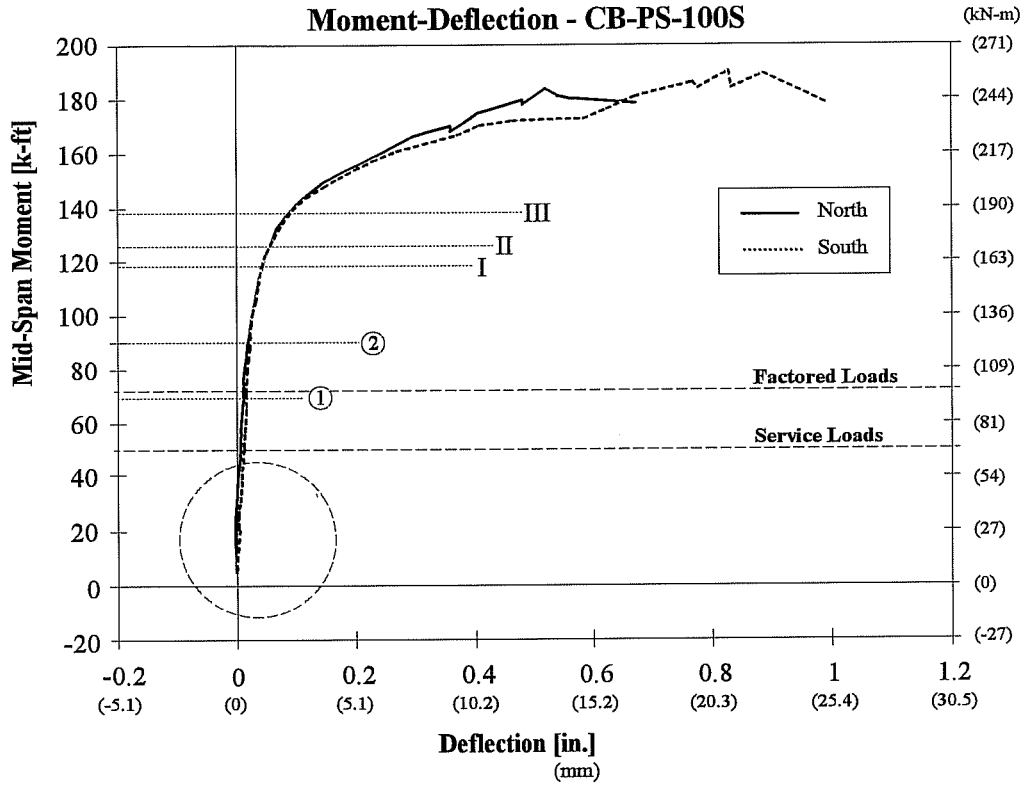


Figure 4.27 Load-Deflection Behavior - CB-PS-100S



- i. Full Dead Load, Begin Post-tensioning
 - ii. Complete Stage 1 of Post-tensioning, $Q=0$
 - iii. Stage 2 of Post-tensioning, $Q=11k$ (49kN)
 - iv. Complete Post-tensioning, $Q=11k$ (49kN)
 - v. Begin Testing (5 days after Post-tensioning)
- ① ② - First Cracking Behavior, refer to Figure 4.21
- I. Yield of Non-prestressed Steel, Mid-Span South
 - II. Yield of Non-prestressed Steel, Mid-Span North
 - III. Yield of Non-prestressed Steel, Center

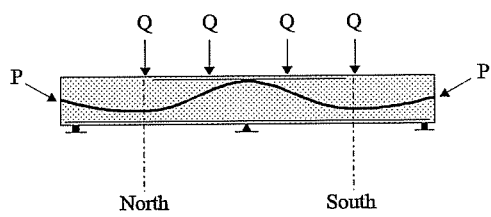


Figure 4.28 Mid-Span Moment-Deflection Behavior for CB-PS-100S

a reliable representation of the actual behavior. These changes were typically of 0.005 in. (0.127mm) which had negligible effects on the overall moment-deflection readings.

There is no distinct point where yielding seems to occur. Rather, as is typical with "fully prestressed" members, there is a gradual change in slope. (This corresponds to the properties of the prestressing strand. See Figure 3.20.) The gradual change in slope began to occur after the initial cracking of the mid-spans. This change was more marked where yielding of the non-prestressed steel at the critical moment regions began. Both mid-span regions behaved similarly with the south span exhibiting slightly more ductility than the north span.

The highest moments measured in the critical sections before testing was stopped were 417 k-ft. (566kN-m) over the center support and 190 k-ft. (258 kN-m) and 184 ft-k (250 kN-m) at mid-span of the south and north spans, respectively. It is clear from this figure that this beam was excessively strong. Its strength was 3.2 times the necessary strength to carry factored loads. This is basically because the amount of post-tensioning strand was dictated by service load stress limits and not by ultimate load requirements.

4.2.3.6 Post-mortem Investigation - CB-PS-100S

The model was opened at the southern mid-span. Figure 4.29 shows the location of the fractured and yielded bars at the failed south mid-span. Here one of the four longitudinal cage steel elements in the tension zone yielded and the remaining three fractured. Much of the side face crack control steel wires in the tension zone fractured. The wires at the same depth as the post-tensioned strands only yielded as did some of the wires on the east side between the strands and the cage steel.

The effective depth of the strands was 12.25 in. (311mm). This was 0.25 in. (6.4mm) smaller than the designed depth of 12.5 in. (317mm). The strand locations across the width of the section were constructed as designed.

4.2.3.7 Further Discussion - CB-PS-100S

The early cracking stress over the center support indicates that the assumed full effective prestressing force was not there. Due to the construction error (see Section 3.3.1.2), the tendon over the center support had a small radius of curvature of 18 in. (457mm). The over-stressing performed during prestressing operations was most likely not enough to account fully for friction losses in this region. The cracking stresses at the mid-spans may also have been low due to the slightly smaller (than designed) effective depth of the strands as discovered in the post-mortem investigation.

In looking at the failure mode of this beam, testing was stopped when a loud bang was heard and the load dropped off rapidly. At this same load, crushing of the concrete at the southern mid-span was also apparent (see Figure 4.30). The noise was thought to have been a strand that fractured. However none of the cage steel bars at a larger effective depth had fractured and it was assumed that no strands had fractured either. The noise heard may have been fracturing of cage steel at mid-spans or an adjustment (release of built-up force) in the testing frame.

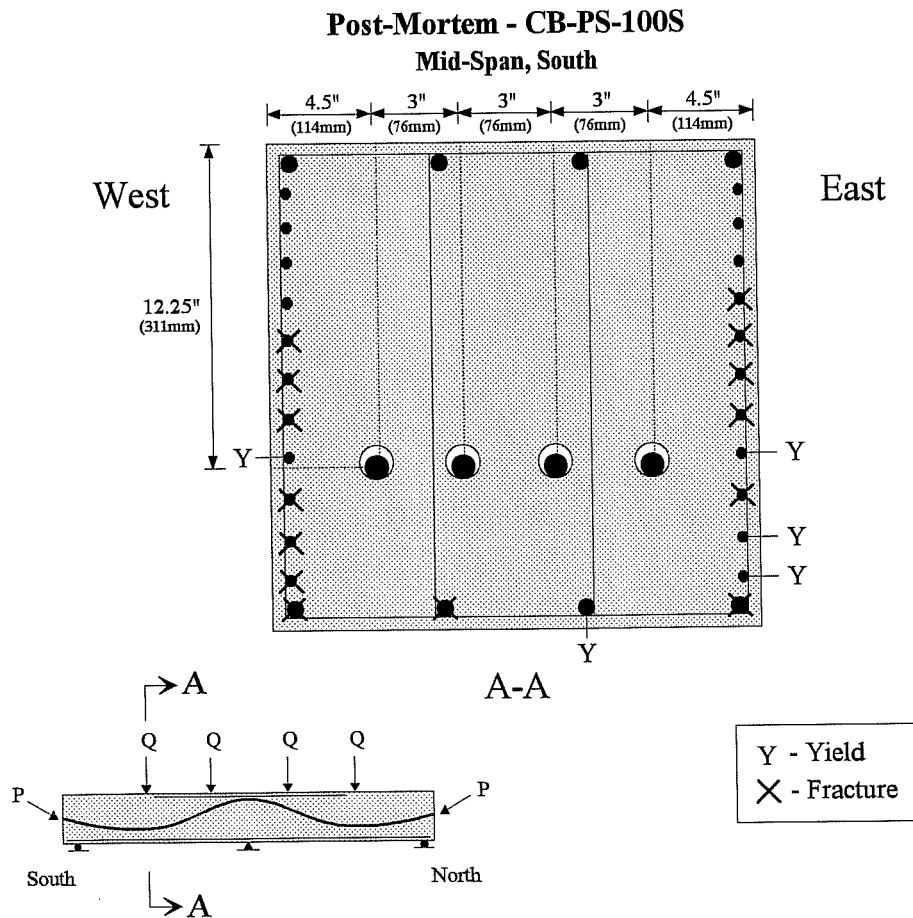


Figure 4.29 Post-mortem Investigation of Failed Cross-Section for CB-PS-100S

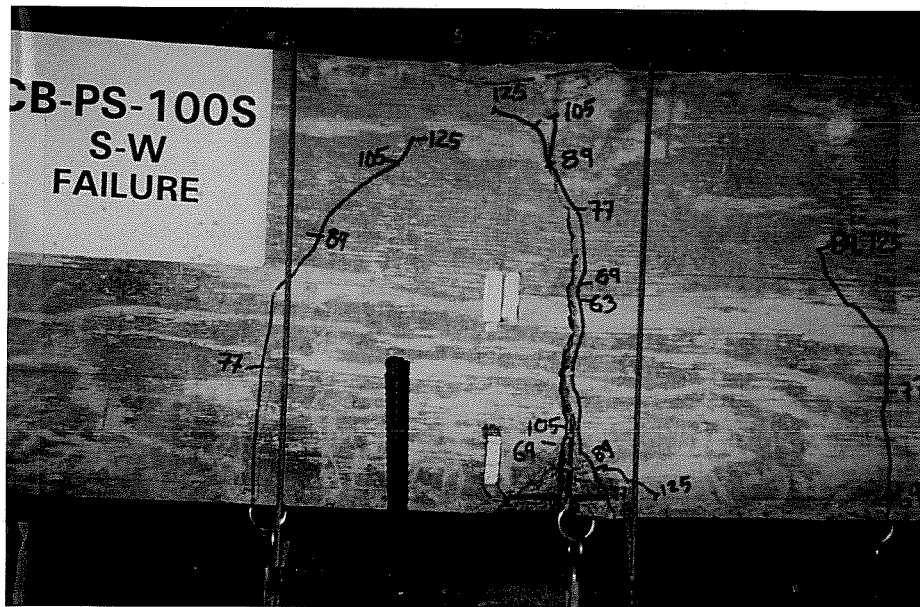


Figure 4.30 Crushing Failure of Mid-Span, North - CB-PS-100S

4.3 Designs According to Proposed Integrated Design Method

4.3.1 CB-PU-100S - 100% Prestress Reinforcing (100% of nominal resistance provided by the prestressing strand)

This model was post-tensioned and grouted 3 days before it was first tested. On the first day of testing, the model was loaded to 13% above factored loads ($Q = 51\text{k}, 227\text{kN}$). The next day the beam was loaded to failure. This beam failed in compression of the concrete at mid-span of the north span.

4.3.1.1 Cracking Behavior - CB-PU-100S

First Cracking - First cracking occurred at the center support under point loads of 27k (120kN) (see Figure 4.31). The moment at this section was -81 k-ft. (-110 kN-m). This corresponds to a cracking tensile stress of $4.6\sqrt{f'_c}$ ($0.37\sqrt{f'_c}$).

The first crack in the mid-span region of the south span near station 1 appeared under point loads of 33.5k (149kN) where the moment at that section was 54 k-ft. (73 kN-m). This corresponds to a calculated

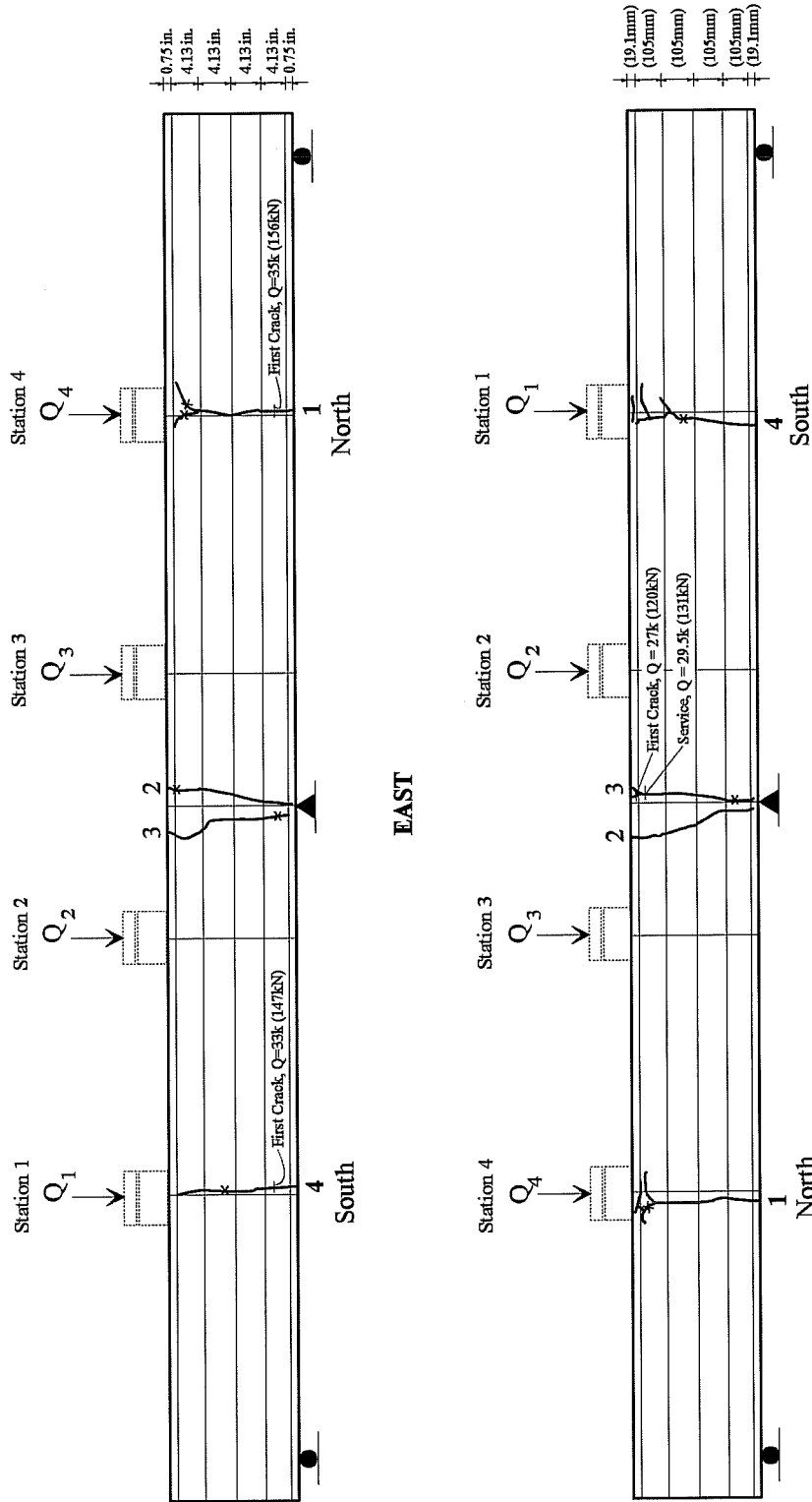


Figure 4.31 Cracking of CB-PU-100S at Ultimate Load Levels

cracking tensile stress of $4.6\sqrt{f'_c}$ ($0.37\sqrt{f'_c}$) assuming full effective prestress. The first crack in the mid-span region of the north span near station 4 appeared under point loads of 36k (160kN) where the moment at that section was 52 k-ft. (71 kN-m). This corresponds with a calculated cracking tensile stress of $4.3\sqrt{f'_c}$ ($0.34\sqrt{f'_c}$) again assuming full effective prestress.

Crack Widths & Serviceability - Figure 4.31 shows the crack locations under service and factored loads and at failure. Maximum crack widths for certain load steps are recorded in Table 4.4. The maximum crack width "envelope" is presented in Figure 4.32.

First cracking occurred just before service loads were applied. The maximum crack width when the crack first became visible was 0.002 in. (0.025mm). At service loads the crack width remained 0.002 in. (0.025mm). This width corresponds to a full-scale prototype crack width of 0.008 in. (0.203mm), and therefore satisfies the current serviceability criterion implicit in the AASHTO Bridge Design Specifications. Crack widths however increase dramatically between service and factored loads and beyond (Figure 4.32).

Cracking Distribution - At service loads only one crack had formed over the center support thus there was no significance to crack distribution. At ultimate loads however, cracks were not very well distributed particularly in the mid-span regions near stations 1 and 4. There was only one major crack at each mid-span and two over the center support. As mentioned previously, the moment required to crack the mid-span region was between 52-54 k-ft. (70-76 kN-m). Predicted yielding of the non-prestressed steel in this region was 65.3 k-ft. (This non-prestressed steel was in fact only cage steel. No tensile crack control steel was required by the finite element analysis based method of crack control used.) A moment of approximately 65 ft-k was reached in these sections two load steps later at factored loads (45k, 200kN), at which point the bars should have yielded (see Section 4.3.1.2). The yielding points would have the characteristics of developing a plastic hinging zone thus preventing increased tensile forces in the uncracked portions of the beam. Therefore, new cracks would not form. The developed tensile forces before the steel had yielded were not enough to distribute cracking.

(a) CB-PU-100S - East

LOAD, Q Kips	CRACK WIDTH, in.			
	1	2	3	4
27	-	-	-	-
28	-	-	-	-
29.5 - Service	-	-	-	-
34	0.002	-	0.002	-
36	n.m.	0.002	n.m.	-
38	n.m.	n.m.	n.m.	0.0015
39	0.02	0.002	0.014	0.004
43	0.04	0.003	0.027	0.007
45 - Factored	n.m.	n.m.	n.m.	n.m.
49	0.12	0.014	0.06	0.035
55	0.188	0.06	0.1	0.125
71	0.875	0.188	0.375	0.625

(b) CB-PU-100S - West

LOAD, Q Kips	CRACK WIDTH, in.			
	1	2	3	4
27	-	-	0.0015	-
28	-	-	0.002	-
29.5 - Service	-	-	0.002	-
34	-	-	0.003	-
36	0.003	-	n.m.	-
38	n.m.	-	n.m.	0.0015
39	0.018	-	0.008	0.004
43	0.03	-	0.02	0.008
45 - Factored	n.m.	n.m.	n.m.	n.m.
49	0.125	0.013	0.06	0.05
55	0.25	0.06	0.1	0.125
71	0.875	0.188	0.375	0.438

Table 4.4E Maximum Crack Widths for CB-PU-100S, English Units

(a) CB-PU-100S - East

LOAD, Q kN	CRACK WIDTH, mm			
	1	2	3	4
27	-	-	-	-
28	-	-	-	-
29.5 - Service	-	-	-	-
34	0.051	-	0.051	-
36	n.m.	0.051	n.m.	-
38	n.m.	n.m.	n.m.	0.038
39	0.051	0.051	0.356	1.02
43	1.02	0.076	0.686	0.178
45 - Factored	n.m.	n.m.	n.m.	n.m.
49	3.05	0.356	1.52	0.889
55	4.78	1.52	2.54	3.18
71	22.23	4.78	9.53	15.88

(b) CB-PU-100S - West

LOAD, Q kN	CRACK WIDTH, mm			
	1	2	3	4
27	-	-	0.038	-
28	-	-	0.051	-
29.5 - Service	-	-	0.051	-
34	-	-	0.076	-
36	0.076	-	n.m.	-
38	n.m.	-	n.m.	0.038
39	0.457	-	0.203	0.102
43	0.762	-	0.508	0.203
45 - Factored	n.m.	n.m.	n.m.	n.m.
49	3.18	0.33	1.52	1.27
55	6.35	1.52	2.54	3.18
71	22.23	4.76	9.53	11.13

Table 4.4S Maximum Crack Widths for CB-PU-100S, S.I. Units

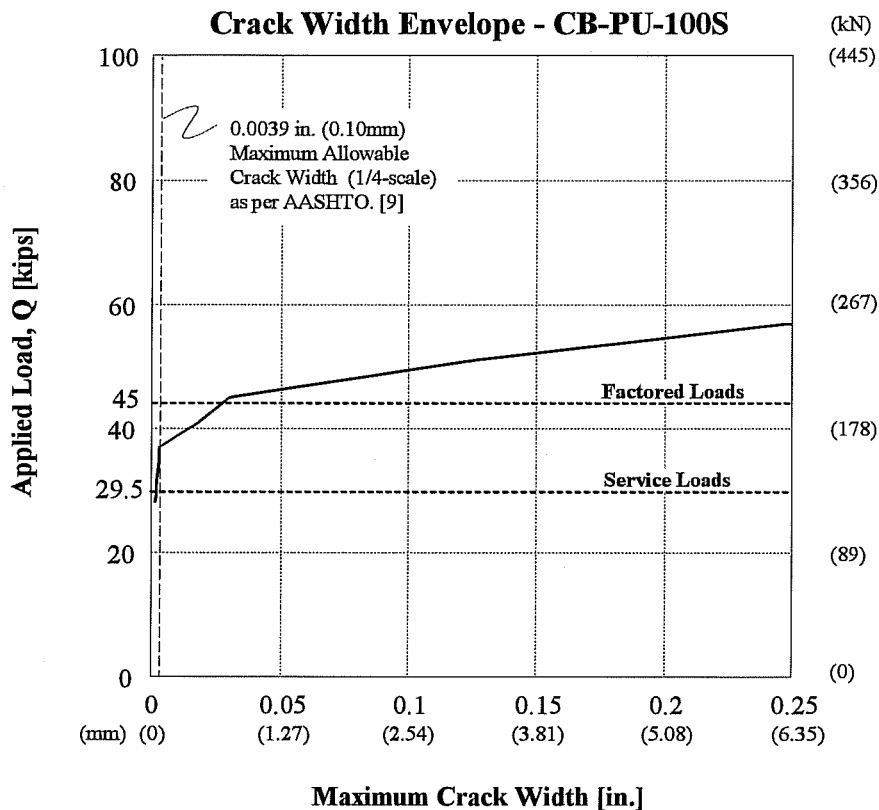


Figure 4.32 Maximum Crack Width Envelope - CB-PU-100S

4.3.1.2 Moment-Strain Behavior - CB-PU-100S

Moment-strain data for the non-prestressed cage steel in the tension zone of the critical moment regions is presented in Figures 4.33-4.36. No stage loading was required for this model and the resulting compression of the non-prestressed steel during post-tensioning operations can be seen in the moment-strain plots.

Once testing was started, Figure 4.33 shows that the non-prestressed tension steel over the center support behaved elastically up to when the first crack appeared at the mid-span just before service loads. A slight decrease in stiffness of the section continued up through first cracking of the mid-spans. At a

moment of approximately 110 ft-k (149 kN-m), a large increase in strain occurred in all of the gages. As the strain was not very close to the yield strain of the steel, it is most likely that at this point the gages are first recording the effects of the crack over the center support. General trends show the steel continuing to carry load and to begin to yield and further increase in strain slightly after factored loads were applied.

Figure 4.34a shows that the non-prestressed cage steel in the tensile zone of the south mid-span responded linearly up to first cracking over the center support. Looking at gage 2, the section then began to lose stiffness and the steel eventually yielded at factored loads. Gage G1 appeared to have malfunctioned shortly after the mid-span crack formed. Figure 4.34b shows that in the north span, the cage steel at mid-span picked up increases in strain after both the north and south mid-span regions had cracked. The gage then seems to have malfunctioned under a moment of approximately 60 k-ft (86kN-m). At this point the stress in the steel may have increased so rapidly, approaching yield, that the gage attachment was negatively effected.

Shear force vs. stirrup strain behavior for the negative moment region is shown in Figure 4.35. Both the gaged inner and outer stirrup measured very little strain throughout the test. The outer gage showed a slight increase (followed by a decrease) in strain after factored loads. Shear force vs. stirrup strain results for the remainder of the gaged stirrups similarly showed little change in strain throughout testing.

Looking at the side face crack control steel at the southern mid-span shown in Figure 4.36a, the steel closer to the extreme tensile fiber began to strain considerably immediately above service loads. This was initiated after a crack formed over the center support and before the mid-spans first cracked. This steel continued to strain considerably under the next few load steps (of 2k each step) and yielded before factored loads were reached. The side face crack control steel closer to the centroid of the section behaved similarly but at higher loads. Strain first increased here after the mid-span cracks had formed and the gage appears to have malfunctioned directly after factored loads. This steel had not yet yielded. The gage may have malfunctioned as a result of yielding, however. This crack control steel was not controlling cracks at service loads (there were no cracks). Once these sections were cracked the steel helped with crack control. With its early yielding however, it was not controlling cracks well at factored loads.

At the center support, Figure 4.36b shows that the crack control steel did not yield before factored loads. Small increases in steel strain could be seen with the formation of cracks. However the steel did not approach yielding until after factored loads. Both gages malfunctioned before the steel yielded. Again, actual yielding may have caused the gages to malfunction.

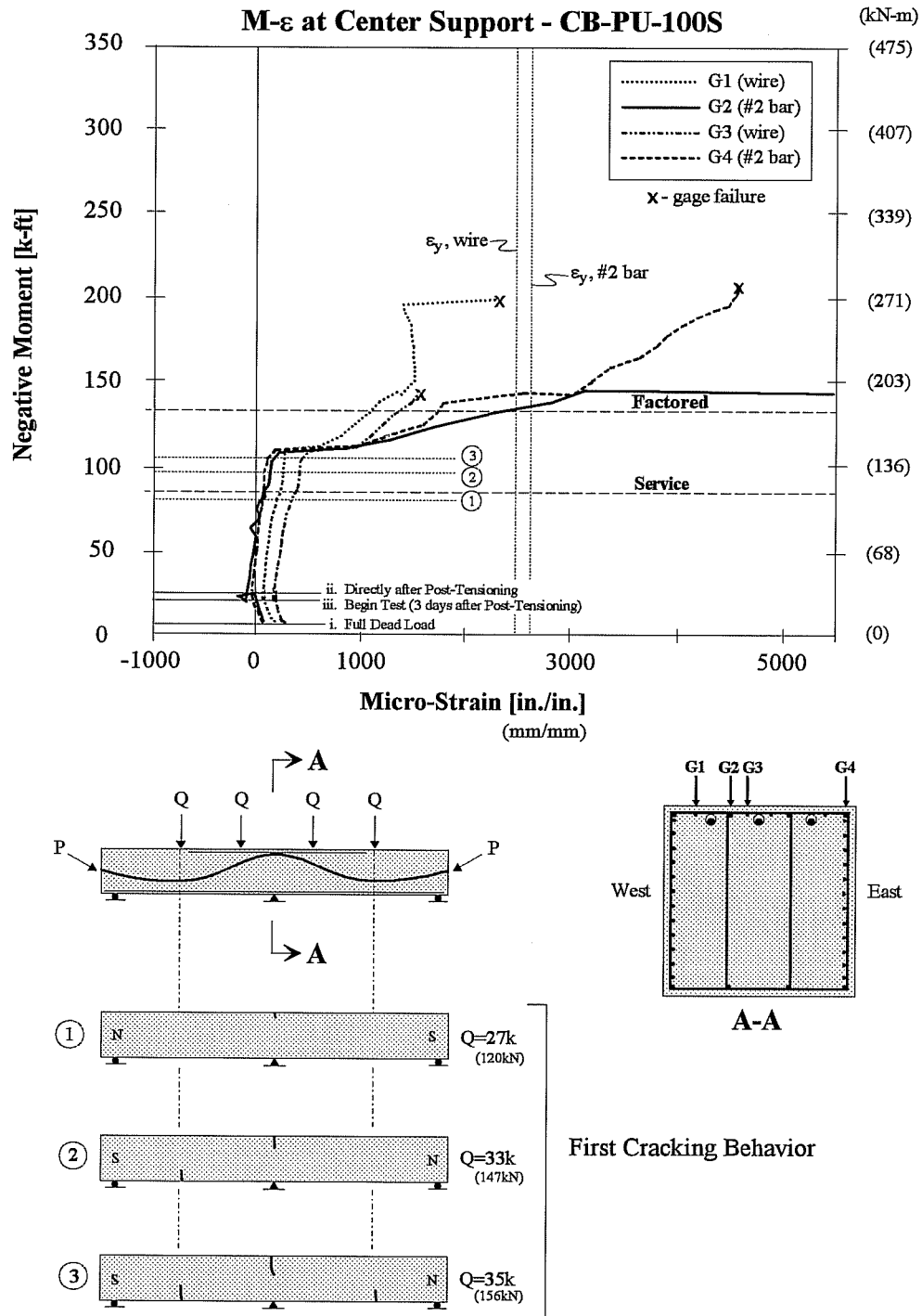


Figure 4.33 Moment Strain Behavior for Non-Prestressed Steel in the Negative Moment Region - CB-PU-100S

M-ε for CB-PU-100S

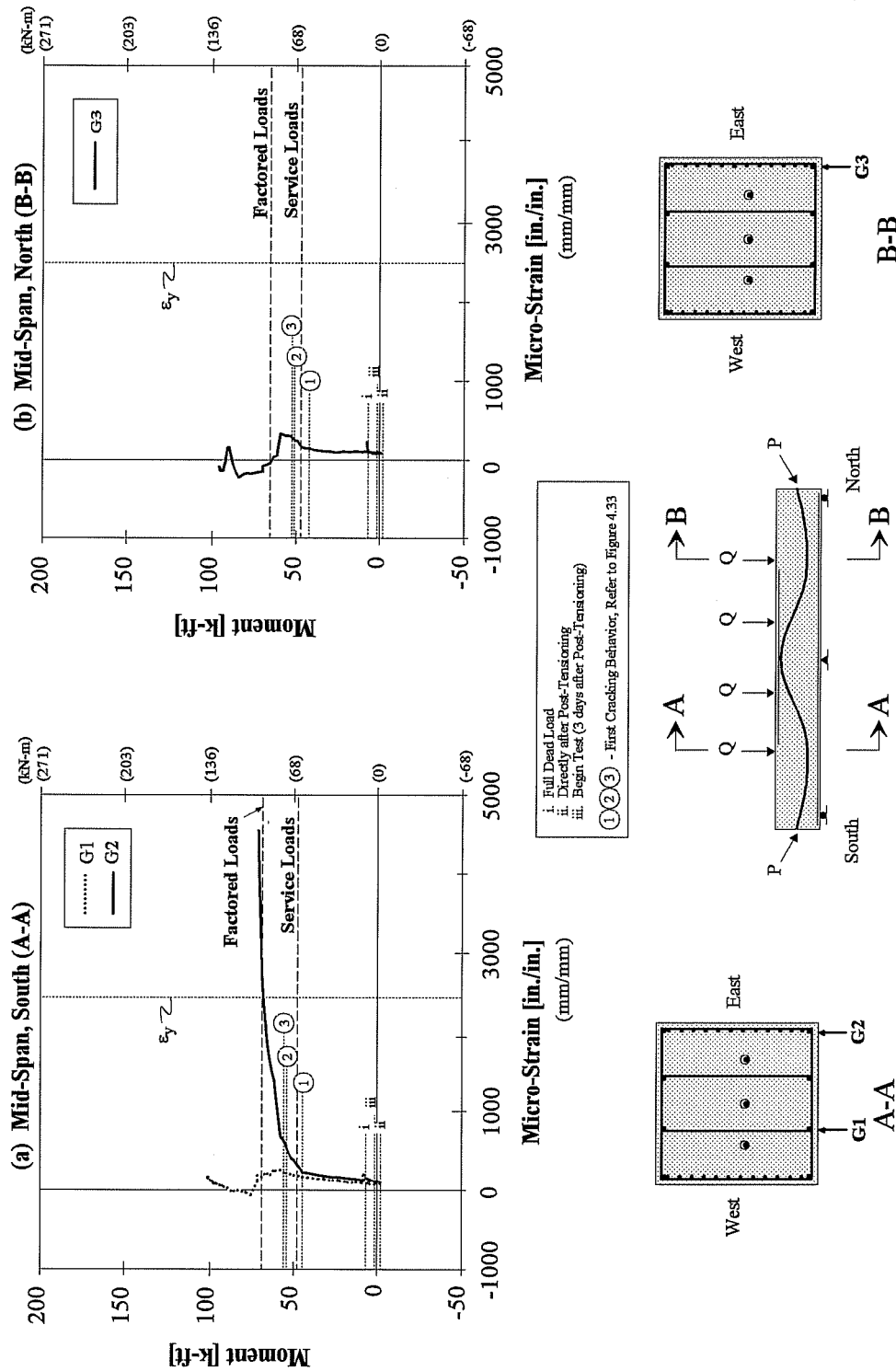


Figure 4.34 Moment-Strain Behavior of Mid-Span Non-prestressed Tensile Steel - CB-PU-100S

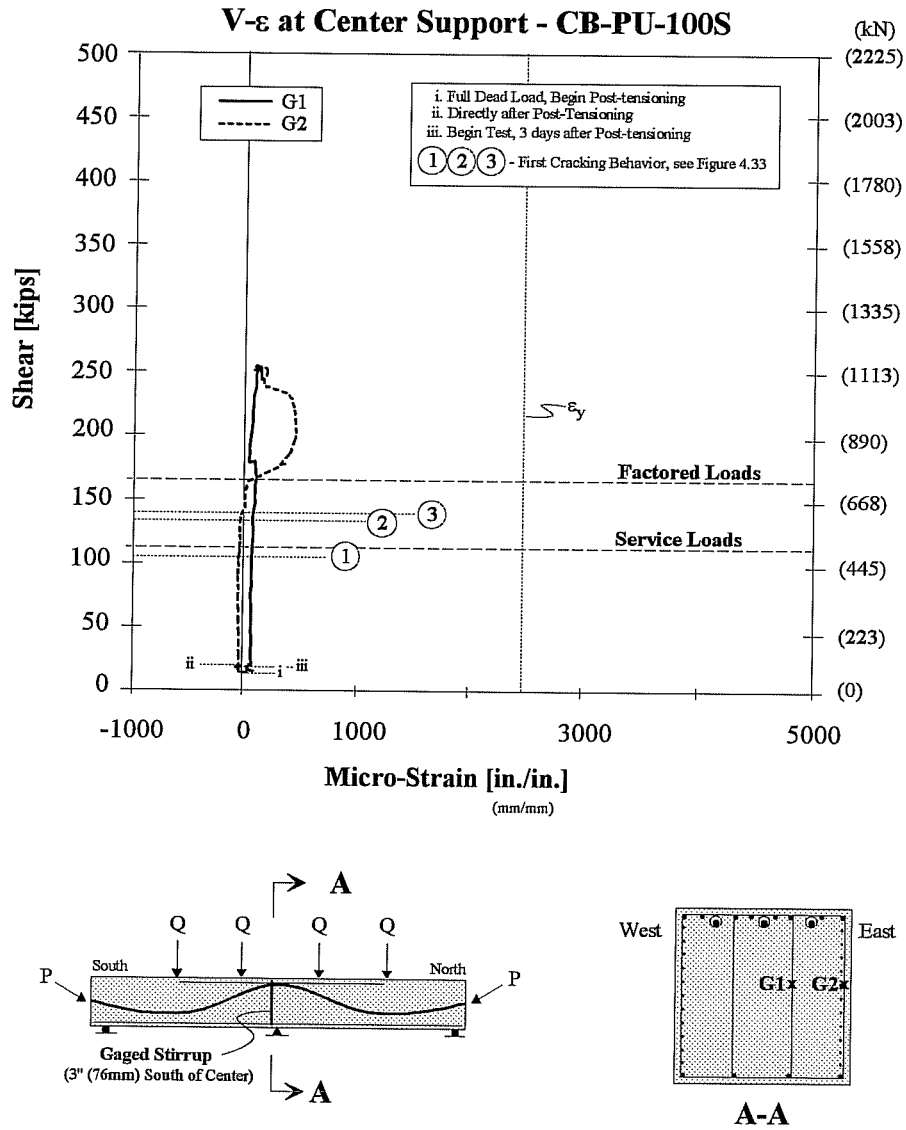


Figure 4.35 Center Support - Strain Behavior for Shear Stirrups - CB-PU-100S

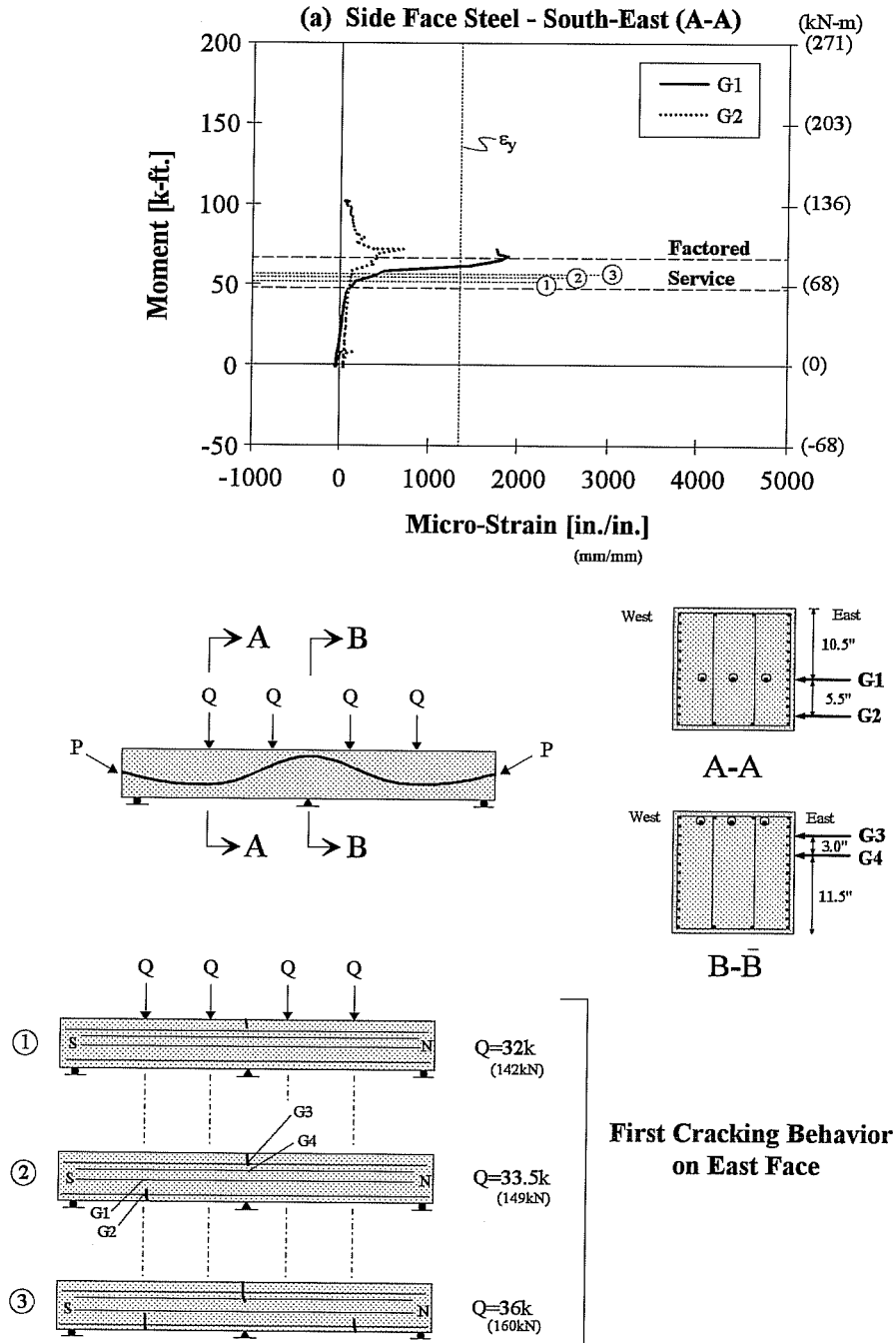


Figure 4.36 Moment-Strain Behavior of Side Face Crack Control Steel for CB-PU-100S (continued on next page)

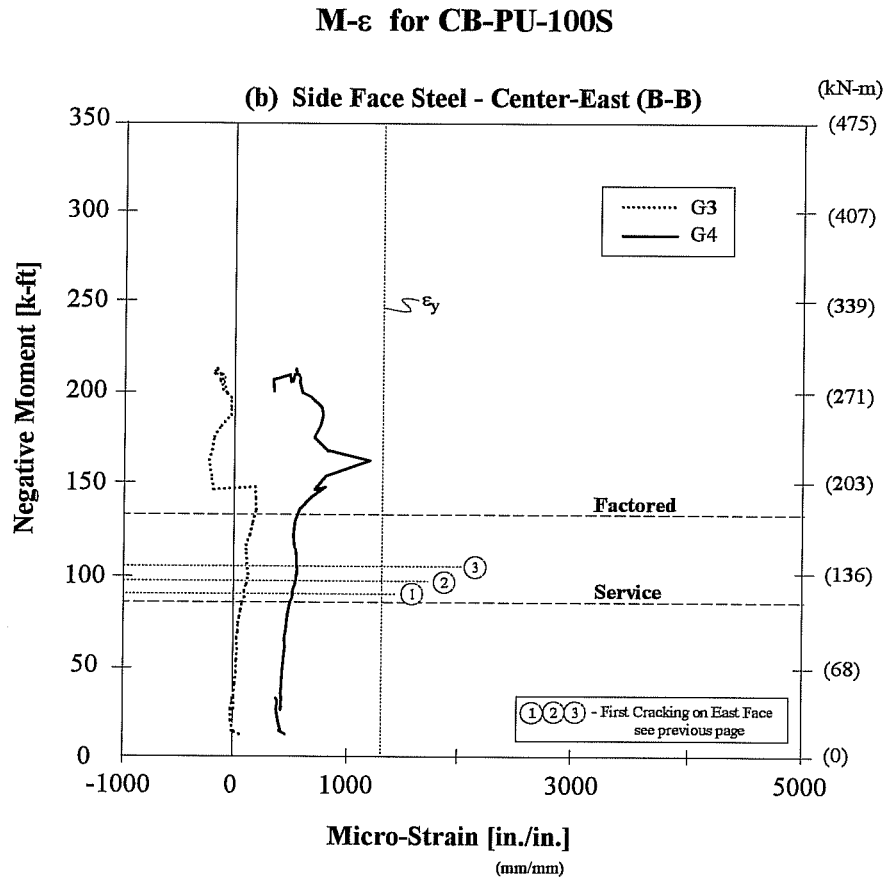


Figure 4.36 (cont.) Moment-Strain Behavior of Side Face Crack Control Steel for CB-PU-100S

4.3.1.3 Moment vs. Applied Load Behavior - CB-PU-100S

Figure 4.37 is a plot of the applied point loads, Q , versus the moment at the mid-spans and over the center support.

Looking at the equivalent load portion of the figure (explained in Section 4.2.3.3), the moments in the positive and negative moments increased under the effects of the dead load. During post-tensioning, the positive moments decreased and the negative moment increased. This exhibited the action of secondary moments. The overall secondary moment was predicted to be negative and this was supported by the behavior shown in Figure 4.37. After three days, creep or temperature changes may have caused the resulting slight decrease in negative moment over the center support and increase in positive moments at the mid-spans. At this point testing began.

The first evidence of moment redistribution occurred around the point load of 33k (147kN) where there was a shift in the slope of the plots. This corresponds to when first cracking occurred in the southern mid-span. The center support began to gain negative moment more rapidly while the mid-span moment gain decreased. Aside from a few minor shifts, most likely due to the propagation of cracks, this behavior continued. Therefore the general trend was for moment to redistribute from the mid-span positive moment regions to the negative moment region over the center support. Testing was stopped due to compression failure. When testing was stopped and the load was allowed to drop off from 71k (316kN) to 67k (298kN), there was a slight increase in moment at the mid-spans and decrease in the moment over the center support compared to the moments measured during initial testing.

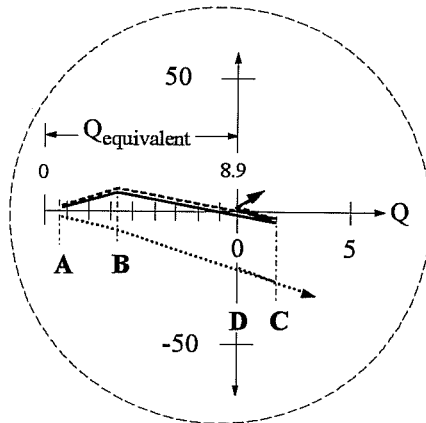
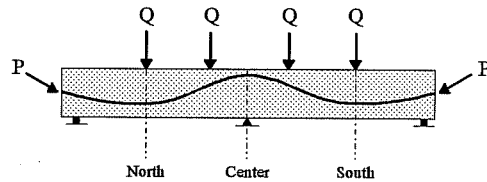
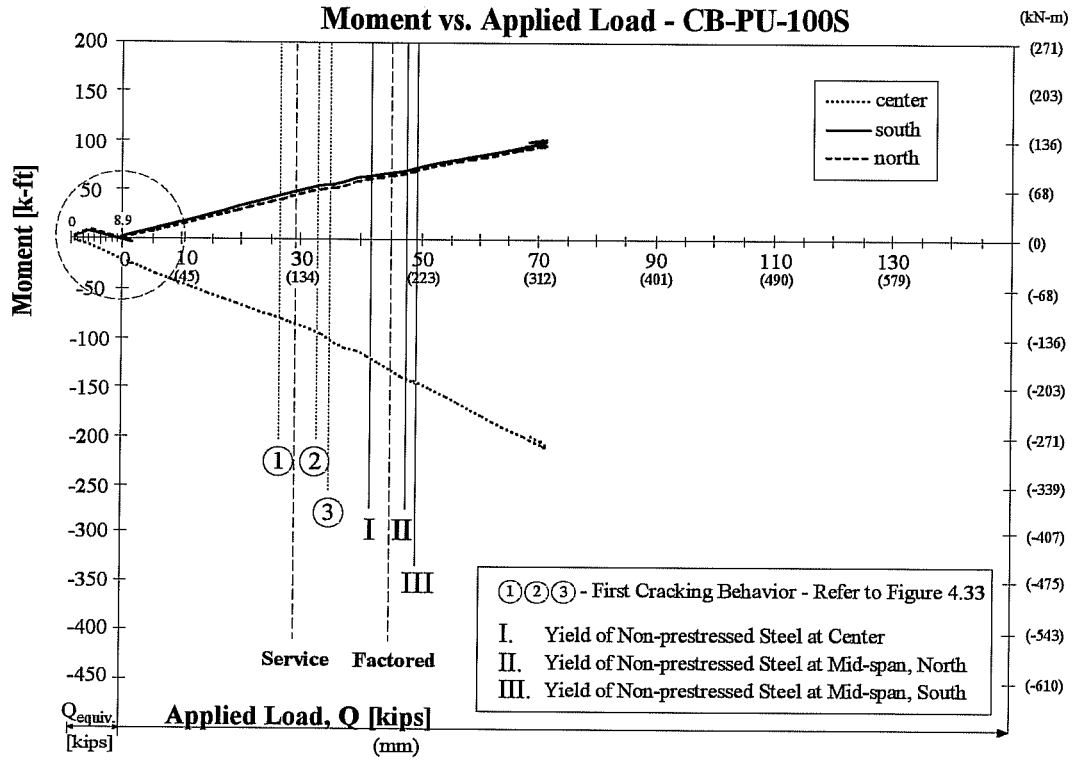
4.3.1.4 Load-Deflection Behavior - CB-PU-100S

Load-deflection behavior for this model is shown in Figure 4.38. Service load deflection criteria in accordance with AASHTO 1992 and ACI-318-89 were satisfied. The maximum service load deflection corresponded to $L/7000$.

A considerable stiffness change was first apparent in the south span with the onset of yielding of the non-prestressed reinforcement between service and factored load levels. Similar behavior occurred in the north span when yielding of the non-prestressed steel began slightly beyond factored loads. This beam exhibited considerable ductility before failure, particularly in the north span. When the north span began to deflect considerably with very little or no load increase (formation of a plastic hinge), the south span effectively "locked up" and showed very little increase in deflection. This beam also exhibited substantial over-strength reaching an ultimate load 1.6 times greater than the factored load.

4.3.1.5 Moment-Deflection Behavior - CB-PU-100S

The moment-deflection plot for CB-PU-100S is shown in Figure 4.39. The beginning of the plot is shown underneath to a larger scale in an effort to show deflection behavior during post-tensioning operations and to determine where decompression of the sections occurred. During post-tensioning, mid-span deflections were negative meaning the beam was cambering upward. During the three days between post-tensioning and testing, the mid-span deflection increased positively. This corresponds with the apparent increase in positive moment seen in the close-up of Figure 4.39. As with model CB-PS-100S, the calculated and observed decompression moments were not comparable. The deflections at these low loads were quite small and temperature changes could have effected the deflection readings by over 100%. The observed behavior is therefore not a reliable representation of the actual behavior.



Where $Q_{equivalent}$ is the force corresponding to loads Q , that would produce the negative moment over the center support resulting from the dead load and prestressing forces. Both negative and positive moments are plotted using the same $Q_{equivalent}$.

- A - Beam Only
- B - Full Dead Load
- C - Directly After Post-Tensioning
- D - Begin Test (3 days after post-tensioning)

Figure 4.37 Moment vs. Applied Load - CB-PU-100S

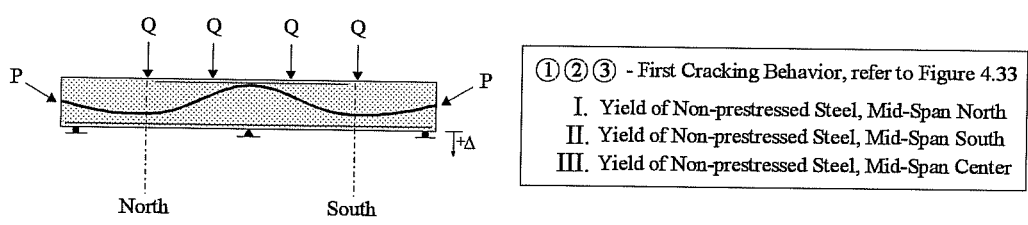
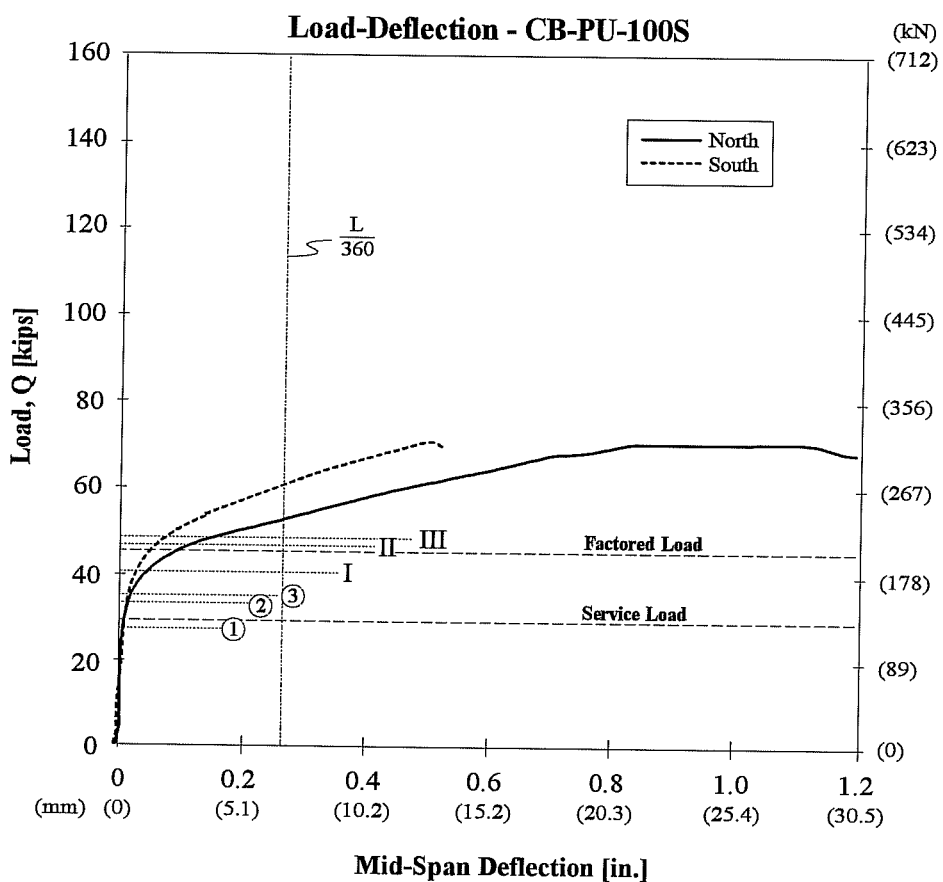
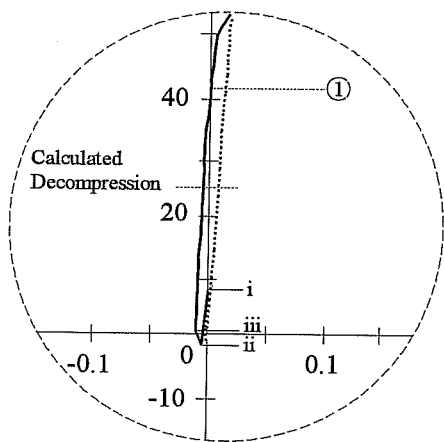
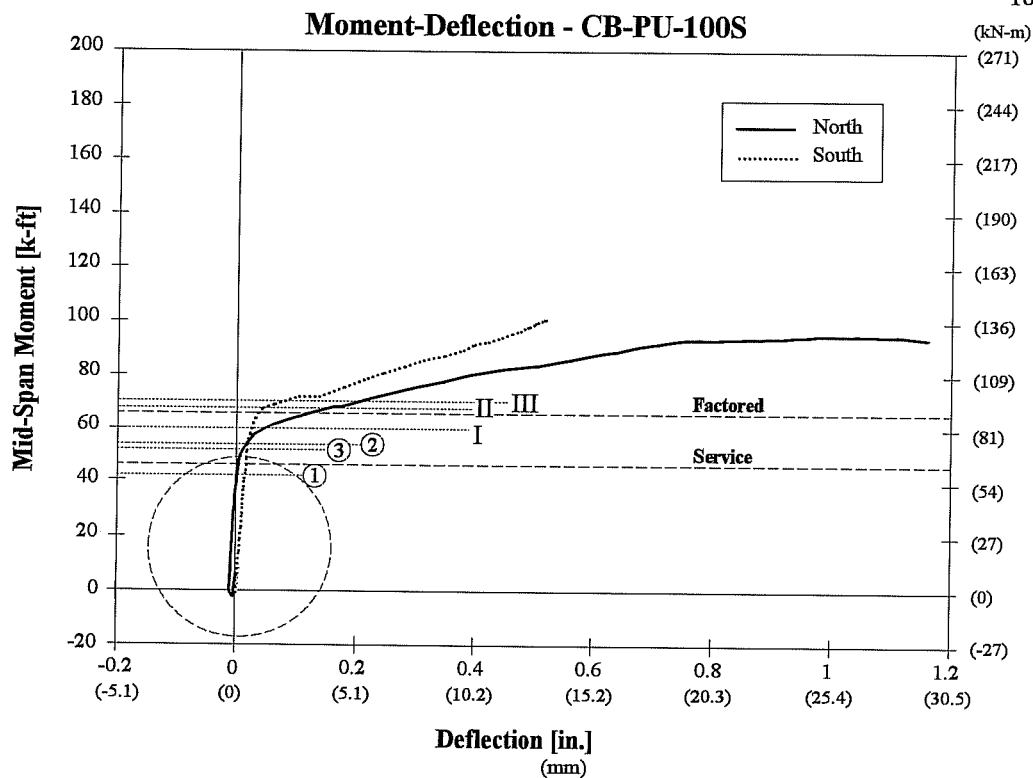


Figure 4.38 Load-Deflection Behavior - CB-PU-100S



- i. Full Dead Load
- ii. Directly after Post-tensioning
- iii. Begin Testing (3 days after Post-tensioning)
- ① ② ③ - First Cracking Behavior, refer to Figure 4.33
- I. Yield of Non-prestressed Steel, Mid-Span North
- II. Yield of Non-prestressed Steel, Mid-Span South
- III. Yield of Non-prestressed Steel, Mid-Span South

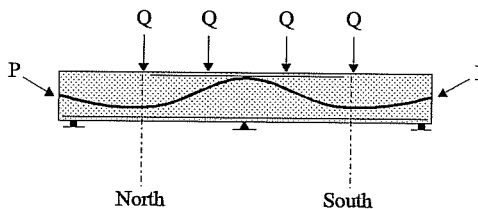


Figure 4.39 Mid-Span Moment-Deflection Behavior for CB-PU-100S

Yielding for this model is quite noticeable from the load-deflection curve and for the north span it begins after first cracking occurs at the mid-spans. The apparent yield points for both the north and south spans from this figure correspond well with the yield points determined from studying the moment-strain behavior at these sections.

In general, the north span was "softer" than the south span. As well, this section exhibited much more ductile behavior. The north span deflected over four times more than the south span as failure was approached (between applied loads of 69-71k (307-316kN)).

As hinges developed at all three critical sections, deflections increased with very slight increases in applied load. As a "collapse mechanism" formed and deflections increased without any or very little increases in load, failure occurred with concrete crushing at mid-span of the north span.

This beam also had substantial strength in excess of what was required for factored loads. The loads it was able to carry were 1.6 times the factored loads.

4.3.1.6 Post-mortem Investigation - CB-PU-100S

The model was opened at the failed section; the northern mid-span. Figure 4.40 shows the beam at this failed location and Figure 4.41 shows the location of the fractured and yielded bars at this same location.

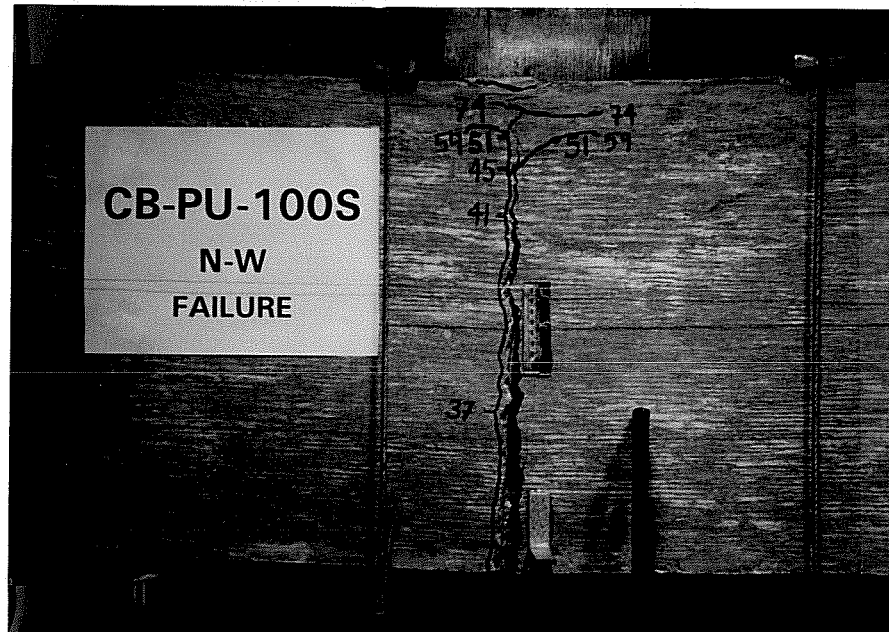


Figure 4.40 Crushing Failure of Mid-Span, North - CB-PU-100S

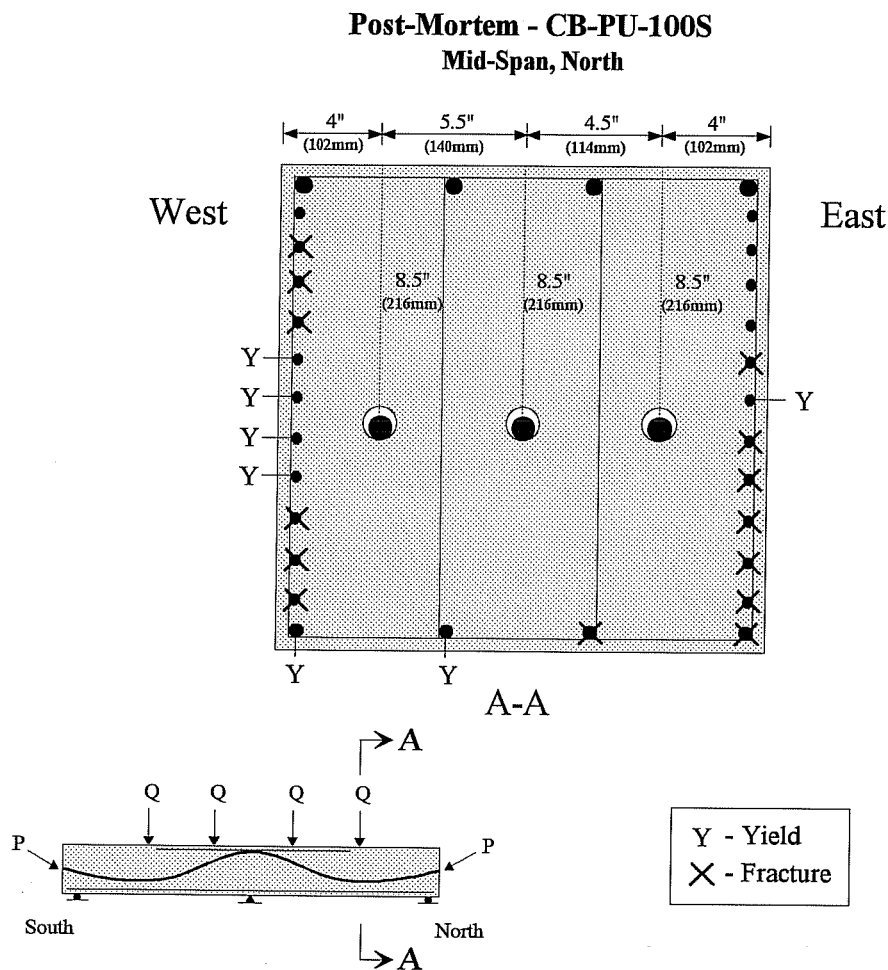


Figure 4.41 Post-mortem Investigation of Failed Cross-Section for CB-PU-100S

The two eastern longitudinal cage steel elements in the tension zone fractured while the western ones fractured. Many of the side face crack control steel wires in the tension zone fractured. Four wires on the west face that were near the depth of the post-tensioned strands only yielded as did one wire on the east face also near the depth of the post-tensioned strands.

All of the strands were constructed with a smaller effective depth than was used for design. The strands were all built with an effective depth of 9.5 in. (241mm). This depth was 1 in. (25.4mm) smaller than designed. The strand locations across the width of the section varied slightly from the designed locations as well. The center strand was 0.5 in. (12.7mm) further to the east than was designed.

4.3.1.7 Further Discussion - CB-PU-100S

The somewhat low calculated first cracking stresses near the mid-span regions may have been the result of the construction errors discussed in the post-mortem investigation. The smaller effective depth of the strands would result in less compressive stress on the section than was assumed, resulting in lower first cracking stresses.

4.3.2 CB-PU-71S - 71% Prestress Reinforcing (71% of nominal resistance provided by the prestressing strand, 29% provided by non-prestressed steel)

This model was post-tensioned and grouted 5 days before it was first tested. On the first day of testing, the model was loaded to factored loads ($Q = 45\text{k}, 200\text{kN}$). The next day the beam was loaded to failure. Failure occurred with the fracturing of a complete tendon as well as a single prestressing wire in another tendon over the center support.

4.3.2.1 Cracking Behavior - CB-PU-71S

First Cracking - First cracking behavior is indicated on Figure 4.42. First cracking occurred at the center support under point loads of 25k (111kN). The moment at this section was -73 k-ft. (-99 kN-m). This corresponds to a cracking tensile stress of $6.1\sqrt{f'_c}$ ($0.49\sqrt{f'_c}$).

The first crack in the mid-span regions of both the north and south spans (stations 4 and 1 respectively) appeared under point loads of 33k (147kN) when the moments at the mid-spans were 55 k-ft. (73 kN-m) at the north span and 59 k-ft. (80 kN-m) at the south span. These correspond to calculated cracking tensile stresses of $5.9\sqrt{f'_c}$ ($0.47\sqrt{f'_c}$) and $6.5\sqrt{f'_c}$ ($0.52\sqrt{f'_c}$), respectively.

Crack Widths & Serviceability - Figure 4.42 shows the crack locations under service and factored loads and at failure. Maximum crack widths for certain load steps are recorded in Table 4.5. The maximum crack width "envelope" is presented in Figure 4.43.

First cracking occurred when 86% of service load was applied. The maximum crack width when the crack first became visible was 0.0015 in. (0.038mm). At service loads the maximum crack width was 0.002 in. (0.025mm). This width corresponds to a full-scale prototype crack width of 0.008 in. (0.203mm), and therefore satisfies the current serviceability criterion in the AASHTO Highway Bridge

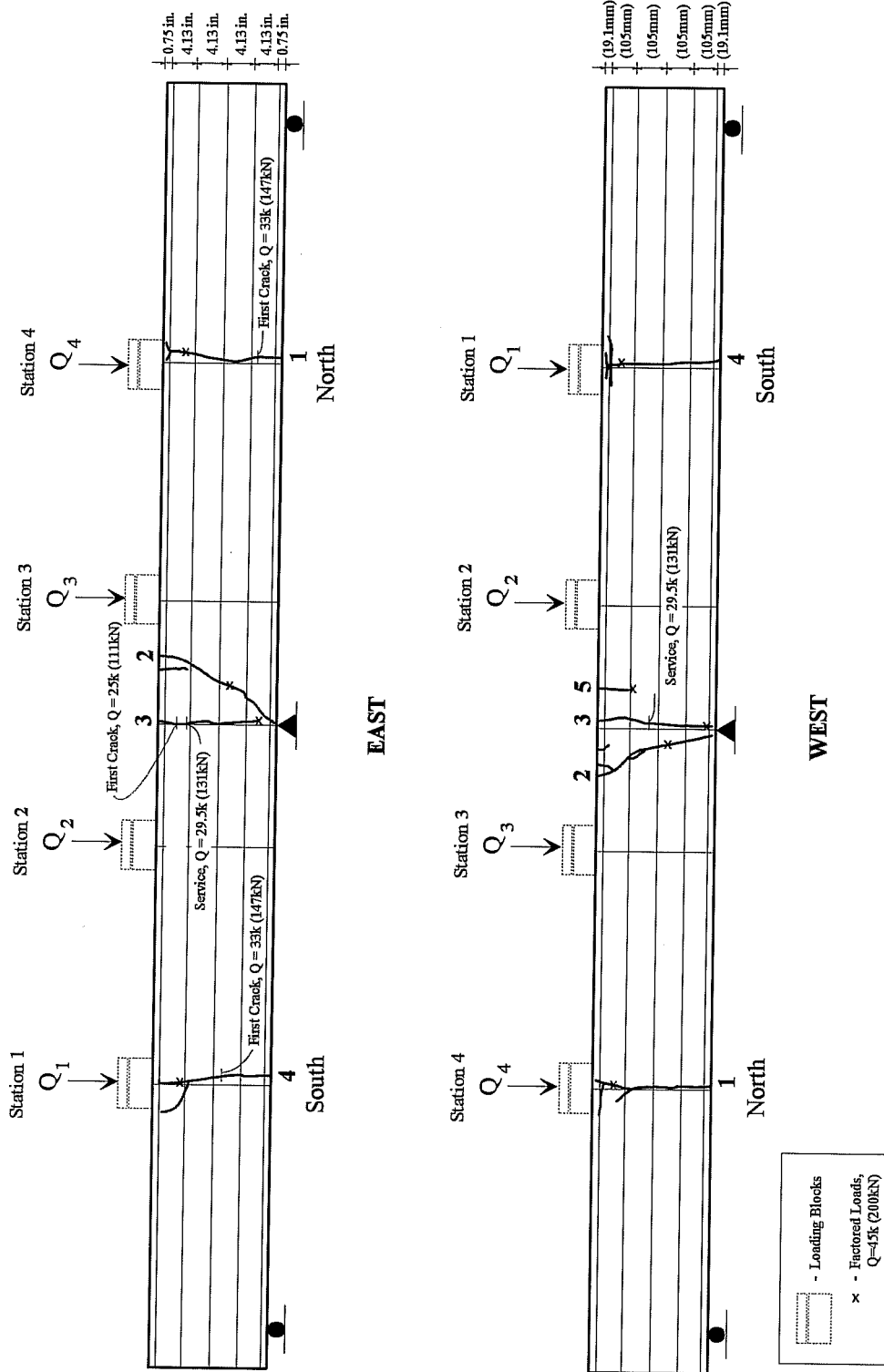


Figure 4.42 Cracking of CB-PU-71S at Ultimate Load Levels

(a) CB-PU-71S - East

LOAD, Q Kips	CRACK WIDTH, in.			
	1	2	3	4
25	-	-	0.0015	-
28	-	-	0.0015	-
29.5 - Service	-	-	0.005	-
33	0.005	-	0.005	-
39	0.014	-	0.017	0.014
43	0.04	0.01	0.04	0.04
43	0.05	0.06	0.042	0.04
45 - Factored	n.m.	n.m.	n.m.	n.m.
49	0.09	0.035	0.07	0.08

(b) CB-PU-71S - West

LOAD, Q Kips	CRACK WIDTH, in.				
	1	2	3	4	5
28	-	-	0.002	-	-
29.5 - Service	-	-	0.003	-	-
33	0.004	-	0.005	-	-
39	0.016	-	0.015	0.016	0.035
43	0.04	0.01	0.033	0.04	0.005
43	0.05	n.m.	0.034	0.037	n.m.
45 - Factored	n.m.	n.m.	n.m.	n.m.	n.m.
49	0.1	0.045	0.055	0.09	n.m.

Table 4.5E Maximum Crack Widths for CB-PU-71S, English Units

(a) CB-PU-71S - East

LOAD, Q kN	CRACK WIDTH, mm			
	1	2	3	4
111	-	-	0.038	-
125	-	-	0.038	-
131 - Service	-	-	0.127	-
147	0.127	-	0.127	-
174	0.356	-	0.432	0.356
191	1.02	0.254	1.02	1.02
191	1.27	1.52	1.07	1.02
200 - Factored	n.m.	n.m.	n.m.	n.m.
218	2.29	0.889	1.78	2.03

(b) CB-PU-71S - West

LOAD, Q kN	CRACK WIDTH, mm				
	1	2	3	4	5
125	-	-	0.051	-	-
131 - Service	-	-	0.076	-	-
147	0.102	-	0.127	-	-
174	0.406	-	0.381	0.406	0.889
191	1.02	0.254	0.838	1.02	0.127
191	1.27	n.m.	0.864	0.94	n.m.
200 - Factored	n.m.	n.m.	n.m.	n.m.	n.m.
218	2.54	1.14	1.4	2.29	n.m.

Table 4.5S Maximum Crack Widths for CB-PU-71S, S.I. Units

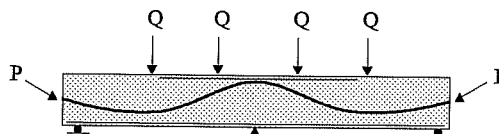
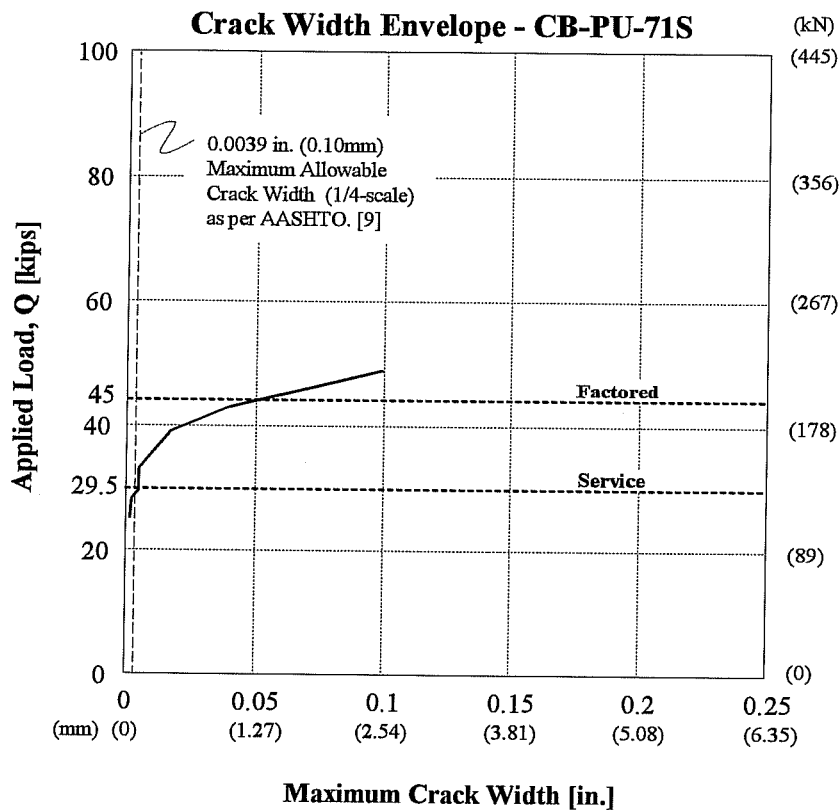


Figure 4.43 Maximum Crack Width Envelope - CB-PU-71S

Specifications. Crack widths however increased considerably between service and factored loads and beyond (Figure 4.43).

Side face crack control steel was placed in the tension zone to specifically control crack widths at levels where there was no flexural steel. As seen in Figure 4.44, the crack widths did tend to be larger below the level of the primary flexural steel at the center support. The side face crack control was therefore contributing to control of these crack widths. Mid-span sections had not yet cracked at service loads and the effectiveness of the side face crack control steel could therefore not be evaluated.

Cracking Distribution - Similar to model CB-PU-100S, crack distribution is not meaningful at service loads as only one crack had formed over the center support. However under factored loads and up to failure, cracks were not very well distributed particularly in the mid-span regions near stations 1 and 4. There was only one major crack at each mid-span and two major cracks over the center support. As mentioned previously, the moment required to crack the mid-span region was between 55-59 k-ft. (73-80 kN-m). This occurred under point loads of 33k (147kN). Predicted yielding of the non-prestressed steel in this region was at a moment of 67 k-ft. This moment was reached in the southern mid-span under point loads of 40k (178kN) and in the northern mid-span under point loads of 43k (191kN). At these loads, the bars would have yielded. These yielding points would have the characteristics of developing a plastic hinging zone thus preventing increased tensile forces in the uncracked portions of the beam. Therefore, new cracks would not form. The developed tensile forces before the steel had yielded were not enough to distribute cracking.

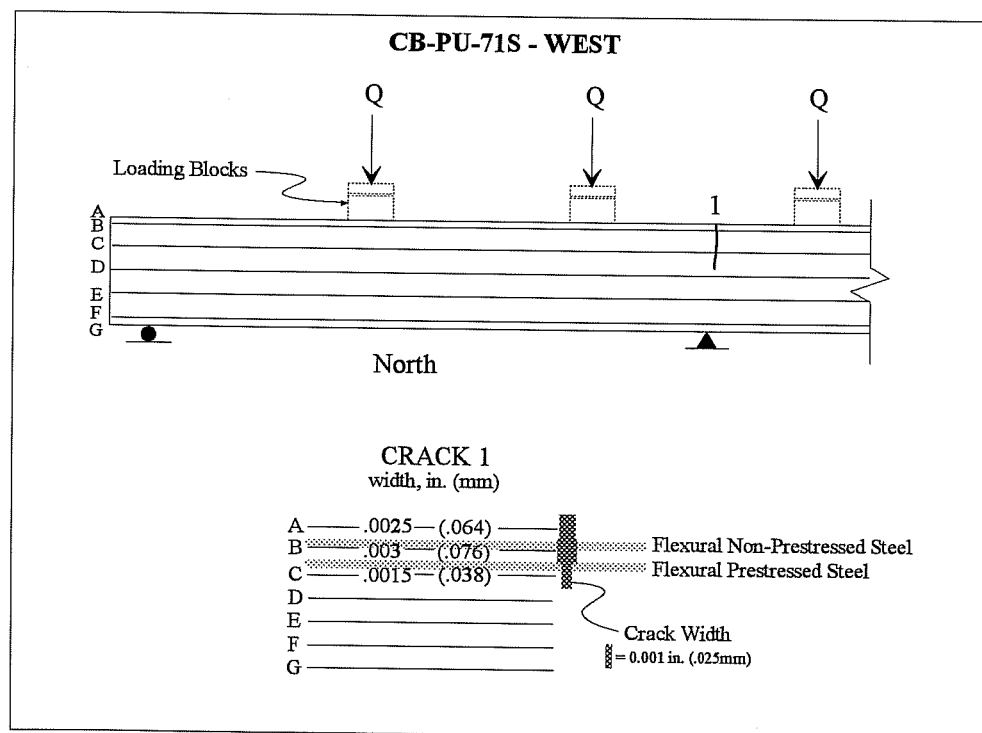


Figure 4.44 Behavior of Side Face Crack Control Steel at Service Loads for Model CB-PU-71S

4.3.2.2 Moment-Strain Behavior - CB-PU-71S

Moment-strain data for the non-prestressed steel in the tension zone of the critical moment regions is presented in Figures 4.45 - 4.48. No stage loading was required for this model and the resulting compression of the non-prestressed steel during post-tensioning operations can be seen particularly in the moment-strain plot for the region over the center support in Figure 4.45.

Once testing was started, the non-prestressed tension steel over the center support behaved elastically up to when the first crack appeared in the mid-span shortly before service loads. A slight decrease in stiffness of the section continued up through service loads. When first cracking occurred at the mid-spans, at a center support moment of -85 ft-k (-115 kN-m), inelastic behavior began as seen in the large increase in strain that occurred in all of the gages in Figure 4.45. General trends show that the steel continued to carry load and began to yield around factored loads.

Figure 4.46a shows that two of the gaged tensile steel bars in the south mid-span responded linearly up through factored loads and yielded almost immediately when an increase in strain was first recorded. These gages were most likely not at crack locations. The third gage registered an increase in strain upon first cracking of the negative moment region. Elastic behavior then continued until cracking occurred at the mid-spans. At this time inelastic behavior ensued until the gage failed near the steel's theoretical yield point and at loads 30% higher than factored loads. At the north span shown in Figure 4.46b, the tensile steel was elastic until first cracking occurred at the mid-spans. Behavior was then inelastic and yielding occurred near factored loads.

Shear force vs. stirrup strain behavior for the negative moment region is shown in Figure 4.47. The gaged inner stirrup measured very little strain up to a shear force of 200k (890kN). This corresponds to 1.36 times factored loads. At this point a sudden increase in strain occurred. Failure of the model followed shortly and this steel did not yield. Shear force vs. stirrup strain results for the other gaged stirrups showed very little change in strain throughout testing.

Looking at the side face crack control steel at the southern mid-span shown in Figure 4.48a, the steel closest to the extreme tensile fiber increased in strain when the negative moment region cracked before service loads. The steel continued to behave elastically through service loads and began to behave inelastically when cracks first formed at the mid-spans. When this occurred, the gages seemed to have failed. The crack control steel closest to the centroid of the section remained in compression beyond factored loads. At the north span shown in Figure 4.48b, all of the crack control steel behaved elastically until cracking of the mid-spans occurred. The behavior was then inelastic and led quickly to yielding of the steel (and gage failure) around factored loads. This crack control steel was not controlling cracks at service

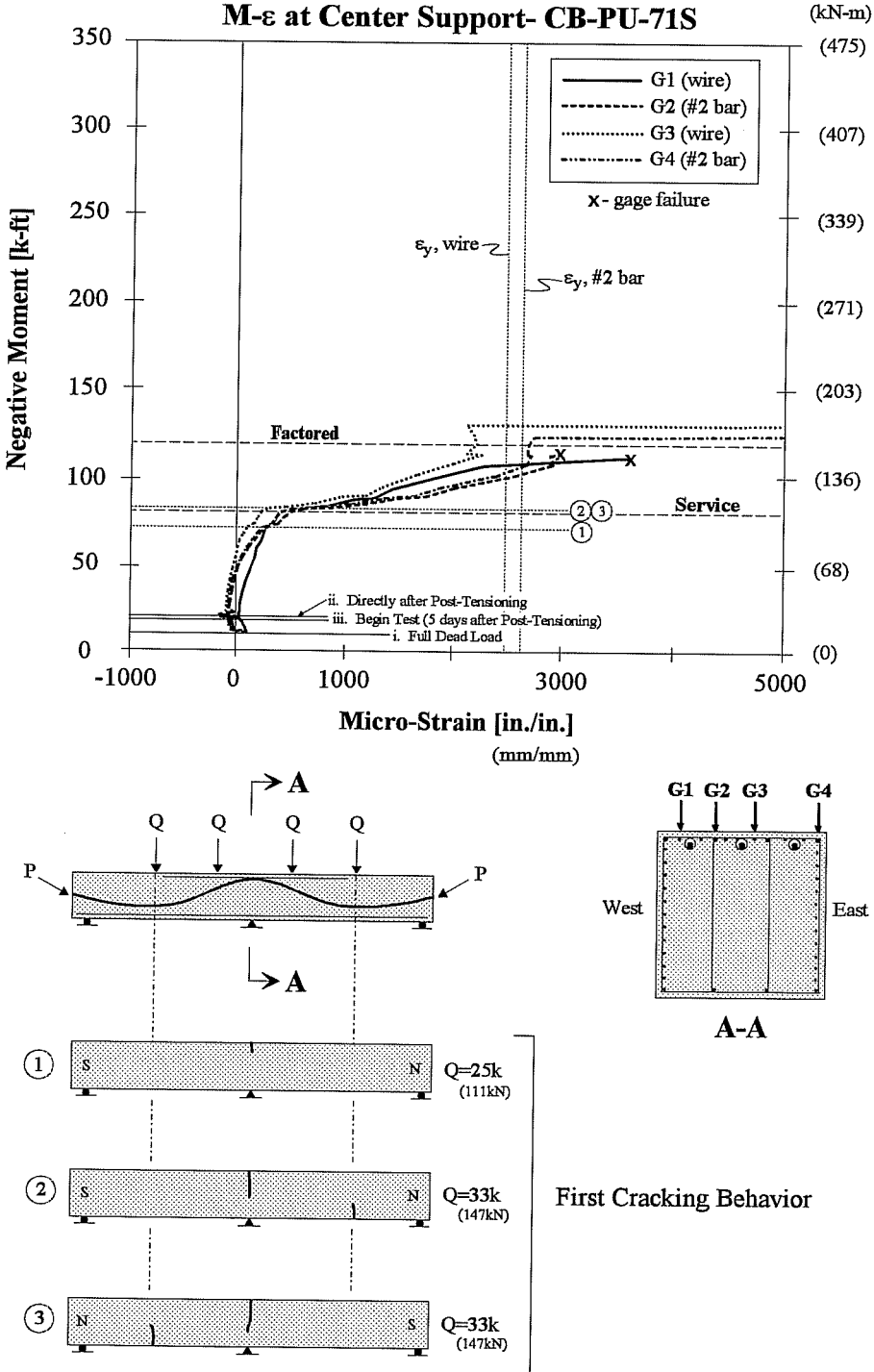
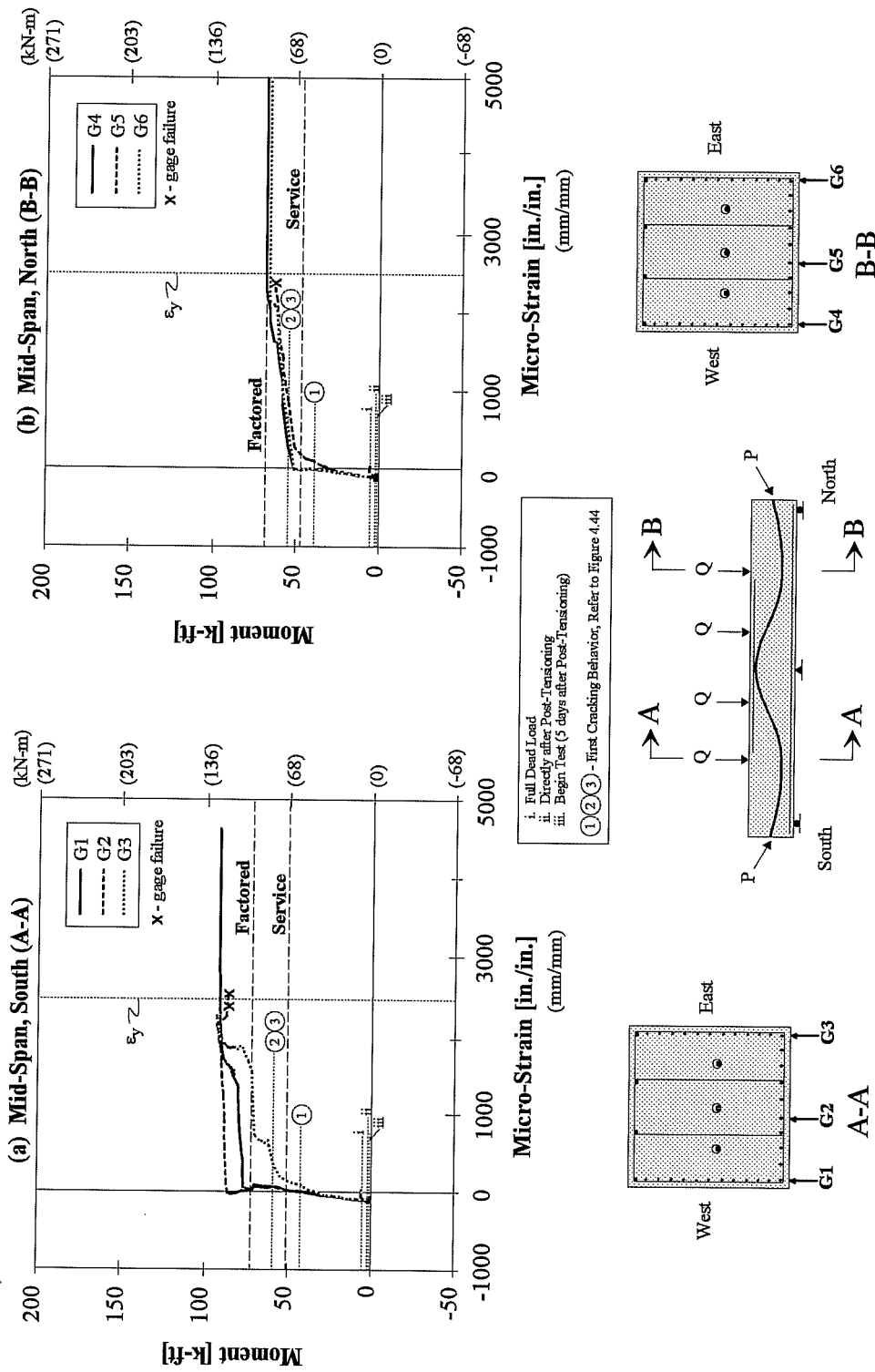


Figure 4.45 Moment-Strain Behavior for Non-Prestressed Steel in the Negative Moment Region - CB-PU-71S

M-ε for CB-PU-71S



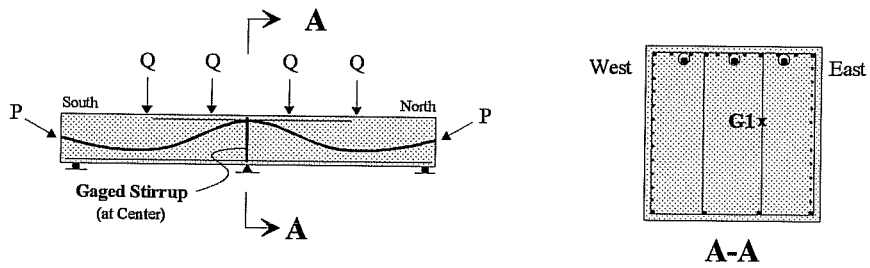
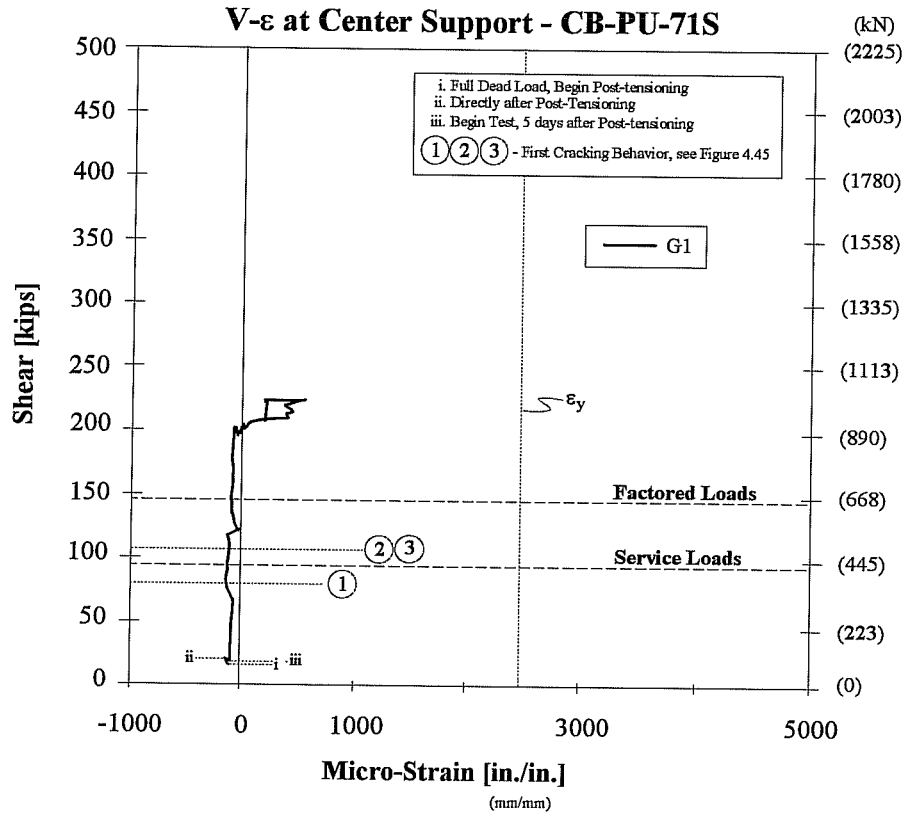


Figure 4.47 Center Support - Strain Behavior for Shear Stirrups - CB-PU-71S

M-ε for CB-PU-71S

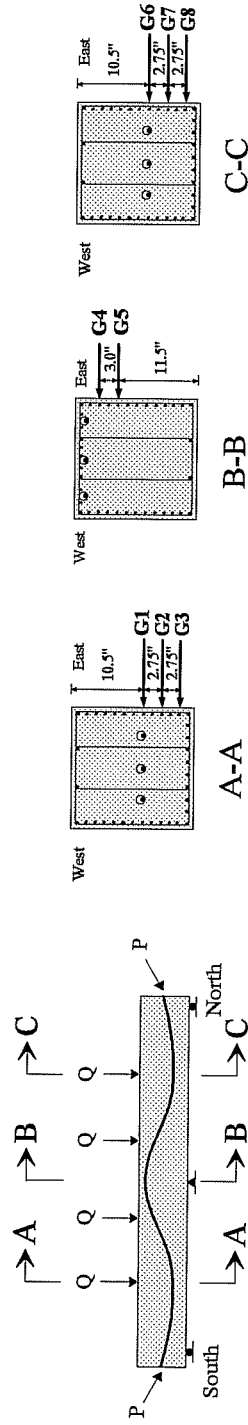
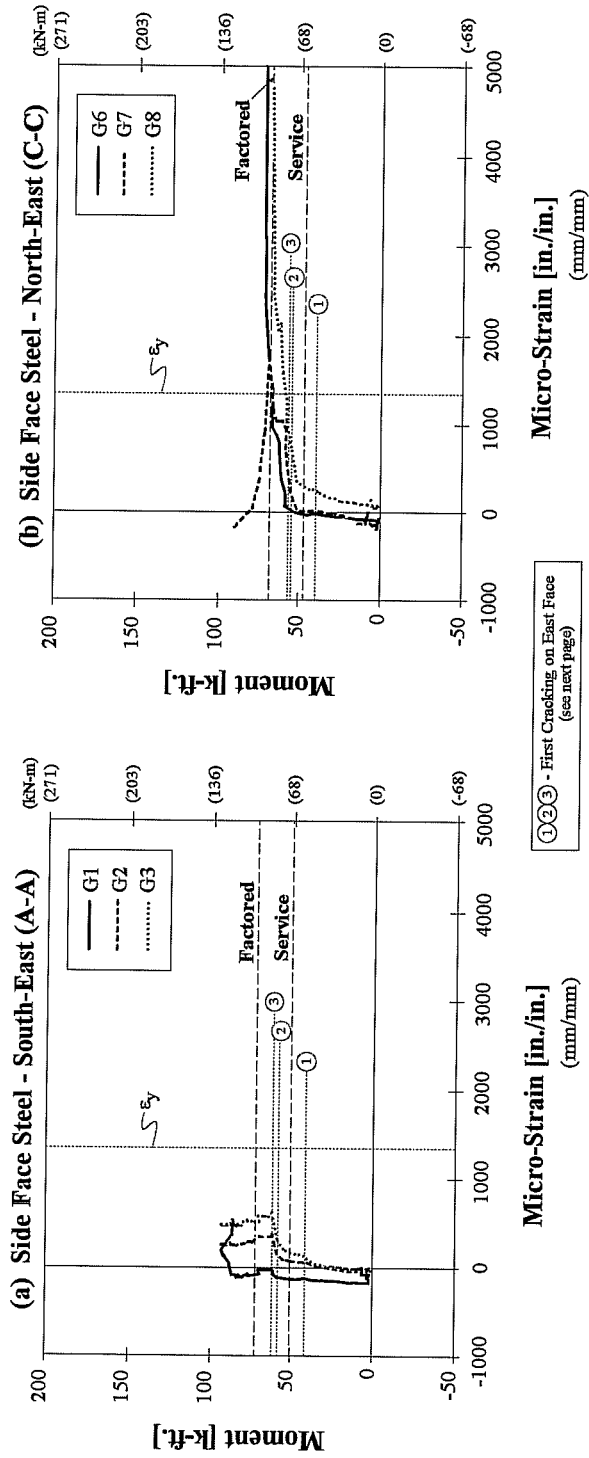


Figure 4.48 Moment-Strain Behavior of Side Face Crack Control Steel for CB-PU-71S (continued on next page)

M-ε for CB-PU-71S

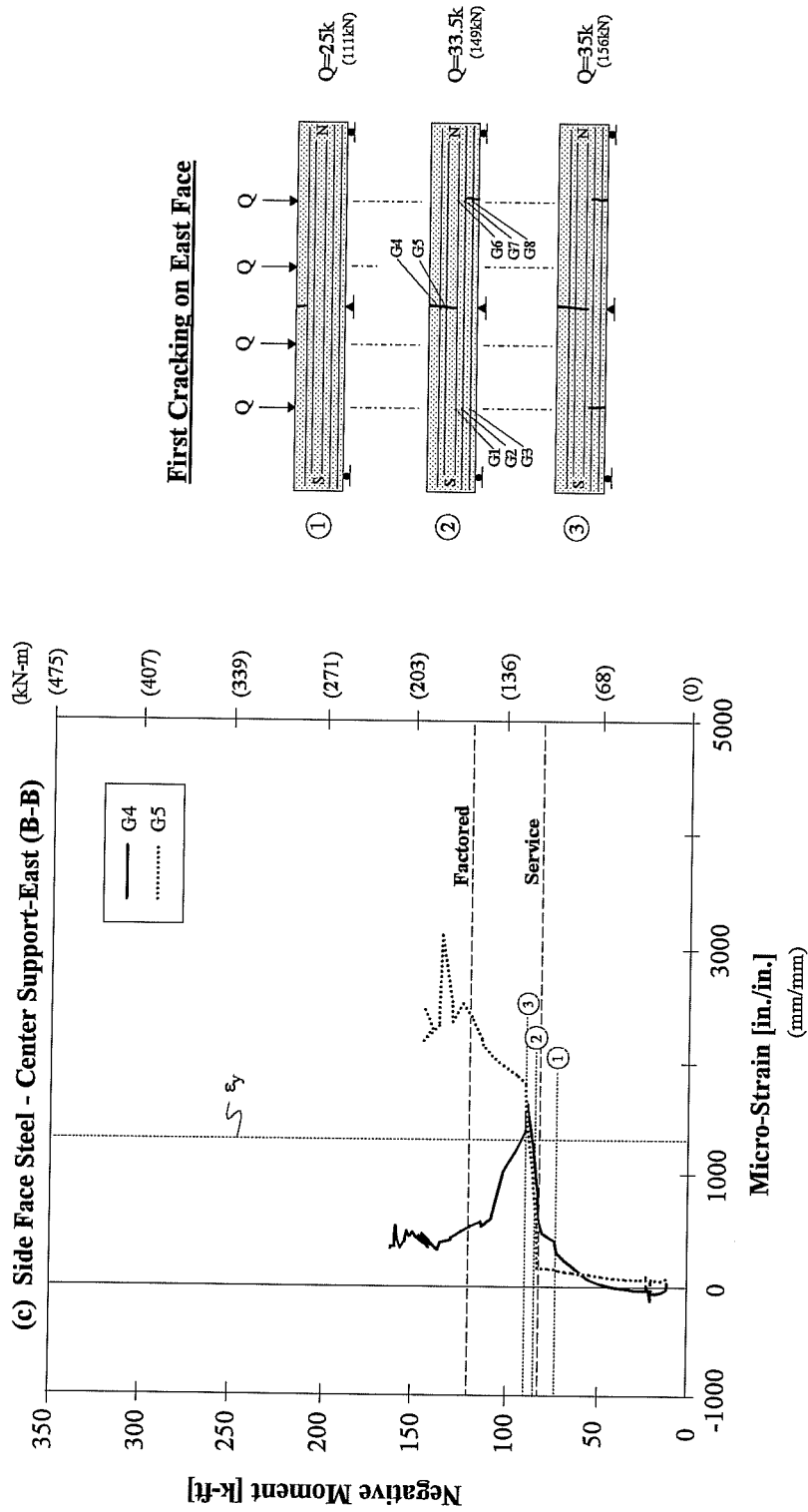


Figure 4.48 (cont.) Moment-Strain Behavior of Side Face Crack Control Steel for CB-PU-71S

loads as there were no cracks in these regions. Once these sections were cracked however, the steel was contributing to crack width control. With its early yielding, the steel was not effectively controlling cracks at factored loads.

At the center support as shown in Figure 4.48c, the crack control steel closest to the extreme tensile fiber initially behaved elastically. As the first cracking load at this section was approached, the steel began to increase in strain more rapidly, most likely due to micro-cracking. A jump in strain occurred when the crack formed. The crack control steel closer to the centroid of the section behaved elastically through first cracking of the region and through service loads. Both gaged steel elements showed large increases in strain when cracking first occurred at the mid-spans and yielding followed almost immediately. This steel seems to have been contributing to crack control at service loads but yielded and would not effectively control cracking shortly thereafter.

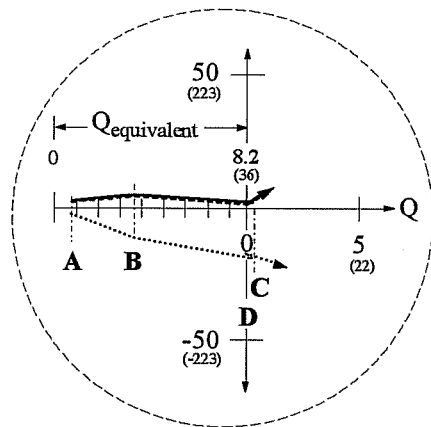
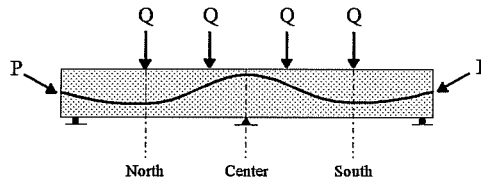
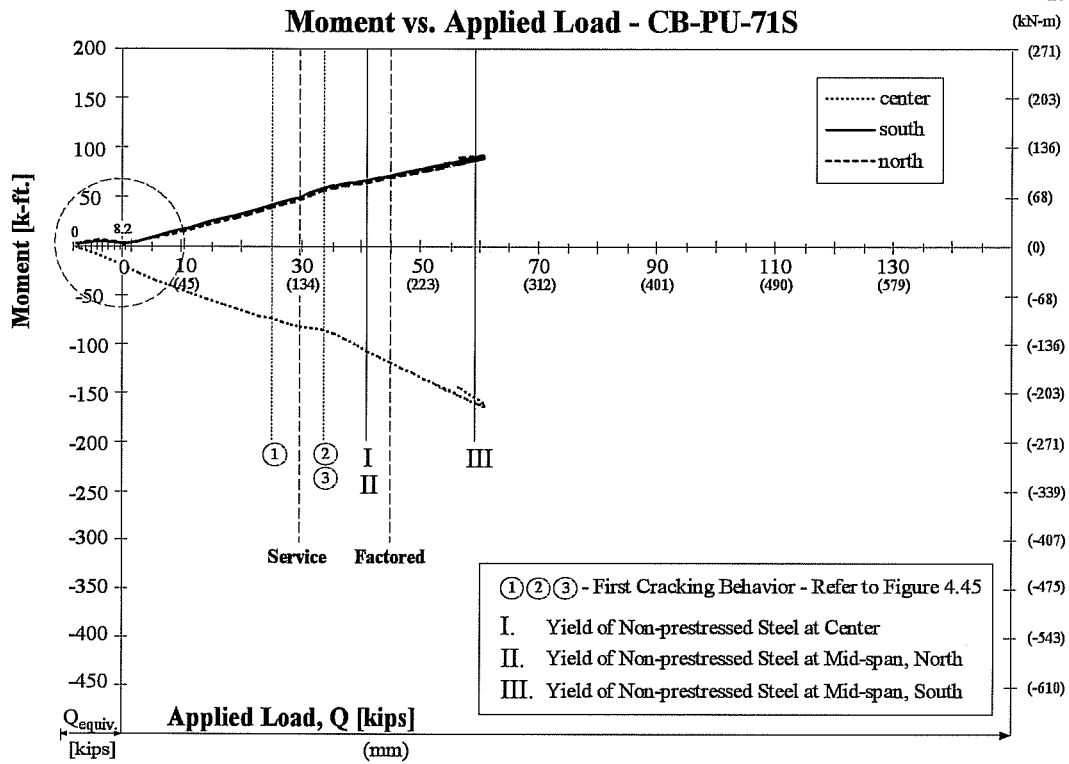
The side face crack control steel is only required for controlling cracks at service loads. The steel used for modeling had a yield strength of 38 ksi (262 MPa). Normally side face crack control steel would have the standard 60 ksi (414MPa) strength and would therefore continue to control cracks at higher loads and contribute more to the ultimate capacity of the member as well.

4.3.2.3 Moment vs. Applied Load Behavior - CB-PU-71S

Figure 4.49 is a plot of the applied point loads, Q , versus the moment at the mid-spans and over the center support.

Looking at the equivalent load portion of the figure (explained in Section 4.2.3.3), the positive and negative moments increased under the effects of the dead load. During post-tensioning, the positive moments decreased and the negative moment increased. This exhibits the action of secondary moments. After five days, creep or temperature changes may have caused the resulting slight decrease in negative moment over the center support. At this point testing began.

The first evidence of moment redistribution occurred when the first crack over the center support appeared under point loads of 25k (34kN). At this point, the moment increase at the center support lessened. Moment was being redistributed to the mid-span regions. However once cracking of the mid-span regions occurred under point loads of 33k (147 kN), the center support moment increased more rapidly than it did initially. Moment was then being redistributed from the mid-span positive moment regions to the negative moment region over the center support. This trend continued up to failure. Testing was stopped when a loud bang was heard which was the fracturing of a strand over the center support.



Where $Q_{equivalent}$ is the force corresponding to loads Q , that would produce the negative moment over the center support resulting from the dead load and prestressing forces. Both negative and positive moments are plotted using the same $Q_{equivalent}$.

- A - Beam Only
- B - Full Dead Load
- C - Directly After Post-Tensioning
- D - Begin Test (5 days after post-tensioning)

Figure 4.49 Moment vs. Applied Load - CB-PU-71S

4.3.2.4 Load-Deflection Behavior - CB-PU-71S

Load-deflection behavior for this model is shown in Figure 4.50. Service load deflection criteria in accordance with AASHTO 1992 and ACI-318-89 were satisfied. The maximum service load deflection corresponded to $L/6400$.

Considerable stiffness changes occurred in both the north and south spans with the onset of yielding of the non-prestressed reinforcement at these sections between service and factored load levels. Failure of this beam was ductile, with hinges appearing to first form at the mid-spans and a full collapse mechanism forming with the yielding and fracture of reinforcement over the center support. This beam exhibited more reasonable over-strength reaching an ultimate load 1.3 times greater than the factored load.

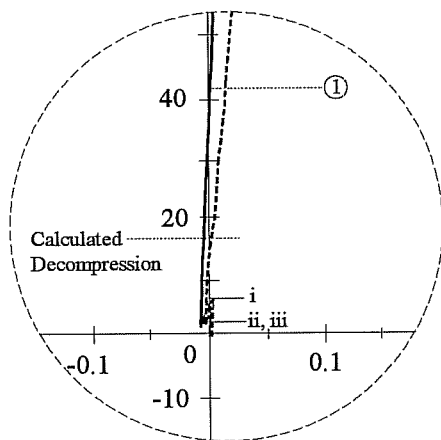
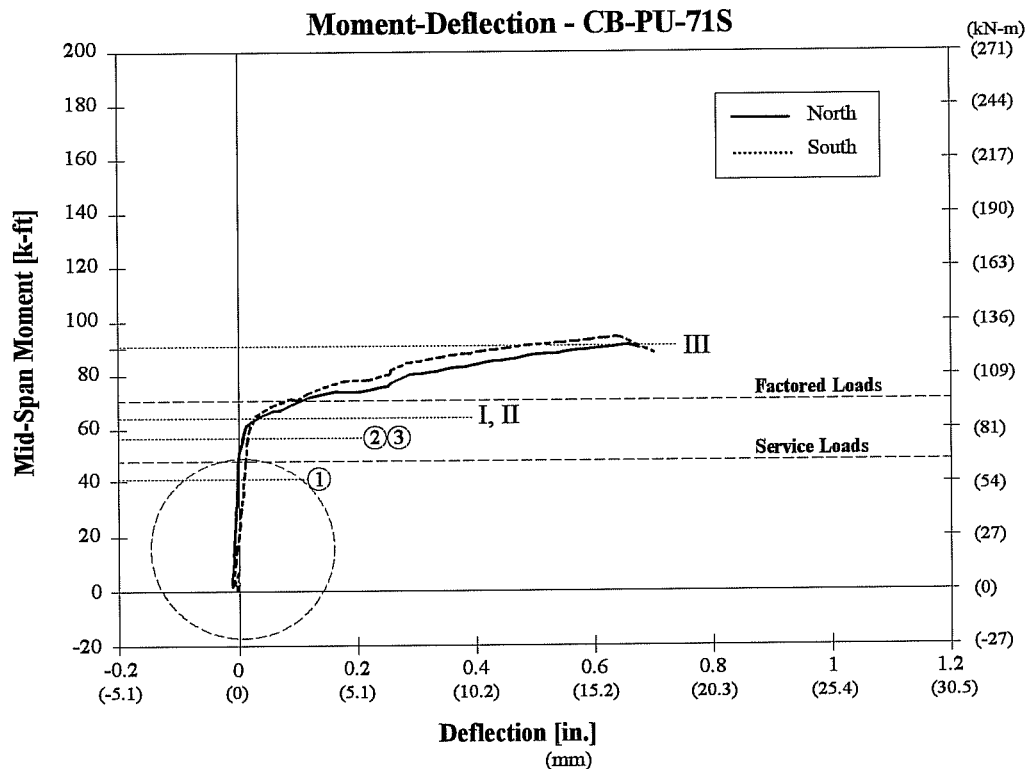
4.3.2.5 Moment-Deflection Behavior - CB-PU-71S

The moment-deflection plot for CB-PU-71S is shown in Figure 4.51.

Yielding for this model was quite noticeable from the moment-deflection curve and began between service and factored loads shortly after initial cracks at the mid-spans formed. The mid-span moments were approximately 63 k-ft. (85 kN-m). This corresponded well with the yield moments determined from studying the moment-strain behavior of the mid-span and center support sections. As with the previous post-tensioned models, the calculated and observed decompression moments were not comparable. Again due to possible temperature effects, the observed behavior was not a reliable representation of the actual behavior.

Failure occurred under point loads of 56k (249kN) with a loud bang that was believed to be a tendon fracturing (see Section 4.3.2.6). The point loads had reached 60k (267kN) and gradually dropped off until the loud bang occurred. The load then dropped further quickly thereafter. The highest moments reached at the critical sections were -172 k-ft. (-233 kN-m) over the center support, 92 k-ft (125 kN-m) at mid-span of the south span, and 82 k-ft. (111 kN-m) at mid-span of the north span.

As can be seen from the moment-deflection curve, both spans of this model behaved similarly and exhibited ductile behavior. Behavior was similar to model CB-PU-100S in that as hinges developed in all three critical sections (at mid-spans and over the center support), deflections increased with very slight increases in applied load. Load could still be applied when failure occurred from the fracturing of a strand. Therefore while a yielding mechanism was reached, full capacity of the section was not quite reached due to final tendon rupture.



- i. Full Dead Load
- ii. Directly after Post-tensioning
- iii. Begin Testing (5 days after Post-tensioning)
- ① ② ③ - First Cracking Behavior, refer to Figure 4.45
- I. Yield of Non-prestressed Steel, Center
- II. Yield of Non-prestressed Steel, Mid-Span North
- III. Yield of Non-prestressed Steel, Mid-Span South

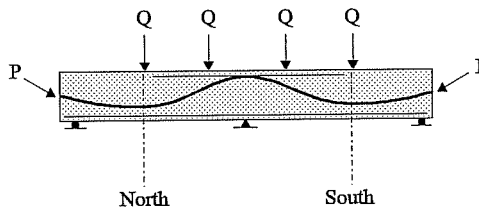


Figure 4.51 Mid-Span Moment-Deflection Behavior for CB-PU-71S

4.3.2.6 Post-mortem Investigation - CB-PU-71S

In a post-mortem investigation of this model, the negative moment region was examined in particular. Figure 4.52 shows a cross section of this region marking reinforcement that yielded or fractured and giving actual locations of prestressing strands. Figure 4.53 shows the actual failure of this region during testing. The west tendon was completely fractured and one wire of the center tendon had fractured. All of the cage steel (#2 bars) as well as 2 of the 7 wires fractured. Two more wires showed definite signs of yielding.

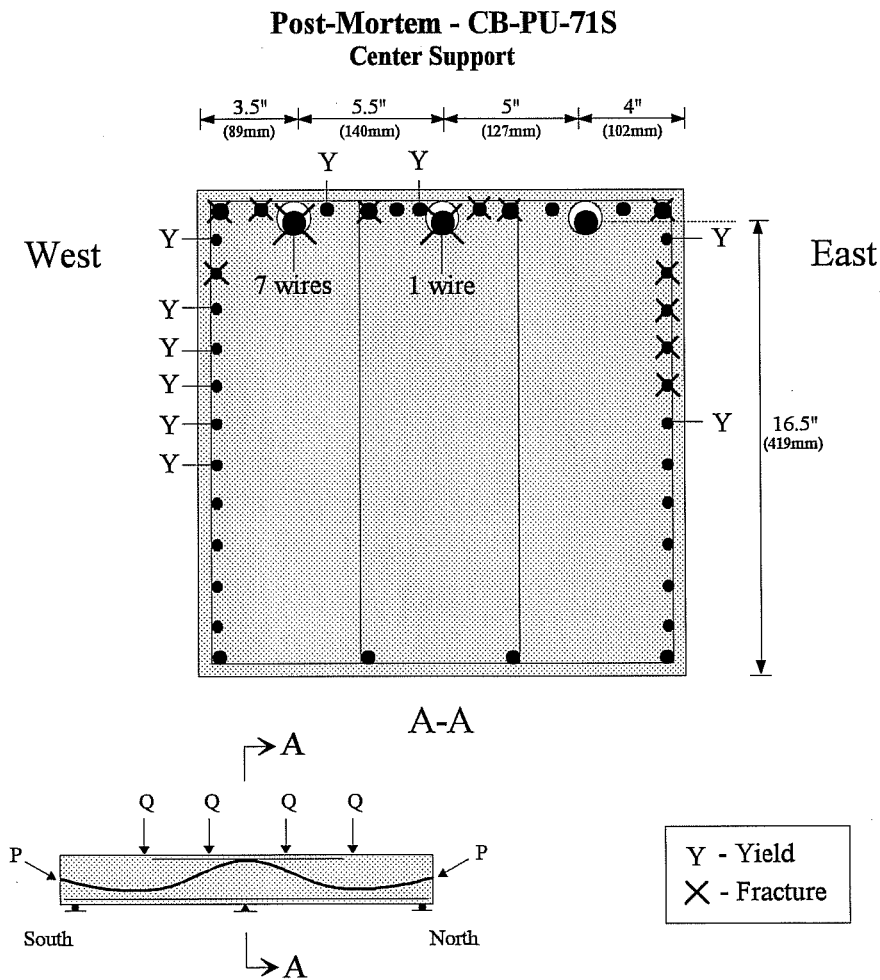


Figure 4.52 Post-mortem Investigation of Failed Cross-Section for CB-PU-71S

All of the side face crack control steel wires up to the centroid of the section yielded and many of the wires fractured as well. The wires with a similar effective depth as the prestressing strand yielded but did not fracture.

All of the strands were constructed with the effective depths that were used for design (16.5 in., 419mm). The strand locations across the width of the section varied slightly from the designed locations. The western and center strands were located as designed. The eastern strand was 0.5 in. (12.7mm) further to the west than was designed.

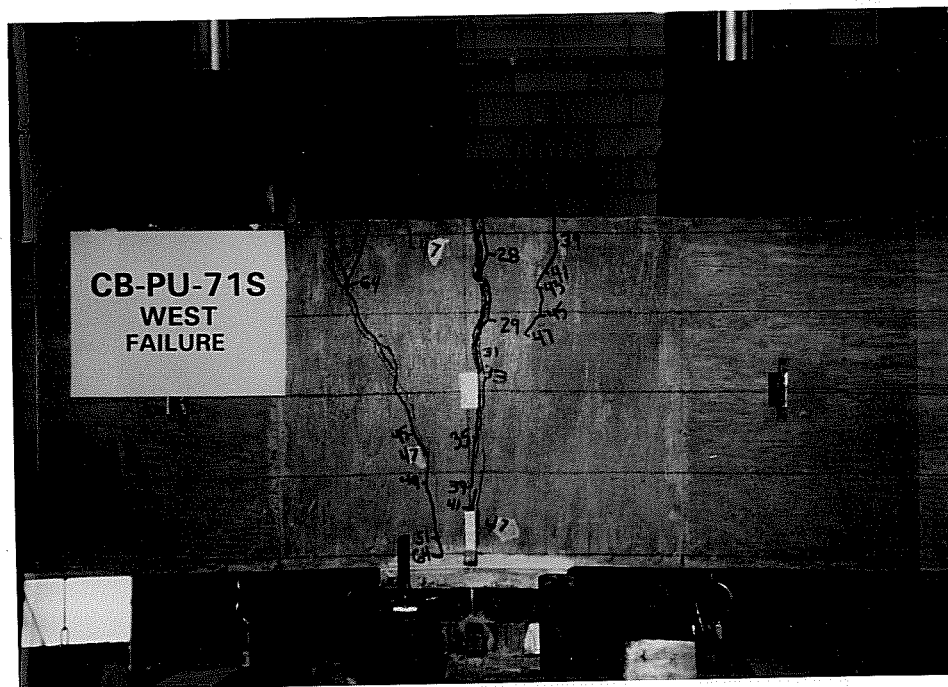


Figure 4.53 Failure over the Center Support - CB-PU-71S

CHAPTER 5

COMPARISON OF TEST RESULTS

5.1 Introduction

In this chapter, comparisons are drawn between all of the models tested. Comparisons will include:

- 1) *First cracking behavior* - including experimental and predicted results.
- 2) *Maximum crack width envelopes* - including where service load crack widths lie in relation to the limitations implied or set forth in American and European standards of practice.
- 3) *Measured vs. predicted crack widths* - using predictions based on actual and simplified versions of crack width equations developed by Gergely and Lutz.[34]
- 4) *Crack distribution characteristics* - including minimum steel requirements for adequate crack distribution as called for by both American and European standards of practice.
- 5) *Moment Redistribution Behavior*
- 6) *Behavior at ultimate loads* - including predicted vs. observed failure modes and loads.
- 7) *Load-deflection Behavior* - including where results lie in relation to American service load deflection criteria.
- 8) *Moment-deflection behavior* - to emphasize section ductilities.
- 9) *Fatigue considerations* -including stress range predictions compared with recommendations by Wollmann.[65]
- 10) *Constructability of each model.*
- 11) *Economic considerations for each model.*

Summaries are made in each section of comparisons.

5.2 First Cracking Behavior

First cracking moment predictions for sections over the center support and at the mid-spans were calculated based on the following equation:

$$M_{cr} = \left(f_r + \frac{A_{ps} f_{pe}}{A_g} \right) \frac{I}{c} \pm M_{dl} \pm M_{ps} \quad (5-1)$$

where: M_{cr} : Applied moment at first cracking.
 f_r : Modulus of rupture of concrete.
 A_{ps} : Area of prestressed reinforcement.
 A_g : Area of concrete section.
 f_{pe} : Effective prestress in prestressed reinforcement, after losses.
 M_{dl} : Moment due to dead load (+ compression, - tension, in extreme tensile fiber).
 M_{ps} : Moment due to prestressed reinforcement, including secondary moments
(+ compression, - tension, in extreme tensile fiber).

This equation was developed as follows:

$$f_t = \frac{P}{A} \pm \frac{Mc}{I}; \quad \text{where } f_t \text{ is a tensile stress, } \therefore \text{ use } -f_t$$

$$-f_t - \frac{P}{A} = \pm (M_{dl} + M_{cr} + M_{ps}) \frac{c}{I}; \quad \text{where } M_{cr} \text{ creates a tensile stress } \therefore \text{ use } -M_{cr}$$

$$M_{cr} = (f_t + \frac{P}{A}) \frac{I}{c} \pm M_{dl} \pm M_{ps}; \quad \text{where } M_{dl} \text{ and } M_{ps} \text{ are problem dependent (+ compr., - tension)}$$

In all cases, the modulus of rupture of concrete for these predictions was assumed to be $6\sqrt{f'_c}$ ($0.5\sqrt{f'_c}$).

Table 5.1 shows that the predicted and measured first cracking values correspond well with each other with one exception (CB-RU center support). In all models, cracking occurred over the center support sooner than expected. In the case of the conventionally reinforced model, CB-RU, the center moment measured may be in error due to the unknown exact support settlement at this location. In the case of the prestressed models, the lower cracking moment is most likely due to higher friction losses than expected along the curve of the duct over the center support. Higher friction losses would have lowered the effective prestress thus lowering the resistance the prestressing could provide against cracking.

In the case of model CB-PU-100S, designed to carry 100% of the ultimate loads with prestressing strand, the effective prestress appears to be low along the entire model, not just over the center support where the higher friction losses were expected. The combination of a lower effective prestress as well as the smaller eccentricity of the strands at the north mid-span (see post-mortem investigation, Section 4.3.1.6) most likely led to the earlier-than-expected cracking moments.

MODEL	M _{CR} - PREDICTED f _t = 6√f' _c (0.5√f' _c) kip-ft (kN-m)			M _{CR} - TEST kip-ft (kN-m) [M _{CR,Test} /M _{CR,Preld}]			M _{CR} / M _{SEB} *		
	Mid-Span North	Center Support	Mid-Span South	Mid-Span North	Center Support	Mid-Span South	Mid-Span North	Center Support	Mid-Span South
CB-RU-initial	+38.3 (52.0)	-38.3 (-52.0)	+38.3 (52.0)	-	-22 (-30) [0.57]	+53 (72) [1.38]	-	0.38	0.90
CB-RU-final	+38.3 (52.0)	-	-	+42 (57) [1.10]	-	-	0.72	-	-
CB-PS-100S	+84.8 (115.0)	-120.1 (-162.9)	+84.8 (115.0)	+88 (119) [1.04]	-112 (-152) [0.93]	+92 (125) [1.08]	1.83	1.38	1.80
CB-PU-100S	+57.6 (78.1)	-92.7 (-125.7)	+57.6 (78.1)	+52 (71) [0.90]	-81 (-110) [0.87]	+54 (73) [0.94]	1.16	0.94	1.13
CB-PU-71S	+49.9 (67.7)	-74.8 (-101.5)	+49.9 (67.7)	+55 (75) [1.10]	-73 (-99) [0.98]	+59 (80) [1.18]	1.18	0.89	1.17
Average Ratio [M _{CR,Test} /M _{CR,Preld}]	-	-	-	[1.04] [1.01]**	[0.84] [0.93]**	[1.15] [1.07]**	-	-	-

* M_{SEB} is the moment at the section under service loads. This moment varies with each test. See Moment-Strain figures in Chapter 4 for service moment data.

**For prestressed models only

Table S.1 Comparison of First Cracking Predictions and Observed Behavior for all Models

Summary

All models except for CB-PS-100S first cracked before service loads were applied. This was to be expected as model CB-PS-100S was designed based on limiting service load stresses according to the 1992 AASHTO Standard Specifications for Highway Bridges.[9] Even with the lower effective prestress over the center support, model CB-PU-100S first cracked at loads very close to service loads. With adequate effective prestress values this model may not have cracked until after service loads.

5.3 Maximum Crack Width Envelopes

Figure 5.1 shows the maximum crack widths for each model from first cracking to beyond factored loads. Since these are all 1/4-scale models, these crack widths correspond to 1/4 of the width of an expected prototype crack.[23] Maximum crack widths typically occurred at the extreme tensile fibers of the maximum moment sections. The two models designed according to current American codes and standards, CB-RU and CB-PS-100S, control crack widths more effectively well beyond factored loads. This is far in excess of serviceability requirements. The two models designed according to the integrated design approach, CB-PU-100S and CB-PU-71S control crack widths well through service loads and then crack widths increase up to and beyond factored loads. The primary reason for this was the formation of only one major crack at each mid-span (see crack distribution discussion, Section 5.5).

Figure 5.2 is a close-up of Figure 5.1 showing where the crack width results lie with respect to the maximum allowable crack widths implied by or called for in American and European standards of practice. The AASHTO criterion is the most lenient while the CEB-FIP codes are the most restrictive. American standards are based on equations developed by Gergely and Lutz.[34] Detailed requirements for crack width control in ACI-318-89 correspond to crack widths of 0.013 in. (0.330mm) and 0.016 in. (0.406mm) for exterior and interior exposure, respectively. The 1992 AASHTO Specification requirements correspond to 0.012 in. (0.305mm) and 0.0155 in. (0.394mm) for extreme and moderate exposure respectively.

Model CB-PS-100S, the AASHTO-based prestressed design was intended not to crack at service loads and did not crack during testing until just before factored loads were reached. This design therefore satisfies both American and European criteria for crack width control.

The conventionally reinforced model CB-RU, on the other hand does not satisfy any of the criteria outlined here. A model crack width of 0.005 in. (0.127mm) was measured which exceeded the AASHTO implied limit of a model crack width of 0.0039 in. (0.10mm).

Model CB-PU-100S designed according to the proposed integrated design method satisfied both the ACI and AASHTO implied maximum allowable crack widths as well as the CEB-FIP Model Code 1990 criterion. Model CB-PU-71S behaved similarly to model CB-RU and did not satisfy any of the criteria outlined here.

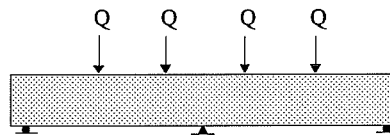
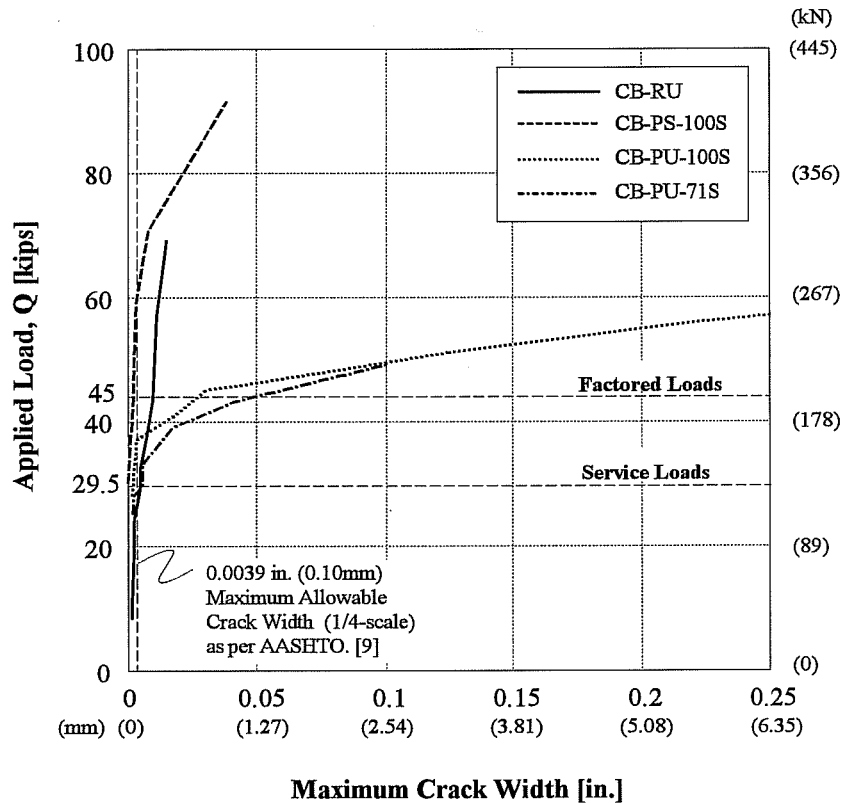
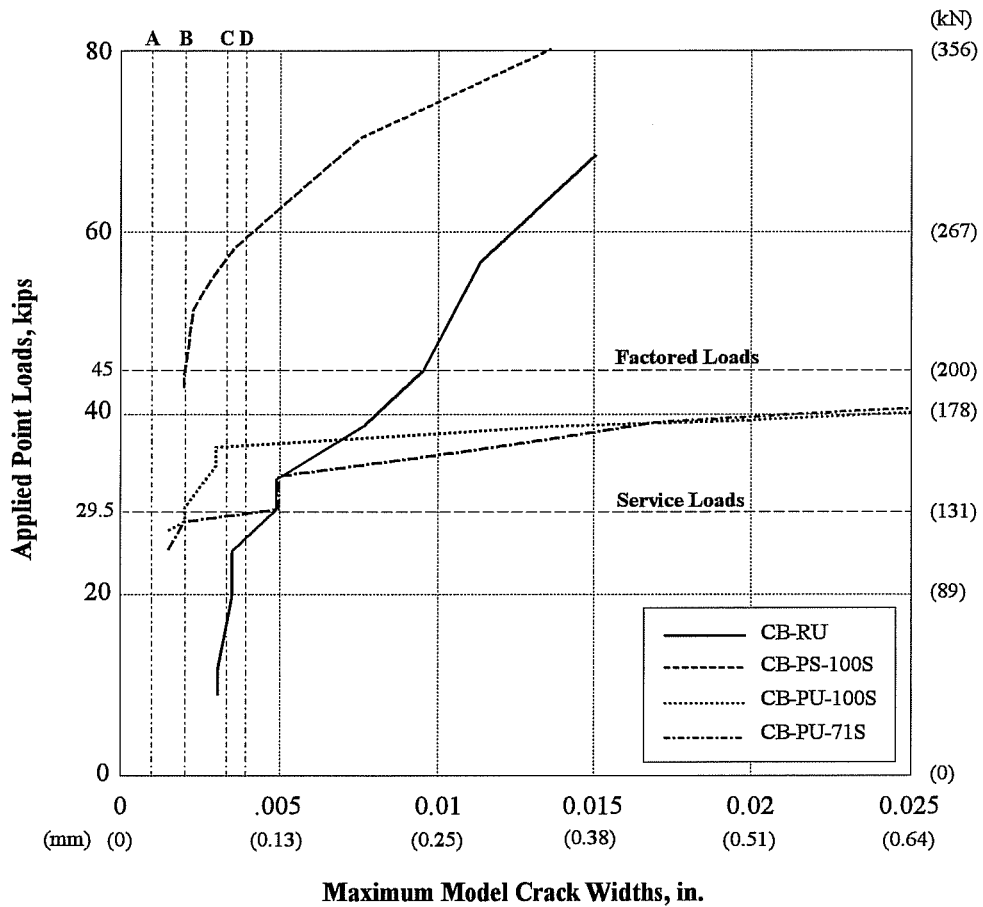


Figure 5.1 Maximum Crack Width Envelopes - All Models



Allowable Crack Widths from Various Specifications and Codes

SPECIFICATION or CODE	Max. Crack Width, Prototype in. (mm)	Max. Crack Width, Model in. (mm)
A - CEB-FIP-78	0.004 (0.1)	0.001 (0.025)
B - CEB-FIP-90	0.008 (0.2)	0.002 (0.051)
C - ACI-89	0.013 (0.34)	0.0033 (0.084)
D - AASHTO-92	0.0155 (0.39)	0.0039 (0.098)

Note: Maximum Crack Width values correspond to conditions for the prototypes modelled - usual (not severe environment) exterior exposure.

Figure 5.2 Maximum Crack Width Envelopes for All Models

Summary

Model CB-RU was designed according to current practice and would be widely accepted as an adequate means of design. In the case of this model, the first measurement of crack widths at service loads was within the AASHTO limit (0.003 in., 0.076mm). The model had been loaded up to service loads and not beyond for the fifth time when this maximum measurement was made. As service loads had not yet been exceeded, the plotted result is still considered a service load crack width. Since this method of design for conventionally reinforced members is widely accepted, since a large scatter in crack widths is acknowledged, and since the use of the maximum crack width envelope is a very strict analysis of data, it may be assumed that the larger crack width for this model represents an acceptable practice. If CB-RU is acceptable, therefore the behavior of model CB-PU-71S may also be termed as acceptable according to current American practice. More experimental evidence should be performed to determine the adequacy of this statement. Neither of these models satisfied CEB-FIP model Code 78 or 90.

Models CB-PS-100S and CB-PU-100S satisfied American maximum service load crack widths criteria as well as the CEB-FIP Model Code 90 criterion. These models did not however, satisfy the CEB-FIP Model Code 78 criterion. This particular criterion appears to be extremely conservative for normal exposure conditions.

In all cases, maximum crack widths at service loads are shown. There is naturally a large scatter in crack widths depending on the depth at which the crack is measured and when the crack began to form. In the case of all of the models studied here, maximum crack widths for single cracks were within 0.002 in. (0.051mm) when measured on both the east and west faces. Rather than averaging these values, maximum values have been reported for the crack width envelopes for conservative comparisons.

5.4 Measured vs. Predicted Crack Widths

Table 5.2 shows measured crack widths at service loads in comparison with crack widths as predicted by equations based on research conducted by Gergely and Lutz.[34] First cracking at the center and mid-spans for the conventionally reinforced concrete model, CB-RU are given as well as first cracking at the first crack location for the prestressed models (center support in all cases). All measured crack widths are taken as the average width of the major crack at service loads.

Three equations are used for these predictions. The first is a simplified version of the original Gergely and Lutz equations adopted by both ACI-318-89 and the 1992 AASHTO Specifications. This equation is the basis of the design criterion for crack width control in both of these standards:

$$w = 0.076 \beta f_s (d_c A)^{1/3} \quad (5.2)$$

- where: w: Crack width in units of 0.001 in..
- β : Ratio of distances to the neutral axis from the extreme tension fiber and from the centroid of the main reinforcement, approximate value of 1.2 for beams is used.
- f_s : Calculated stress in reinforcement at service loads, ksi.
- d_c : Thickness of concrete cover measured from extreme tension fiber to center of bar or wire located closest thereto, in.
- A: Effective tension area of concrete surrounding the flexural tension reinforcement and having the same centroid as that reinforcement, divided by the number of bars or wires, m, in.²

The original two equations of Gergely and Lutz are:

$$w = 0.076 \frac{h_2}{h_1} f_s (d_c A)^{1/3} \quad (5.3)$$

$$w = 0.091 \frac{h_2}{h_1} (f_s - 5) (d_c A)^{1/3} \quad (5.4)$$

- where: h_1 : d-kd, in.
- h_2 : h-kd, in.
- h: overall depth of the beam, in.
- d: Effective depth of the beam, distance from extreme compression fiber to the centroid of the tensile reinforcement, in.
- k: Distance from the neutral axis to the extreme compression fiber divided by the effective depth of beam.

All of these equations were developed only for conventionally reinforced members. For this reason, several modifications were necessary to apply these equations to members with prestressed reinforcement as suggested by Wood [66] and Salas [54]. In determining the effective tension area the number of bars, m, was determined in three ways. The first, m_1 , was simply the number of all longitudinal bars and strands in the effective tension area. This includes all mild steel, post-tensioning ducts and side face crack control steel in this region. The second determination of the number of bars, m_2 , was the total area of all longitudinal steel in the effective tension area divided by the size of the largest non-prestressed reinforcing

bar or wire. The third number of bars used, m_3 , was determined by adding the area of all longitudinal steel in the effective tension area divided by the size of the largest prestressing strand or non-prestressed reinforcing bar or wire. Another adaptation for prestressed members included taking f_s as the steel stress in the non-prestressed reinforcement under service loads. The results of these comparisons are shown in Table 5.2.

For the conventionally reinforced model, CB-RU, for which the Gergely-Lutz equations would be most applicable, the measured cracks were generally smaller than the predicted crack widths. Considering the ± 0.0005 in. (± 0.013 mm) error in measurements, these measured results are quite close to the predicted values.

In the case of the prestressed models designed based on ultimate loads (according to the integrated design approach) the predictions do not seem to accurately represent the measured crack widths for CB-PU-100S but are more accurate for CB-PU-71S. Equation 5.4 is the most accurate for CB-PU-100S. Equations 5.2 and 5.3 are more accurate for model CB-PS-71S.

However, as seen by the post-mortem investigation of CB-PU-100S (see Section 4.3.1.6) as well as the first cracking behavior of this model (Section 5.2), the effective prestress of this model seems to have been lower than intended in design. Cracks would therefore be wider than expected, at service loads, thus increasing the differences with the predicted crack widths.

These crack width prediction equations use theoretical values for the steel stress at service loads, as predicted by a strain compatibility analysis. Service load stresses on some of the non-prestressed steel were experimentally measured as well. To compare the prediction equations using theoretical and experimental service load stresses, Table 5.3 repeats the comparisons of Table 5.2 using experimentally measured service load stresses.

Summary

In general, Equations 5.2 and 5.3 give the most accurate results for this series. Looking at model CB-PU-71S, predictions were examined based on which assumption of the number of bars, m , was used. Predictions using both m_1 and m_2 were close to each other and closest to the measured values. Even in model CB-PU-100S, the predicted widths were consistent with each other (despite not matching the measured values). Either method could be recommended as a result of these tests. Using m_1 is perhaps easier. Equation 5-4 was particularly inaccurate for model CB-PU-100S using m_1 and m_2 . This is a result of the theoretical service load stress being close to 5ksi (34MPa). When this is the case, the difference in predictions between Equations 5-2 or 5-3 and Equation 5-4 can be quite large. In the case of model CB-

MODEL	MEASURED CRACK WIDTHS AT SERVICE. in. (mm)	PREDICTED CRACK WIDTHS, in. (mm) GERGELY-LUTZ ACI-318 Simplification* Equation 5-2			PREDICTED CRACK WIDTHS, in. (mm) GERGELY-LUTZ* Equation 5-3			PREDICTED CRACK WIDTHS, in. (mm) GERGELY-LUTZ* Equation 5-4		
		using m_1^{**}	using m_2	using m_3	using m_1	using m_2	using m_3	using m_1	using m_2	using m_3
CB-RU-initial Mid-Span, South	.0025 (.064)	.0027 (.069) [0.92]***	-	-	.0024 (.061) [1.04]	-	-	.0024 (.061) [1.04]	-	-
CB-RU-initial Center Support	.0035 (.089)	.0042 (.106) [0.84]	-	-	.0037 (.093) [0.96]	-	-	.0038 (.098) [0.91]	-	-
CB-RU-final Mid-Span, North	.00175 (.044)	.0027 (.069) [0.64]	-	-	.0024 (.061) [0.73]	-	-	.0024 (.061) [0.73]	-	-
CB-PU-100S Center Support	.002 (.051)	.0009 (.023) [2.23]	.0009 (.022) [2.29]	.0013 (.033) [1.56]	.0008 (.020) [2.55]	.0008 (.019) [2.62]	.0011 (.029) [1.78]	.0003 (.007) [7.72]	.0003 (.006) [7.94]	.0015 (.038) [1.33]
CB-PU-71S Center Support	.004 (.102)	.0039 (.100) [1.02]	.0043 (.108) [0.94]	.0051 (.131) [0.78]	.0034 (.087) [1.16]	.0037 (.095) [1.07]	.0045 (.115) [0.89]	.0035 (.088) [1.15]	.0038 (.096) [1.06]	.0186 (.471) [0.22]

* Gergely-Lutz equations were developed only for non-prestressed members. They have been modified in this study to see if they apply to prestressed members.
 ** Refer to Section 5.4 for calculations of m , the number of tensile elements used in crack width control equations.
 *** Ratio of measured crack width to predicted crack width.

Table 5.2 Comparison of Measured Crack Widths and Predicted Crack Widths under Service Loads

MODEL	MEASURED CRACK WIDTHS AT SERVICE. in. (mm)	PREDICTED CRACK WIDTHS, in. (mm) GERGELY-LUTZ* ACI-318 Simplification, using gaged steel stress Equation 5-2			PREDICTED CRACK WIDTHS, in. (mm) GERGELY-LUTZ* using gaged steel stress Equation 5-3			PREDICTED CRACK WIDTHS, in. (mm) GERGELY-LUTZ* using gaged steel stress Equation 5-4		
		using m ₁ **	using m ₂	using m ₃	using m ₁	using m ₂	using m ₃	using m ₁	using m ₂	using m ₃
CB-RU-initial Mid-Span, South	.0025 (.064)	.0021 (.053) [1.19]***	-	-	.0018 (.047) [1.35]	-	-	.0017 (.044) [1.43]	-	-
CB-RU-initial Center Support	.0035 (.089)	.002 (.052) [1.72]	-	-	.0018 (.045) [1.96]	-	-	.0016 (.041) [2.19]	-	-
CB-RU-final Mid-Span, North	.00175 (.044)	.0014 (.036) [1.23]	-	-	.0013 (.032) [1.40]	-	-	.001 (.026) [1.7]	-	-
CB-PU-100S Center Support	.002 (.051)	.0008 (.020) [2.52]	.0008 (.020) [2.59]	.0011 (.029) [1.76]	.0007 (.018) [2.88]	.0007 (.017) [2.96]	.0002 (.004) [13.33]	.0001 (.004) [13.70]	.0009 (.022) [2.29]	
CB-PU-71S Center Support	.004 (.102)	.0017 (.042) [2.40]	.0018 (.046) [2.21]	.0022 (.055) [1.83]	.0015 (.037) [2.74]	.0016 (.040) [2.53]	.0011 (.028) [3.61]	.0012 (.031) [3.32]	.0059 (.150) [0.68]	

* Gergely-Lutz equations were developed only for non-prestressed members. They have been modified in this study to see if they apply to prestressed members.

** Refer to Section 5.4 for calculations of m, the number of tensile elements used in crack width control equations.

*** Ratio of measured crack width to predicted crack width.

Table 5.3 Comparison of Measured Crack Widths and Predicted Crack Widths using Measured Steel Stresses under Service Loads

PU-100S, using Equation 5-4 results in a predicted crack width of roughly one third that of Equation 5-3. As prestressed members may often have service load stresses near 5ksi (34MPa), this equation is not recommended for predicting crack widths of prestressed models.

In the tests performed in this series, only mono-strands were used. A more complete 1/4-scale model could have included use of smaller multi-strand wires to model the prototype's multi-strand tendons. It is unclear if these crack width predictions would be applicable to prototypes with larger ducts and tendons made up of many strands. Full-scale tests would be best to investigate the credibility of such prediction equations.

In comparing the predictions using theoretical and experimental service load steel stresses, it was found that the experimental stresses led to predictions slightly larger than the theoretical stresses for model CB-RU-initial at the south span and model CB-PU-100S. However, predictions for the rest of model CB-RU-initial, model CB-RU-final and model CB-PU-71S using experimental steel stresses were roughly twice the predictions using theoretical steel stresses.

5.5 Crack Distribution Characteristics

A comparison of crack distributions at the service limit state for the four models is shown in Figure 5.3. Adequate crack distribution at service loads was found with all of the models. Beyond service loads, the conventionally reinforced concrete model, CB-RU had the most favorable crack distribution. The prestressed models, particularly those following the proposed integrated design approach, CB-PU-100S and CB-PU-71S, had less favorable crack distributions beyond service loads. However crack distributions beyond service loads are irrelevant. Beyond service loads, only the ultimate load carrying capacity is important.

There are currently no provisions in American standards for minimum steel required to provide adequate crack distribution for prestressed members. The only minimum steel requirements are called for to prevent sudden failure at first cracking. (There are also minimum steel requirements for shrinkage and temperature effects.) Table 5.4 shows these requirements to prevent sudden failure as specified by both AASHTO 1992 [9] and ACI-318-89 [15] as well as the newly proposed ACI-318-95 minimum steel requirements. Table 5.4 also shows what the requirements would be for the prestressed models using the current crack distribution criterion for conventionally reinforced sections in accordance to AASHTO 1992 and ACI-318-89.

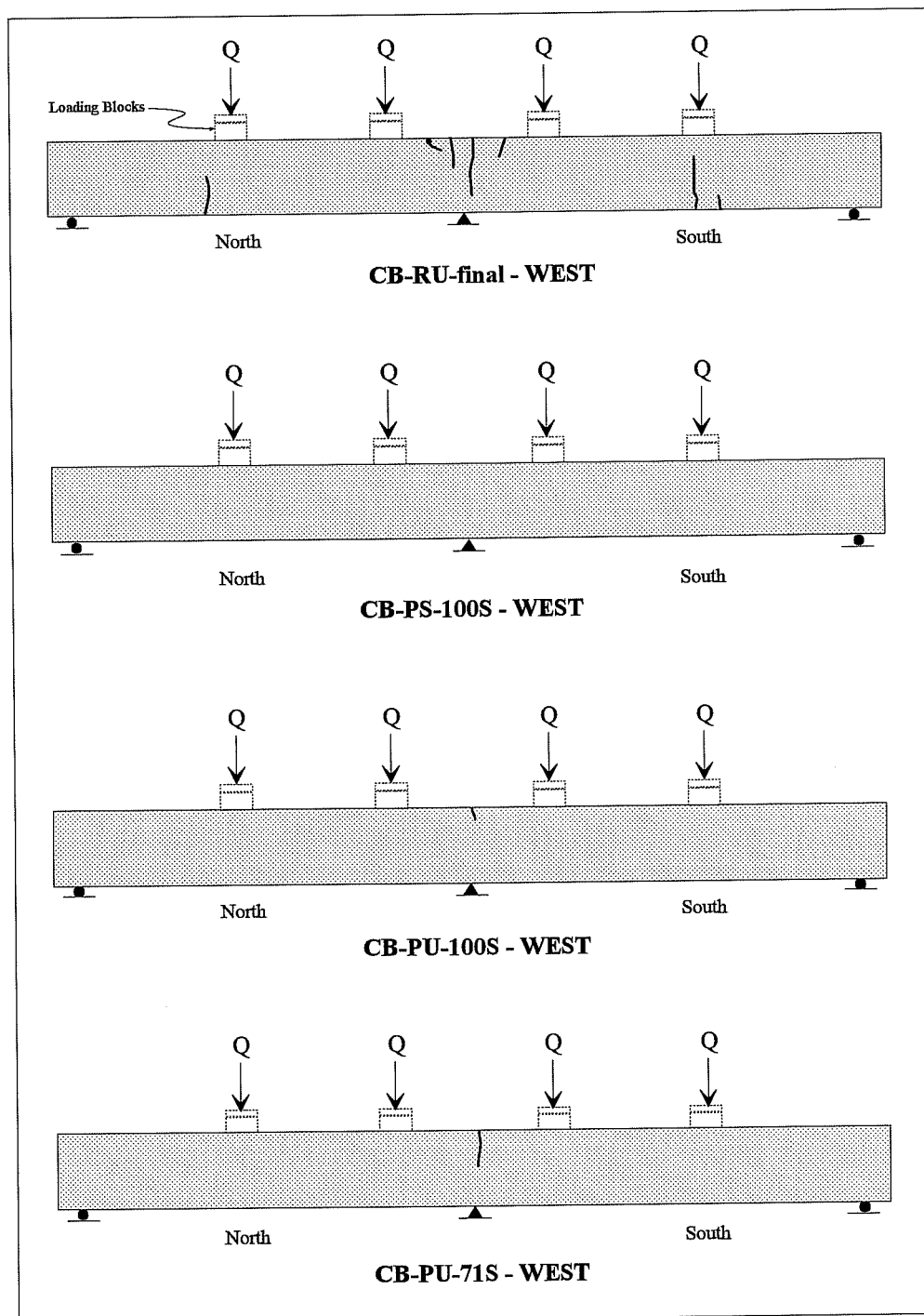


Figure 5.3 Comparison of Crack Distribution of all Models at the Service Limit State

The requirement by AASHTO 1992 and ACI-318-89 is that:

$$\Phi M_n \geq 1.2 M_{cr} \quad (5.5)$$

where: ΦM_n : Nominal resistance (moment) provided by the section.
 M_{cr} : Cracking moment.

The proposed requirement by ACI-318-95 applicable to the models tested here is:

$$A_{s,\min} = \frac{3\sqrt{f'_c}}{f_y} b_w d \geq \frac{200 b_w d}{f_y} \quad (5.6)$$

where: $A_{s,\min}$: Minimum area of prestressed and non-prestressed steel required at a section.
 f'_c : Concrete compressive strength.
 f_y : Yield strength of non-prestressed reinforcement.
 b_w : Web width.
 d : Effective depth of non-prestressed reinforcement.

The crack distribution requirement equation for conventionally reinforced members is:

$$z = f_s \sqrt[3]{d_c A} \quad (5-7)$$

where: z : 170 kips/in. (kN/mm)
 f_s : Steel stress at service loads, ksi (Mpa).
 d_c : Depth of concrete cover from outer fiber to centroid of first layer of steel, in. (mm).
 A : Effective tension area, refer to Equation 5.2, in² (mm²), use m_1 .

As can be seen in Table 5.4, all of the prestressed models were designed adequately for the 1992 AASHTO and ACI-318-89 criterion as well as the newly proposed provision for ACI-318-95. They also clearly satisfy the crack distribution steel requirements (Equation 5-7) typically used by current standards for conventionally reinforced concrete members.

Both ACI-318-89 Code and the 1992 AASHTO Bridge Design Specifications follow the prestressed design philosophy of limiting concrete tensile stresses at service loads. It is not intended that such designs would experience large amounts of cracking in their service life and therefore no provisions are made to require minimum amounts of steel specifically for adequate crack distribution.

While the American design philosophy for prestressed concrete does not always recognize the presence of cracking at service loads, many European practices do. European standards therefore have

MODEL	AASHTO 1992 & ACI-318-89 Equation 5-5		Proposed ACI-318-95 Equation 5-6			AASHTO 1992 & ACI-318-89 Equation 5-7			
	Provided: M_u k-ft. (kN-m)	Required: $1.2 \cdot M_u$ k-ft. (kN-m)	M_{prov}/M_{req}	Provided: $A_s, prov$ in ² (mm ²)	Required: A_s, min in ² (mm ²)	$A_s, prov/A_s, min$	z kips/in. (kN/mm)	$z < 42.57^*$ ($z \leq 7.45?$)	
CB-RU	Center Support	141 (191)	46 (62)	3.07	1.54 (734)	1.14 (994)	1.35	41 (7.18)	O.K.
	Mid-Spans	124 (168)	46 (62)	2.7	1.18 (628)	0.97 (761)	1.21	42.5 (7.45)	O.K.
CB-FS-100S	Center Support	236 (320)	142 (193)	1.66	2.43 (1568)	0.99 (639)	2.44	8.1 (1.42)	O.K.
	Mid-Spans	180 (240)	115 (156)	1.56	2.43 (1568)	0.78 (503)	3.13	5.4 (0.95)	O.K.
CB-PU-100S	Center Support	174 (236)	91 (123)	1.91	1.71 (1103)	1.01 (652)	1.69	9.8 (1.72)	O.K.
	Mid-Spans	99 (134)	91 (123)	1.09	1.52 (981)	0.67 (432)	2.28	1.6 (0.28)	O.K.
CB-PU-71S	Center Support	132 (179)	69 (94)	1.9	1.27 (819)	1.01 (652)	1.25	43 (7.53)	~ O.K.
	Mid-Spans	82 (111)	81 (110)	1.01	1.15 (742)	0.72 (465)	1.61	2.1 (0.37)	O.K.

* The limit at 1/4-scale

Table 5.4 Minimum Reinforcement Requirements in American Specifications and Codes

specific provisions to ensure adequate crack distribution. Table 5.5 presents three different methods for such provisions. The first is according to the CEB-FIP Model 1990 Code [30] where:

$$A_{s, \min} = \frac{k_c k f_{ct, \max} A_{ct}}{\sigma_{s2}} \quad (5.8)$$

- where: k_c : Factor accounting for tensile stress distribution, use 0.35 for the models tested.
 k : Factor correcting the value $A_{s, \min}$ as found by technical theory, against the real A_{ct} -values taking into account non-linear stress distributions, use 0.6 for the models tested.
 $f_{ct, \max}$: Upper fractile of the concrete strength in tension at the moment when the first crack is expected to appear, from Table 2.1.2 in Reference 30.
 A_{ct} : Area of concrete tensile zone just before the formation of cracks.
 σ_{s2} : May be taken equal to f_y (yield strength of steel) if adequate anchorage is secured. A lower value may be needed to satisfy crack width limits (see Reference 30).

Two other approaches are outlined by Favre et al. in Reference 33. The first is the requirements of the Swiss standard, SIA 162. Here, the minimum amount of steel required, $A_{s, \min}$, is:

$$A_{s, \min} = \gamma \frac{\alpha \beta f_{ct} A_{ct}}{f_y} \quad (5-9)$$

- where: γ : Factor of 1.0 for normal requirements.
 Factor of 1.3 for increased requirements.
 α : Factor to account for the influence of bar spacing (Section 3.2.2.2, Reference 33).
 β : Factor of 0.5 for flexure.
 f_{ct} : Design value of concrete tensile strength.
 A_{ct} : Area of concrete tensile zone before first cracking.
 f_y : Yield strength of reinforcing steel.

Another approach developed and outlined by Favre et al. requires:

$$A_{s, \min} = 0.5 A_{ct} \frac{f_{ct, ef}}{f_y} ; \quad \text{where: } f_{ct, ef} = \eta_t \eta_h f_{ctm} \quad (5.10)$$

- where: A_{ct} : Area of concrete tensile zone before the formation of cracks.
 η_t : Factor to account for lower modulus of rupture for concrete not yet at its 28-day strength.
 η_h : Factor according to the thickness of the member to account for micro-cracking and the beginning of cracks formed by the self-equilibrating stresses due to restraint, such as temperature and shrinkage.
 f_{ctm} : The average 28-day tensile strength of the concrete.
 f_y : Yield strength of the non-prestressed steel.

MODEL	CEB-FIP MODEL CODE 90 Equation 5-8			SLA 162 Equation 5-9			FAVRE, et. al. Equation 5-10			
	Provided: $A_{sp,prov}$ in ² (mm ²)	Required: $A_{sp,min}$ in ² (mm ²)	$A_{sp}/A_{sp,m}$	Provided: $A_{sp,prov}$ in ² (mm ²)	Required: $A_{sp,min}$ in ² (mm ²)	$A_{sp}/A_{sp,m}$	Provided: $A_{sp,prov}$ in ² (mm ²)	Required: $A_{sp,min}$ in ² (mm ²)	$A_{sp}/A_{sp,m}$	
CB-PS-100S	Cen. Support	.25 (158)	.34 (222)	.74	.25 (158)	.39 (253)	.63	.25 (158)	.38 (245)	.65
	Mid-Spans	.25 (158)	.34 (222)	.74	.25 (158)	.39 (253)	.63	.25 (158)	.38 (245)	.65
CB-PU-100S	Cen. Support	.32 (205)	.35 (229)	.91	.32 (205)	.39 (253)	.81	.32 (205)	.38 (248)	.83
	Mid-Spans	.13 (86)	.35 (229)	.37	.13 (86)	.39 (253)	.34	.13 (86)	.41 (262)	.33
CB-PU-71S	Cen. Support	.37 (240)	.35 (229)	1.06	.37 (240)	.39 (253)	.95	.37 (240)	.38 (248)	.97
	Mid-Spans	.25 (160)	.35 (229)	.71	.25 (160)	.39 (253)	.63	.25 (160)	.41 (262)	.61

Table 5.5 Comparison of European Practice of Minimum Reinforcing for Crack Control of Members with Prestressed Reinforcement

As shown in Table 5.5, the provisions for CEB-FIP Model Code 1990 are satisfied only at the mid-span of model CB-PU-71S which was designed to carry 71% of the ultimate loads with prestressing strand and 29% of the ultimate loads with non-prestressed reinforcement. Crack distribution behavior for this specimen was however, unfavorable in this region. One reason for the unfavorable crack distribution may have been the strength of the side face crack control steel used. This steel had a yield strength of 38 ksi rather than the 60 ksi that would be used in prototype designs. This was assumed to be all right for service load cracking as service load stresses did not exceed the yield strength. However, when cracks formed, much of the side face steel began to yield and was unable to control or aid in the distribution of cracks.

The early yielding of lower strength side face crack control steel for all of the models may have contributed to the poor crack control behavior observed, especially at the mid-span regions of models CB-PU-100S and CB-PU-71S. Here, poor crack distribution was observed at factored loads. At service loads however, the single cracks of small crack width were acceptable.

Summary

Due to the service load design philosophy currently used by American standards of practice, there are no provisions for providing steel for adequate crack distribution in members with prestressed steel. The only minimum reinforcement requirement for such members is based on providing enough steel so as to prevent sudden failure at first cracking. However, current American crack control steel requirements for non-prestressed members (Equation 5-7) seems to be adequate for both non-prestressed members as well as members with both prestressed and non-prestressed steel. This could be seen in the acceptable crack distribution in all of the models at service loads. The proposed integrated design method suggests using an elastic finite element analysis at service loads to dimension crack control steel. However, simply using the present reinforced concrete provision for adequate crack distribution would be simpler and would lead to acceptable (conservative) design. (This Equation, 5-7 is based on the crack width prediction Equation, 5-2.)

A specific crack distribution provision for prestressed members is required in many European standards of practice. Of the three European methods examined here, the Swiss SIA 162 specifications as well as those developed by Favre et al. are the most conservative and predicted poor crack distribution behavior for all of the prestressed models. The CEB-FIP Model Code 90 provisions were less conservative yet also predicted poor crack distribution behavior for all of the prestressed models. These predictions proved to be conservative for the actual behavior of the models designed with prestressing based on ultimate loads. Only model CB-PU-71S was close to being unacceptable according to the AASHTO and

ACI provisions for non-prestressed members. European predictions showed this model to be over 60% underreinforced for adequate crack distribution.

5.6 Moment Redistribution Behavior

All members exhibited moment redistribution behavior as can be seen in Figures 4.14, 4.25, 4.36, and 4.47 (see also Section 5.8). Plastic hinges began forming over the center support for all of the models and collapse mechanisms formed when hinging occurred at a mid-span of the post-tensioned models and at the flexure-shear crack location of the conventionally reinforced model.

As a result of this hinging behavior, all designs could be modified to account for moment redistribution, to produce more efficient members. The 1992 AASHTO Bridge Design Specification does not allow for negative moment redistribution. However the ACI-318-89 Building Code does. In accordance with the ACI-318-89 specifications, the required negative moment capacity for model CB-RU could be lowered by approximately 17%. The corresponding required negative moment capacity for model CB-PS-100S could be lowered by approximately 13% while that for models CB-PU-100S and CB-PU-71S could be lowered by approximately 18%. Therefore these last two models in particular, designed according to the proposed integrated design method, could have a further increase in efficiency and economic savings if designed considering negative moment redistribution. The recent adoption of R. Mast's proposal for unified design provisions (Reference 45) for ACI-318-95, also allows for negative moment redistribution, following a new approach. This new approach allows for easier application to both non-prestressed and prestressed members.

In all cases, moment redistribution requires ductile detailing. In turn, moment redistribution must be considered to provide adequate detailing for ductility.

5.7 Ultimate Behavior

A comparison of the experimental and predicted ultimate load capacities is given in Table 5.6. Here, a simple plastic event-to-event analysis was used to predict a lower-bound estimate of the ultimate load carrying capacity of each member. The widths of the loading blocks and plates above the pin and roller supports were considered in this analysis. In all cases, the models carried loads higher than these predicted capacities. Models CB-PU-100S and CB-PU-71S were however quite close to their estimated capacities. Models CB-RU and CB-PS-100S exceeded their estimated capacities by approximately 20%. The most

MODEL	Q_{ult} - TEST kips (kN)	Q_{ult} - PREDICTED* kips (kN)	$Q_{n, test}/Q_{n, pred}$	$Q_{n, test}/Q_{n, fac}^{**}$	$Q_{n, pred}/Q_{n, fac}$
CB-RU-final	84 (374)	72 (320)	1.17	1.87	1.60
CB-PS-100S	144 (641)	120 (534)	1.2	3.20	2.67
CB-PU-100S	71 (316)	70 (312)	1.01	1.58	1.56
CB-PU-71S	60 (267)	56 (249)	1.07	1.33	1.24

* Q_{ult} predictions were made using a simple plastic event-to-event analysis

** $Q_{n, fac}$ is the factored load used for design, 45k (200kN)

Table 5.6 Comparison of Ultimate Applied Load Predictions and Observed Behavior for All Models

plausible reason for this over-strength appears to be due to restraint forces caused by the arrangement of the test set-up for these first two tests.

In the first model tested, CB-RU, thin fiber-glass bearing pads were used between the ram piston and the loading blocks (refer to Figure 3.30). These were however crushed during testing and were essentially non-existent at ultimate loads. In the second model, no pads were used. The major problem with not using adequate bearing pads is that with increasing deflections, the loading blocks tilt with the deflection. Friction between the blocks and ram piston kept these two elements in contact and this may have caused the ram piston to rotate slightly. This would essentially "lock up" the free movement of the piston inside the ram's casing. The actual applied load may therefore not have been as high as the load recorded. Some of the recorded load may have been lost in friction inside the ram casing.

The two integrated design models, CB-PU-100S and CB-PU-71S were tested using steel reinforced elastomeric bearing pads between the ram piston and the loading blocks. Figure 5.4 shows the behavior of these pads at ultimate loads for model CB-PU-71S. The possibility of friction in the earlier tests appears reasonable as evidenced by the amount of shear deformation these pads experienced (approximately 0.5 in. (12.7mm)).

Summary

Models CB-PU-100S and CB-PU-71S reached ultimate loads very close to their predicted ultimate loads based on a simple plastic event-to-event analysis. Models CB-RU and CB-PS-100S however reached loads roughly 20% greater than their predicted values. This apparent over-strength may be attributed to the use of inadequate or no elastomeric bearing pads between the ram piston and the loading blocks on the beams.

5.8 Load-Deflection Behavior

Figure 5.5 shows the load-deflection behavior of all of the models. The load-deflection curves give a good comparison of the ultimate load carrying capacities of these models regardless of how moment was being redistributed. A comparison of the experimental and theoretical ultimate load capacities reached and ultimate factored loads which the models were required to carry is shown in Table 5.6.

As seen in both Figures 5.5 and 5.6, all models clearly satisfied the AASHTO and ACI service load deflection criteria of a maximum allowable deflection of $L/360$, where L is the span length in inches (mm).

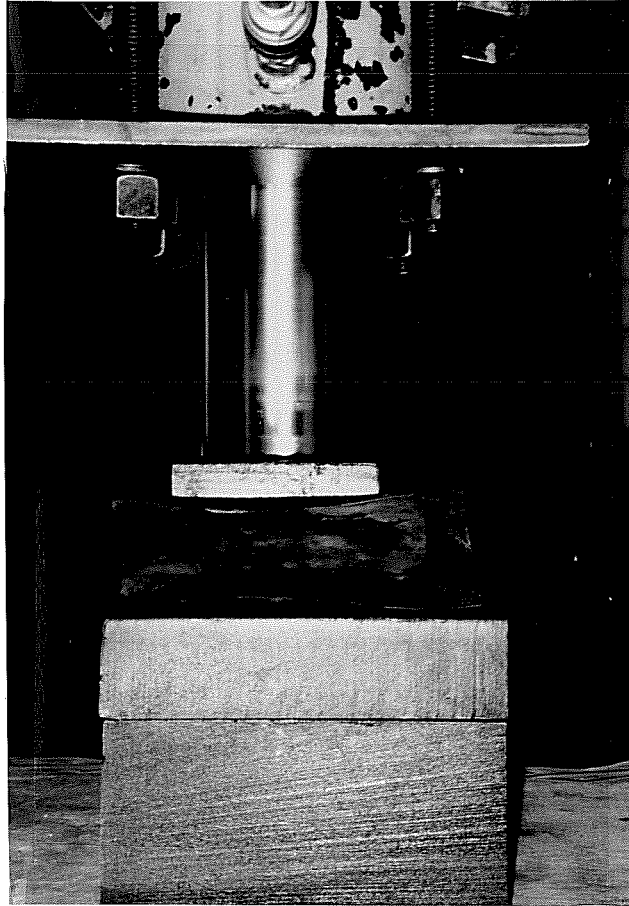


Figure 5.4 Shear Deformation in Elastomeric Bearing Pads

In terms of ultimate capacity, the AASHTO service load design model, CB-PS-100S had excessive strength, reaching an ultimate load of 3.2 times the factored load which it was required to carry (Figure 5.5 and Table 5.6). Part of this over-strength may be attributed to the lack of elastomeric bearing pads between the rams and the loading blocks. However, even the predicted ultimate load was 2.7 times greater than the required factored load (Table 5.6). The conventionally reinforced design according to AASHTO Specifications, CB-RU, exhibited considerable over-strength as well. The beam was carrying loads 1.9 times higher than factored loads and appeared to be continuing to carry load when the sudden failure from the formation of a flexure-shear crack occurred. Again considering the inadequate bearing pads used, the ultimate load may have been less. The predicted load however was still 1.6 times higher than the factored load.

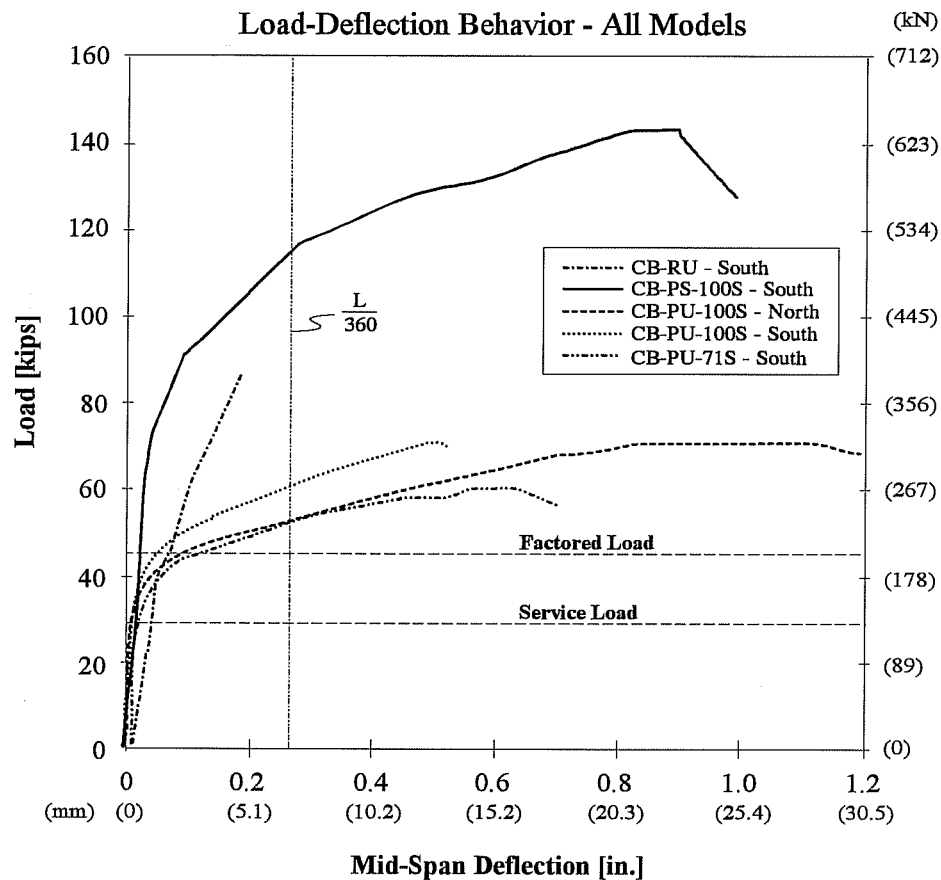


Figure 5.5 Load-Deflection Behavior of All Models

Excessive strength above factored loads for both of these members was to be expected due to service load crack control requirements. In the positive moment region of conventionally reinforced model CB-RU, additional steel was required to provide adequate crack control. In the fully prestressed model, CB-PS-100S, the required prestressing force and steel area were to limit concrete tensile stresses and effectively prevent cracking at service loads. This required a considerable amount more steel than necessary to carry factored loads. Both of these designs are very over-conservative. Fully prestressed model CB-PS-100S however, provides an extremely unnecessary amount of over-strength.

The two models designed according to the proposed integrated design method, CB-PU-100S and CB-PU-71S reached loads higher than factored loads as well. Their amount of over-strength, particularly for model CB-PU-71S, was not as excessive as with the previous fully prestressed model, CB-PS-100S. Model CB-PU-100S reached loads 1.6 times factored loads. Although this design was based on ultimate

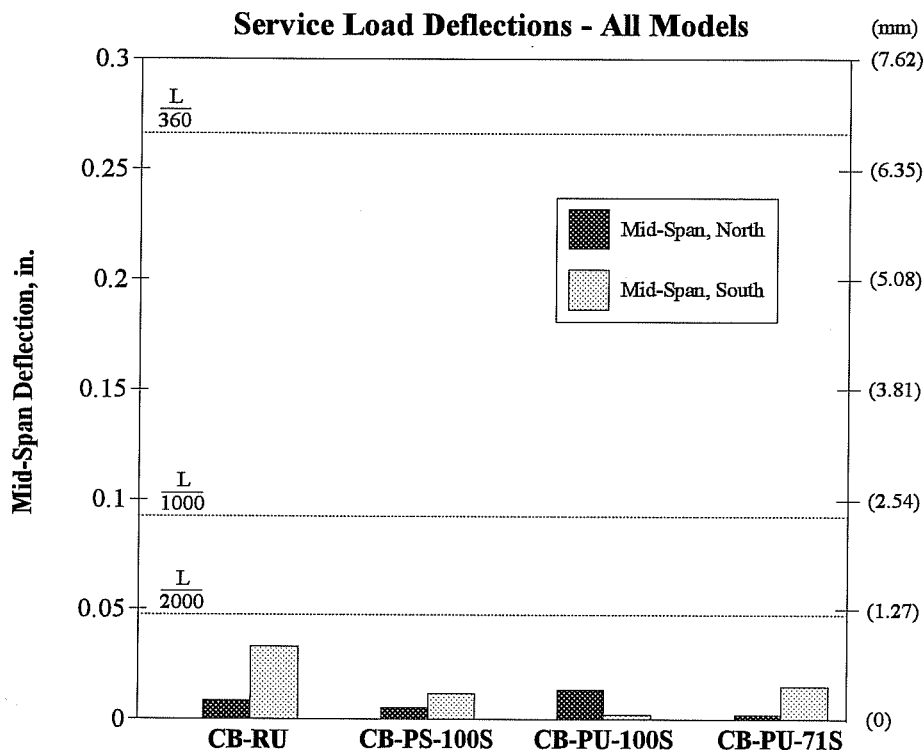


Figure 5.6 Mid-Span Deflection for all Models under Service Loads

loads with serviceability checks, this over-strength was expected. Non-prestressed steel was required in addition to the prestressed steel to provide adequate crack control in the negative moment region. Model CB-PU-71S reached ultimate loads that were 1.33 times greater than the factored loads for which this model was designed. This more accurate design for factored loads was the result of using non-prestressed steel in design for both carrying factored loads and providing crack control.

Summary

All models satisfied the current American maximum service load deflection criterion.

Due to excessive crack control criteria inherent in current American standards of prestressed concrete design, model CB-PS-100S reached loads in considerable excess of those required by the ultimate limit state. The amount of excess may be considered a wasteful use of materials. Conventionally reinforced model CB-RU was similarly very conservative in carrying loads in excess of those required. The prestressed models designed based on ultimate loads were conservative but more realistic. Model CB-PU-100S carried substantial excess load and it was quite ductile. Model CB-PU-71S carried loads that were

closest in magnitude to the required loads for which it was designed. This model was therefore the most efficient in terms of its use of materials.

As mentioned in Section 5.6, accounting for negative moment redistribution in such members is not specified in AASHTO 1992. None of these models therefore had negative moment redistribution considered in their designs. As can be seen in the overstrength of all of the models, accounting for negative moment redistribution would seem to lead to more efficient designs in terms of having ultimate capacities closer to the factored loads which they are designed to carry.

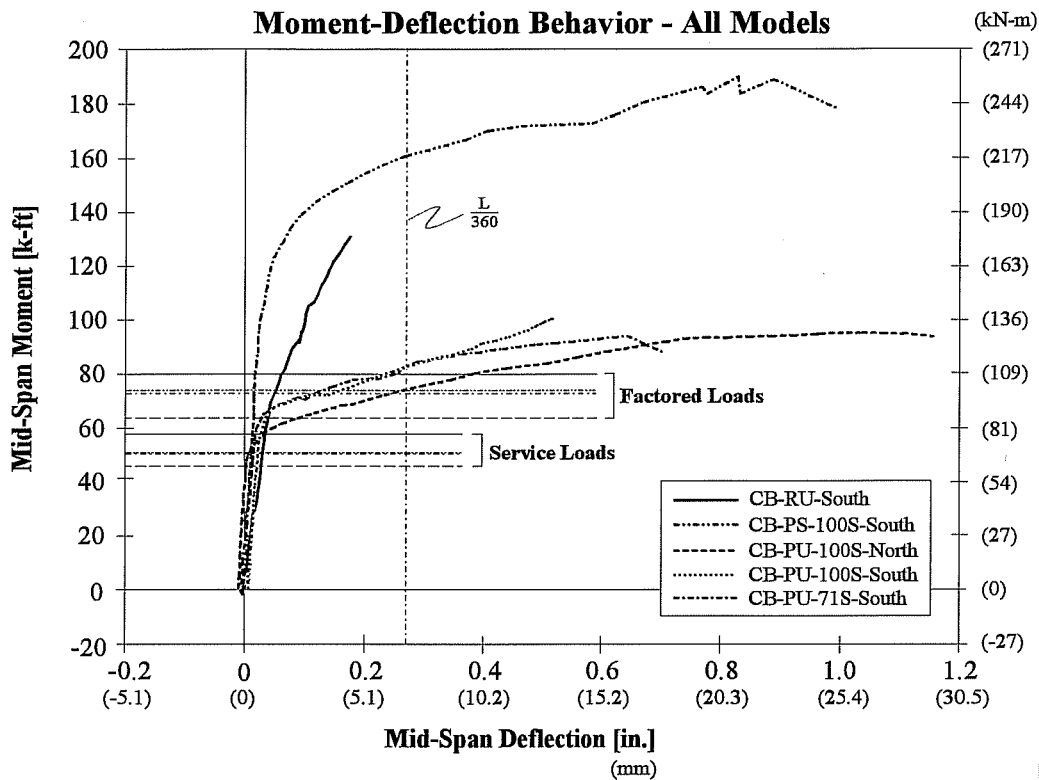
5.9 Moment-Deflection Behavior

The moment-deflection curves of Figure 5.7 show relative ductilities of each model. Results for one typical span for each beam are presented except for the case of model CB-PU-100S. For this model, results from both spans are given due to the marked difference between them (explained more fully in this section). In terms of moment capacity, the results here correspond well with the load-deflection response shown in Figure 5.5. Again it is clear that all models satisfied the 1992 AASHTO maximum service load deflection criterion of being less than $L/360$.

The mid-span section of fully prestressed model CB-PS-100S showed excessive over-strength. Conventionally reinforced model CB-RU showed similar over-strength and appeared to be continuing to resist more moment when sudden failure occurred. As expected from the design requirements for crack control, both of these beams behaved conservatively.

Models CB-PU-100S and CB-PU-71S behaved conservatively as well but with less wasteful over-strength. Both models began to show signs of yielding at the mid-spans between service and factored loads. In Figure 5.7, both mid-span sections for model CB-PU-100S are shown. Each span began to yield between service and factored loads. However the service load moment was approximately 10% lower for the north span due to moment redistribution and differing stiffnesses. This was the weak spot for this beam as failure in compression eventually occurred here. The weakness may be attributed to the smaller eccentricity built at this location than was accounted for in design (see post-mortem investigation, Section 4.3.1.6). The mid spans of model CB-PU-71S behaved similarly to the south span of model CB-PU-100S, yielding between service and factored loads and reaching ultimate slightly above factored loads.

Model CB-RU showed extremely non-ductile performance. This was the result of a design detail near the end supports. In accordance with AASHTO provision 8.24.1.4.1, flexural reinforcement may be cut off where the shear force does not exceed $2/3$ that permitted (the resistance provided). This was the case



at a distance 1 ft. (305mm) from the end supports. As well, provision 8.24.1.4.3 states that flexural reinforcement in a positive tension zone may be cut off if continuing bars provide "double the area required for flexure at the cutoff point and the shear does not exceed three-fourths that permitted." [9] This again was the case for a section 1 ft. (305mm) from the end supports and as a result all but 7 #2-bars were cut off at this point.

This model did carry loads well beyond factored loads. Therefore, this detail performed satisfactorily for actual design loads. However, in terms of overall member ductility this is not acceptable behavior. Beyond factored loads, when the cracking moment of this section was reached, a flexure-shear crack formed. This then developed almost immediately into a shear crack and failure occurred, resulting in very non-ductile behavior. Although factored load behavior was sufficient, such cutoff details in tension zones should be avoided to prevent "weak spots" and to achieve ductile behavior. Ductile behavior is necessary to allow for negative moment redistribution. As well, with the allowance of negative moment redistribution provisions, resulting changes in moments and shear forces need to be considered in satisfying specification detail requirements such as provisions 8.24.1.4.1 and 8.24.1.4.3 [9] described above.

Summary

Models CB-PS-100S and CB-RU had the most excessively over-strength sections. Models CB-PU-100S and CB-PU-71S exhibited more efficient sectional capacity, reaching their ultimate state at loads closer to the ultimate limit state loads for which they were designed.

Both fully prestressed models, CB-PS-100S based on service loads and CB-PU-100S based on ultimate loads showed the most ductile behavior. Model CB-RU was the least ductile although it was designed in accordance with current AASHTO specifications. More ductility would be desirable to be able to account for negative moment redistribution in design. Such redistribution would then need to be accounted for when designing details for ductility.

5.10 Fatigue Considerations

Conventionally reinforced model CB-RU satisfied the 1992 AASHTO Bridge Design Specifications by having predicted stress ranges (between full dead load and service live load plus impact) within the allowable limits. The AASHTO-based fully prestressed model, CB-PS-100S was designed for limited extreme fiber concrete tensile stresses (most likely not to crack at service loads) and as a result had very low predicted stress ranges at the critical sections. Allowable stress ranges for post-tensioned members should be less than 14.5 ksi (100MPa) in accordance with Wollmann.[65] Model CB-PU-100S satisfied Wollmann's recommendation by having a maximum predicted service load stress range over the center support of 7 ksi (48MPa). Model CB-PU-71S however did not satisfy Wollmann's recommendation as it had a maximum predicted stress range of 27 ksi (186MPa) over the center support. This model would need to be redesigned, perhaps using a higher prestressing force, closer to the 100% prestressed (based on ultimate load) model or using less prestressing and more non-prestressed steel to reduce the stress range.

5.11 Constructability of Models

The ease or difficulty in constructing each model was noted throughout the experimental program. Construction of all models involved building formwork, tying reinforcing cages and placing concrete. In addition to this, the post-tensioned models required the securing of post-tensioning ducts before concrete placement and performing post-tensioning operations before testing.

The formwork was generally the same for all models. A small additional block-out was required at the ends for the anchor zone of the post-tensioned models.

The conventionally reinforced model had the most difficult reinforcing cage to tie. The reinforcement was very closely spaced particularly in the negative moment region where larger bars and more closely spaced shear stirrups were required. This congestion as well as that in the positive moment regions near the mid-spans made adequate consolidation of the concrete difficult.

The AASHTO-based fully prestressed model's non-prestressed cage was much simpler to construct, as it was considerably less congested and therefore lighter. Securing the draped post-tensioning ducts required careful attention. However, this was not difficult due to the openness of the cage. Anchor zone reinforcement was somewhat congested but not to the extent that consolidation of the concrete was difficult. Of most significance in terms of constructability, was the attention required of this model during post-tensioning operations. Due to the high post-tensioning force required by this service load based design, staged loading was necessary so as not to crack the beam before service loads were applied. In the field this would require two stages of post-tensioning operations; one before placement of the superstructure and one afterwards, before traffic loads are present.

The prestressed models based on ultimate loads, CB-PU-100S and CB-PU-71S were the simplest to construct. Model CB-PU-100S had an uncongested very light cage, similar to the fully prestressed AASHTO model. CB-PU-100S had one less duct which made securing of the ducts and placement of the concrete simpler than was the case for the AASHTO service load design. This model required less anchor zone reinforcement as well. In terms of post-tensioning operations, staged loading was not required. All post-tensioning was carried out in one operation. Having fewer tendons also meant that the post tensioning operations took less time.

Model CB-PU-71S was similarly constructed. Here, due to discreet strand sizes three tendons were used for the model. However in a prototype it would be possible to use only two tendons, greatly easing the congestion of the cage. Required tensile crack control steel did not cause congestion or difficulty of tying reinforcement or placement of concrete. Due to the smaller post-tensioning force, even less anchor zone steel was required of this model than was required for the previous two post-tensioned models. Staged loading was not required for this model. As mentioned previously, a prototype design may only require two tendons. In this case, post-tensioning operations as well as general construction would have been the fastest of all of the post-tensioned models.

Summary

In general the two models designed according to the proposed integrated design method, CB-PU-100S and CB-PU-71S, were the easiest to construct. The conventionally reinforced model, CB-RU required no

post-tensioning operations. The excessive steel congestion of this model however, led to difficulty in adequately consolidating the concrete. This is an important consideration particularly where durability of the concrete is of concern. The AASHTO service load based fully prestressed model, CB-PS-100S had an extremely light cage. However, this model was the most labor-intensive in terms of construction primarily due to the higher number of tendons required and the resulting need for staged post-tensioning. The two integrated design method models required fewer post-tensioned tendons and did not require staged post-tensioning. The cages were light and simple to construct and consolidating the concrete was not difficult.

5.12 Economic Considerations

A further consideration in comparing the four models designed and tested is the economics of such designs. Pricing estimates for the steel reinforcement including materials and labor were supplied by a local bridge contractor. For reasonable cost estimates, material prices were based on the assumption that 25 such prototypes would be built. The estimates did not include the cost of formwork, concrete and concrete placement as the contractor felt that despite the varying levels of difficulty in properly consolidating the concrete, such costs would be the same for each design.

The following prices were used for the cost of the material and labor involved with the steel reinforcement:

Mild Reinforcement:

Buy reinforcing	\$0.22/lb
Buy chairs, etc.	\$0.01/lb
Handle & haul	\$0.03/lb
Tie & erect	\$0.115 to \$0.138/lb

Prestressing Reinforcement:

Buy strand	\$0.35/linear ft* . x 1.15
Buy duct	\$1.00/linear ft x 1.15
Buy anchors	\$200 ea., 2 per tendon
Duct couplers	\$1.00 ea., 1 per every 20 ft
Grout	\$1.50/ft ³
Placing duct	0.15 hrs./linear ft @ \$13/hr.
Place tendon, stress, grout	0.5 hrs. ea. @ \$13/hr.
Anchor placement	3 hrs. ea., 2 per tendon @ \$13/hr.
Misc. labor	2 hrs. per tendon @ \$13/hr.
Patching, misc. steel around anchors	\$100 per tendon

Table 5.7 shows the steel quantities for a prototype of each model, broken down into non-prestressed steel and prestressed steel. Figure 5.8 then shows the steel material and labor costs for a prototype of each model.

The cost comparison in Figure 5.8 shows only the net cost difference of the steel. As the costs of concrete material and placement are not included, the percentage difference in construction cost between the designs would probably be lower.

REINFORCEMENT	CB-RU		CB-PS-100S		CB-PU-100S		CB-PU-71S	
	ft. (m)	lbs. (kg)	ft. (m)	lbs. (kg)	ft. (m)	lbs. (kg)	ft. (m)	lbs. (kg)
#11 Bars	680 (207)	3610 (1639)	-	-	-	-	-	-
#9 Bars	910 (277)	3097 (1403)	540 (165)	1838 (833)	270 (82)	919 (416)	270 (82)	919 (416)
#5 Bars	570 (174)	601 (270)	460 (140)	485 (218)	828 (252)	873 (392)	1265 (386)	1334 (598)
#3 Bars	240 (73)	90 (41)	240 (73)	90 (41)	240 (73)	90 (41)	240 (73)	90 (41)
TOTAL Non-Prestressing Reinforcement	2400 (730)	7397 (3355)	1240 (378)	2413 (1092)	1338 (407)	1882 (849)	1775 (541)	2343 (1055)
Φ -0.6" Strand	-	-	4200 (1280)	182 (84)	2480 (756)	106 (49)	1120 (341)	46 (21)
TOTAL Prestressing Reinforcement	-	-	4200 (1280)	182 (84)	2480 (756)	106 (49)	1120 (341)	46 (21)
TOTAL REINFORCEMENT	2400 (730)	7400 (3355)	5440 (1660)	2595 (1175)	3820 (1165)	1990 (900)	2895 (885)	2390 (1075)

Table 5.7 Reinforcement Lengths and Weights for Each Model

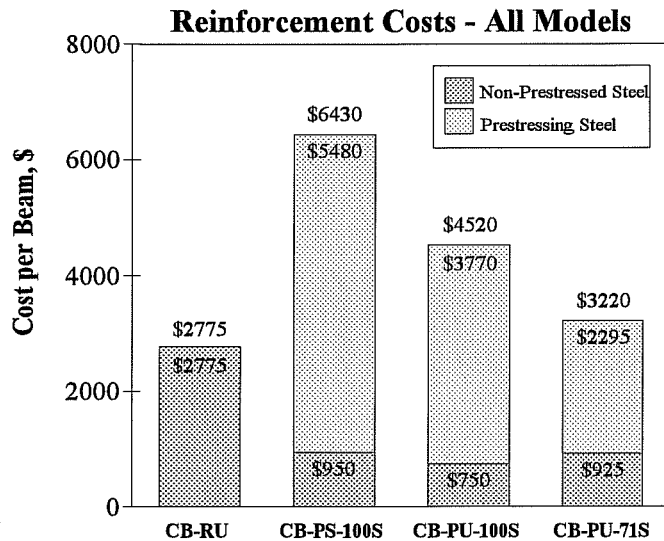


Figure 5.8 Cost of Reinforcing Steel for Prototypes of Each Model

Summary

The conventionally reinforced beam, model CB-RU would have the least expensive steel costs and is followed closely by model CB-PU-71S, the beam designed for 71% of ultimate loads carried by prestressed steel and 29% carried by non-prestressed steel. A prototype for model CB-PU-100S designed for 100% of ultimate loads to be carried by prestressed steel would be about 50% more expensive than a prototype of model CB-RU. The fully prestressed model based on service loads, CB-PS-100S would be by far the most expensive in terms of steel costs and would be approximately twice the cost of prototypes for both models CB-RU and CB-PU-71S.

5.13 Design Recommendations

Based on the results of these tests summarized in each of the previous sections, many recommendations can be made with regard to the design of two-span continuous large-scale stocky members:

Analysis/Design: Consider prestressed reinforcement as both a load and a resistance as discussed in Chapter 2. This will lead to a clearer understanding of secondary moments due to prestressing and general member behavior.

Consider negative moment redistribution in accordance to ACI-318-89, Sections 8.4.1 for members with 100% non-prestressed reinforcement based on ultimate loads and Section 18.10.4.1 for members with combinations of non-prestressed and prestressed or 100% prestressed reinforcement based on ultimate loads. Negative moment redistribution may also be considered with respect to the newly adopted unified design specifications for ACI-318-95 as outlined in Reference 45.

Flexure Design: Design members using between 70-100% prestressing based on ultimate loads.

Checking the service limit state to meet fatigue criteria or crack control, may control the percentage of prestressed reinforcement to be used. (The designer has considerable room to "play" with eccentricities of prestressed steel and percentages of non-prestressed steel to satisfy both the service and ultimate limit states.) Designs using lower percentages of prestressing reinforcement may be permissible but were not investigated in this study.

Shear Design: Design for shear based on ultimate loads in accordance with current standards for normal conditions. Where members are very sensitive to shear, refer to shear design procedures outlined by Armstrong.[17] (This recommendation is made as shear design did not control in this study but was very important in other studies under this same project. Refer to Chapter 1.)

Crack Width and Distribution Control: As an interim recommendation, use Equation 5-7 to check the "z" parameter against allowable limits (depending on exposure conditions) for members with prestressed and non-prestressed members. Additional work is needed to support this recommendation more fully. Provide side face crack control steel in accordance with Frantz and Breen.[25]

Anchor Zone Design: Provide anchor zone reinforcement in accordance with NCHRP Report 356.[24]

Fatigue Check: Determine the maximum stress range in the reinforcement between full dead load and service live load plus impact including all steel in the tension zone (flexural and crack control steel). For members with post-tensioned reinforcement, restrict the stress range to 14.5 ksi (100MPa) as recommended by Wollmann.[65] For members with only non-prestressed reinforcement, restrict stress ranges to limits specified in AASHTO 1992.

CHAPTER 6

SUMMARY & CONCLUSIONS

6.1 Summary

The 1992 AASHTO Bridge Design Specifications are presently compartmentalized in terms of reinforced concrete design and prestressed concrete design. Each type of design follows a different design philosophy. Reinforced concrete members are primarily designed based on the ultimate limit state with additional secondary serviceability checks. Prestressed concrete members are primarily designed based on the service limit state with additional secondary ultimate limit state checks which seldom govern. There is presently no provision for using anything but full prestressing based on the service limit state if any prestressing is used.

This problem of differing design philosophies is also found in the confusion between deep beam and corbel design. On the recent San Antonio Y project in Texas, designers faced difficulties when designing large-scale cantilever overhangs for the elevated highway substructure. Following the AASHTO Specifications it was unclear whether the members should be designed as deep beams or corbels, each following different design philosophies. As a result, members were designed for both. This led to inefficient uneconomical designs that were difficult to construct.

This confusion caused by current standards results from the lack of clear behavioral models to follow which would lead to a better understanding of overall structural action. Instead, the current design philosophies lead to confusion and preclude more advantageous types of engineering design.

This thesis focuses on developing a clearer design method for two-span continuous stocky beams such as those used as straddle bents for elevated highways in Texas. This integrated design method examines the behavior of such members using varying amounts of prestressed and non-prestressed reinforcement primarily designed based on ultimate loads. The goal is to develop an integrated design method that may be applied to structures using any amount of non-prestressed and/or prestressed reinforcement. Recent proposals to unify codes have involved unifying and revising terminology so that it may apply to members with nonprestressed and prestressed reinforcement. This however, is not the aim of this study. Rather, this study examines designing members with both prestressed and non-prestressed reinforcement in conjunction with a unified design philosophy. The philosophy is one that bases flexural and shear designs

on the ultimate limit state, carrying out adequate serviceability checks.

For this study, four 1/4-scale models of large-scale straddle bents were constructed and loaded to failure. The four models were:

CB-RU - A conventionally reinforced beam based on the 1992 AASHTO Bridge Design Specifications. Both flexure and shear design were based on the ultimate limit state. Crack distribution was satisfied by "z" requirements and side face crack control steel was provided in accordance with Frantz and Breen.[25]

CB-PS-100S - A fully prestressed model based on service load design in accordance with the 1992 AASHTO Bridge Design Specifications. Prestressing strand was provided to limit extreme fiber concrete tensile stresses at service loads, with a check for ultimate load carrying capacity which did not govern. Shear design was based on the ultimate limit state. Side face crack control steel was provided in accordance with Frantz and Breen.[25]

CB-PU-100S - Prestressed beam designed for 100% of the factored loads to be carried by the prestressing strand. Shear design was based on the ultimate limit state as well. Crack control was provided based on results of an elastic finite element analysis. Side face crack control steel was provided in accordance with Frantz and Breen.[25]

CB-PU-71S - Prestressed beam designed for 71% of the factored loads to be carried by prestressing strand and 29% of factored loads to be carried by non-prestressed reinforcement. Shear design was based on the ultimate limit state as well. Crack control was provided based on results of an elastic finite element analysis. Side face crack control steel was provided in accordance with Frantz and Breen.[25]

Behavior of these models during loading was recorded in terms of cracking behavior (including first cracking, maximum crack widths at service loads and overall crack distribution behavior), load-deflection and moment-deflection response, moment redistribution, and ultimate load carrying capacity. Predicted fatigue capacity as well as constructability and economic considerations were examined. Many conclusions resulted from this study.

6.2 Conclusions

Based on the results presented in Chapters 4 and 5, the following important conclusions are drawn from this study.

- 1) In spite of some crack width measurements indicating locally large crack values, overall it may be concluded that all designs resulted in generally acceptable cracking behavior at service loads in terms of allowable crack widths in accordance with AASHTO 1992 and ACI-318-89. Model CB-PS-100S did not crack at all at service loads and model CB-PU-100S was more conservative than the remaining models in terms of service load crack widths.
- 2) Current estimates of crack widths adopted in the form of a crack distribution equation in AASHTO and ACI predict crack widths well for the conventionally reinforced members (equivalent crack width equation is Equation 5-2, a form of the Gergely and Lutz equations discussed in Reference 34). No specific AASHTO or ACI predictive equations for crack widths of prestressed members exist. However, crack width estimates for prestressed models were best predicted by Equations 5-2 and 5-3 as discussed in Section 5.4 when modifications were made for prestressed steel as discussed in that section.
- 3) Current crack distribution equations in American standards for crack control of non-prestressed members were modified to apply to members with both non-prestressed and prestressed reinforcement. These modified expressions predicted the acceptable cracking behavior observed in the models containing both non-prestressed and prestressed steel. Use of these equations is simpler than using the originally proposed finite element analysis based method for crack control (Chapters 2 & 3). Many European requirements for adequate crack distribution appear to be quite over-conservative.
- 4) Model CB-PS-100S, designed based on limiting stresses at service loads, had an excessive over-strength to the point of being wasteful of the structural materials used. Models CB-RU had substantial over-strength that was however considerably less excessive than that of model CB-PS-100S. Model CB-PU-100S had substantial overstrength that was less than both model CB-PS-100S and model CB-RU. Model CB-PU-71S behaved most efficiently in terms of ultimate load carrying capacity as it had the least amount of over-strength while still satisfying the ultimate limit state.
- 5) All models satisfied service load deflection requirements according to AASHTO 1992 and ACI-318-89.

- 6) Model CB-PU-100S exhibited the most overall member ductility. All models with the exception of model CB-RU exhibited acceptable ductility.
- 7) Moment redistribution occurred in all models, and plastic hinges formed or were forming over the center supports in all models when failure occurred.
- 8) Moment redistribution should be considered when designing details for ductile members.
- 9) When designing members with post-tensioning based on ultimate loads, fatigue life of members should be examined in terms of allowable stress ranges between full dead load and service live load plus impact. Stress ranges should be compared with recommendations made by Wollmann.[65]
- 10) Anchor zone reinforcement designed as per NCHRP Report 356 [24] performs well.
- 11) Secondary moments as a result of uneven support settlements may be considerable for such stiff members as those studied in this thesis.
- 12) Conventionally reinforced model CB-RU and prestressed model CB-PU-71S were the simplest models to construct and prepare for loading. Although model CB-RU did not require any post-tensioning operations, model CB-PU-71S contained considerably less steel making fabrication simpler and concrete placement with adequate consolidation easier. Model CB-PS-100S was clearly the most difficult to construct and prepare for loading particularly due to the need for staged post-tensioning operations.
- 13) In terms of reinforcement material and labor costs, models CB-RU and CB-PU-71S were the least expensive. Model CB-PU-100S had reinforcement costs approximately 50% higher while the reinforcement cost for model CB-PS-100S was over twice that of models CB-RU and CB-PU-71S.
- 14) Consideration of prestressed reinforcement as both a load and a resistance can greatly simplify understanding of indeterminate beam behavior.

APPENDIX A

DESIGN EQUATIONS FOR MODELS CB-RU AND CB-PU-100S

Design Equations for Model CB-RU

All references to AASHTO correspond to the 1992 Standard Specifications for Highway Bridges. [9]

Flexure:

$$M_u = A_s f_y \left(d - \frac{a}{2} \right); \quad a = \frac{A_s f_y}{0.85 f'_c b} \quad (\text{A-1})$$

where: M_u :	factored moment at B:	124 k-ft	(168 kN-m)
A_s :	required area of reinforcing steel:	unknown	
f_y :	yield strength of reinforcing steel:	60 ksi	(414 MPa)
d:	effective depth of section:	17.25 in.	(438 mm)
f'_c :	concrete compressive strength:	5000 psi	(34.5 MPa)
b:	width of section:	18 in.	(457 mm)

$$\therefore A_s = 1.49 \text{ in}^2 \quad (961 \text{ mm}^2)$$

This could be satisfied with 14-#3 bars which provide an area of 1.54 in². (994 mm²).

For the positive moment region, M_u at D was 78 k-ft. (105.8 kN-m). This required an area of 0.74 in² (477 mm²), which could be satisfied with 16-#2 bars providing an area of 0.78 in². (506 mm²)

Each of these flexural requirements was then checked to see if crack control criteria were satisfied.

Check Crack Control Criterion:

In accordance with AASHTO provision 8.16.8.4, the following number of bars was required over the center support:

$$f_r = \frac{z}{\sqrt[3]{d_c A}} \leq 0.6 f_y; \quad A = \frac{2(h-d)b}{n} \quad (\text{A-2})$$

where:	f_r :	stress in reinforcement at service loads (use $0.6 f_y = 36 \text{ ksi}$, 248 MPa)
	z:	measure related to crack width control $\leq 42.5 \text{ k/in}$ (7.4 kN/mm)
	d_c :	thickness of concrete cover = 0.75 in. (19.1 mm) (to center of bottom bars)
	f_y :	yield strength of reinforcement = 60 ksi (414 MPa)
	A:	effective tension area, defined above

- h: height of effective tension area = 1.5 in. (38.1 mm)
 b: width of tension area = 18 in. (457 mm)
 n: number of bars = 14

$$A = 1.93 \text{ in.}^2 (1245 \text{ mm}^2) ;$$

$$\therefore z = 40.7 \text{ k/in. (7.1 kN/mm)} \leq 42.5 \text{ k/in. (7.4 kN/mm)} \quad O.K.$$

In terms of spacing of bars, the controlling limit was a minimum spacing of 1.5 times the maximum aggregate size (or bar size, which was the same in this case) as required by AASHTO section 8.21.1. With the 3/8" (9.52mm) aggregate and bar diameter, this meant a minimum spacing of 0.56 in. (14.29mm) which was satisfied by using 14 #3 bars (see Figure 3.7).

In checking the crack width control criteria (Eq. A-2) at the positive moment region, the following changes in variables were required:

- f_s : stress in reinforcement at service loads (use $0.6f_y = 36\text{ksi}$, 248MPa)
 f_y : yield strength of reinforcement = 60 ksi (414 MPa)
 A: effective tension area, defined in Equation A-1.
 n: number of bars = 16

$$A = 1.69 \text{ in.}^2 (1090 \text{ mm}^2) ;$$

$$\therefore z = 48.7 \text{ k/in. (8.5 kN/mm)} \leq 42.5 \text{ k/in. (7.4 kN/mm)} \quad \text{No Good.}$$

Therefore the number of bars needed to be increased to 24 bars giving an effective tension area of 1.12 in.² (723 mm²) and a "z" of 42.5 k/in. (7.4 kN/mm). This provided an ultimate resistance of 123 k-ft (167 kN-m) which is 57% higher than the factored moment that this section is required to carry.

Shear:

Shear design was based on full factored loads. Maximum factored shear was taken as the shear force at a distance "d" from the center support plus the applied concentrated load, 45k (200kN) between this point and the center support in accordance to AASHTO provision 8.16.6.1.2. The factored shear load used for design was 90k (449kN). The shear diagrams used for design are given in Figure 3.7. (90 kips was chosen

as that was the calculated shear at ultimate for the beam already designed for flexure.) The concrete shear strength in accordance to AASHTO provision 8.16.6.2.1 was:

$$V_c = 2\sqrt{f'_c} * b_w * d = 44 \text{ k} \quad (196 \text{ kN}) \quad (\text{A-3})$$

where: V_c : concrete shear strength
 f'_c : concrete compressive strength = 5000 psi, (34.5 MPa)
 b_w : width of section = 18 in., (457 mm)
 d : effective depth of section = 17.25 in., (438 mm)

The remaining amount of shear force was 46k (205kN). Using a design yield strength of 60 ksi (414 MPa) for the 5/32" (4mm) diameter wire, the required steel area as per AASHTO 8.16.6.3.2 was:

$$V_s = \frac{A_v f_y d}{s}; \quad \therefore s = 1.5 \text{ in.} \quad (38 \text{ mm}) \quad (\text{A-4})$$

where: V_s : shear force to be carried by stirrups
 A_v : total cross sectional area of stirrup = 0.077 in.², (49.7 mm²)
 f_y : yield strength of stirrups, assumed = 60 ksi, (414 MPa)
 d : effective depth = 17.25 in., (438mm)

With all designing complete, assuming the typical 2.25 in. (57mm) cover used by TxDOT for these members, the effective depth was actually 17.17 in. (436mm), making virtually no difference in overall design.

The remainder of the section required only minimum shear reinforcement as per AASHTO 8.19.1.2:

$$A_v = \frac{50 b_w s}{f_y} \text{ in}^2; \quad = \left(\frac{0.345 b_w s}{f_y} \text{ mm}^2 \right) \quad (\text{A-4})$$

where A_v : Area of shear reinforcement within a distance s , in² (mm²)
 b : Web width = 18 in., (457mm)
 s : spacing of shear reinforcement parallel to the longitudinal reinforcement
 f_y : specified yield strength of reinforcement = 60ksi, (414MPa)

Assuming the same size double stirrups, a spacing of 5 in. (127 mm) was required.

The actual yield strength of the stirrups was 71 ksi (490 MPa). Therefore the provisions here were conservative.

Side Face Crack Control:

Side face crack control steel was provided in accordance with recommendations by Breen and Frantz [25], similar to AASHTO provision 8.17.2.1.3 where:

$$\rho_{sk} = \frac{A_{sk}}{\frac{d}{2} b_{sk}} \geq 0.00024(d-30) \quad (A-5)$$

where ρ_{sk} : Ratio of skin reinforcement to skin area in tension zone.
 A_{sk} : Area of skin reinforcement, in² (mm²)
 d : Effective depth = 66 in., (1676mm)
 b_{sk} : "Skin" width, total width of cover on both sides = 5 in., (127mm).

Note that skin reinforcement was determined for the full-scale prototype and the required area was then scaled down for use in the model. The area required for the model was 0.045 in² for each side. The controlling minimum spacing was 1.5 in. (38mm). This was satisfied with 12-gauge wire.

As discussed in Chapter 3, for simplicity, 12-gauge (Φ -2.7mm) wire was placed along the entire depth of the section throughout the beam.

Development of Reinforcement:

In accordance with AASHTO provision 8.24.1.4.1, flexural reinforcement may be cut off where the shear force does not exceed 2/3 of the shear resistance provided. This was the case at a section 1 ft. (305mm) from the end supports where the ultimate shear force was 24k (107kN) and the shear capacity was 60k (267kN). As well, provision 8.24.1.4.3 allows for positive moment reinforcement to be cut off at a section where continuing bars provide double the area for flexure and the shear is less than 3/4 of the shear resistance provided. This was also the case at a distance of 12 in. (305mm) from the end supports where 7 continuing bars and the side face crack control steel provided a flexural capacity of ~40 k-ft. (54kN-m) and the ultimate moment at this section was ~20 k-ft. (27kN-m). Again, the shear capacity was 60k (267kN) and the ultimate shear was 24k (107kN).

Other development lengths were provided in accordance with AASHTO provisions 8.24 and 8.25.

Negative moment reinforcement that was cut off beyond the point of inflection had a development length of 18 in. (457mm) which was approximately the effective depth of the section. Positive moment reinforcement near the center support that was cut off had a development length of ~14in. (356mm).

Design Equations for Model CB-PU-100S

Flexure Design:

This required steel was determined using the traditional equation from AASHTO 9.17.2:

$$M_u = \Phi M_n = \Phi [A_s^* f_{su}^* d (1 - 0.6 \frac{\rho^* f_{su}^*}{f_c'})] \quad (\text{A-6})$$

where: M_u : Ultimate (factored load) moment.
 Φ : Resistance factor (1.0 for these designs)
 M_n : Nominal moment strength of a section
 A_s^* : Area of prestressing steel
 d : Distance from extreme compression fiber to centroid of prestressing force (this is also 9 in. (229mm) plus the strand eccentricity).
 ρ^* : Ratio of prestressing steel (A_s^*/bd ; b = width of flange or rectangular member)
 f_{su}^* : Average stress in prestressing steel at ultimate load (AASHTO provision 9.17.4)
 f_c' : Compressive strength of concrete at 28 days

This equation is an approximation of a more accurate analysis based on strain compatibility and equilibrium.

The optimum amount of prestressing steel and layout (eccentricities) required for this model was determined by iteration using a spreadsheet and was based on the following conditions:

M_u over center support:	124 k-ft.	(168 kN-m)
M_u at mid-span:	72 k-ft.	(98 kN-m)
f_c' :	6200 psi	(42.8 MPa)

Considering the maximum allowable eccentricity of 7.5 in. (191mm) at the most critical section - the negative moment region over the center support, the amount of steel required to carry factored loads was determined to be 0.366 in². Due to discrete strand sizes, 3- Φ 0.5in. strands were chosen, providing 0.391 in². With this amount of strand, the eccentricity at the mid-spans required to carry factored loads was 1.5 in. (38mm).

Crack Control:

Based on the service load concrete tensile stress results from the elastic finite element analysis (see Figure 3.11b), it was determined that additional crack control steel was required only over the center support where the maximum concrete tensile stress reached $5\sqrt{f'_c}$ psi ($0.035\sqrt{f'_c}$ MPa). The concrete was assumed to carry $2\sqrt{f'_c}$ psi ($0.014\sqrt{f'_c}$ MPa) and crack control steel was therefore required to carry $3\sqrt{f'_c}$ psi ($0.021\sqrt{f'_c}$ Mpa). The required amount of steel was then determined using Equation 2-1 presented in Chapter 2 of this thesis with the following values:

$$\begin{aligned} A_c: & 2" \times 18" = 36 \text{ in}^2, (51\text{mm} \times 457\text{mm} = 23,226 \text{ mm}^2) \\ f'_c: & 6200 \text{ psi}, (42.8 \text{ MPa}) \\ f_c: & 3\sqrt{f'_c} = 236 \text{ psi}, (1.6 \text{ MPa}) \\ f_s: & 36 \text{ ksi}, (248 \text{ MPa}) \end{aligned}$$

The area of steel required was 0.236 in^2 (152mm^2). The cage steel provided 0.192 in^2 (124mm^2) and an additional 4- Φ 5/32 in. (4mm) wires were used to provide 0.269 in^2 (173mm^2).

Shear:

Shear design was based on ultimate loads and followed a similar procedure as described in this appendix for model CB-RU. However, rather than using the V_c equation (Equation A-3), V_{ci} and V_{cw} were calculated instead. These equations correspond to the concrete shear strength for inclined-shear crack failure and web-shear crack failure respectively and can be found in AASHTO provision 9.20.2).

Side Face Crack Control:

Side face crack control steel design followed the design outlined in this appendix for model CB-RU.

Anchor Zone Design:

Anchor zone design was in accordance with NCHRP Report 356 [24]. Three bearing plates of 4.25"x3"x1" (108mmx76mmx25mm) were used. The first check involved checking the bearing strength of the concrete in the anchor zone using the following equations:

$$f_b \leq 0.7 \Phi f_{ci} \sqrt{\frac{A}{A_g}} \quad (\text{A-7})$$

$$f_b \leq 2.25 \Phi f_{ci}' \quad (\text{A-8})$$

$$\text{where } f_b = \frac{P_u}{A} \quad \text{and} \quad P_u = 0.972 f_{su} A_{ps}$$

- where:
- f_b : Maximum factored tendon load, P_u , divided by the effective bearing area, A_b .
 - Φ : 0.85
 - f_{ci}' : Concrete compressive strength at stressing = 5000psi, (34.5MPa)
 - A : Maximum area of the portion of the supporting surface that is geometrically similar to the loaded area and concentric with it.
 - A_g : Gross area of bearing plate = 12.75 in², (8225mm²). (see Reference 24 for special conditions).
 - A_b : Effective net area of the bearing plate calculated as the area A_g minus the area of openings in the bearing plate.
 - P_u : Maximum factored tendon load.
 - f_{su} : Ultimate stress of prestressing steel = 270ksi, (1862MPa).
 - A_{ps} : Area of prestressing steel = 0.391 in², (252mm²).

Individual plates were checked first having a bearing area of 42.9 in² (27,677mm²). Equation A-7 controlled for this case requiring a bearing stress less than 5.4 ksi (37.2 MPa). Based on a calculated P_u of 40.2k (179kN), the maximum bearing stress would be 3.3 ksi (22.8MPa). Therefore the bearing plates are adequate for individual plate bearing.

The bearing plates were then checked as a group having a bearing area of 98.4 in² (63,485mm²). Equation A-7 again controlled requiring a bearing stress less than 4.8 ksi (33.1MPa). The maximum bearing stress was calculated as 2.9 ksi (20MPa). Therefore the bearing plates were also adequate for group plate bearing.

Bearing stiffness of the individual plates was checked next. In accordance with Reference 40, it is required that:

$$\frac{n}{t} = 0.8 \sqrt[3]{\frac{E_b}{f_b}} \quad (\text{A-9})$$

- where
- n : Maximum distance from the outer edge of the wedge plate to the outer edge of the bearing plate = 0.88 in., (22.4mm).
 - t : Average thickness of bearing plate = 1 in., (25.4mm).

E_b : Modulus of elasticity of bearing plate material = 29,000 ksi, (200,000MPa).

f_b : (see above) = 3.3 ksi, (22.8 MPa).

Bearing plate stiffness was found to be adequate.

Anchor zone stirrups were then designed based on the bursting forces calculated in accordance with Figure 3.7. For this model, the maximum bursting force was 25k (111kN) within the depth of the beam. Considering a Φ -factor of 0.85 and the yield stress of the stirrups as 71 ksi (490MPa), a total of 7 stirrups at 3 in. (76mm) was required. As mentioned in Section 3.3.2.1 of this thesis, 10 stirrups at 2 in. (51mm) were used.

APPENDIX B
FATIGUE STUDY FOR MODEL CB-PU-100S

Fatigue study for CB-PU-100S

Of interest in a fatigue study is the stress range in the prestressed and non-prestressed steel between full dead load and service live load plus impact. For the prestressed steel, this will be done by means of a strain compatibility analysis. Stresses in the initial stage (before application of full dead load) are determined first. For this model the entire section is initially in compression. Therefore the decompression load is calculated next. This corresponds to the applied load required to create zero stress at the extreme tension fiber (the extreme fiber that goes into tension under increased applied loads). With the decompression load determined, a cracked section analysis is then used to continue the analysis up to service loads. This analysis includes assuming a concrete compressive strain and determining the steel stresses and location of the neutral axis by iteration until equilibrium is reached. The moment (and therefore applied load) corresponding to the steel stresses for each assumed concrete strain is then calculated. A plot is made of applied load versus steel stress to determine the range of stress experienced by the steel between dead and service loads.

This method is shown here as it applies to the load versus stress range relationship for the negative moment region of model CB-PU-100S. As the stress range for the prestressed steel was well within the recommended limit for post-tensioned steel, the non-prestressed steel was not checked. This could however be done using a strain compatibility analysis or by following AASHTO provision 8.16.8.3.[9]

The following cross sectional and material properties as well as forces are used:

b, h:	18 in.	(457mm)	f _c ':	7170 psi	(49.4 MPa)
d _{ps} :	16.5 in.	(419mm)	f _{pu} :	270 ksi	(1724 MPa)
d _s :	17 in.	(432mm)	f _{se} :	150 ksi	(1034 MPa)
c:	9 in.	(229mm)	f _y :	75.1 ksi	(518 MPa)
I:	8748 in ⁴	(3.64x10 ⁹ mm ⁴)	E _c :	4825 ksi	(33275 MPa)
A _{ps} :	0.391 in ²	(252mm ²)	E _s :	29000 ksi	(200,000 MPa)
A _s :	0.3 in ²	(194mm ²)	F _{ps} = A _{ps} * f _{se} :	58.7k	(261kN)
A _{eff} = b*h:	324 in ²	(209030mm ²)	M _{DL} :	-10.8 k-ft.	(-14.65 kN-m)
e:	7.5 in.	(191mm)	M _{sec} :	-16.4 k-ft.	(-22.2 kN-m)

Initial Stage:

$$\sigma_{top} = - \frac{F_{ps}}{A_{eff}} - (F_{ps} e) \frac{c}{I} - (M_{DL} + M_{sec}) \frac{c}{I} = - 301 \text{ psi} \quad (- 2.08 \text{ MPa}) \quad (\text{compression})$$

$$\sigma_{bot} = -\frac{F_{ps}}{A_{eff}} + (F_{ps} e) \frac{c}{I} + (M_{DL} + M_{sec}) \frac{c}{I} = -61 \text{ psi} \quad (-0.42 \text{ MPa}) \quad (\text{compression})$$

Note: M_{DL} and M_{sec} are negative moments and therefore produce tension at the top fiber and compression at the bottom fiber.

Corresponding concrete and steel strains at this initial stage are shown graphically in Figure B.1.

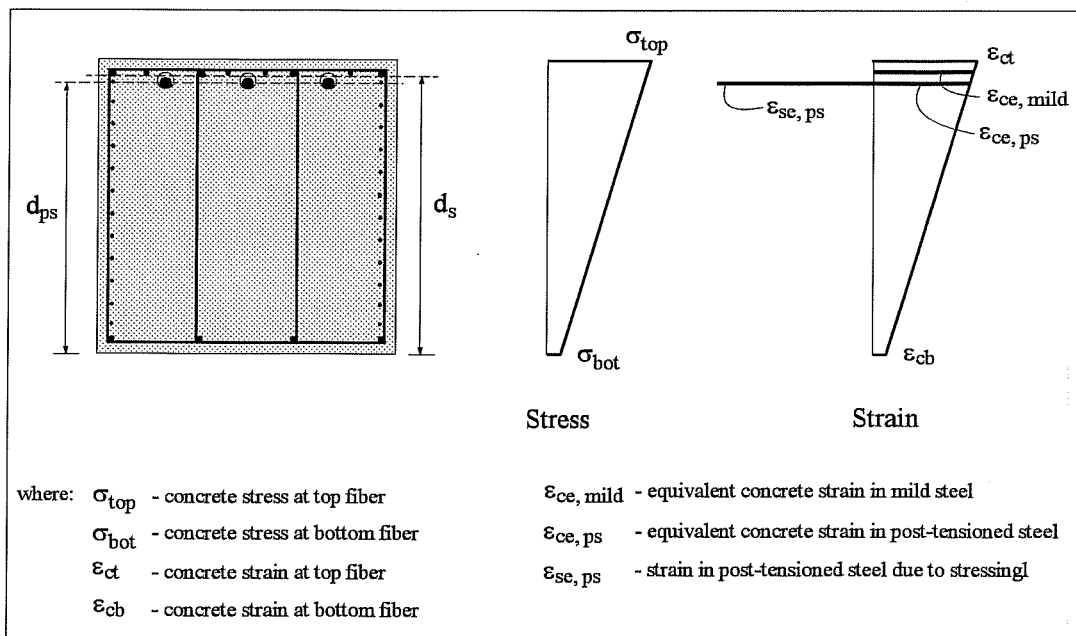


Figure B.1 Concrete and Steel Strains in Initial Stage for Fatigue Study

The strains are:

ϵ_{ct} :	0.000062
ϵ_{cb} :	0.000013
$\epsilon_{ce, ps}$:	0.000053
$\epsilon_{sc, ps}$:	0.005172

Decompression Moment and Load:

The applied load to give an extreme tensile fiber stress of zero requires enough moment to overcome the initial strain in the concrete and steel in the tension zone. Therefore the decompression moment must overcome prestressing strains of:

$$\epsilon_{ps} = \epsilon_{se,ps} + \epsilon_{ce,ps} = 0.00523$$

$$f_{ps} = \epsilon_{ps} * E_s = 151.7 \text{ ksi} \quad (1046 \text{ MPa})$$

$$F_{ps} = f_{ps} * A_{ps} = 59.3 \text{ k} \quad (264 \text{ kN})$$

This corresponds to extreme fiber stresses of -303 psi (-2.09 MPa) at the top ($\epsilon_{ct,dec} = -6.3 \times 10^{-5}$) and -63 psi (-0.43 MPa) at the bottom ($\epsilon_{cb,dec} = -1.3 \times 10^{-5}$). To create an extreme fiber stress of zero at the top, the following moment must be applied:

$$M_{dec} = \sigma_{top} * \frac{I}{c} = 303 * \frac{8748}{9} * \frac{1}{12} = 24.5 \text{ k-ft.} \quad (33.2 \text{ kN-m})$$

From statics, this decompression moment, M_{dec} , can be created by point loads of $Q = M/2.435 = 10.1\text{k}$ (45kN) (refer to Figure 3.2 for point load arrangement.)

Cracked Section Analysis:

To determine the load vs. stress range relationship for the post-tensioned steel at this section, both the prestressed and non-prestressed steel are considered, using a strain compatibility analysis. A triangular compressive block is assumed to balance the tensile forces as compressive concrete strains do not exceed 0.001 in./in. (mm/mm) (see Figure B-2).

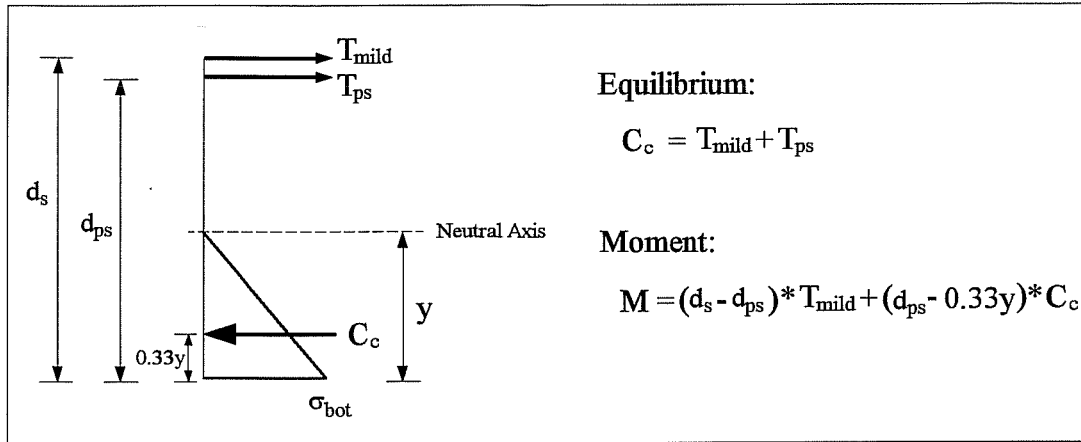


Figure B.2 Cracked Section Analysis for Fatigue Study

Point (1) $\epsilon_c = 0.00016$

Assume Neutral Axis = $y = 9$ in. (229mm)

$$C_c = 0.5 * \epsilon_c * E_c * b * y = 62.6k \quad (278kN)$$

$$\epsilon_{ips} = (d_{ps} - y) * \epsilon_c / y = 0.000133$$

$$\epsilon_{pse} = \epsilon_{ips} + \epsilon_{ps} = 0.005364$$

$$f_{ps} = \epsilon_{pse} * E_s = 155.6 \text{ ksi} \quad (1073 \text{ MPa})$$

$$F_{ps} = A_{ps} * f_{ps} = 60.8k \quad (271kN)$$

$$\epsilon_{mild, dec} = (\epsilon_{ct, dec} - \epsilon_{cb, dec}) * d_s / h + \epsilon_{cb, dec} = 0.000064$$

$$\epsilon_{imild} = (d_s - y) * \epsilon_c / y = 0.000142$$

$$\epsilon_{mild} = \epsilon_{imild} + \epsilon_{mild, dec} = 0.000206$$

$$f_{mild} = \epsilon_{mild} * E_s = 6.0 \text{ ksi} \quad (41.4 \text{ MPa})$$

$$F_{mild} = A_s * f_{mild} = 1.8k \quad (8.0kN)$$

$$T = 62.6k \quad (279kN) = C_c \quad \text{O.K.} \quad \therefore y = 9 \text{ in. (229mm)}$$

$$M = F_{mild} * (d_s - d_{ps}) + C_c * (d_{ps} - 0.33y) = 70.5 \text{ k-ft.} \quad (95.6 \text{ kN-m})$$

$$Q = M / 2.435 = 29.0k \quad (129kN)$$

$$f_{ps} = 155.6 \text{ ksi} \quad (1073 \text{ MPa})$$

Many other points were found by choosing a concrete compressive strain and determining the neutral axis location that fulfills equilibrium. Figure B-3 shows a final load versus stress range curve. The critical stress range is 7 ksi (48.3 MPa) which is within the allowable limit of 14.5 ksi (100 MPa) recommended by Wollmann.[65].

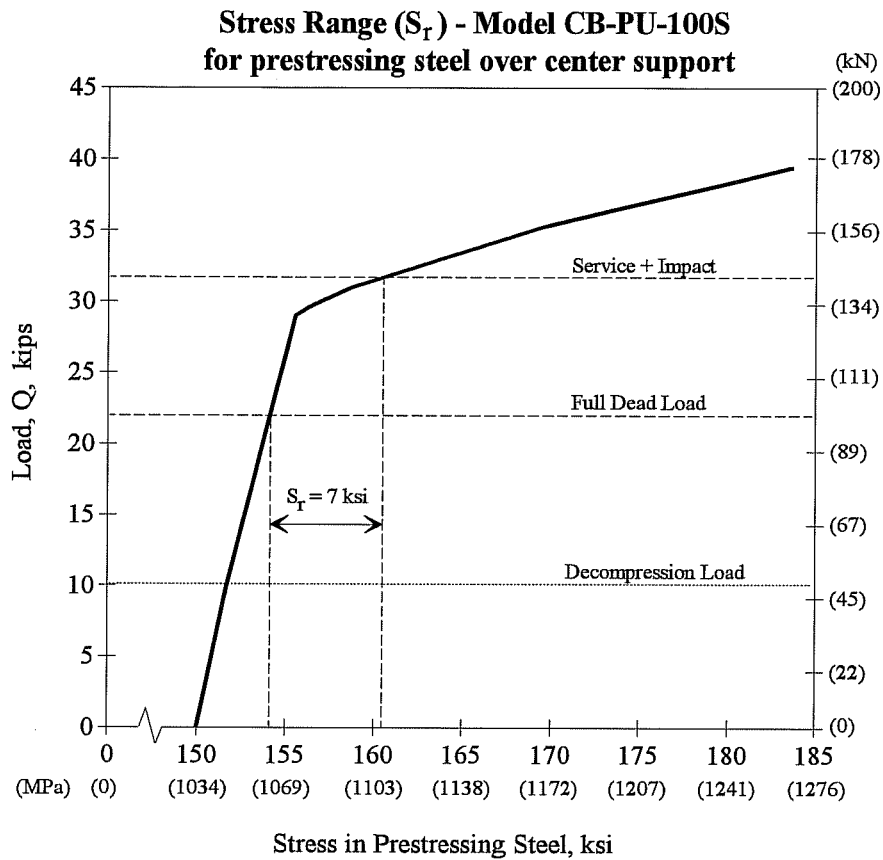


Figure B.3 Stress Range for Prestressed Steel over Center Support - CB-PU-100S

Notation:

- b: Width of member
- h: Height of member
- d_{ps} : Effective depth to centroid of prestressed reinforcement
- d_s : Effective depth to centroid of non-prestressed reinforcement
- c: Distance from extreme compression fiber to neutral axis
- I: Moment of inertia of member
- A_{ps} : Area of prestressed reinforcement
- A_s : Area of non-prestressed reinforcement
- A_{eff} : Gross area of member
- e: Eccentricity of load parallel to axis of member measured from centroid of the gross section

f'_c :	28-day compressive strength of concrete
f_{pu} :	Ultimate tensile strength of prestressed reinforcement
f_{se} :	Effective stress in prestressed reinforcement (after all prestress losses)
f_y :	Yield strength of non-prestressed reinforcement
E_c :	Modulus of elasticity of concrete
E_s :	Modulus of elasticity of steel
F_{ps} :	Force in prestressed reinforcement after all prestress losses
M_{DL} :	Moment induced by dead loads
M_{sec} :	Secondary moments

REFERENCES

- [1] Abeles, P.W., "Philosophy of Partial Prestressing," American Concrete Institute SP-59, from 1976 Symposium on "Concrete Design: U.S. and European Practices", 1979, pp287-304
- [2] American Association of State Highway Officials (AASHO), Standard Specifications for Highway Bridges, Eighth Edition, Washington, D.C., 1961.
- [3] AASHO, Standard Specifications for Highway Bridges, Tenth Edition, Washington, D.C., 1969.
- [4] AASHO, Standard Specifications for Highway Bridges, Eleventh Edition, Washington, D.C., 1973.
- [5] AASHO Road Test Advisory Panel on Bridges, "Tensile Stresses in Concrete in Prestressed Concrete Beams," Memorandum to the AASHO Committee on Bridges and Structures, April, 1962.
- [6] American Association of State Highway and Transportation Officials (AASHTO), Guide Specification for the Design and Construction of Segmental Concrete Bridges, 1989.
- [7] AASHTO, Standard Specifications for Highway Bridges, Twelfth Edition, Washington, D.C., 1977.
- [8] AASHTO, Standard Specifications for Highway Bridges, Thirteenth Edition, Washington, D.C., 1983.
- [9] AASHTO, Standard Specifications for Highway Bridges, Fifteenth Edition, Washington, D.C., 1992.
- [10] American Concrete Institute (ACI), Building Code Requirements for Reinforced Concrete and Commentary - 318-63, Detroit, 1963.
- [11] ACI, Building Code Requirements for Reinforced Concrete and Commentary - 318-63, Detroit, 1963.
- [12] ACI, Building Code Requirements for Reinforced Concrete and Commentary - 318-71, Detroit, 1971.
- [13] ACI, Building Code Requirements for Reinforced Concrete and Commentary - 318-77, Detroit, 1977.

- [14] ACI, Building Code Requirements for Reinforced Concrete and Commentary - 318-83, Detroit, 1983.
- [15] ACI, Building Code Requirements for Reinforced Concrete and Commentary - 318-89, Detroit, 1989.
- [16] ACI-ASCE Joint Committee 323, "Tentative Recommendations for Prestressed Concrete," Journal of the American Concrete Institute, Detroit, January 1958, Vol. 29. No. 7, pp. 545-578.
- [17] Armstrong, S., "Design and Behavior of Large Cantilever Overhangs with Combinations of Prestressed and Non-Prestressed Reinforcement," Masters Thesis, The University of Texas at Austin, August, 1992.
- [18] Beeby, A.W., "Cracking, Cover, and Corrosion of Reinforcement," *Concrete International*, February 1983, pp. 35-40.
- [19] Beeby, A.W., Darwin, D., Ghowrwal, A.Q., Hognestad, E., Manning, D.G., Rice, P.F., "Debate: Crack width, cover, and corrosion," *Concrete International*, May 1985, pp. 20-35.
- [20] Bennett, W.Burr, Interview, W.Burr Bennett Ltd., Northbrook, Illinois.
- [21] Billington, D.P., "Historical Perspective on Prestressed Concrete," *Prestressed Concrete Institute (PCI) Journal*, September-October, 1976, pp 48-71.
- [22] Billington, D.P., The Tower and the Bridge, Princeton University Press, Princeton, NJ, 1985.
- [23] Borges, F., Lima, A., "Crack Deformation Similitude in Reinforced Concrete," RILEM, No. 7, June 1960
- [24] Breen, J.E., Burdet, O., Roberts, C., Sanders, D., Wollmann, G., "Anchorage Zone Reinforcement for Post-tensioned Concrete Girders," NCHRP, Report 356, Transportation Research Board, National Research Council, 1994.
- [25] Breen, J.E., Frantz, G.C., "Control of Cracking on the Side Faces of Large Reinforced Concrete Beams," Research Report 198-1F, Center for Highway Research, The University of Texas at Austin, September 1978.
- [26] Brueggeling, A.S.G., "Partially Prestressed Concrete Structures - A Design Challenge," *PCI Journal*, March-April, 1985, pp140-171.

- [27] Bureau of Public Roads, "Criteria for Prestressed Concrete Bridges," U.S. Department of Commerce, Washington D.C., 1954.
- [28] Cohn, M.Z., "Continuity in Prestressed Concrete," Proceedings of the NATO Advanced Workshop on "Partial Prestressing, From Theory to Practice," Paris, France, 1984, Ch. 8.
- [29] Cohn, M.Z. (editor), Nonlinearity and Continuity in Prestressed Concrete, International Symposium, University of Waterloo, Waterloo, Ontario, Canada, July 1983.
- [30] Comité Euro-International du Béton, CEB-FIP Model Code 1990 (Design Code), Thomas Telford, London, 1993.
- [31] Depman, F., Hollander, E.F., Nagle, J., Zollman, C.C., "Building and Rebuilding of Philadelphia's Walnut Lane Memorial Bridge," *PCI Journal*, May-June 1992, pp 66-82.
- [32] Dunker, K.F., Rabbat, B.G., "Performance of Highway Bridges," *Concrete International*, Volume 12, No. 8, August 1990, pp. 40-42.
- [33] Favre, R., Jaccoud, J.P., Koprna, M., Radojicic, A., Dimensionnement des Structures en Béton; Dalles, murs, colonnes et fondations, Traité de Génie Civil, Volume 8, Presses Polytechniques et Universitaires Romandes, 1990.
- [34] Gergely, P., Lutz, L.A., "Maximum Crack Width in Reinforced Concrete Flexural Members," Causes, Mechanism, and Control of Cracking in Concrete, ACI SP-20, Detroit, 1968, pp. 87-117.
- [35] Hawkins, N.M., "Impact of Research on Prestressed Concrete Specifications," ACI SP-72, pp. 163-176.
- [36] Inomata, S., "A Design Procedure for Partially Prestressed Concrete Beams Based on Strength and Serviceability," *PCI Journal*, September-October 1982, pp 100-116.
- [37] Kerekes, F., Reid, H.B. Jr., "Fifty Years of Development in Building Code Requirements for Reinforced Concrete," *Journal of the American Concrete Institute*, Vol. 25, No. 6, February 1954, pp. 441-470.
- [38] Kong, F.K., Reinforced Concrete Deep Beams, Van Nostrand Reinhold, New York, 1990.
- [39] Leonhardt, F., "To New Frontiers for Prestressed Concrete Design and Construction," Keynote Address, *PCI Journal*, Volume 19, No. 5, September 1974, pp 54-69.

- [40] Leonhardt, F., "Recommendations for the Degree of Prestressing in Prestressed Concrete Structures," ACI SP-59, from 1976 Symposium on "Concrete Design: U.S. and European Practices," 1979, pp. 269-285.
- [41] Lin, T.Y., Burns, N.H., Design of Prestressed Concrete Structures, Third Edition, John Wiley & Sons, New York, 1981.
- [42] Lin T.Y., "Partial Prestressing Design -- Philosophy and Approach," ACI SP-59, from 1976 Symposium on "Concrete Design: U.S. and European Practices", 1979, pp. 257-267.
- [43] Lin, T.Y., Thornton, K., "Secondary Moment and Moment Redistribution in Continuous Prestressed Concrete Beams," *PCI Journal*, January-February, 1972, pp. 8-20
- [44] Maples, W.A., Wilde, R.E., "A Story of Progress - Fifty Years of the American Concrete Institute," *ACI Journal*, Vol. 25, No. 6, February 1954, pp. 409-436.
- [45] Mast, R., "Unified Design Provisions for Reinforced and Prestressed Concrete Flexural and Compression Members," *ACI Structural Journal*, March-April 1992, pp 185-199.
- [46] Naaman, A.E., Siriakorn, A., "Serviceability based Design of Partially Prestressed Beams," *PCI Journal*, March-April, 1979, pp 64-89.
- [47] NATO, "Partial Prestressing, From Theory to Practice," Proceedings of the NATO Advanced Workshop, Paris, France, 1984.
- [48] NCHRP 12-33, Development of Comprehensive Bridge Specifications and Commentary, Third Edition LFRD Specifications and Commentary, April, 1992.
- [49] Nilson, A.H., Winter, G., Design of Concrete Structures, Tenth Edition, McGraw-Hill Book Company, 1982.
- [50] Overman, T.R., "Flexural Fatigue Behavior of Pretensioned Concrete Girders," Masters Thesis, The University of Texas at Austin, December 1984.
- [51] Posten, R.W., "Improving Durability of Bridge Decks by Transverse Prestressing," Doctoral Dissertation, The University of Texas at Austin, December, 1984.
- [52] Regan, P., "The Treatment of Prestress in the CEB-FIP Model Code 90," CEB Bulletin D'Information No. 212, December 1992.

- [53] Rickets, D.R., MacGregor, J.G., "Ultimate Behavior of Continuous Deep Reinforced Concrete Beams," Masters Thesis, The University of Alberta, Edmonton, Alberta, 1985.
- [54] Salas, R., "Behavior of Structural Concrete Cantilever Piers using Thheaded Reinforcing Bars and Varied Prestressing Design Criteria," Masters Thesis, The University of Texas at Austin, August 1992.
- [55] Schlaich, J., Schäfer, K., Jennewein, M., "Towards a Consistant Design of Structural Concrete," *PCI Journal*, Vol. 32, No. 3, May/June 1987, pp 74-150.
- [56] Scholz, H., "Simple Deflection & Cracking Rules for Partially Prestressed Members," *ACI Structural Journal*, Vol. 88, No. 2, March-April 1991, pp. 199-203.
- [57] SIA Standard 162, Concrete Structures, Swiss Society of Engineers and Architects, Zürich, Switzerland, July, 1989.
- [58] Siess, Prof. C.P., Interview, University of Illinois at Champaign-Urbana.
- [59] Siess, C.P., "Research, Building Codes and Engineering Practice," *ACI Journal*, Vol. 31, No. 11, May 1960, pp 1105-1122.
- [60] Siess, C.P., "Research in Prestressed Concrete," Paper presented at the First U.S. Conference on Prestressed Concrete, Massachusetts Institute of Technology, July 1951.
- [61] "Structural Concrete: Unifying Design Approaches," *Concrete International*, October 1991, pp. 74-77.
- [62] Tan, K.H., Mansur, M.A., "Partial Prestressing in Concrete Corbels and Deep Beams," *ACI Structural Journal*, May-June 1992, pp 251-262.
- [63] Thürlimann, B., "Considerations to the Design of Prestressed Concrete Bridges," International Association for Bridge and Structural Engineering (IABSE), Proceedings, P-70/83, pp. 237-252.
- [64] Winter, G., "Development of a National Building Code for Reinforced Concrete 1908-1977," *Concrete International*, December 1982, pp 27-37.
- [65] Wollmann, G.P., Yates, D.L., Breen, J.E., Kreger, M.E., "Fretting Fatigue in Post-tensioned Concrete," Report 465-2F, Center for Transportation Research, The University of Texas at Austin, November 1988.
- [66] Wood, B. Unpublished Doctoral Dissertation, University of Texas at Austin, 1995.

VITA

Sarah Longstreth Billington was born in Princeton, New Jersey on October 28, 1968 to David Perkins and Phyllis Bergquist Billington. After graduating as valedictorian from Princeton High School in Princeton, New Jersey she attended Princeton University. She received her Bachelor of Science in Engineering with high honors and a Certificate in Architecture and Engineering from Princeton in June, 1990. During the summers throughout college she worked for Nomura Securities in Tokyo, Japan and as a structural engineering intern for Skidmore, Owings & Merrill in Chicago, Illinois and London, England. Upon receiving her Bachelor's degree, she was awarded a Fulbright Fellowship for studies in Switzerland. From October 1990 to December 1991 she attended the Swiss Federal Institute of Technology in Zurich where she attended classes in civil engineering and carried out a research project in the Hydraulic Engineering Department. During September and October, 1991 she worked for Elektrowatt Engineers, Inc., as a structural engineering intern on the construction site of a water power plant in Laufenburg, Switzerland. Upon returning to the United States, she worked as a structural engineer for Greiner Engineering in Timonium, Maryland for four months before entering the Master's degree program at the University of Texas at Austin.

Permanent Address: 45 Hodge Road
 Princeton, NJ 08540

This thesis was typed by the author.